

Oil & Natural Gas Technology

DOE Award No.: DE-FE0024297

Quarterly Research Performance Progress Report

(Period ending: 06/30/2017)

Marcellus Shale Energy and Environment Laboratory (MSEEL)

Project Period: October 1, 2014 – September 30, 2019

Submitted by:
Samuel Taylor



West Virginia University Research Corporation
DUN's Number: 191510239
886 Chestnut Ridge Road,
PO Box 6845, Morgantown WV, 26505
Tim.Carr@mail.wvu.edu
304-293-9660

Prepared for:
United States Department of Energy
National Energy Technology Laboratory

April 21, 2017



Office of Fossil Energy

Quarterly Progress Report

April 1 – June 30, 2017

Executive Summary

The objective of the Marcellus Shale Energy and Environment Laboratory (MSEEL) is to provide a long-term field site to develop and validate new knowledge and technology to improve recovery efficiency and minimize environmental implications of unconventional resource development.

This quarter field work focused on developing presentations for the MSEEL session at URTEC in Austin, TX and at other venues. Production data for gas and water is now on the MSEEL.org website and is updated at the first of the month. We have developed geophysical techniques to process the fiber-optic DAS data from the MIP-3H that can image cross-stage fluid communication during hydraulic stimulation. These results have been submitted for presentation at the SPE Hydraulic Fracturing Conference. We are undertaking a new reservoir simulation using a Discrete Fracture Network Model (Schlumberger's Mangrove).

Deliverables this quarter include:

- Subtask 1.3.2 – Initial Economic Impact. Report from RRI is attached as an appendix.
- Subtask 1.6.4 – Data Collection and analysis of fiber optic measurements. Abstract is attached as an appendix.
- Subtask 2.2.2 – Long term monitoring of production. Results are ongoing, and data is on the MSEEL website.

The project team is tracking eight (8) milestones in this budget period:

- 3/1/2017 - Completed Production Logging (Scheduled 2/15/2017; Completed 3/15/2017)
- 4/30/17 - Conduct preliminary analysis of production log data and present to DOE. (Completed and being worked into a new reservoir simulation – Review meeting held at WVU 4/11/2017)
- 8/15/17 - Coordinate and hold MSEEL session at URTEC 2017
- 8/30/17 - Complete rock geochemistry and geomechanical data analysis and integration with log & microseismic data to develop preliminary reservoir simulation and fracture model(s)
- 8/30/17 – Create a comprehensive online library of MSEEL presentations and papers that can be downloaded. Maintain with additional material through end of project.
- 8/30/17 – Reorganize MSEEL data portal and prepare to transfer to NETL for public dissemination.
- 12/31/17 – Complete a detailed reservoir simulation incorporating fracture geometry and flow simulation
- 12/31/17 - Determine changes in kerogen structure and bulk rock interactions and composition on interaction with fracturing fluids under simulated subsurface conditions.

Quarterly Progress Report

April 1 – June 30, 2017

Project Performance

This report summarizes the activities of Cooperative Agreement DE-FE0024297 (Marcellus Shale Energy and Environment Laboratory – MSEEL) with the West Virginia University Research Corporation (WVURC) during the third quarter of FY2017 (April 1 through June 30, 2017).

This report outlines the approach taken, including specific actions by subtopic. If there was no identified activity during the reporting period, the appropriate section is included but without additional information.

A summary of major lessons learned to this point of the project are provided as bullet points and will be added to as research is completed. New lessons are highlighted.

- 1) Synthetic based drilling mud is ecofriendly as well as helps with friction which resulted in faster drilling and reduced costs while leading to drilling waste from both the vertical and horizontal portions of the wells that passed all toxicity standards.
- 2) Microseismic monitoring does not completely define propped fractures and the extent of stimulated reservoir volume from hydraulic fracture stimulation. Requires integration of data from core, logs and slow slip seismic monitoring.
- 3) Production logging documents significant variations in production between completion types, stages and even clusters. Variations in production provide the necessary data for robust reservoir simulation.
- 4) Complex geology in laterals can lead to intercommunication between stages and reduced fracture stimulation efficiency. This can be mitigated with limited entry (engineered completions) that significantly improves fracture stimulation efficiency. NNE has continued the practice in subsequent wells. Planned production logging will help to define production efficiency.
- 5) The significant part of air emissions are in truck traffic, not in drilling and fracture operations on the pad. Emissions from both the pad and trucking can be reduced with operational modifications such as reducing dust and truck traffic during fracture stimulation (e.g., Sandbox) from bifuel (natural gas-diesel) engine operations.
- 6) Dual fuel engines demonstrated lower carbon monoxide (CO) emissions than diesel only operation. Dual fuel operations could reduce onsite diesel fuel consumption by 19 to 63% for drilling and 52% for hydraulic stimulation.
- 7) Biologic activity cannot be eliminated with biocides, only delayed. The biologic activity results in a unique biota that may affect operations. There may be other methods to control/influence biologic activity.
- 8) Water production changes rapidly after fracture stimulation in terms of volume (500 bbl/day to less than 1 bbl/day) and total dissolved solids (TDS from freshwater, 100 to 150g/L). Radioactivity is associated with produced water, not drill cuttings.
- 9) Drill cutting radioactivity levels were within West Virginia DEP standards of 5 pCi/g above background. This was true of both vertical and horizontal (Marcellus) sections.
- 10) Using the green drilling fluid Bio-Base 365, all drill cutting samples, vertical and horizontal, passed the USEPA's method 1311 (Toxicity Characteristics Leaching Procedure or TCLP) for inorganic and organic contaminants. This indicates that under

Federal and West Virginia solid waste rules, these solid wastes would not be considered hazardous.

- 11) The absence of hazardous TCLP findings suggest that drilling fluids, not the inherent properties of the Marcellus formation, play the dominant role in determining drill cutting toxicity.
- 12) Concerning produced water quality, hydraulic fracturing fluid was nearly identical to makeup (Monongahela River) water. Initial produced water underwent a radical change in ionic composition and a two order of magnitude increase in total dissolved solids (TDS).
- 13) Produced water is highly saline and total dissolved solids (TDS) rapidly increased to a maximum between 100 and 150 g/L. There was negligible change in ionic composition between the initially produced water and that sampled five years post completion.
- 14) Concentrations of both 226 Ra and 228 Ra increased rapidly through the produced water cycle to combined maximum concentrations of 20,000 pCi/L in the first year post completion. These radium isotopes are critical regulatory determinants.
- 15) The volume of produced water decreased rapidly from nearly 500 bbl/day to less than 1 bbl/day after one year. Over this cycle produced water averaged about 6 bbl/day.
- 16) Developed a new frequency attribute calculated from the DAS data that reveals cross-stage fluid communication during hydraulic fracturing.

Dr. Carr presented MSEEL results to the North American Coal Bed Methane forum on 4/12/2017. The slides from this talk are attached as an appendix.

Summary report for Task 8 by RRI is included as an appendix. RRI Report “MSEEL Project Context: State of the Region (2001-2014)” is attached, and can be downloaded from

<http://rri.wvu.edu/resource-documents/>

A MSEEL session and related presentations is scheduled for Unconventional Resources Technology Conference (<http://urtec.org/2017/>) on 24-26 July. MSEEL has a dedicated session for Monday afternoon (<http://urtec.org/2017/Technical-Program/Monday/Monday-Afternoon-Oral-Presentations>). Full copies of these papers are included as an appendix to this report.

Oral Session

Marcellus Shale Energy and Environment Laboratory (MSEEL)

Introductory Remarks – NETL, DOE

Marcellus Shale Energy and Environment Laboratory (MSEEL): Subsurface Reservoir Characterization and Engineered Completion; Presenter: Tim Carr; West Virginia University (2670437)

Depositional environment and impact on pore structure and gas storage potential of middle Devonian organic rich shale, Northeastern West Virginia, Appalachian Basin; Presenter: Liaosha Song, Department of Geology and Geography, West Virginia University, Morgantown, WV, (2667397)

Seismic monitoring of hydraulic fracturing activity at the Marcellus Shale Energy and Environment Laboratory (MSEEL) site, West Virginia; Presenter: Abhash Kumar, DOE, National Energy Technology Laboratory (2670481)

Geomechanics of the microseismic response in Devonian organic shales at the Marcellus Shale Energy and Environment Laboratory (MSEEL) site, West Virginia; Presenter: Erich Zorn, DOE, National Energy Technology Laboratory (2669946)

Application of Fiber-optic Temperature Data Analysis in Hydraulic Fracturing Evaluation- a Case Study in the Marcellus Shale; Presenter: Shohreh Amini (Presented by Tim Carr), West Virginia University (2686732)

The Marcellus Shale Energy and Environmental Laboratory (MSEEL): water and solid waste findings-year one; Presenter: Paul Ziemkiewicz WRI, West Virginia University (2669914)

Role of organic acids in controlling mineral scale formation during hydraulic fracturing at the Marcellus Shale Energy and Environmental Laboratory (MSEEL) site; Presenter: Alexandra Hakala, National Energy Technology Laboratory, DOE (2670833)

**MSEEL URTeC eSession Agenda
Geochemical Studies from the Marcellus Shale Energy and Environment Laboratory
(MSEEL)**

CONTROL ID	TITLE	PRESENTER
2670833	Role of Organic Acids in Controlling Mineral Scale Formation During Hydraulic Fracturing at the Marcellus Shale Energy and Environmental Laboratory (MSEEL) Site	Alexandra Hakala
2670060	Diglyceride Fatty Acid Profiles at the Marcellus Shale Energy and Environment Laboratory as Evidence of Non-Viable Microbial Community and Paleo-Environmental Conditions	Rawlings Akondi
2669965	Biogeochemical Characterization of Core, Fluids, and Gas at MSEEL Site	Shikha Sharma

Additional MSEEL Related Presentation at URTeC

Integrating High-Tier Measurements and Advanced Engineering Workflows to Understand and Improve Production Performance in the Marcellus Shale: A Field Case Study (2671506): Presenter Olatunbosun Anifowoshe in Theme 10: Well Completion Integration, Optimization, and Refracturing III

Also submitted were extended abstracts for the Society of Exploration Geophysicists (SEG) Annual meeting in Houston, TX, 24-29 September, 2017 (<http://seg.org/Annual-Meeting-2017>). Titles and authors are:

Correlating distributed acoustic sensing (DAS) to natural fracture intensity for the Marcellus Shale, Authors: Payam Kavousi*, Timothy Carr, Thomas Wilson, and Shohreh Amini, West Virginia University; Collin Wilson, Mandy Thomas, Keith MacPhail, Schlumberger; Dustin Crandall, US Department of Energy/National Energy Technology Laboratory; BJ Carney, Ian Costello, and Jay Hewitt, Northeast Natural Energy LLC.

Relationships of $\lambda\rho$, $\mu\rho$, brittleness index, Young's modulus, Poisson's ratio and high TOC for the Marcellus Shale, Morgantown, West Virginia, Authors: Thomas H. Wilson*, Payam Kavousi, Tim Carr, West Virginia University; B. J. Carney, Northeast Natural Energy LLC; Natalie Uschner, Oluwaseun Magbagbeola and Lili Xu, Schlumberger

Dominant Frequency Attribute Analysis of the Distributed Acoustic Sensing Data for the Marcellus Shale for Society Petroleum Engineers, Hydraulic Fracturing Technology Conference, January 23-25, Woodlands, TX, Authors: Payam Kavousi, Tim Carr, West Virginia University; Priyavrat Shukla, Schlumberger

Meso- and Macro-Scale Facies and Chemostratigraphic Analysis of Middle Devonian Marcellus Shale in Northern West Virginia, USA for Eastern Section American Association of Petroleum Geologists Annual Meeting September 26-27. Authors: Thomas Paronish, Timothy Carr, West Virginia University; Dustin Crandall and Jonathan Moore, National Energy Technology Laboratory, U.S. Department of Energy

Project Management Update

Approach

The project management team will work to generate timely and accurate reporting, and to maintain project operations, including contracting, reporting, meeting organization, and general oversight.

Results and Discussion

The project team is tracking eight (8) milestones in this budget period.

3/1/2017 - Completed Production Logging (Scheduled 2/15/2017; Completed 3/15/2017)

4/30/17 - Conduct preliminary analysis of production log data and present to DOE (Completed and being worked into a new reservoir simulation)

8/15/17 - Coordinate and hold MSEEL session at URTEC 2017

8/30/17 - Complete rock geochemistry and geomechanical data analysis and integration with log & microseismic data to develop preliminary reservoir simulation and fracture model(s)

8/30/17 – Create a comprehensive online library of MSEEL presentations and papers that can be downloaded. Maintain with additional material through end of project.

8/30/17 – Reorganize MSEEL data portal and prepare to transfer to NETL for public dissemination.

12/31/17 – Complete a detailed reservoir simulation incorporating fracture geometry and flow simulation

12/31/17 - Determine changes in kerogen structure and bulk rock interactions and composition on interaction with fracturing fluids under simulated subsurface conditions.

Topic 1 – Geologic Engineering

Approach

The core plug experiments are continuing. The permeability of the samples 59, 75, 78, 80, 84, 99, 102, and 110 have been measured. The permeability of the samples 101 and 101.2 cannot be measured due to non-cylindrical shape of the plugs.

Results and Discussion

Core Plugs

The core plugs exhibited permeability values in the range of 0.7-14 micro darcy. The analysis of the permeability measurement results indicate that the flow regime is transition flow for pore pressures below 900 psia and slip flow for pore pressure above 1000 psia. To determine the absolute permeability, the modified Klinkenberg correction is necessary when the flow regime is transition flow while Klinkenberg correction is sufficient under the slip flow conditions.

Production Logging

The analysis of the production and stimulation data are continuing to determine the optimum well spacing and production decline performance.

Products

M. El Sgher, K. Aminian, S. Ameri: "The impact of the hydraulic fracture properties on gas recovery from Marcellus Shale," SPE 185628, SPE Western Regional Conf., Bakersfield, California, April 2017.

Elsaig, M., Aminian, K., Ameri, S. and M. Zamirian: "Accurate Evaluation of Marcellus Shale Petrophysical Properties," SPE-**Error! Reference source not found.**84042, SPE Eastern Regional Conf., Canton, OH, September 2016.

Filchock, J.J., Aminian, K. and S. Ameri: "Impact of Completion Parameters on Marcellus Shale Production," SPE-184073, SPE Eastern Regional Conf., Canton, OH, September 2016.

Tawfik Elshehabi and H. Ilkin Bilgesu: "Well Integrity and Pressure Control in Unconventional Reservoirs: A Comparative Study of Marcellus and Utica Shales," SPE 184056, SPE Eastern Regional Conf., Canton, OH, September 2016.

Plan for Next Quarter

The drilling and log data are correlated for estimating of formation properties during drilling. Also, spinner survey data is under review to determine the factors contributing to the natural gas production.

Topic 2 – Geophysical & Geomechanical

Approach

Geophysical

The effort this past quarter concentrated on: 1) Moderate revision to the Journal Interpretation paper. Revisions were completed and submitted. 2) The SEG Expanded Abstract was accepted. 3) 3D-3C survey design and processing approach used in the Appalachian region has been investigated. 4) Hydraulic fracture modeling. 5) Research advising (see also plans for next quarter).

Geomechanical

During this quarterly period, the influence of a discrete fracture network on the growth of hydraulic fractures was investigated through the use of numerical modeling. The model used in previous quarters was updated to include the use of acid in the treatment schedule to more closely match what was carried out using actual pumping schedules A and B. Stages completed in previous reports were remodeled and 6 new stages were modeled with the inclusion of acid.

Results & Discussion

Geophysical

The results of last quarter's study revealed that the high TOC zone in the Marcellus Shale is associated with parameters derivable from 3D-3C seismic data. These associations have been recognized for many years: notably Goodway et al. (1997). Acquisition and processing workflows designed to extract elastic moduli from 3D-3C seismic data have been advanced since

2005 based on the work of Hampson and Russell. Recent uses of 3D-3C seismic surveys to characterize unconventional reservoirs have been presented by Alzate and Devegowda (2013) and Perez and Marfurt (2015).

Recent surveys in the region conducted by ION Geophysical motivated an extended inquiry into 3D-3C processing and acquisition in the area. ION collected an impressive 3D-3C seismic data set just east in Preston Co. Something for operators in the basin to consider.

Hydraulic fracture modeling using the NNE pump and proppant schedule for stage 10 revealed the following some interesting features of the hydraulic fractures. Hydraulic fracture width contours and profiles are shown (Figures 2.1 and 2.2). A close up of the fracture width contours is shown for comparison in Figure 2.3.

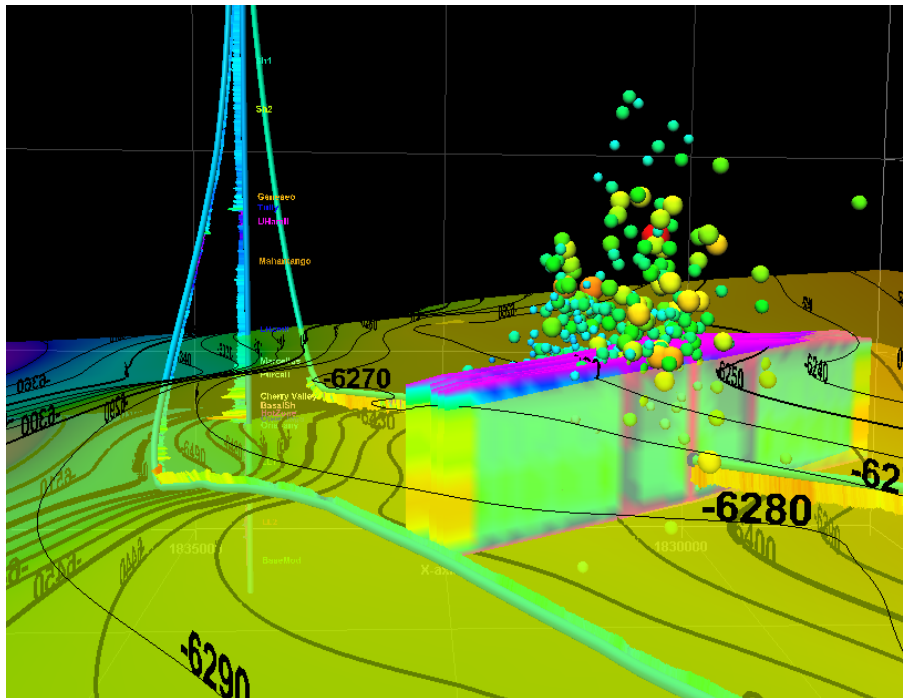


Figure 2.1. Hydraulic fractures developed across 5 perforation clusters (Stage 10).

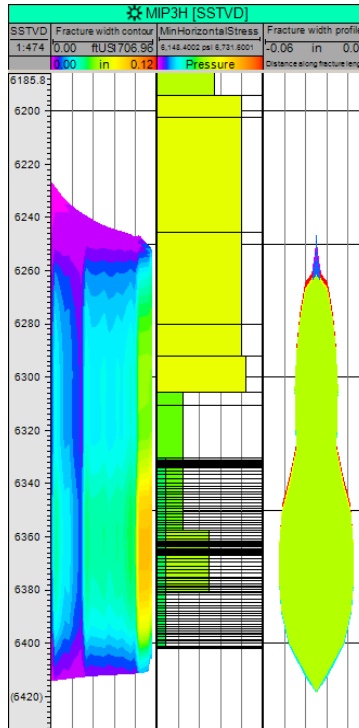


Figure 2.2. Fracture width contour, Shmin, and fracture width profile.

The model indicates the fracture pinches to narrower aperture with changes in proppant concentration in the later quarter of the stimulation (see Figures 2.3 and 2.4). Proppant, as expected tends to settle into the lower larger aperture region of the hydraulic fracture (Figures 2.2 and 2.3).

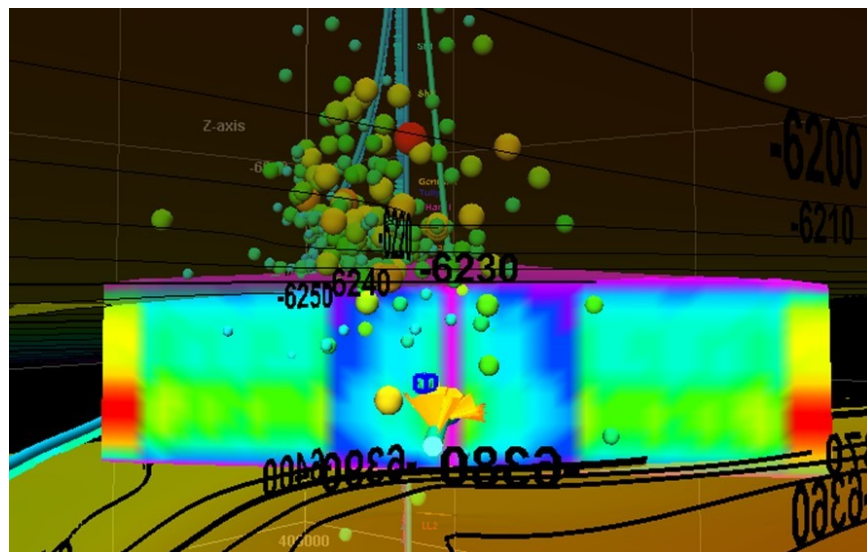


Figure 2.3. Area-based proppant concentration versus distance and height out along the hydraulic fracture.

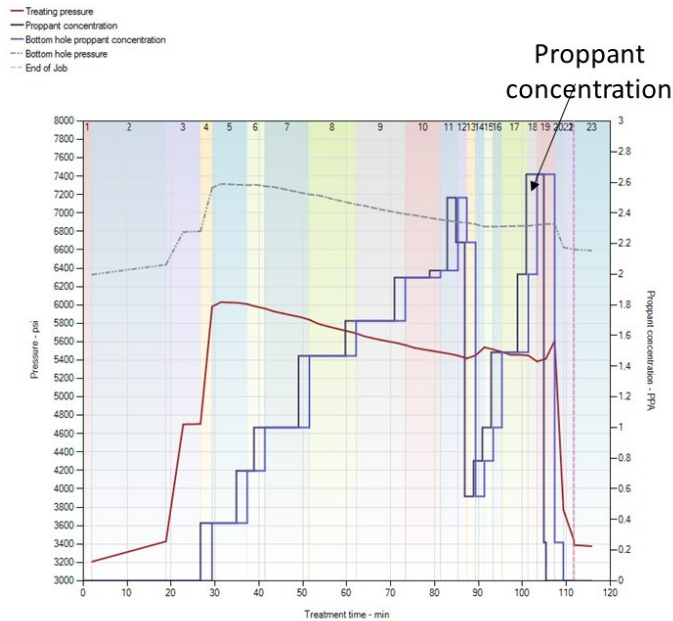


Figure 2.4. Variations of proppant concentration during stimulation

The rationale for doing this may be worth investigating and modifying to ensure more uniform fracture width. This might increase overall connectivity along the length of the hydraulic fracture.

Lastly, assistance was also provided to Payam Kavousi (post-doc working with fiber data) and Yixuan Zhu (Ph. D. student working with microseismic).

Geomechanical

Table 2.1 shows the updated fracture geometries for MIP 3H stages 1 through 10. Figure 2.5 shows the fracture geometry for one of the primary induced hydraulic fractures in stage 10 of well MIP 3H. Figure 2.6 shows the cumulative proppant mass versus time (modeled vs measured), Figure 2.7 shows the slurry volume injected versus time (modeled vs measured), and Figure 2.8 shows the surface pressure versus time (modeled vs measured) for stage 10 of well MIP 3H. These figures show a good match between the numerical model and the reported data.

Microseismic data was available for four of the stages modeled during this quarter (stages 7, 8, 9, and 10). Microseismic, well, and hydraulic fracture geometric data were visualized in three dimensions. Figure 2.9, Figure 2.10, Figure 2.11, and Figure 2.12 show side views of calculated hydraulic fracture geometries and measured microseismic events and magnitudes for stage 7, stage 8, stage 9, and stage 10, respectively, for well MIP 3H. Figure 2.13 shows an overview of all four hydraulic fracture geometries, microseismic events, and the entire MIP 3H wellbore. Figure 2.14 shows an orthogonal projection of the four hydraulic fracture geometries, microseismic events, and the nearby section of the MIP 3H wellbore. In Figure 2.8 through Figure 2.14, the measured microseismic events appear to be more prevalent on one side of the MIP 3H wellbore.

Table 2.1. Updated Fracture Geometries – Stage 1 through Stage 10 – MIP 3H

STAGE	Fracture Half-Length (ft)	Fracture Height (ft)	Average Fracture Width (in)
1	704.7	348	0.028462
2	647.6	306.7	0.026497
3	659.7	329.9	0.02899
4	684.7	326.9	0.027285
5	594.6	300.1	0.016779
6	698.7	326.5	0.026389
7	687.1	329	0.027577
8	615.5	355.2	0.021193
9	656.7	335.6	0.029723
10	649.6	332.4	0.03001

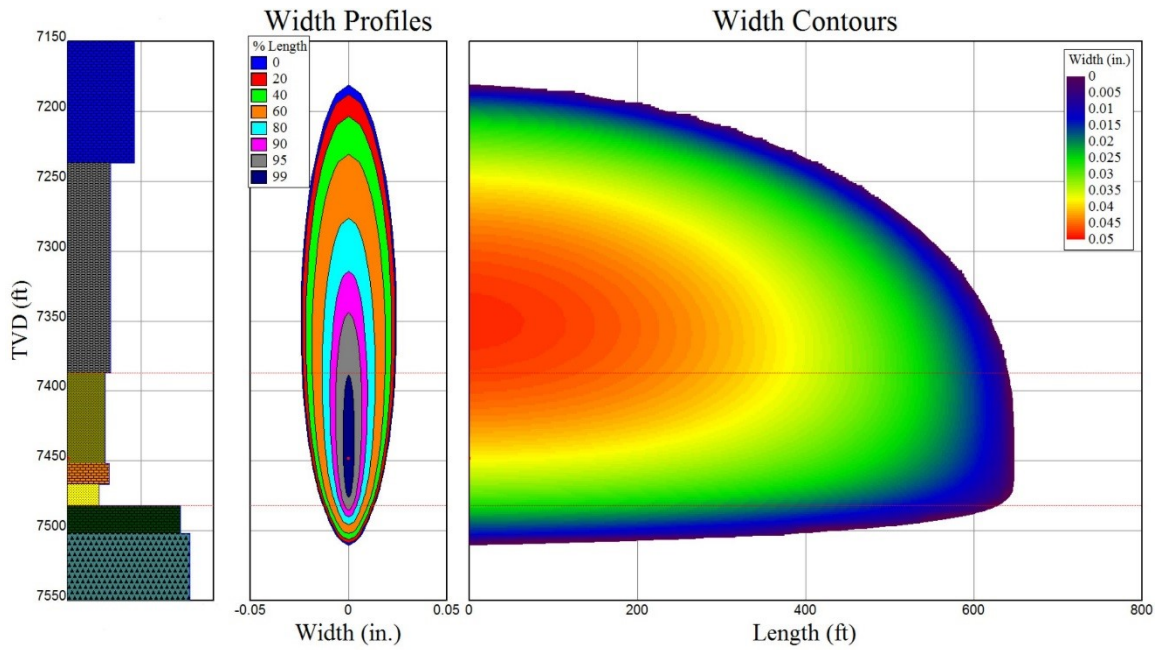


Figure 2.5. Fracture Geometry for Stage 10 - MIP 3H

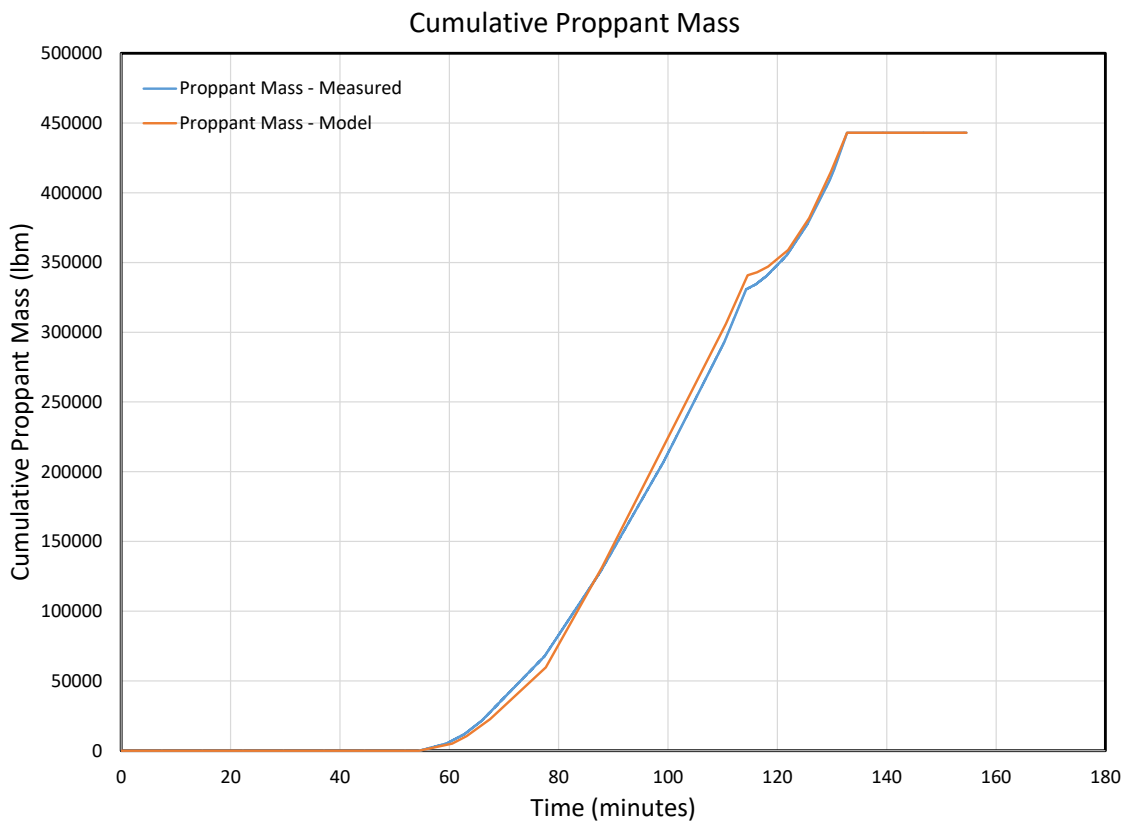


Figure 2.6. Cumulative Proppant Mass for Stage 10 - MIP 3H

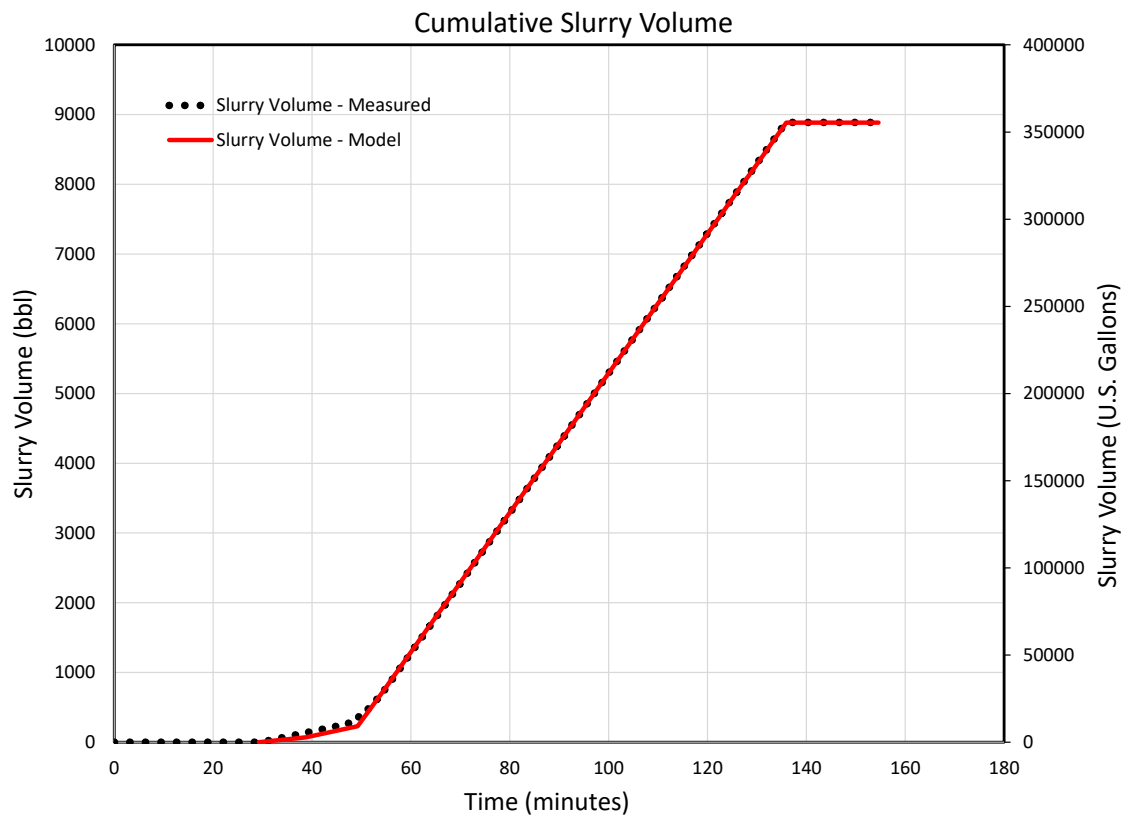


Figure 2.7. Cumulative Slurry Volume for Stage 10 - MIP 3H

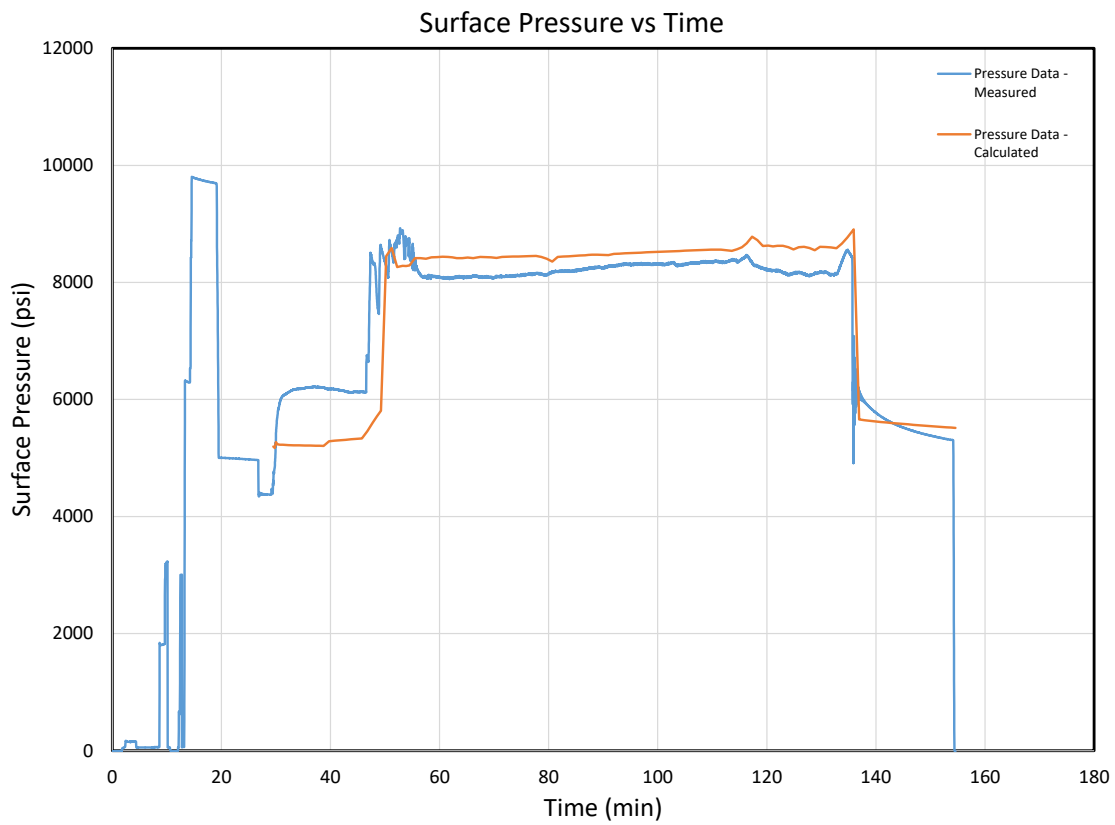


Figure 2.8. Surface Pressure versus Time for Stage 10 - MIP 3H

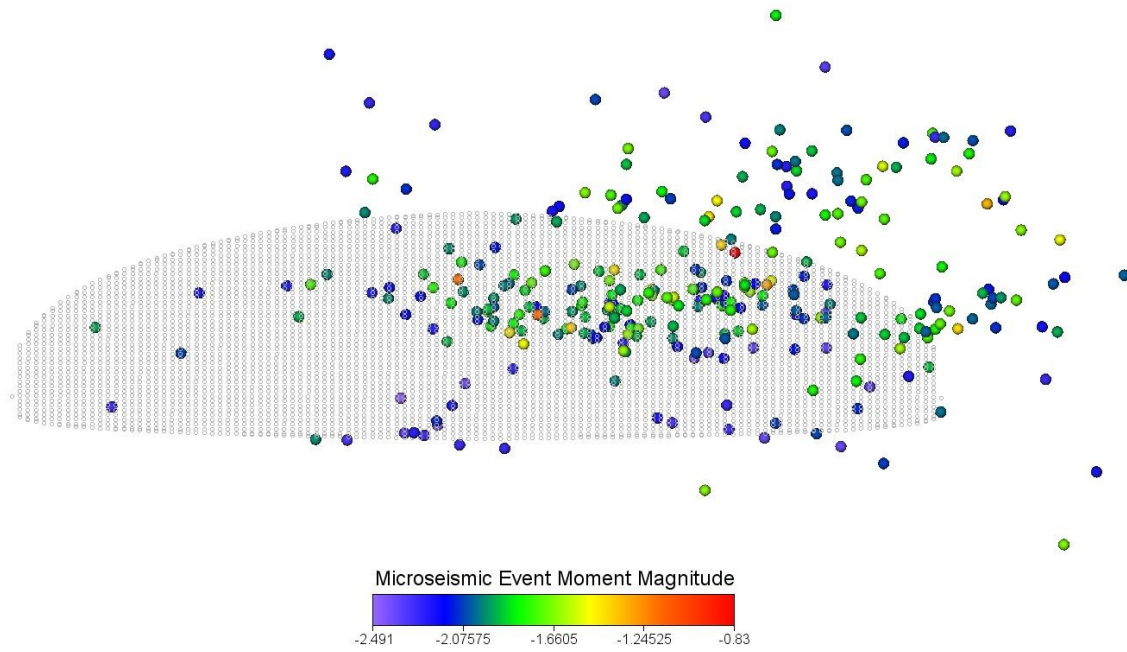


Figure 2.9. Side View of Calculated Hydraulic Fracture and Measured Microseismic Events and Magnitudes for Stage 7 - MIP 3H

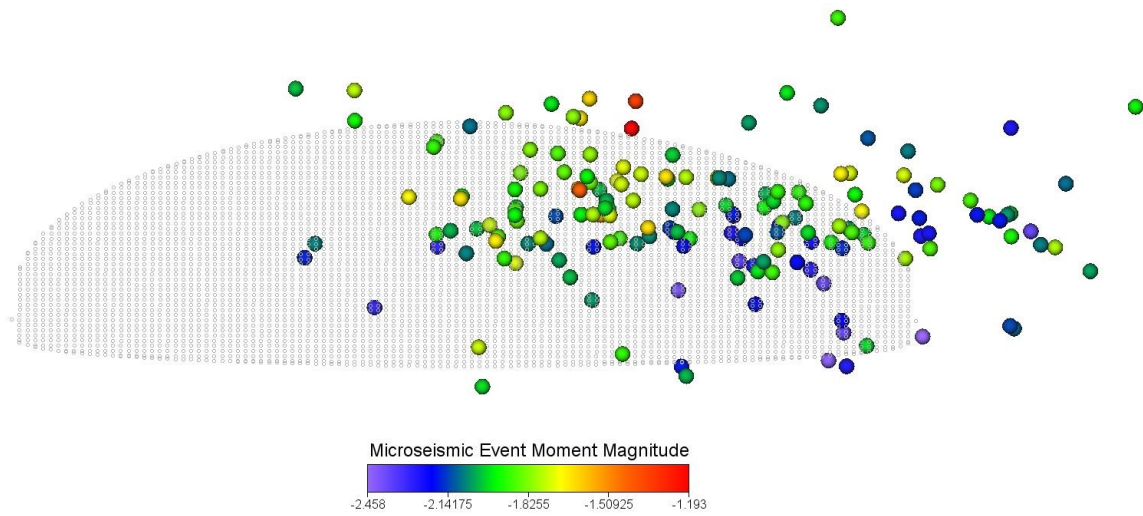


Figure 2.10. Side View of Calculated Hydraulic Fracture and Measured Microseismic Events and Magnitudes for Stage 8 - MIP 3H

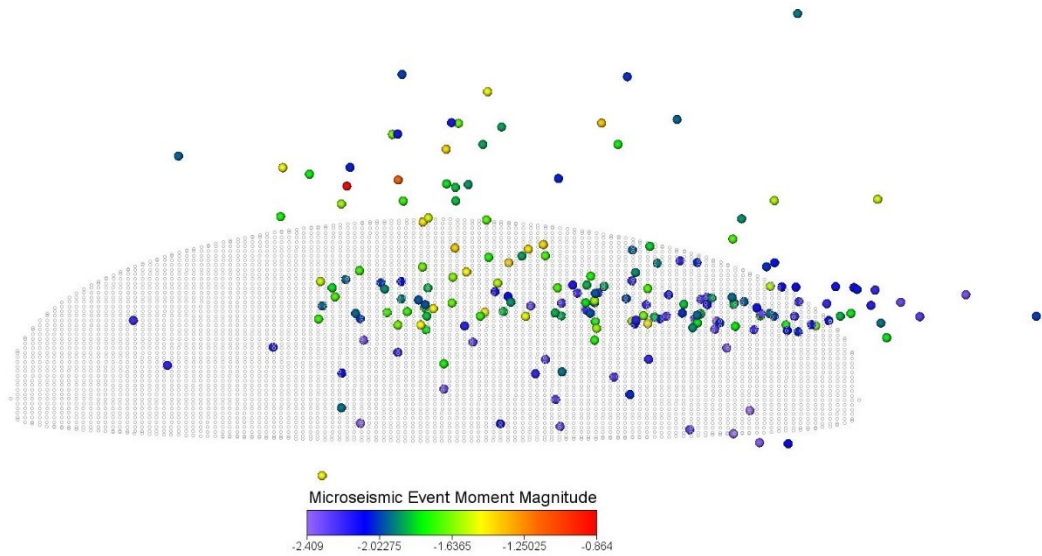


Figure 2.11. Side View of Calculated Hydraulic Fracture and Measured Microseismic Events and Magnitudes for Stage 9 - MIP 3H

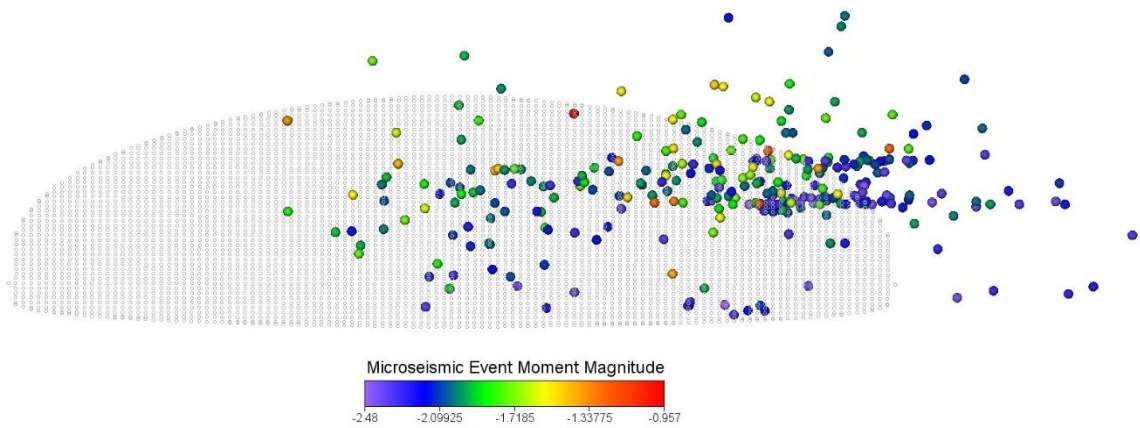


Figure 2.12. Side View of Calculated Hydraulic Fracture and Measured Microseismic Events and Magnitudes for Stage 10 - MIP 3H

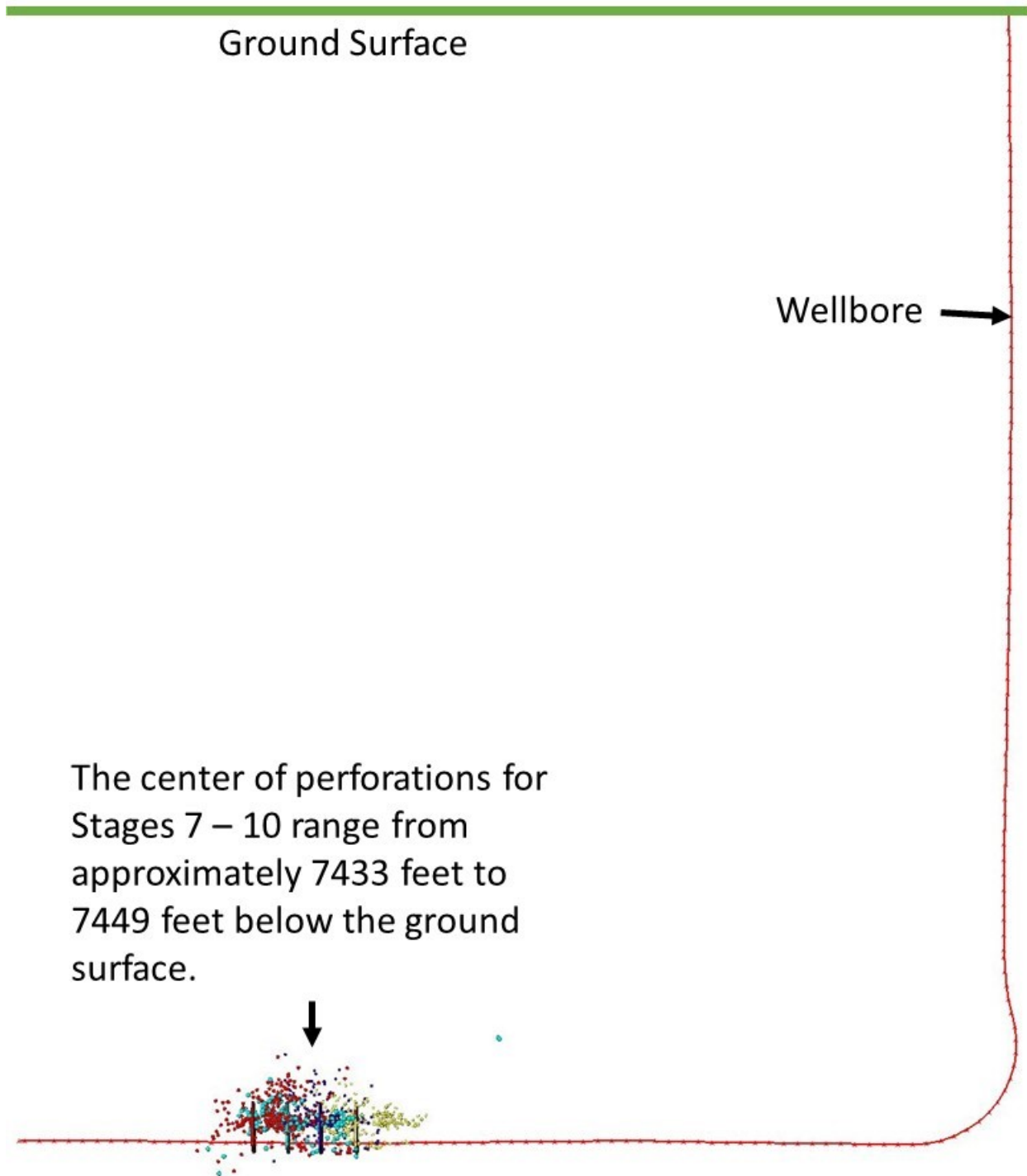


Figure 2.13. Overview of Calculated Hydraulic Fracture Geometries, Measured Microseismic Events, and Entire Wellbore for Stage 7 through Stage 10 - MIP 3H

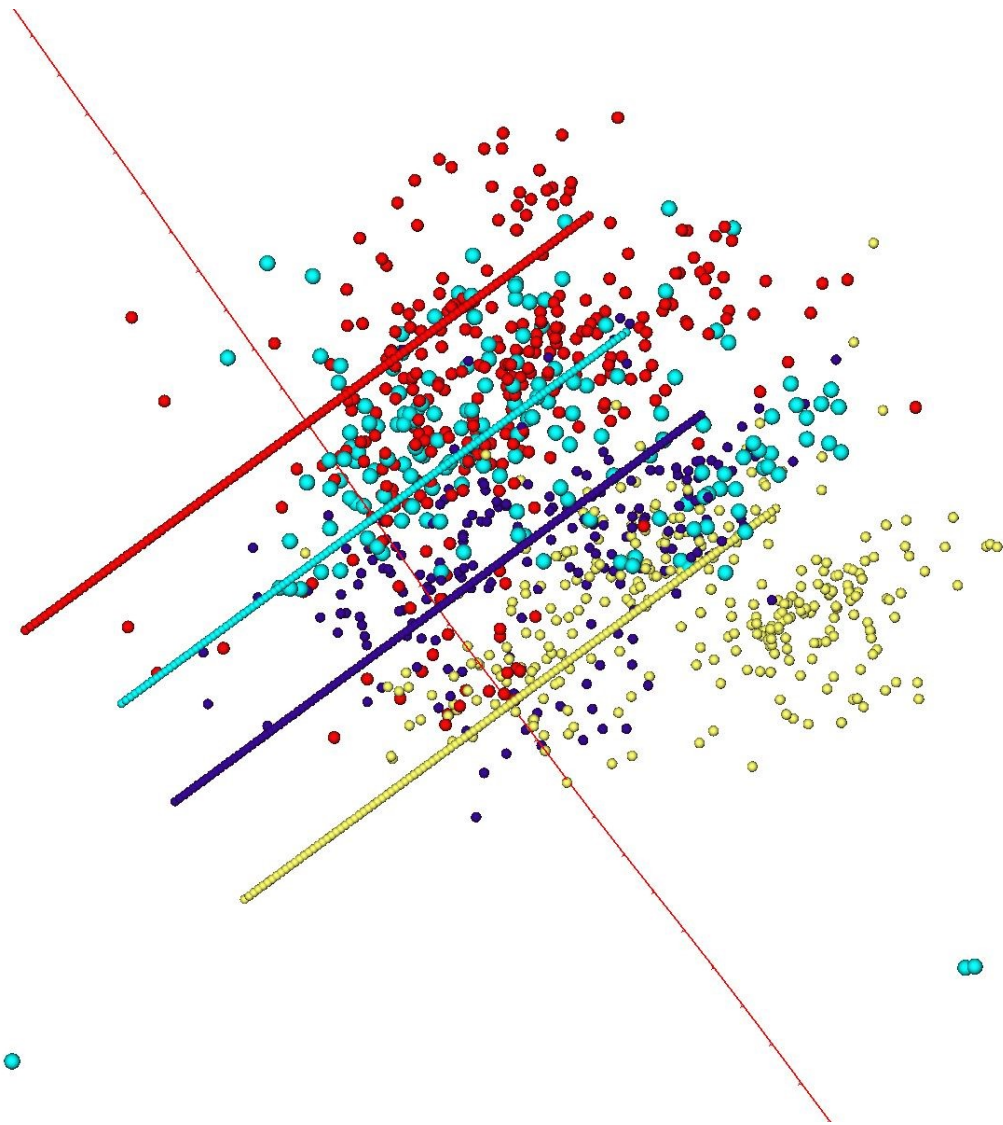


Figure 2.14. Top View of Calculated Hydraulic Fracture Geometries, Measured Microseismic Events, and Nearby Wellbore for Stage 7 through Stage 10 - MIP 3H

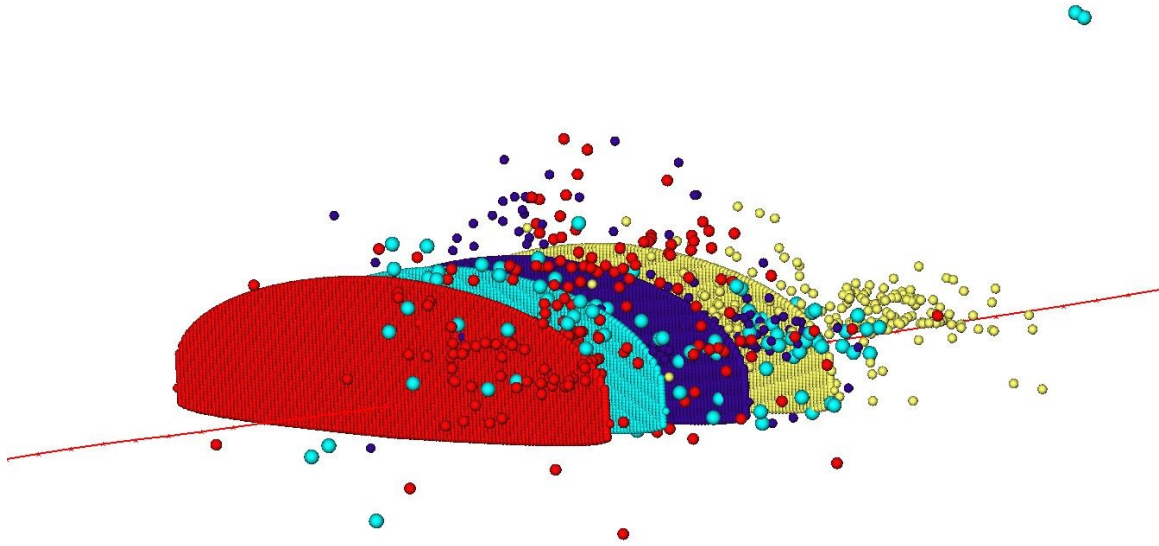


Figure 2.15. Orthogonal View of Calculated Hydraulic Fracture Geometries, Measured Microseismic Events, and Nearby Wellbore for Stage 7 through Stage 10 - MIP 3H

Products

The paper titled *Marcellus Shale model stimulation tests and microseismic response yield insights into mechanical properties and the reservoir DFN* was accepted with moderate revisions. Revisions were completed and submitted.

Submission of an abstract for the 2017 Annual International SEG meeting:

The paper titled “Relationships of $\lambda\rho$, $\mu\rho$, brittleness index, Young’s modulus, Poisson’s ratio and high TOC for the Marcellus Shale, Morgantown, West Virginia” by *Thomas H. Wilson**, *Payam Kavousi*, *Tim Carr*, *West Virginia University*; *B. J. Carney*, *Northeast Natural Energy LLC*; *Natalie Uschner*, *Oluwaseun Magbagbeola* and *Lili Xu*, *Schlumberger*, was submitted to SEG for consideration.

This paper was accepted for publication and presentation at the Society of Exploration Geophysics annual international meeting and exposition this fall in Houston. Paper was attached to the last quarterly report.

Plan for Next Quarter

Geophysical

Attend SEG conference in late September to present results noted in paper noted above.

With efforts to date exceeding expectations, future efforts will be limited to support role for team members Payam Kavousi (post-doc working with fiber data) and Yixuan Zhu (Ph. D. student working with microseismic).

Geomechanical

The modeling study will be continued with the use of an assumed natural discrete fracture network which was presented in this report to investigate other stimulation stages at well MIP 3H through the use of available information on the hydraulic fracturing field parameters (fluid volumes, pumping rate, proppant schedule, and geophysical data). Results presented in this report show that the computed fracture heights are higher than those which were computed without discrete fracture networks and are closer to the height of the microseismic data cloud. The analysis of microseismic data will be continued and a comparison of fracture geometries will be made with available microseismic data.

Topic 3 – Deep Subsurface Rock, Fluids, & Gas

Approach

The main focus of the subsurface team led by Sharma this quarter was to analyze core, fluid and gas samples collected from the MSEEL site. Members of Sharma's lab group (Dr. Warriar and Mr. Wilson) and Dr. Hanson from Mouser's lab group continue to coordinate and supervise all sample collection. Samples were also distributed to the research team at OSU and NETL for analysis under different sub-tasks. Several talks and presentations were given at local and regional conferences /universities.

Results & Discussion

Progress on Sidewall Core, Vertical Core & Cutting Analysis

The side wall cores are curated at OSU and WVU. Based on the geophysical logs eight samples were selected from different lithologies (i.e. zones that were expected to present maximum biogeochemical variations). Samples were homogenized and distributed among different PI's, and are currently being processed for the biomarker, isotope analysis, elemental analysis, porosity/pore structure, and noble gas analysis.

For whole core analysis, cores were taken from 1-foot intervals through the 111 feet of whole vertical core. Samples were ground, homogenized, and distributed to different groups at WVU, OSU, and NETL for different analysis.

In Sharma's Lab Ph.D. Student Rawlings Akondi just published a methods paper (*frontiers in microbiology*) examining how lipid biomarker extraction methods from deep subsurface shale samples can be optimized. These

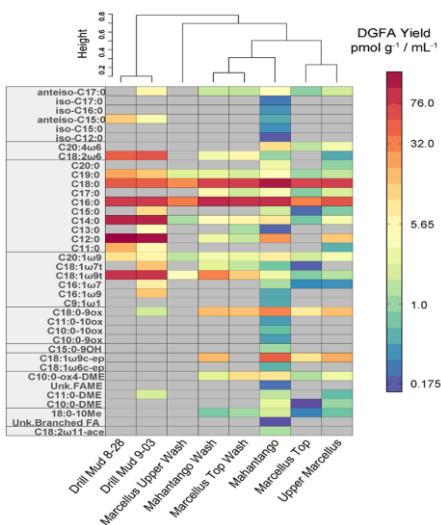


Figure 3.1. Heat map showing absolute abundances of DGFA biomarkers in the drill muds, core washes, and various core formations. Samples sorted based on dendrogram groupings calculated from Bray-Curtis dissimilarities.

methodological improvements would be very useful for recovering a diverse lipid pool from pristine deep shale cores. Rawlings is also working on a paper that is focused on examining the lipid fatty acids (DGFAs) indicative of remnant biomass in the samples collected from the MIP 3H well (Figure 3.1). He will send out the manuscript to co-authors in the last weeks of summer. Rawlings has received compound specific isotope results from the University of California at Davies, and together with the major element geochemical analysis of the MSEEL, he will be working on another manuscript in the fall.

Another Ph.D. Student of Sharma, Vikas Agrawal, analyzed extracted kerogen from Mahantango and different zones of Marcellus shale at the MSEEL site using direct analytical techniques: XPS (X-ray photoelectron

spectroscopy), ATR-FTIR (Attenuated total reflection-Fourier transform infrared spectroscopy), ¹³C solid state NMR (Nuclear magnetic resonance), and Raman spectroscopy. These techniques were used to characterize molecular structure of kerogen and to understand HC generative potential of different aliphatic and aromatic carbon chains.

Preliminary direct kerogen analysis at the MSEEL site suggests that majority of carbon chains present in kerogen are mainly aromatic (Figure 3.2). This indicates that most of the aliphatic chains have been already thermally degraded at this maturity stage. Aliphatic biomarkers of pristine sidewall cores showed that contribution of organic matter from marine input increased from Marcellus Top to Lower Marcellus. However, kerogen structural parameters determined by direct kerogen analysis are very similar throughout Marcellus at the MSEEL site. This indicates thermal maturity has the dominant control on kerogen structure.

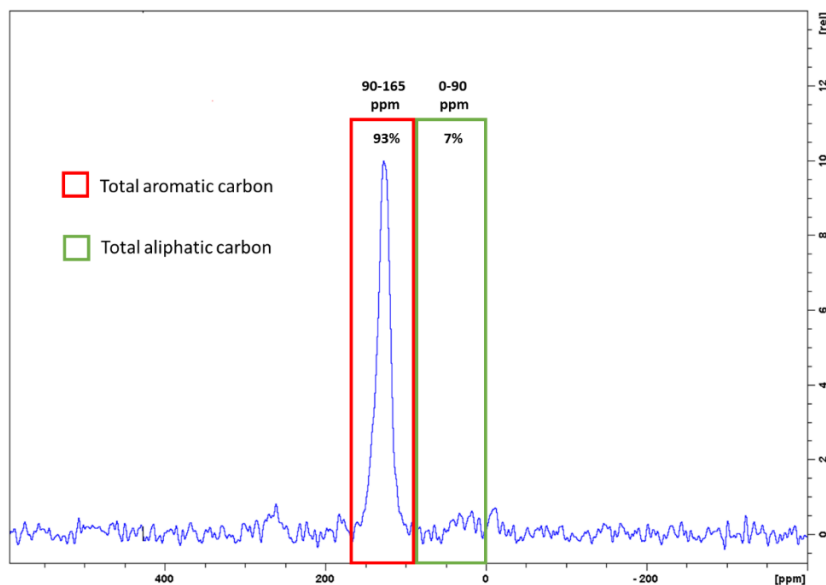


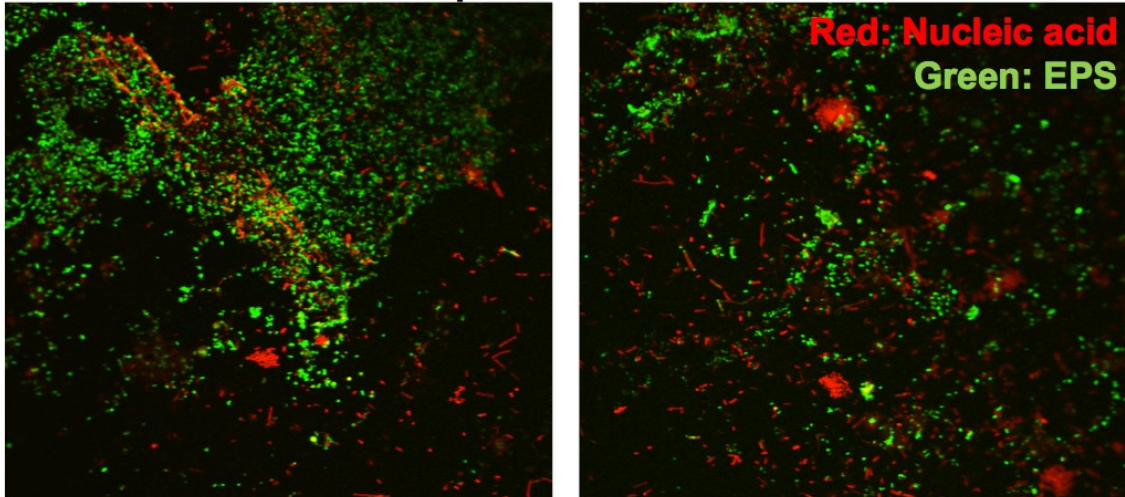
Figure 3.2. Multiple CP (cross polarization) ¹³C NMR spectra of kerogen sample from lower Marcellus shale formation. Peak area distribution shows kerogen contains 7% aliphatic carbon chains and 93% aromatic carbon chains.

In **Cole’s Lab**, QEMSCAN mineral maps (1x1mm) were acquired for polished sections of MT 11, middle Marcellus, and MT 16, Upper Marcellus. Small core chips of MT 11 (Middle Marcellus) were shared with the Wilkins lab for bacterial culturing on natural bedding plane surfaces. Guided simple critical point drying specimen preparation for SEM imaging.

Wilkin’s Lab did some experiments with *Halanaerobium* biofilm forming potential. Prior proteomic investigations have suggested that under pressurized conditions characteristic of the deep shale, dominant *Halanaerobium* strains are more prone to surface attachment and biofilm formation. Recently, the team incubated this microorganism in the presence of quartz chips under atmospheric and high-pressure conditions. Quartz surfaces were subsequently imaged using epifluorescence microscopy and stains specific for both extracellular polymeric substances (EPS; ‘slime’) and biomass itself (Figure 3.3). Despite less biomass growing under high-pressure conditions, four-times more cells were measured on quartz chips incubated at high pressure, relative to atmospheric pressure conditions: EPS ‘slime’, indicating that biomass in the deep subsurface may preferentially attach to shale surfaces within newly formed fracture networks.

Additionally, thicker layers of EPS slime were also measured under pressurized conditions. Ongoing work is assessing the extent of biofilm formation on shale surfaces. Additional experiments are also investigating central metabolic changes to this microorganism when grown at pressure. Preliminary results suggest that hydrogen production is lessened under pressurized conditions, with greater production of organic acids to account for the disposal of reducing equivalents.

Atmospheric Pressure



5k psi pressure

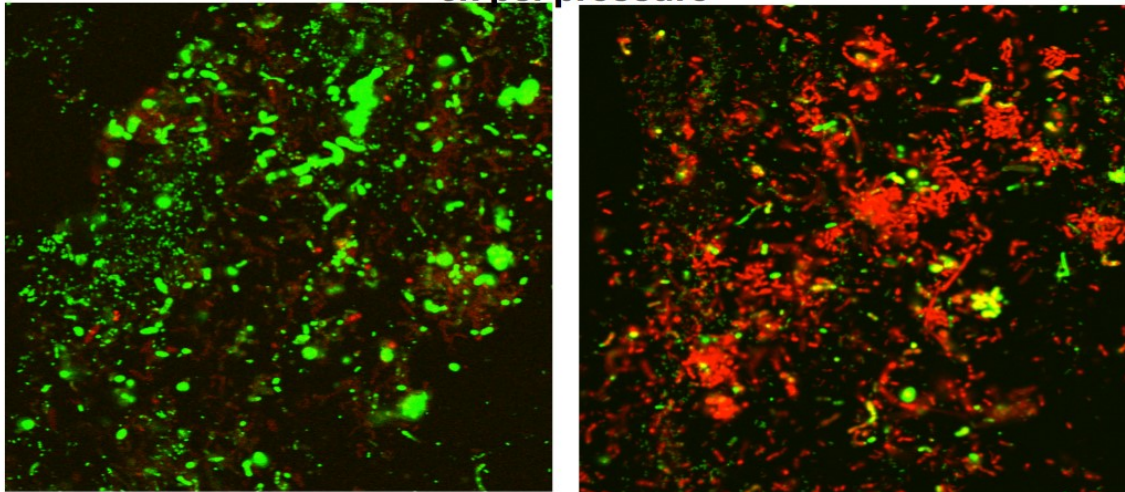


Figure 3.3. Red stain targets DNA and so indicates that extent of cell attachment to quartz surfaces. Green stains target sugars in EPS material. Images show greater cell attachment (red) to surfaces under 5000 psi pressure and thicker production of EPS (solid green regions).

Wrighton's Lab received the sequencing data from pristine sidewall core sample. All sequencing data were quality checked, filtered and assembled. Comparison of core material samples to control samples did not show any clear genomic signatures for indigenous microbial life in the MIP3H well.

In **Mouser's Lab**, Andrea completed the analysis of intact lipids using LC-MS/MS in Germany from May to June. In addition to adding seven dates to the temporal assessment of microbial lipids in flowback and produced water (bringing the total number of dates to 12 from Dec. 2015 to April 2017), Andrea finalized the analysis of the sidewall cores using a highly sensitive

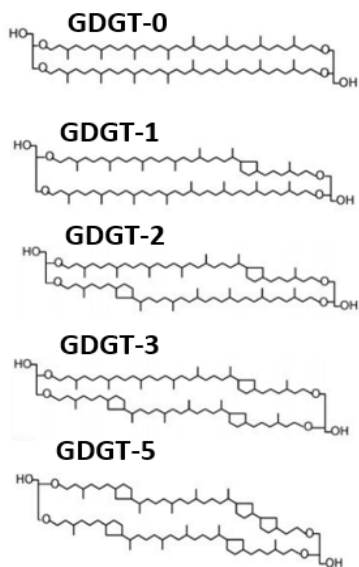


Figure 3.4. Glycerol dialkyl glycerol tetraether (GDGT) core lipids detected in Tully Limestone. Evidence from deep sub-seafloor studies suggests the more number of rings in the core lipid structure results in greater stability at higher temperatures and greater resistance to acid.

the microbial cells from the high salinity as conceptualized in Figure 3.5. The manuscript in preparation is expected to wrap up in early fall.

Lastly, Andrea will be returning to MSEEL in mid-August to collect produced water from MIP 3H and 5H; geochemistry will be analyzed and all samples distributed to the MSEEL team at OSU.

Progress on Produced Fluid and Gas Analysis

Produced water samples were collected in 5-gallon carboys every 6 weeks. The samples were transported, filtered and processed in Sharma Laboratory at WVU. All water samples were collected in different containers using different methods, preservatives, etc. specified for different kinds of analysis. All PI's at OSU and NETL and provided their detailed sampling instructions. Dr. Warrier, Wilson from WVU, and Hanson from OSU were primarily in charge of sample collection and distribution among different PI's at WVU, OSU, and NETL. The collected fluids are currently being processed for biomass, reactive chemistry, organic acids, and noble gas and stable isotope analysis at different institutes.

Sharma lab continues to analyze O, H, and C isotopic composition of produced fluids collected from 3H and 5H. The carbon isotope composition of the dissolved inorganic carbon in the

method specifically designed to target archaeal lipid structures. In doing so, the quantification of archaeal core lipids detected in the Tully Limestone was enhanced (structures of identified lipids are shown in Figure 3.4).

Significant progress has been made in identifying and quantifying the intact bacterial lipids in the MIP 3H fluids; several different structural classes of intact lipids were identified in the MIP 3H fluids. The lipid composition data provide novel insight into the structures (i.e. the microbial membranes) that provide the first line of defense to protect microbes in the shale well system, giving clues as to how the membranes may contribute to microbial persistence. For

example, the data indicates the viable microbial biomass has a high density of negative charges on the surface of the membrane, which likely helps shield

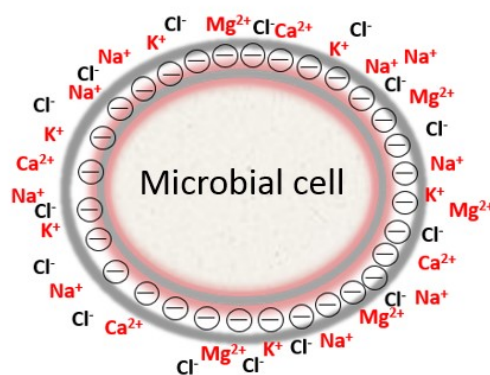


Figure 3.5. Conceptual depiction of how microbial membranes likely contribute to protection from high salinity in produced water. A high density of negative charges on the surface of the membrane may help shield cells from ions and counter the high concentration of cations while increasing the selectivity of ions entering or exiting the cell.

produced water continues to show the enrichment in ^{13}C with $\delta^{13}\text{C}_{\text{DIC}} > +17\text{‰ V-PDB}$. To rule out if the dissolution of carbonates in the reservoir or drilling fluids/mud etc. could contribute to this high ^{13}C signatures, carbonate vein samples in and around the landing zone and all possible sources of carbon put downhole were analyzed for their ^{13}C signatures. The cement and silica sand had no detectable carbon in them. The drilling mud and frac water had $\delta^{13}\text{C}$ values of -1.8 and -7.8‰ V-PDB respectively. Therefore, the high $\delta^{13}\text{C}_{\text{DIC}}$ signatures in produced water are possibly due to the microbial utilization of lighter carbon (^{12}C) by methanogenic bacteria in the reservoir. This indicates that introduction of C containing nutrients like guar, methanol, methylamines, etc. could stimulate certain methanogen species in the reservoir to produce biogenic methane in the reservoir. Wrighton's group is currently analyzing the genomic data on these samples to understand the dominant microbes in the reservoirs.

The $\delta^{18}\text{O}$ and δD analysis have been completed on all samples to date. Both 3H and 5H plot similar trends, showing an 18O shift to more enriched values from the Local Meteoric Water Line indicative of high-temperature exchange within the formation. The molecular and isotopic composition of CH_4 and CO_2 of produced gas sampled concurrently with produced water is underway to constrain methanogenic pathways.

Wrighton's Lab received metagenomic sequencing data for seven produced water samples from wells MIP3H and MIP5H. Metabolite data from produced fluid samples (paired with metagenomic samples) were received from the Pacific Northwest National Laboratory, Environmental Molecular Sciences Laboratory. The data is currently being analyzed to incorporate into a manuscript and is in preparation for submission this fall on comparative genomes of the dominant methane-producing microorganism (*Methanohalophilus* species) in the MSEEL wells.

Another manuscript about the dominant bacterium in the MSEEL wells, a *Halanaerobium* species, is in preparation for submission this fall. This manuscript explores the viral controls on *Halanaerobium* populations in hydraulically fractured shales.

Analysis of fluid samples from the MIP 3H and 5H wells continues in **Cole Lab**. Several of the samples are being re-analyzed in duplicate at different dilutions to determine the reproducibility of the analysis.

Darrah's Lab continued time-series analysis of fluid samples collected monthly from the MIP 3H and 5H wells. Some initial graphs and results from He and Ne analysis are shown in Figure 3.5.

$^4\text{He}/^{20}\text{Ne}$ vs. time

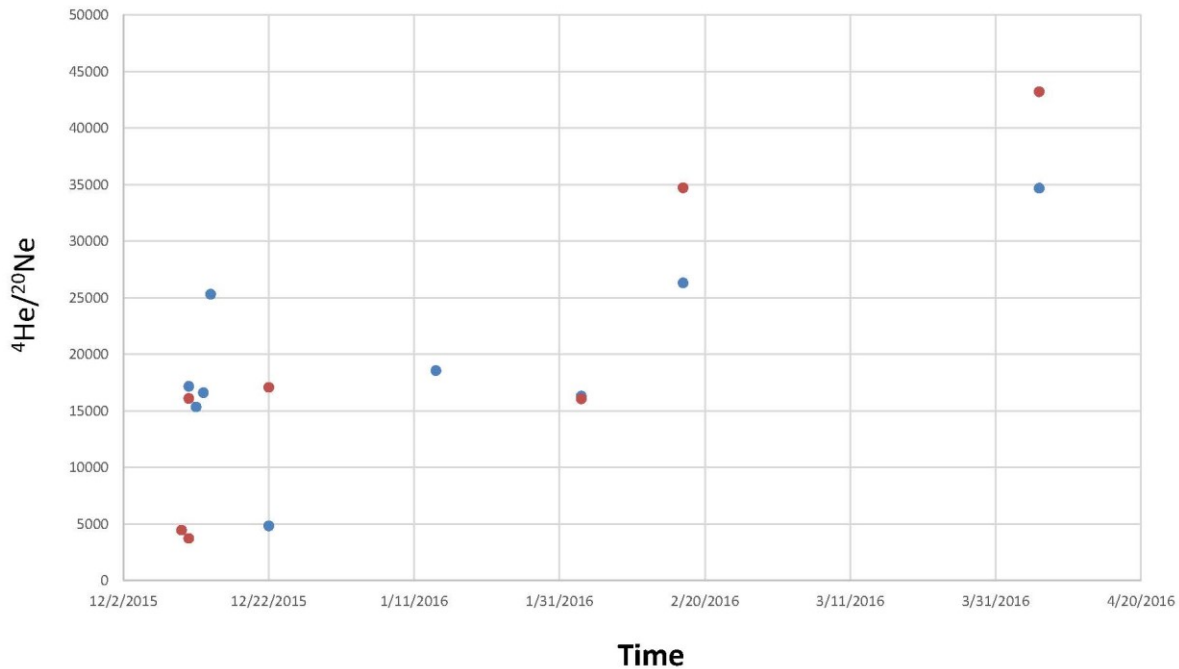


Figure 3.5. Time-series analyses of $^4\text{He}/^{20}\text{Ne}$ versus sampling time frame. Shows a progression changing gas composition. ^4He is derived predominantly from thermogenic natural gas, while ^{20}Ne is derived exclusively from air-saturated water present in the Earth's crust. Here, the figure shows an example of the changing proportion of thermogenic gas and water-derived noble gases following the onset of production. This trend continues through the most recent data, although a rollover has started to occur indicating that most water has been removed from the Marcellus Formation shortly after the onset of production.

Products

1. Akondi R, Trexler R, Pfiffner SM, Mouser PJ, Sharma S 2017. Modified Lipid Extraction Method for Deep Subsurface Shale. *Frontiers in Microbiology*
<https://doi.org/10.3389/fmicb.2017.01408>
2. Sharma S 2017. Shale Research at Marcellus Shale Energy and Environment laboratory. 23rd Annual CNSF Exhibition, May 16, Rayburn House, Washington DC.

Plan for Next Quarter

Several manuscripts in preparation is expected to wrap up in early fall. Andrea will be returning to MSEEL in mid-August to collect produced water from MIP 3H and 5H; geochemistry will be analyzed and all samples distributed to the MSEEL team at OSU.

Topic 4 – Environmental Monitoring – Surface Water & Sludge

Approach

The Marcellus Shale Energy and Environment Laboratory (MSEEL) is the first comprehensive field study coupling same site environmental baseline, completion and production monitoring with environmental outcomes. One year into the post completion part of the program, the water and solid waste component of MSEEL has systematically sampled flowback and produced water volumes, hydraulic fracturing fluid, flowback, produced water, drilling muds, drill cuttings and characterized their inorganic, organic and radio chemistries. In addition, surface water in the nearby Monongahela River was monitored upstream and downstream of the MSEEL drill pad. Toxicity testing per EPA method 1311 (TCLP) was conducted on drill cuttings in both the vertical and horizontal (Marcellus) sections to evaluate their toxicity potential.

Figure 4.1 shows the general processes of fluid flow during hydraulic fracturing and gas production. During well completion, hydraulic fracturing fluids are injected into the target formation and the injected fluids return to surface via the well bore as flowback. Produced water is the fluid returned via the well bore along with gas during production phase. The distinction between flowback and produced water is not well defined and these two terms are sometimes used interchangeably in the vernacular.

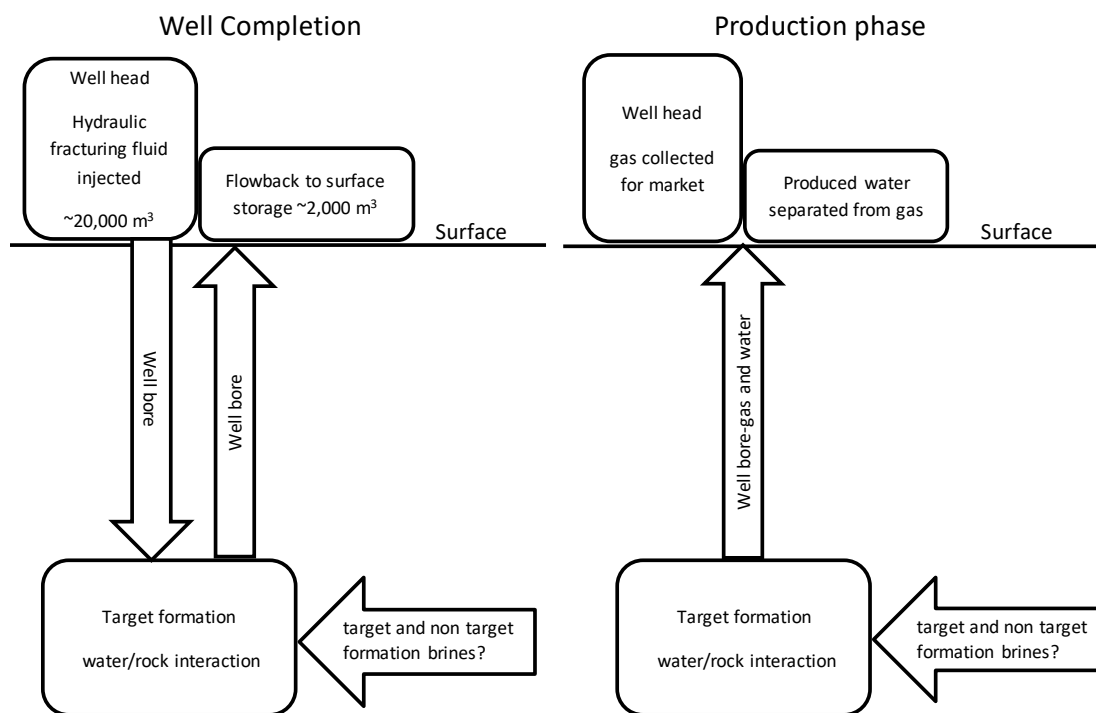


Figure 4.1. Flow of fluids during the well completion (hydraulic fracturing) and production phases of well operations. (From Ziemkiewicz et al., 2014).

The following information for this topic has been rolled over from the previous quarter. Note that Lessons Learned for this topic are highlighted at the beginning of the report.

Previous findings

The MSEEL wells used green completion strategy including a synthetic based drilling fluid (Bio-Base 365). All drill cutting samples fell below TCLP thresholds for organic and inorganic components indicating that they are non-hazardous per the Resource Conservation and Recovery Act. Maximum specific isotopic activity in drill cuttings was recorded for 40 K which was 28.32 pCi/g. Gross alpha accounted for the highest reading at 60 pCi/g. The maximum combined radium isotope values was 10.85 pCi/g. These radioactivity levels are within the background range for the region.

The composition of the hydraulic fracturing (HF) fluids in both wells was similar to the makeup water which was drawn from the Monongahela River. Its chemistry was typical of Monongahela River water. This is true of inorganics, organics and radio chemicals. Organic surrogate recoveries were in the range of 90 to 104% indicating good quality control at the analytical laboratory. There was no evidence that Monongahela River quality was influenced by well development, completion or production at the MSEEL site.

Produced water is severely contaminated indicating care in handling. Concentrations of all parameters increased through the flowback/produced water cycle. 226+228 Ra reached 20,000 pCi/L at post completion day 251 indicating an important trend that will be carefully assessed in ongoing monitoring.

Methods

Table 4.1 summarizes the produced water sampling schedule for the quarter. Makeup water was pumped from the Monongahela River and mixed with the hydraulic fracturing fluids. Produced water samples were taken at the upstream end of each well’s separator.

Table 4.1. Sampling schedule for the quarter.

	Freshwater		Aqueous/Solids: drilling/completion/production					total aqueous	total solids	Sampling Dates	Sampling Notes
	Mon River	Ground water	HF fluid makeup	HF fluids	flowback/produced	drilling fluids	drilling cuttings/muds				
Flowback @ 57 weeks - 3H					1			1		1/13/2017	one sample 3H
Flowback @ 57 weeks - 5H					0			0		-	no sample (5H not producing)
Flowback @ 215* Weeks - 4H					1			1		1/13/2017	one sample 4H
Flowback @ 215* Weeks - 6H					1			1		1/13/2017	one sample 6H
Flowback @ 61 weeks - 3H					1			1		2/14/2017	one sample 3H
Flowback @ 61 weeks - 5H					2			2		2/14/2017	two samples 5H
Flowback @ 219 weeks - 4H					1			1		2/14/2017	one sample 4H
Flowback @ 219 weeks - 6H					1			1		2/14/2017	one sample 6H
Flowback @ 65 weeks - 3H					1			1		3/13/2017	one sample 3H
Flowback @ 65 weeks - 5H					1			1		3/17/2017	one sample 5H
Flowback @ 223 weeks 4H					1			1		3/17/2017	one sample 4H
Flowback @ 223 weeks 6H					1			1		3/17/2017	one sample 6H

Analytical parameters are listed in tables 4.2 and 4.3.

Table 4.2. Aqueous analytical parameters

Aqueous chemistry parameters - HF fluids and PW					
Inorganics				Organics	Radionuclides
	Anions	Cations*			
	pH	Br	Ag		
TDS	Cl	Al	Mn	Toluene	β
TSS	SO ₄	As	Na	Ethylbenzene	⁴⁰ K
Conductance	sulfides	Ba	Ni	Total xylene	²²⁶ Ra
Alkalinity	nitrate	Ca	Pb	m,p-xylene	²²⁸ Ra
Bicarbonate	nitrite	Cr	Se	o-xylene	
Carbonate		Fe	Sr	MBAS	
TP		K	Zn	O&G	

* total and dissolved

Table 4.3. Analytical parameters drill cuttings and mud.

Solids chemistry parameters - Cuttings & Muds								
Inorganics			Organics	Radionuclides	TCLPs			
	Anions	Cations*						
alkalinity**	Br	Ag	Mg	Propane	α	Arsenic	1,4-Dichlorobenzene	Methyl ethyl ketone
conductance	Cl	Al	Mn	DRO	β	Barium	1,2-Dichloroethane	Nitrobenzene
pH	SO ₄	As	Na	GRO	⁴⁰ K	Benzene	1,1-Dichloroethylene	Pentachlorophenol
bicarbonate**	sulfide	Ba	Ni	Ethylbenzene	²²⁶ Ra	Cadmium	2,4-Dinitrotoluene	Pyridine
carbonate**	nitrate	Ca	Pb	m,p-xylene	²²⁸ Ra	Carbon tetrachloride	Endrin	Selenium
TP	nitrite	Cr	Se	o-xylene		Chlordane	Heptachlor	Silver
		Fe	Sr	Styrene		Chlorobenzene	Heptachlor epoxide	Tetrachloroethene
		K	Zn	Toluene		Chloroform	Hexachlorobenzene	Toxaphene
				Total xylenes		Chromium	Hexachlorobutadiene	Trichloroethylene
				TOC		o-Cresol	Hexachloroethane	2,4,5-Trichlorophenol
				COD		m-Cresol	Lead	2,4,6-Trichlorophenol
				O&G		p-Cresol	Lindane	2,4,5-TP (Silvex)
						Cresol	Mercury	Vinyl chloride
						2,4-D	Methoxychlor	

Results & Discussion

Produced water volume trends in wells MIP 3,5H and MIP 4,6H

NNE's water production logs were used to estimate produced water volumes. While water production rates were similar in the first two months post completion, cumulative water production rates soon diverged yielding very different curves for each well (Figure 4.2). Over this cycle produced water averaged about 6 bbl/day. It is noted that the older wells (4H, 6H) were shut in between 12 Dec 15 and 17 Oct 16, an interval of 315 days.

The proportion of hydrofrac fluid returned as produced water, even after 1844 days (5 years) was only 12% at MIP 4H and 7.5% at MIP 6H (Table 4.4). The reason for the variation among wells

both respect to cumulative and proportional produced water returns remains an unanswered question.

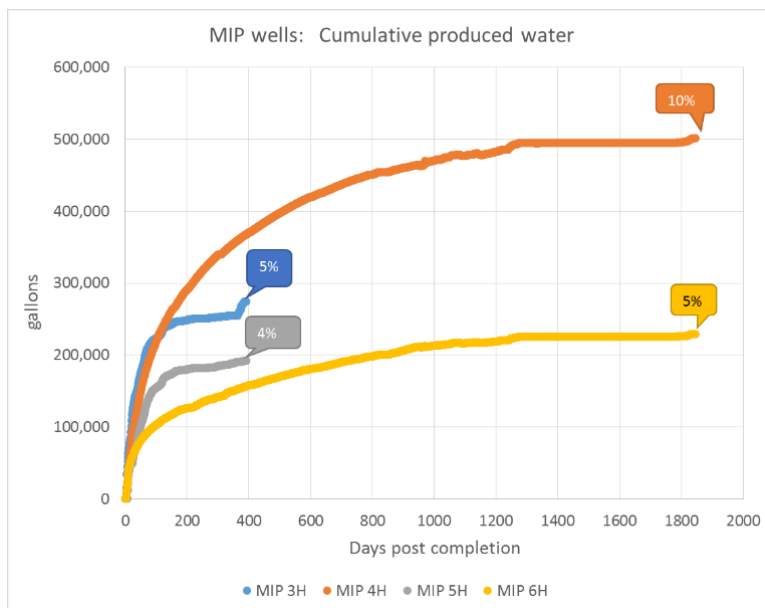


Figure 4.2. Cumulative water production at the four MSEEL wells. The estimated proportion of produced water to HF fluids are shown in the callouts.

Table 2.4. Produced water volumes relative to injected HF fluid for each MSEEL well.

	days post	cumulative produced water		HF injected
	completion	gal	% injected	gal
MIP 3H	392	274,102	2.6%	10,404,198
MIP 5H	392	192,134	2.0%	9,687,888
MIP 4H	1844	501,396	12.0%	4,160,982
MIP 6H	1844	229,183	7.5%	3,042,396

Trends in produced water chemistry

Major ions

While makeup water was characterized by low TDS (total dissolved solids) and a dominance of calcium and sulfate ions, produced water from initial flowback is essentially a sodium/calcium chloride water (Figure 4.3). Other than slight increases in the proportion of barium and strontium, the ionic composition of produced changed very little through 314 days post completion.

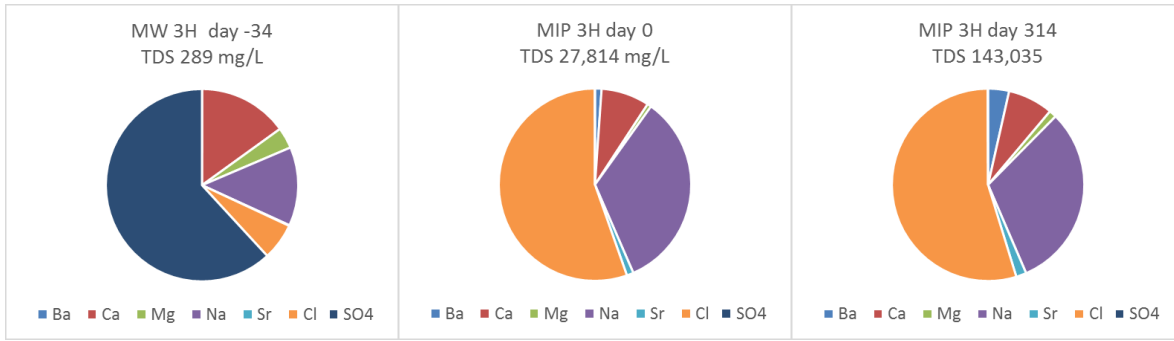


Figure 4.3. Changes in major ion concentrations in produced water from well MIP 3H. From left to right the charts represent makeup water from the Monongahela River, produced water on the first day of flowback and produced water on the 314th day post completion.

In fact, after 1858 days ionic composition remained nearly identical to the initial produced water (Figure 4.4).

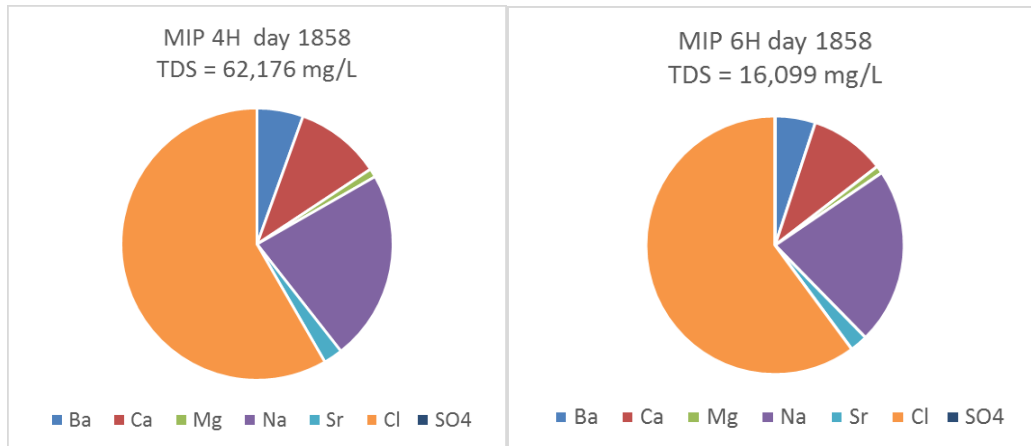


Figure 4.4. Major ion composition of wells MIP 4H and 6H 1858 days after completion.

While TDS increased rapidly over the initial 90 days post completion, it appears to have levelled off between 100,000 and 150,000 mg/L (Figure 4.5). The older 4H and 6H wells offer insight into the longer term TDS trend. Those wells only came back on line during this quarter after a shut in period of 315 days and those results vary but they are much lower than the current values for wells MIP 3H and 5H.

Thus far, results are only available for two sampling dates: 16 Nov 16 and 14 Dec 16. TDS varied between 62,176 mg/L at well MIP 4H and 16,099 mg/L at MIP 6H. If these trends continue, it would suggest that available salt is being exhausted.

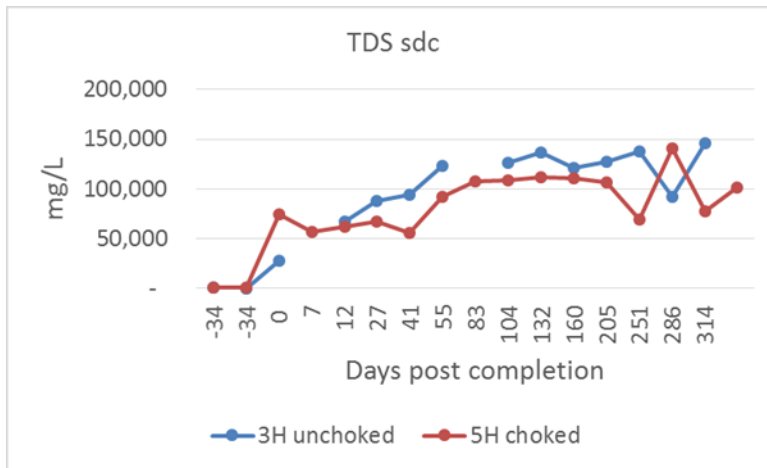


Figure 4.5. Changes in produced water TDS sdc (sum of dissolved constituents) through the first 340 days post Acompletion.

Water soluble organics

The water soluble aromatic compounds in produced water: benzene, toluene, ethylbenzene and xylene were never high. With one exception at post completion day 321, benzene has remained below 30 µg/L (Figure 4.6). This seems to be a characteristic of dry gas geologic units. After five years, benzene has declined below the drinking water standard of 5 µg/L.

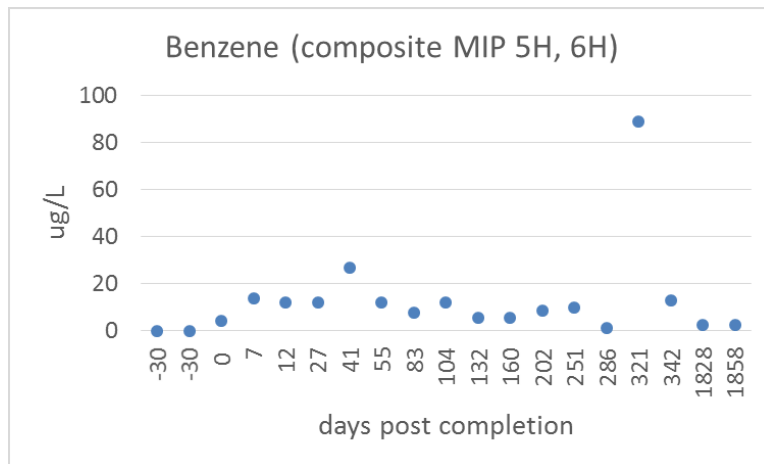


Figure 4.6. Changes in benzene concentration. The figure shows data from well 5H through the first 342 days post completion, followed by results from well 6H.

Radium isotopes

Radioactivity in produced water

Radium concentrations generally increased over the 314 days post completion at wells MIP 3H and 5H. Maximum levels of the radium isotopes reached about 20,000 pCi/L at the unchoked 3H well and about half that amount at 5H.

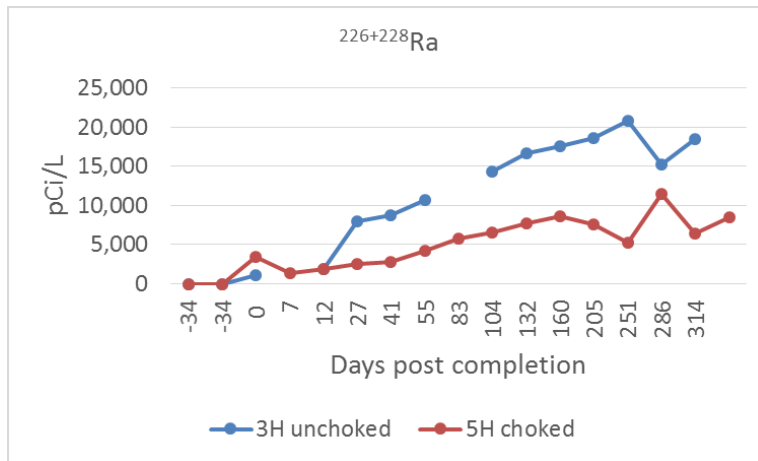


Figure 4.7. The radium isotopes are plotted against days post well completion. Well 5H was choked periodically. It produced less water and lower concentrations of radium.

At the older wells MIP 4H and 6H, all isotope concentrations declined to low levels, often below the MDC (minimum detectable concentration) (Table 4.5). This, like the apparent decline in TDS at the older wells is an interesting result and, if sustained by future sampling, would suggest exhaustion of contaminant reserves within the fracture field.

Table 4.3. Radiochemistry of the older wells 4H and 6H at 1828 (5 years) days post completion.

		16-Nov-16 MIP 4H days post completion: 1828			16-Nov-16 MIP 6H days post completion: 1828		
		act ¹	unc ²	mdc ³	act ¹	unc ²	mdc ³
α	pCi/L	228.0	53.6	27.2	57.7	10.9	1.6
β	pCi/L	48.7	20.1	29.2	7.4	1.6	0.8
²²⁶ Ra	pCi/L	353.3	260.6	309.2	199.3	333.5	390.3
²²⁸ Ra	pCi/L	31.1	31.9	48.6	0.0	20.9	54.6
⁴⁰ K	pCi/L	49.7	95.5	102.7	0.0	21.9	151.4

¹ activity

² +/- uncertainty

³ minimum detectable concentration

Solid waste

The TCLP (toxicity characteristics leaching procedure) or USEPA method 1311 is prescribed under the Resources Conservation and Recovery Act (RCRA) to identify hazardous solid waste. TCLP was applied to thirteen drill cutting samples, twelve from MIP 3H and 5H and one from another well in western Monongalia County. All three wells had been developed using green, synthetic drilling fluid. All samples fell below the TCLP criteria for hazardous waste and would be classified under RCRA subtitle D. This indicates that under Federal and West Virginia solid waste rules, these solid wastes would not be considered hazardous.

Bio-Base 365 drilling fluid (Shrieve Chemical Products, Inc.) had been used at the MSEEL wells and ABS 40 (AES Drilling Fluids Inc.) was used at the other well.

Products

N/A

Plan for Next Quarter

If expanded scope funds are received, the team plans to start work on Tank Bottoms analysis and Precipitate formation, as well as continuing with the current work.

Topic 5 – Environmental Monitoring: Air & Vehicular

Approach

Air

This approach has transitioned to the quantification of methane emissions from typical site operation. The audits will be completed with the use of WVU's Full Flow Sampling System (FFS). Results of the first complete site audit is presented below.

Vehicular

Sampling has been ongoing for estimating the effect of heavy duty diesel traffic such as would be expected from well pad operations.

Results & Discussion

Air

The second Marcellus Shale Energy and Environment Laboratory (MSEEL) site audit was completed on April 10, 2017. The goal of this assessment was to measure the emissions of methane (CH₄) emitted from all onsite equipment. These measurements included an assessment of the enclosed gas production units (EGPUs), produced water tank, dehydration units, wellheads, and stack emissions from the EGPUs were conducted to estimate the carbon dioxide (CO₂), carbon monoxide (CO), and oxides of nitrogen (NO_x) emissions, and CH₄ emissions from these sources.

All equipment on site was checked for potential leaks using an Eagle 2 from RKI Instruments. This instrument uses a pump with a sample rate of 2 SCFH. The lower range can detect methane between 0 and 50,000 ppm with an accuracy of ±25ppm and a resolution of 5ppm (RKI Instruments, 2000). Leak checking involved scanning components of the dehydrators, burners, and attached piping to determine location of leaks. Detected leaks were marked and quantified with the WVU Full Flow Sampling (FFS) system. The FFS system consists of a hose that feeds an explosive-proof blower, which exhausts the collected leak sample and excess dilution air through a mass airflow sensor (MAF) and sample probe. The setup of the system is shown in Figure 5.1.



Figure 5.1. WVU's Full Flow Sampling System

To accurately quantify methane, CO₂, and water vapor (H₂O) the system utilizes laser spectroscopy in the form of an Ultraportable Greenhouse Gas Analyzer (UGGA) from Los Gatos Research (LGR). The UGGA uses off-axis integrated cavity output spectroscopy (OA-ICOS). The operation principle for the UGGA is described in literature. The UGGA records measurements of methane, CO₂, and H₂O. The precision (1 σ , 5 sec / 100 sec) for the three species are as follows: methane (2 ppb / 0.6 ppb), CO₂ (300 ppb / 100 ppb), and H₂O (200 ppm / 60 ppm) (Los Gatos Research, 2016).

EGPU Stack Emissions Rate

Only one stack on site could be sampled. The EGPU stack sampled was designated stack #1. The second stack was stack #2. The EGPUs are rated at 750M BTYU/hr and produced by Exterran. The burners and other connected components evaluated for leaks are shown in Figure 5.2.



Figure 5.2. Natural Gas Burners and Other On-site Equipment

At the time of the audit both EGPUs were operating, however, stack emissions were only able to be taken from stack #1. Estimation of an emission rate was performed by measuring the stack gas flow rate and concentration. The gas flow rate was determined by using an S-type pitot tube, which

was calibrated against a NIST traceable laminar flow element (LFE). The calibration is shown in Figure 5.3.

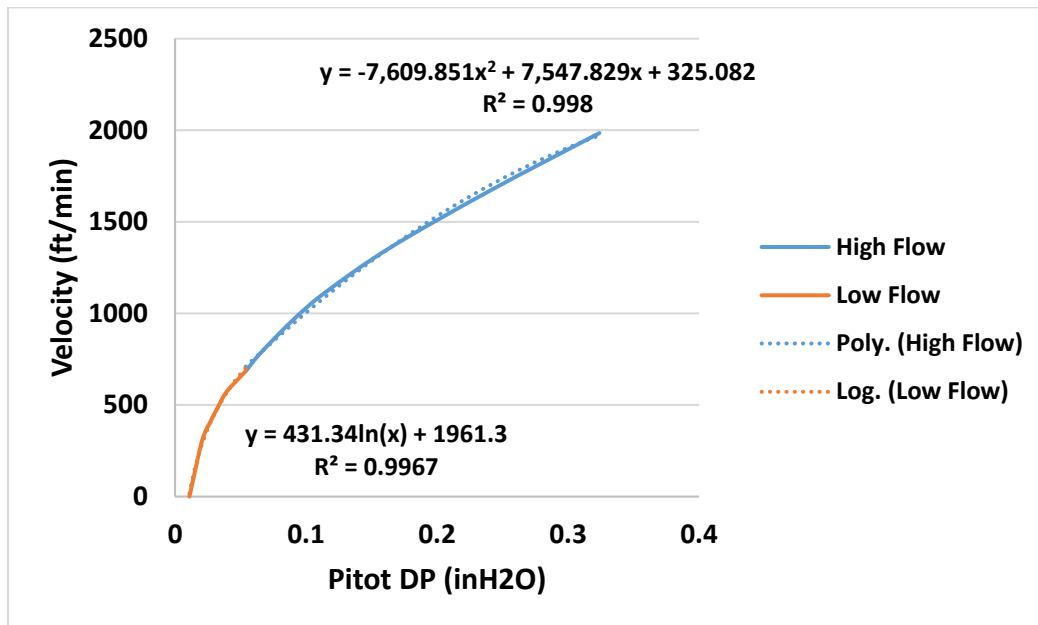


Figure 5.3. S-Type Pitot Tube Calibration for Low and High Range Differential Pressures

The use of an S-type pitot tube allowed for a determination of the average stack velocity. Stack geometry then allowed for an estimated flow rate in cubic feet per minute. The temperature of the stack flow was measured using a standard K-type thermocouple during sampling of velocity and emissions. A sample was collected from the stack using a pump and probe and was captured in a sealed Teflon bag. Bag samples were later evaluated using a MKS Multigas™ 2030 FTIR Continuous Gas Analyzer for concentration measurements on a dry basis (MKS Instruments, 2007). This allowed for determination of up to 20 different gas species including CH₄, CO₂, CO, and NO_x.

Methane fluxes were measured from all four wellheads on site. Leak rates were also measured from two different leaks identified on one of the dehydration units, designated Dehy #1. Methane loss rates from the enclosures of the EGPUs were also measured and were considered separately from the leaks. Emissions from the produced water tank were measured from the open “thief” hatch at the top of the tank. The natural gas thermoelectric power generator previously used for power generation on-site was not actively producing emissions. A diesel generator was being used which was not there during the previous audit. Background CH₄ concentration on site was determined to be 2.04 parts per million (ppm). The average methane lost from each wellhead is presented in Table 5.1. It can be seen from this table that the methane losses from MIP 3H are much larger than those from the other wells. This was due to a nearly continuous venting of pneumatic device attached to the wellhead.

Table 5.1. Methane Loss Rate from Wellheads

Component	CH ₄ Concentration above Background	CH ₄ Loss Rate	CH ₄ Loss Rate
	ppm	g/hr	kg/yr
MIP 3H	599.49	134.36	1177.00
MIP 5H	0.20	0.04	0.36
MIP 4H	22.21	4.99	43.68
MIP 6H	0.17	0.04	0.32
Total		139.43	1221.36

The methane losses from inside of the EGPU housing, shown “opened” in Figure 5.2, and the produced water tank were evaluated separately from the leaks since these emissions may be a product of system design and are represented as methane losses. The results from the vents of the Exterran EGPUs and the water tank are shown in Table 5.2. The table shows an extremely high concentration of methane loss from the produced water tank. The hatch on the tank was open during the site evaluation. This hatch is meant to be kept shut to limit the amount of volatile organic compounds emitted from the tank.

Table 5.2. Methane Losses from EGPUs and Produced Water Tank

Component	CH ₄ Concentration above Background	CH ₄ Loss Rate	CH ₄ Loss Rate
	ppm	g/hr	kg/yr
Tank	17,373.67	3,731.40	32,687.06
Burner #1	147.19	30.34	265.80
Burner #2	197.67	39.55	346.43
Total		3,801.29	33,299.28

Only two major leaks were identified during this audit, both coming from dehydration unit #1. The leak rates are shown in Table 5.3. Pictures of the leak locations are found in Appendix 5A.

Table 5.3. Methane Losses from On-site Leaks

Component	CH ₄ Concentration above Background	CH ₄ Loss Rate	CH ₄ Loss Rate
	ppm	g/hr	kg/yr
Leak 1 on Dehy #1	145.60	30.07	263.40
Leak 2 on Dehy #1	645.93	133.03	1165.37
Total		163.10	1428.76

Emissions from the stacks of the Exterran units were also evaluated but contained minimal CH₄. The levels were below those of the local background, however, the stacks were evaluated for carbon dioxide (CO₂), carbon monoxide (CO), oxides of nitrogen (NO_x), ethane (C₂H₆), formaldehyde (CH₂O) and acetylene (C₂H₂). Only one stack could be evaluated at the time of the audit because the other did not contain a viable sample port. The stack velocity was measured with a pitot tube and the average velocity was determined to be 272.97 ft/min giving a flow rate of 214 standard cubic feet per minute (SCFM). Stack emissions were estimated by multiplying the concentration measured from a bag sample by the estimated flow rate are shown in Table 5.4.

Table 5.4. Emissions from Exterran Stacks

Emission	Concentration	Loss Rate	Loss Rate
	ppm	g/hr	kg/yr
CO ₂	41,765.74	8,448.23	74,006.51
CO	64.70	8.33	72.96
NO _x	10.01	1.58	13.83
C ₂ H ₆	2.26	0.31	2.73
CH ₂ O	0.19	0.03	0.23
C ₂ H ₂	1.70	0.20	1.78

Second Audit Summary

Methane losses were measured from a variety of site components including: wellheads, produced water tank, enclosed gas production unit housings, stacks, and leaking devices. The total estimated methane emissions are shown in Table 5.5. The Exterran stack emissions were also analyzed and showed emissions of CO₂, CO, NO_x, C₂H₆, CH₂O and C₂H₂. These emissions contribute to the total greenhouse gas (GHG) emissions of the site and can be considered in estimating a total GHG emission rate on a CO₂-equivalent basis. The total CO₂-equivalent GHG emissions from methane

and CO₂ are shown in Table 5.6 assuming both Exterran units operated continuously with similar emissions profiles and that all emissions were continuous throughout the year. However, it is known that while auditing the EGPU's were operated intermittently. A CO₂-equivalent of 25 was used for methane (Environmental Protection Agency, 2016). The current GHG Reporting Program Standard is 25,000 metric tons of CO₂-equivalent per year. If the Audit 2 results were used, the MSEEL site only produces 1,047 metric tons of CO₂-equivalent per year, well below the reporting threshold.

Table 5.5. Total Methane Losses

Source	Loss Rate	Loss Rate	Percent of Total Emissions
	g/hr	kg/yr	%
Wellheads	139.43	1221.36	3.40%
Water Tank	3,731.40	32,687.06	90.93%
Burner Housing	69.89	612.22	1.70%
Leaks	163.10	1,428.76	3.97%
Total	4,103.81	35,949.40	100%

Table 5.6. CO₂-Equivalent Greenhouse Gas Emissions (Both EGPUs Running)

Emission	CO ₂ -Equivalent	
	kg/yr	%
CO₂	148,013.03	14.14%
CH₄	898,735.05	85.86%
Total	1,046,748.08	100%

Throughput Normalized Emissions

Reporting of the natural gas throughput from the site lags data collection by one quarter but the methane data from Audit 1 have been normalized by the daily production rate during the day of the audit to present methane as a percentage of throughput. Table 5.7 presents the total natural gas production and methane emissions and the relative percentage of just 0.006%.

Table 5.7. Production and total methane emissions and the relative loss percentage for Audit 1, November 16, 2016.

	Daily Production (MCF)	Daily CH₄ Emissions (MCF)
MIP 3H	1,822.6	0.41
MIP 5H	2,778.4	
MIP 4H	1,576.2	
MIP 6H	1,047.1	
Total	7,224.3	0.006%

Trends From Quarterly Audits

Now that multiple site audits have been completed, the team will start to examine the trends in site emissions. Table 5.8 presents the component level emissions and their relative change from Q1 to Q2. Site wide methane emissions increased by a factor of 5.13 from Audit 1 to Audit 2. These increases were dominated by the additional emissions from MIP 3H and the open thief hatch of the produced water tank (increased by factors of 163 and 43, respectively). While throughput has not yet been presented for this quarter, if the throughput is the same last during the last Audit, this would increase the relative loss as a percentage of throughput to 0.034%.

Table 5.8. Comparison of Audit 1 and Audit 2 Results.

Component	CH₄ Loss Rate (g/hr)		Relative Change
	Nov-16	Apr-17	%
Wellheads	0.85	139.43	16,304
EGPU Housing	356.50	69.89	-80
Produced Water Tank	83.98	3,731.40	4,343
Leaks	227.40	163.10	-28
NG Burner	0.82	N/A	N/A
Total	669.55	4,103.81	513

Conclusions

Measuring the methane emissions from new unconventional well pads of is interest in order for the EPA and other agencies to develop accurate emissions factors for new equipment and technologies. A recent study by Rella, et al., used mobile flux techniques to estimate the total site emissions from well pads in the Barnett Shale region of Texas (Rella, Tsai, Botkin, Crosson, & Steele, 2015). In total, 193 sites were audited and 122 were found to have measureable emissions rates. Other sites may or may not have had emissions rates due to the measurement technique. Of the sites that had measureable fluxes, the geometric mean was 0.63 ± 0.09 kg/hr with an arithmetic mean of 1.74 ± 0.35 kg/hr. During Audit 1, the MSEEL site emissions were 0.67 kg/hr, which is nearly identical to the geometric mean of Rella et al, and only about 1/3rd of their arithmetic mean. However, during Audit 2 the methane emissions rate was 4.1 kg/hr or about 2.4 times the arithmetic mean of Rella et al. Therefore, the MSEEL continuous methane emissions seem similar to expected emissions from well pads but tended to increase during the second audit. The team will work further with NNE to examine if the increases in methane emissions are expected or if the produced water tank and well MIP 3H had malfunctioning components.

References

Environmental Protection Agency. (2016, July 29). For GHG Reporters. Retrieved October 2016, from Greenhouse Gas Reporting Program (GHGRP): <https://www.epa.gov/ghgreporting/ghg-reporters>

Los Gatos Research. (2016). Ultraportable Greenhouse Gas Analyzer (CH₄, CO₂, H₂O). Retrieved September 19, 2016, from Ultraportable Analyzers: <http://www.lgrinc.com/analyzers/ultraportable-greenhouse-gas-analyzer/>

MKS Instruments. (2007, March 15). Multigas 2030 FTIR Continuous Gas Analyzer. Retrieved October 16, 2015, from <http://www.mksinst.com/docs/UR/onlinemultigas2030ds.pdf>

Rella, C. W., Tsai, T. R., Botkin, C. G., Crosson, E. R., & Steele, D. (2015, March 25). Measuring Emissions from Oil and Natural Gas Well Pads Using the Mobile Flux Plane Technique. *Environmental Science and Technology*, 49(7), 4742-4748. doi:10.1021/acs.est.5b00099

RKI Instruments. (2000, August 16). Eagle 2 Model. Retrieved September 19, 2016, from One to Six Gas Portable Monitor: <http://www.rkiinstruments.com/pdf/eagle2.pdf>

Appendix 5A: Photos of Leak Locations



Leak #1



Leak #2

Vehicular

Figure 5.4 shows the most recent data from a valley running perpendicular to a roadway with substantial heavy-duty diesel traffic. Figure 5.5 shows the area on a map. Previous studies have suggested that the ultrafine (<0.1 μm) diesel particulate will agglomerate rapidly and not be detectable beyond 300 m of the roadway (Zhang, K.M., et al. 2005. Atmospheric Environment, 39(22), pp.4155-4166). However, such studies had not considered the effect of topography in their results. With a perpendicular valley it can be seen (Figure 5.4) that a concentration buildup can occur, most likely due to temperature inversions both at sunrise and sunset as well as during other meteorological conditions.

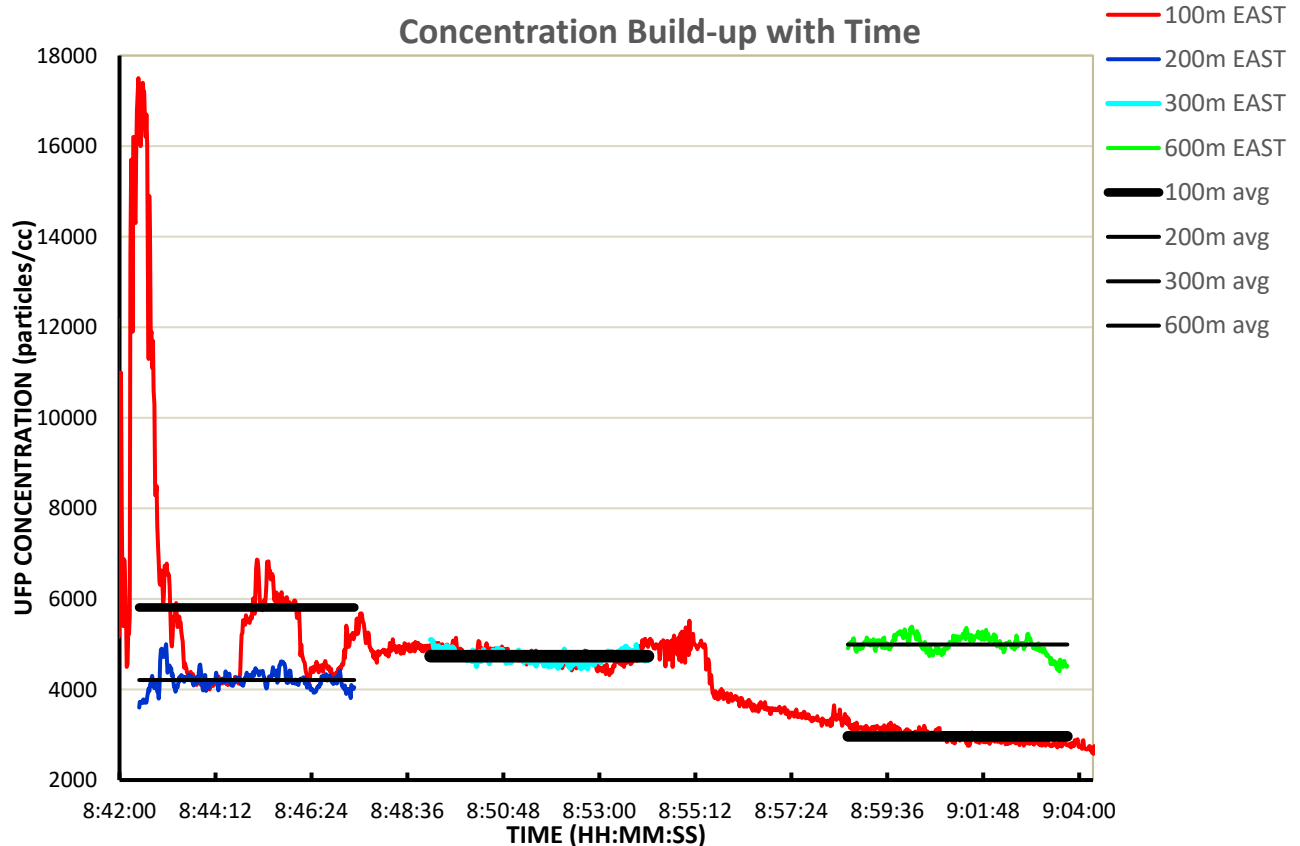


Figure 5.4. Measurements taken using a PTrack (TSI, inc.) condensation particle counter (CPC) that determines the particle number concentration of Ultrafine particles on a real time basis. One CPC was placed within 100 m of the north-south running interstate (red line), on an east-west axis in the valley situated perpendicular to the interstate. One other CPC was moved along the perpendicular axis to sample at three different locations farther away from the interstate. The thin black line is the average concentration at each of those three locations for the sampling time period. The concentration can be seen to be increasing with time and with distance away from the interstate, both observations seemingly contradictory to the findings of the Zhang et al. work.



Figure 5.5. Sampling area with Kirby Rd. used as the perpendicular sampling axis to Interstate 79 just north of Morgantown, WV (north is top of map).

While it is not unexpected that emissions, in this case from diesel traffic, will be confined and expected to increase due to valley inversions, the Zhang et al. paper leads one to expect that they will not remain ultrafine due to agglomeration. The paper has been widely cited as the reason for not considering ultrafine emissions as a far ranging source of exposure. In this case, the emissions appear to reach at least twice the previously supposed maximum distance (300 m vs 600 m).

Products

N/A

Plan for Next Quarter

Air

- Conduct Audit #3
- Possible assess if the retainment pond is a source of methane emissions through collaboration with OSU.
- Seek additional funding to expand the scope of work regarding methane emissions.

Vehicular

Data analysis and sampling is ongoing to better refine the estimates of potential exposure zones along truck routes for well pad deliveries to determine if that is a competing or possibly sole reason for the health effects seen in areas of unconventional gas drilling operations.

Topic 6 – Water Treatment

Approach

The team continued to focus on softening produced water as the first treatment step. A two-chamber electrochemical cell separated by Nafion 115 (cation exchange membrane) was used to identify the optimal condition high pH catholyte generation.

Results & Discussion

Using 0.5 M sodium chloride (NaCl) as a feed solution in batch mode, under cell current of 300 mA and operation time of 15 minutes; catholyte with pH around 12 can be generated in cathode. For this condition, characterization of electrochemical cell was done mainly to find resistance within the cell and membrane. Softening of PW was carried out in batch mode with six different volume ratios of catholyte: PW (0.1:1, 0.5:1, 1:1, 2:1, 5:1, and 10:1). For practical field applications, the ratio of 2:1 was determined as an optimal ratio for softening. With this ratio, calcium and magnesium removal were 65% and 80%, respectively.

Scanning electron microscope (SEM) micrographs and energy dispersive X-ray spectroscopy (EDS) analysis on the chemical sludge from the softening treatment confirmed precipitation of multi-valent cations (e.g., Ca, Mg, Fe) as well as sodium chloride.

Products

N/A

Plan for Next Quarter

Future work include developing a continuous softening process for produced water treatment. Metal and organics removal will be measured to characterize the continuous softening treatment and to optimize the treatment process.

Topic 7 – Database Development

Approach

Other than continued data uploading and quality control, including well production and pressure data, no activity.

Results & Discussion

N/A

Products

N/A

Plan for Next Quarter

N/A

Topic 8 – Economic and Societal

A Deliverable for this topic is attached as an appendix. RRI Report “MSEEL Project Context: State of the Region (2001-2014)” is attached, and can be downloaded from

<http://rri.wvu.edu/resource-documents/>

As reports are completed, they will be indicated here. **Other work in this task is complete and will not be updated in future reports.**

Cost Status

Year 1

Start: 10/01/2014 End:

09/30/2017

Baseline Reporting Quarter

	Q1 (12/31/14)	Q2 (3/30/15)	Q3 (6/30/15)	Q4 (9/30/15)
<u>Baseline Cost Plan</u>	(From 424A, Sec. D)			
<u>(from SF-424A)</u>				
Federal Share	\$549,000		\$3,549,000	
Non-Federal Share	\$0.00		\$0.00	
Total Planned (Federal and Non-Federal)	\$549,000		\$3,549,000	
Cumulative Baseline Costs				
<u>Actual Incurred Costs</u>				
Federal Share	\$0.00	\$14,760.39	\$237,451.36	\$300,925.66
Non-Federal Share	\$0.00	\$0.00	\$0.00	\$0.00
Total Incurred Costs - Quarterly (Federal and Non-Federal)	\$0.00	\$14,760.39	\$237,451.36	\$300,925.66
Cumulative Incurred Costs	\$0.00	\$14,760.39	\$252,211.75	\$553,137.41
<u>Uncosted</u>				
Federal Share	\$549,000	\$534,239.61	\$3,296,788.25	\$2,995,862.59
Non-Federal Share	\$0.00	\$0.00	\$2,814,930.00	\$2,814,930.00
Total Uncosted - Quarterly (Federal and Non-Federal)	\$549,000	\$534,239.61	\$6,111,718.25	\$5,810,792.59

Start: 10/01/2014 End:
09/30/2017

Baseline Reporting Quarter

	Q5 (12/31/15)	Q6 (3/30/16)	Q7 (6/30/16)	Q8 (9/30/16)
<u>Baseline Cost Plan</u>	(From 424A, Sec. D)			
<u>(from SF-424A)</u>				
Federal Share	\$6,247,367		\$7,297,926	
Non-Federal Share	2,814,930		\$4,342,480	
Total Planned (Federal and Non-Federal)	\$9,062,297	\$9,062,297.00	\$11,640,406	
Cumulative Baseline Costs				
<u>Actual Incurred Costs</u>				
Federal Share	\$577,065.91	\$4,480,939.42	\$845,967.23	\$556,511.68
Non-Federal Share	\$0.00	\$2,189,863.30	\$2,154,120.23	\$0.00
Total Incurred Costs - Quarterly (Federal and Non-Federal)	\$577,065.91	\$6,670,802.72	\$3,000,087.46	\$556,551.68
Cumulative Incurred Costs	\$1,130,203.32	\$7,801,006.04	\$10,637,732.23	\$11,194,243.91
<u>Uncosted</u>				
Federal Share	\$5,117,163.68	\$636,224.26	\$1,004,177.30	\$447,665.62
Non-Federal Share	\$2,814,930.00	\$625,066.70	(\$1,503.53)	(\$1,503.53)
Total Uncosted - Quarterly (Federal and Non-Federal)	\$2,418,796.68	\$1,261,290.96	\$1,002,673.77	\$446,162.09

Start: 10/01/2014 End:
09/30/2017

Baseline Reporting
Quarter

	Q9 (12/31/16)	Q10 (3/30/17)	Q11 (6/30/17)	Q12 (9/30/17)
<u>Baseline Cost Plan</u>	(From 424A, Sec. D)			
<u>(from SF-424A)</u>				
Federal Share				
Non-Federal Share				
Total Planned (Federal and Non-Federal)				
Cumulative Baseline Costs				
<u>Actual Incurred Costs</u>				
Federal Share	\$11,223.71	\$196,266.36	\$120,801.19	
Non-Federal Share	\$0.00	\$0.00	\$0.00	
Total Incurred Costs - Quarterly (Federal and Non-Federal)	\$113,223.71	\$196,266.36	\$120,801.19	
Cumulative Incurred Costs	\$11,307,467.62	\$11,503,733.98	\$11,624,535.17	
<u>Uncosted</u>				
Federal Share	\$334,441.91	\$138,175.55	\$17,374.36	
Non-Federal Share	(\$1,503.53)	(\$1,503.53)	(\$1,503.53)	
Total Uncosted - Quarterly (Federal and Non-Federal)	\$332,938.38	\$136,672.02	\$15,870.83	

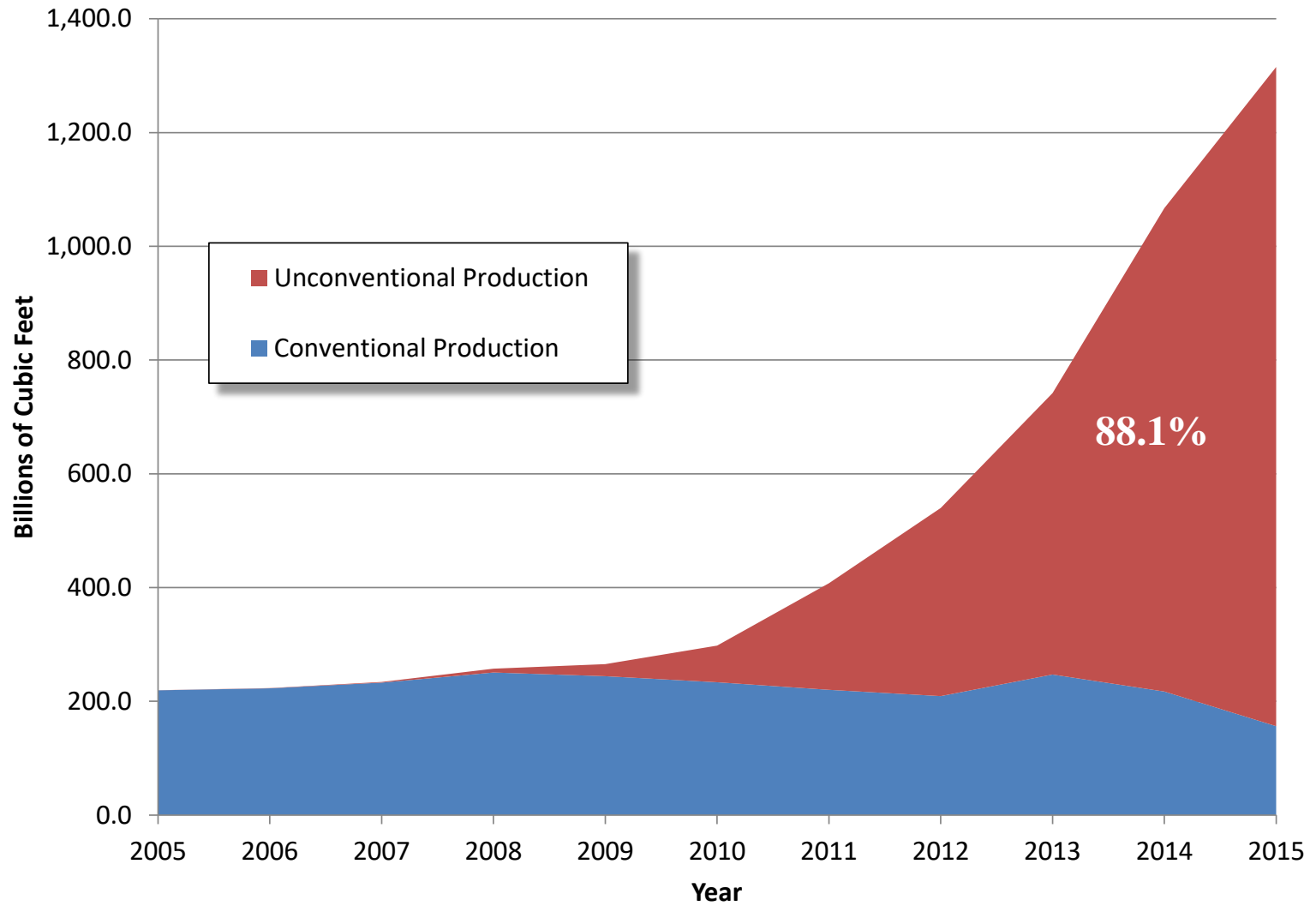
Appendix 1 – NACBM Slides, 4/12/2017

MARCELLUS SHALE ENERGY AND ENVIRONMENT LABORATORY

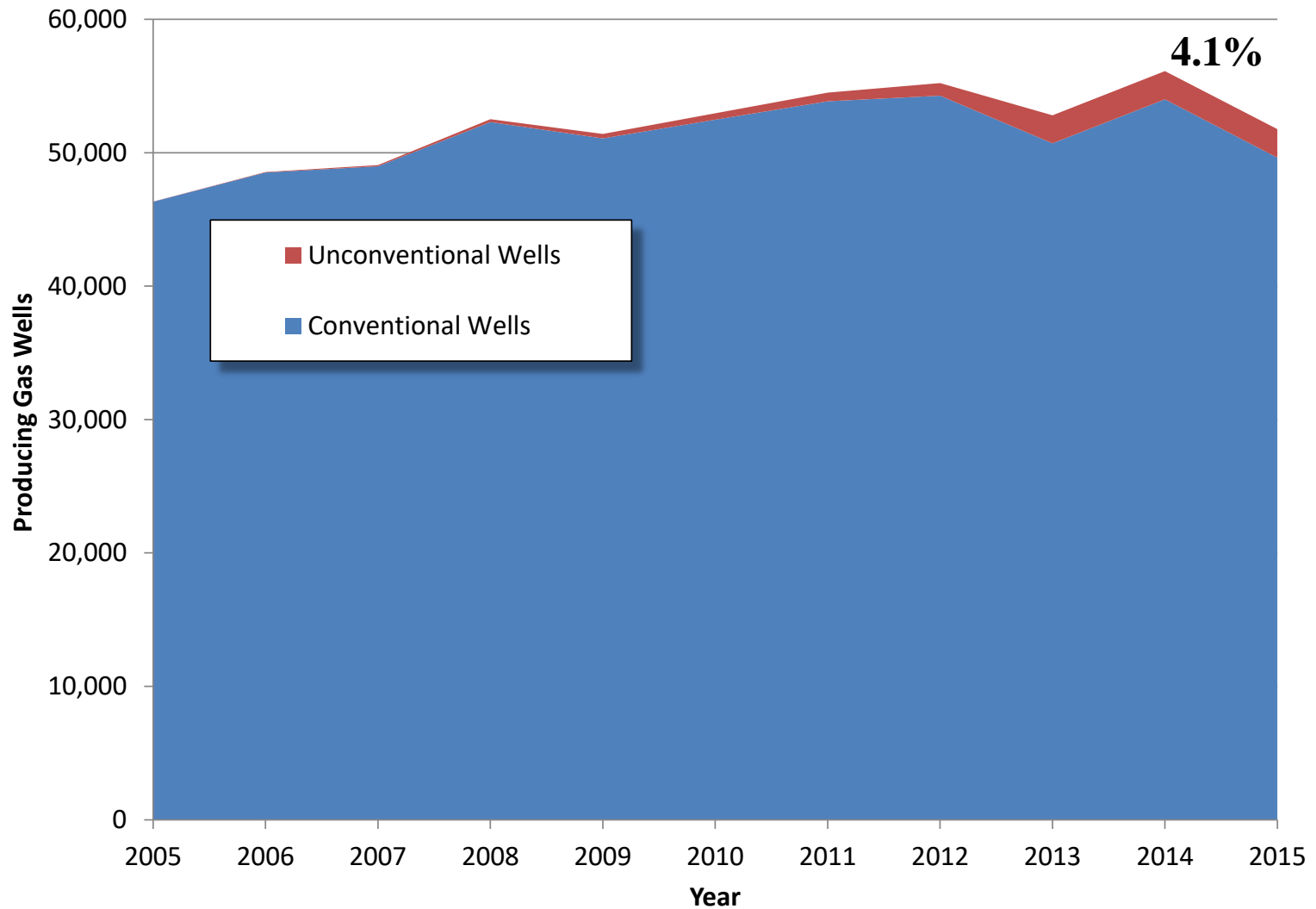
MSEEL



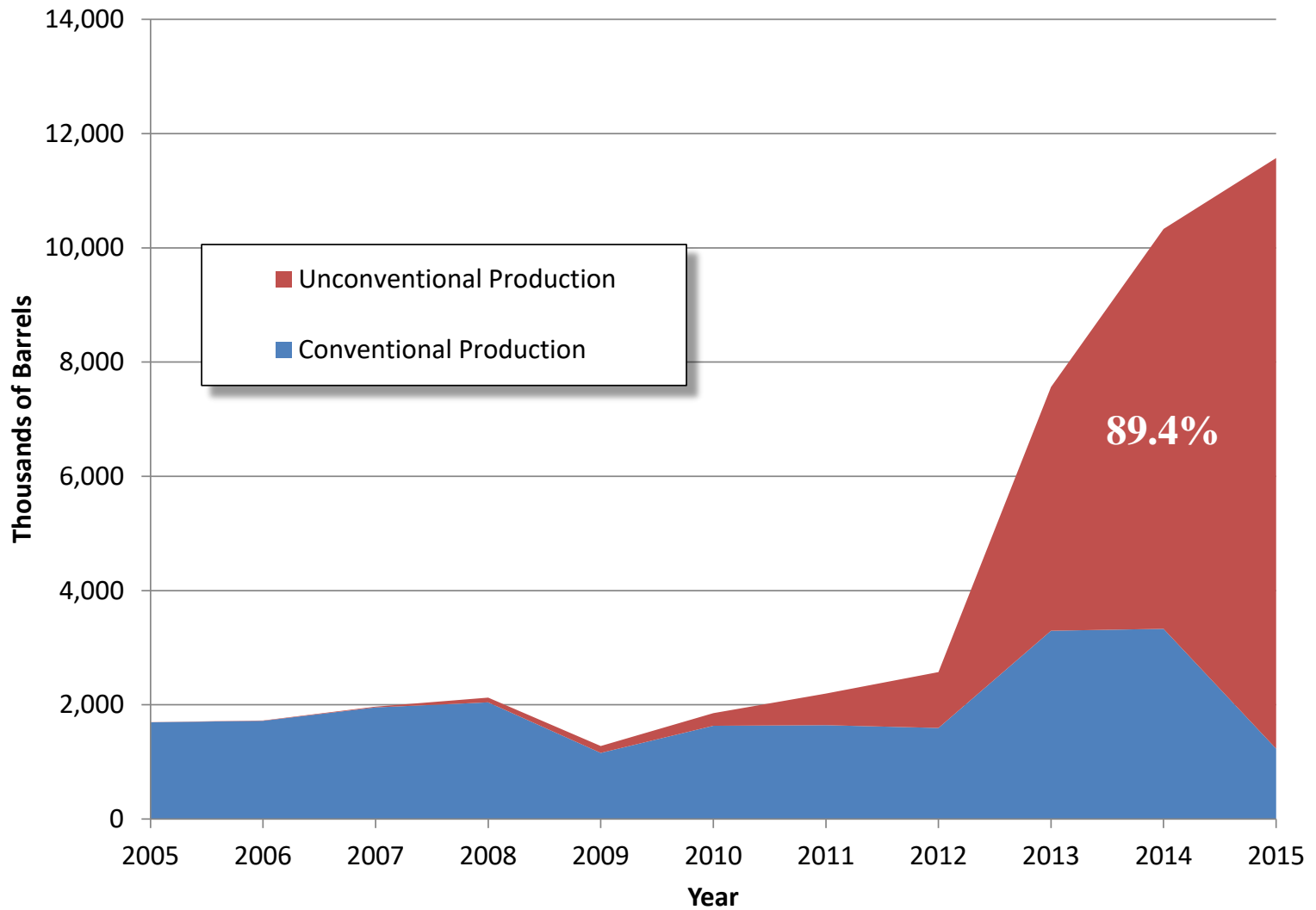
West Virginia Gas Production



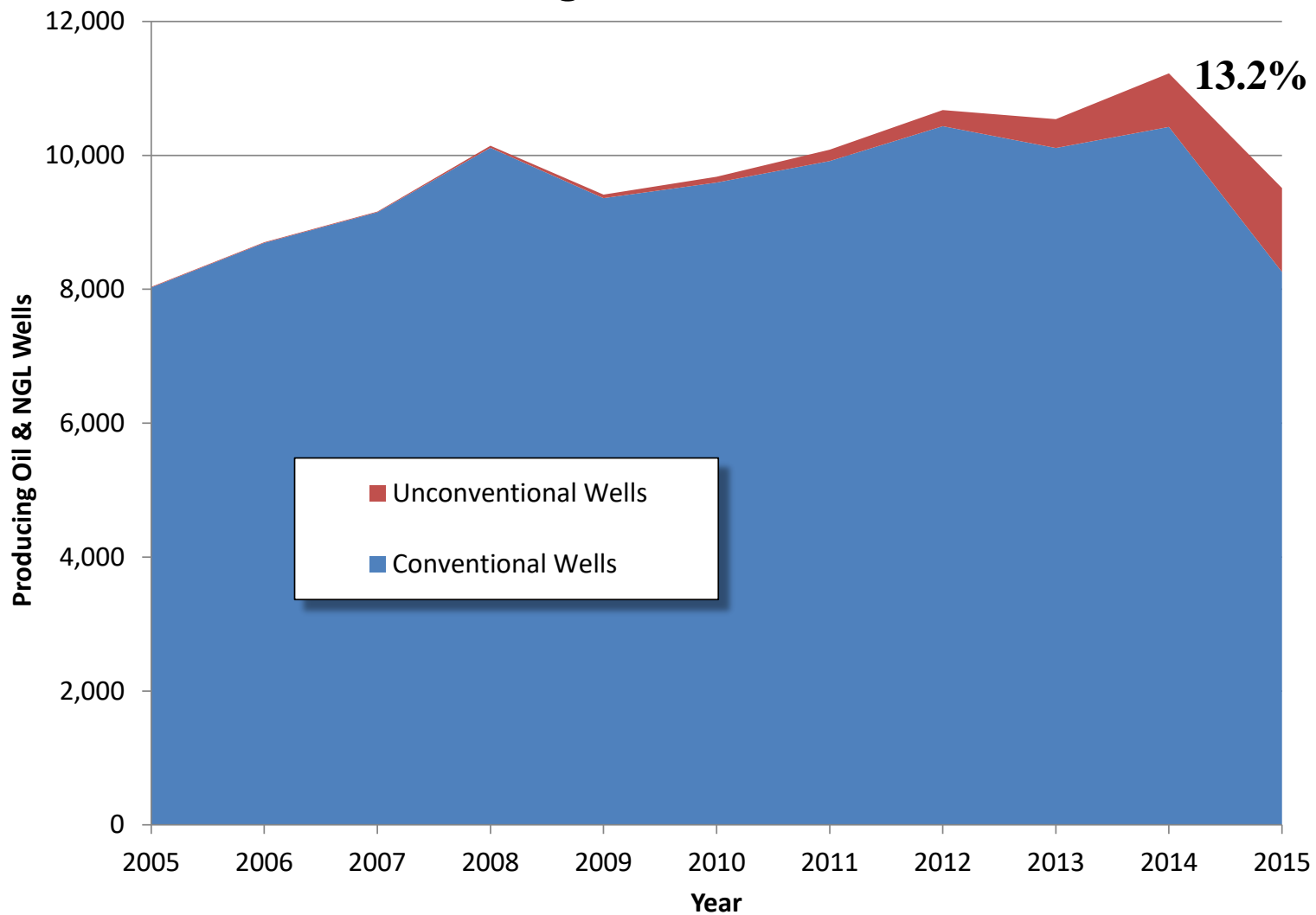
West Virginia Gas Wells



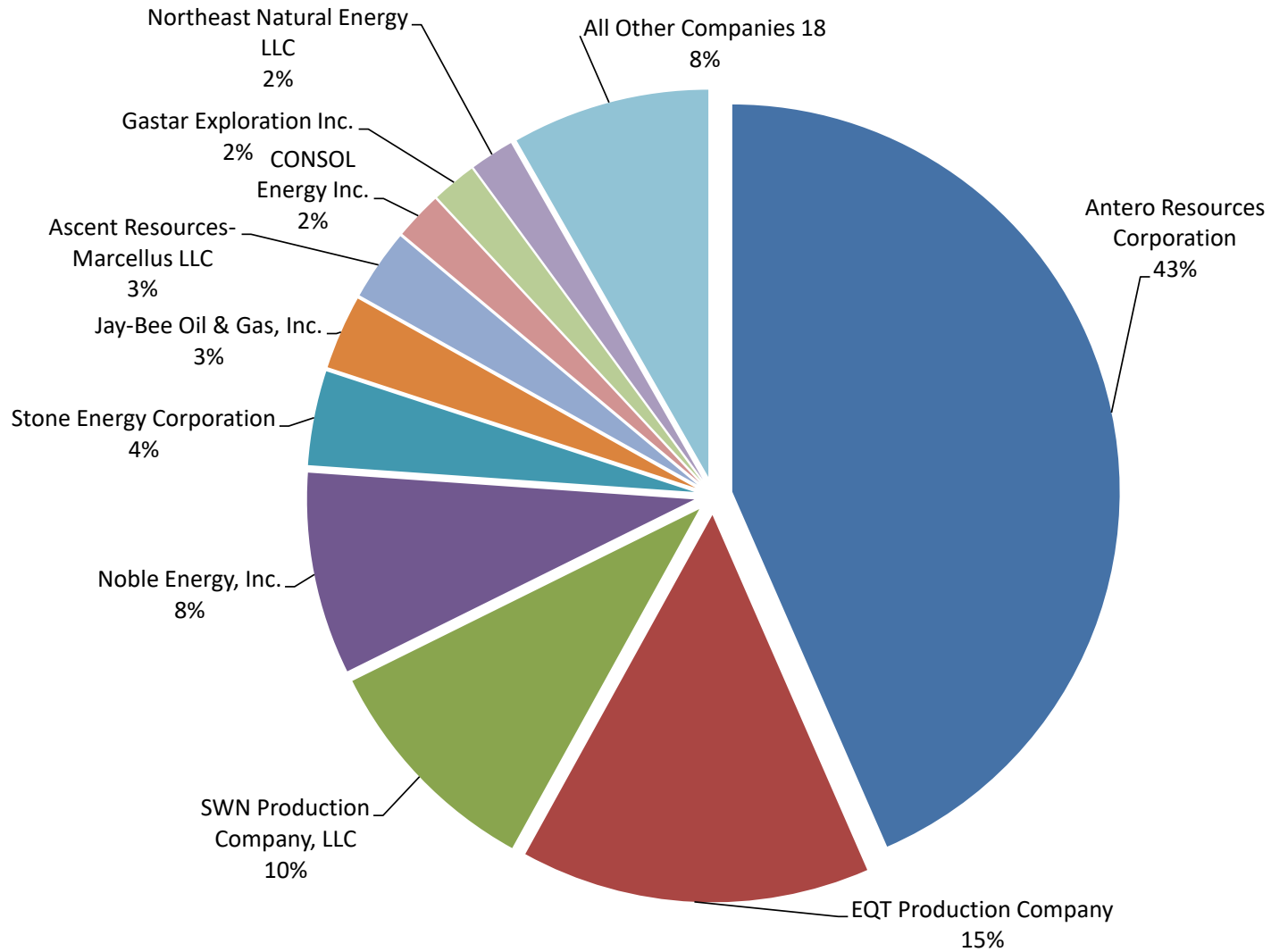
West Virginia Oil & Liquids Production



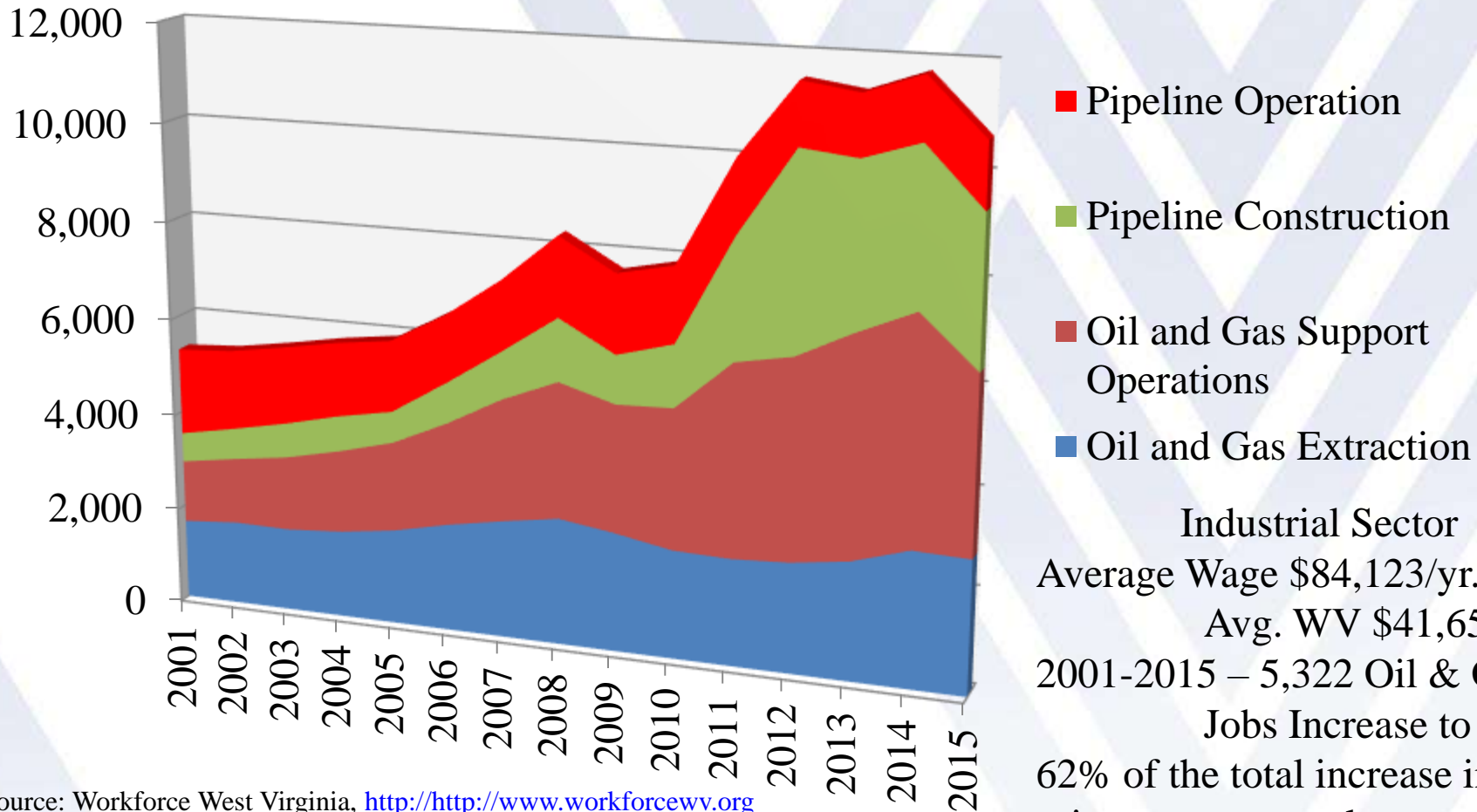
West Virginia Oil & NGL Wells



West Virginia 2015 Marcellus Gas Production by Operator



West Virginia Direct Oil & Gas Industrial Sector Employment



Industrial Sector
 Average Wage \$84,123/yr.
 Avg. WV \$41,655/yr.
 2001-2015 – 5,322 Oil & Gas
 Jobs Increase to 10,635
 62% of the total increase in
 private sector employment

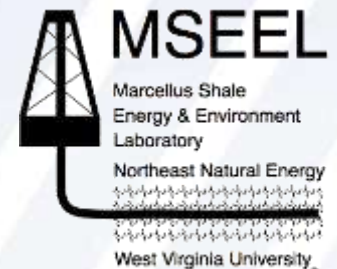
Source: Workforce West Virginia, <http://www.workforcewv.org>
 Through 2015



MARCELLUS SHALE ENERGY AND ENVIRONMENT LABORATORY

MSEEL

The objective of the Marcellus Shale Energy and Environment Laboratory (MSEEL) is to provide a **long-term collaborative field site** to develop and validate new knowledge and technology to improve recovery efficiency and minimize environmental implications of unconventional resource development



MSEEL Site

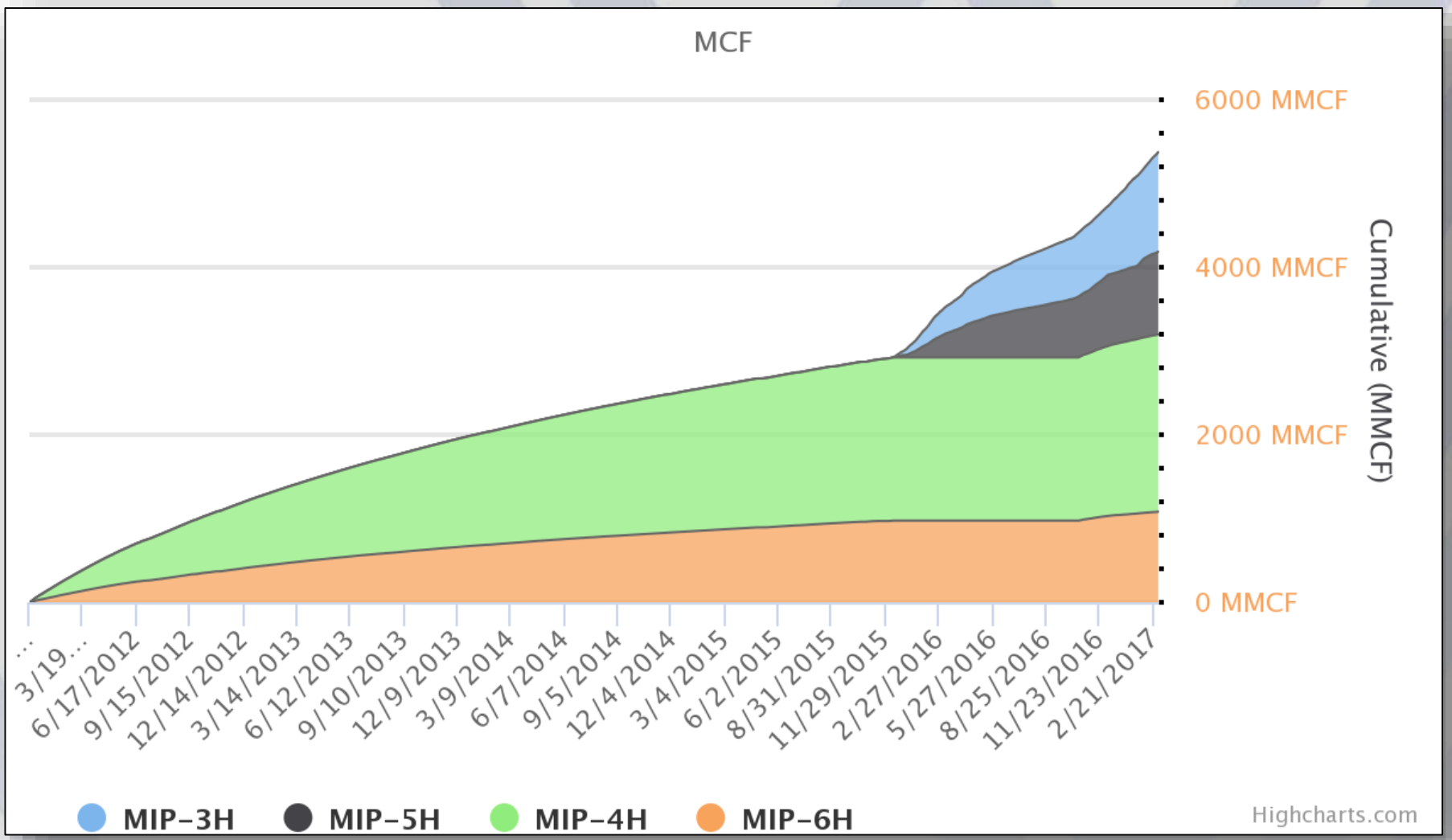


MSEEL

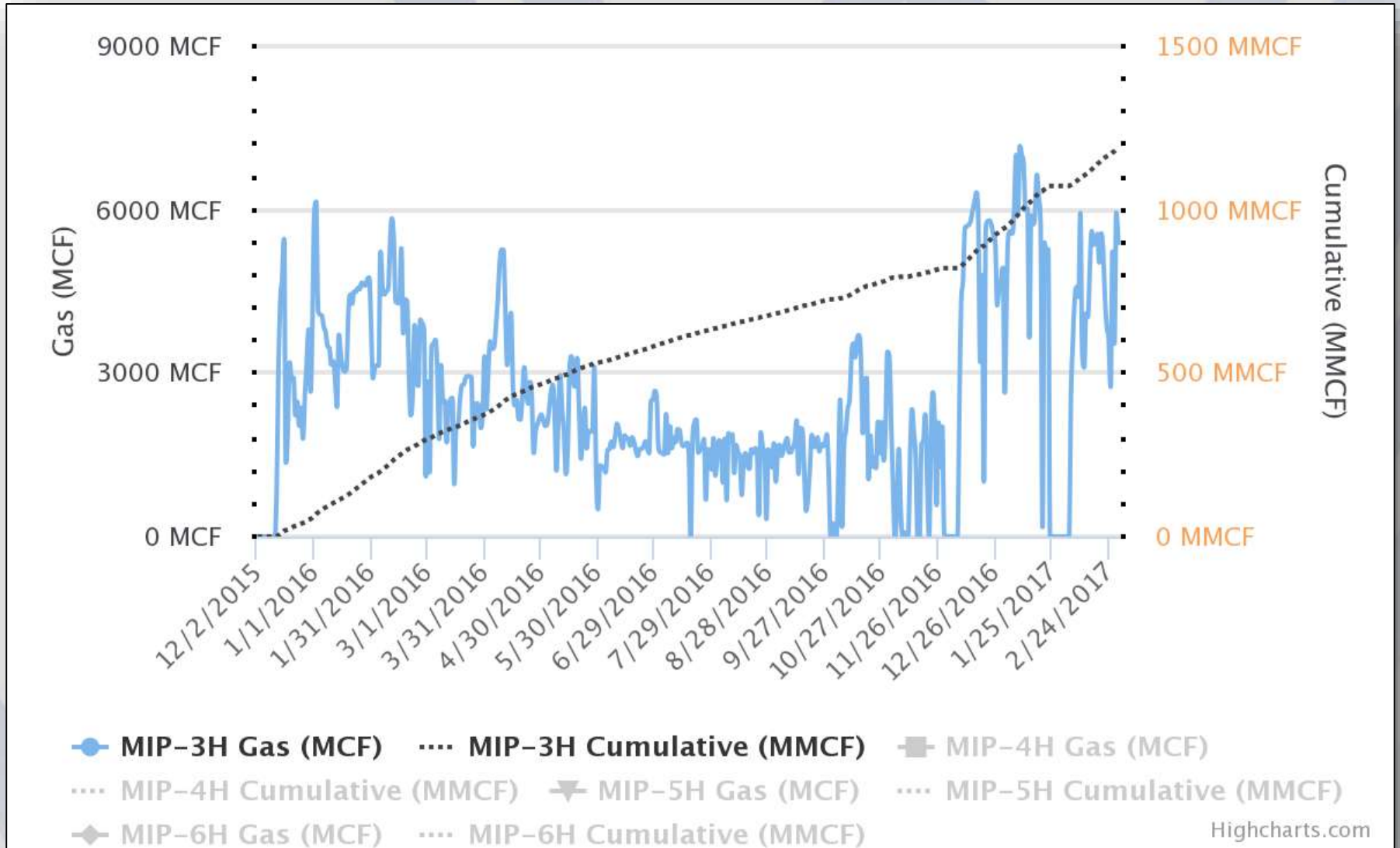
Drilling MIPU 3H and 5H



Production Volumes: MIP 3H, 5H, 4H, 6H



Production Volumes: MIP 3H



Drilling and Produced Water Waste Monitoring

Cuttings

Mud



Using 'Green' Drilling Mud

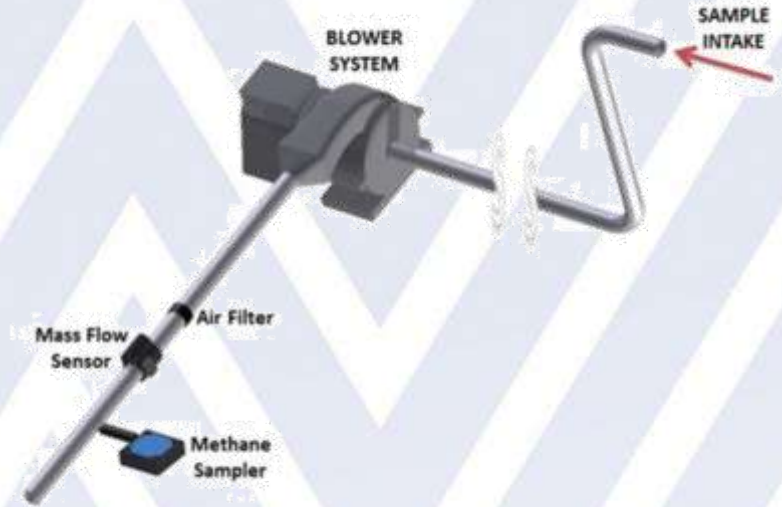
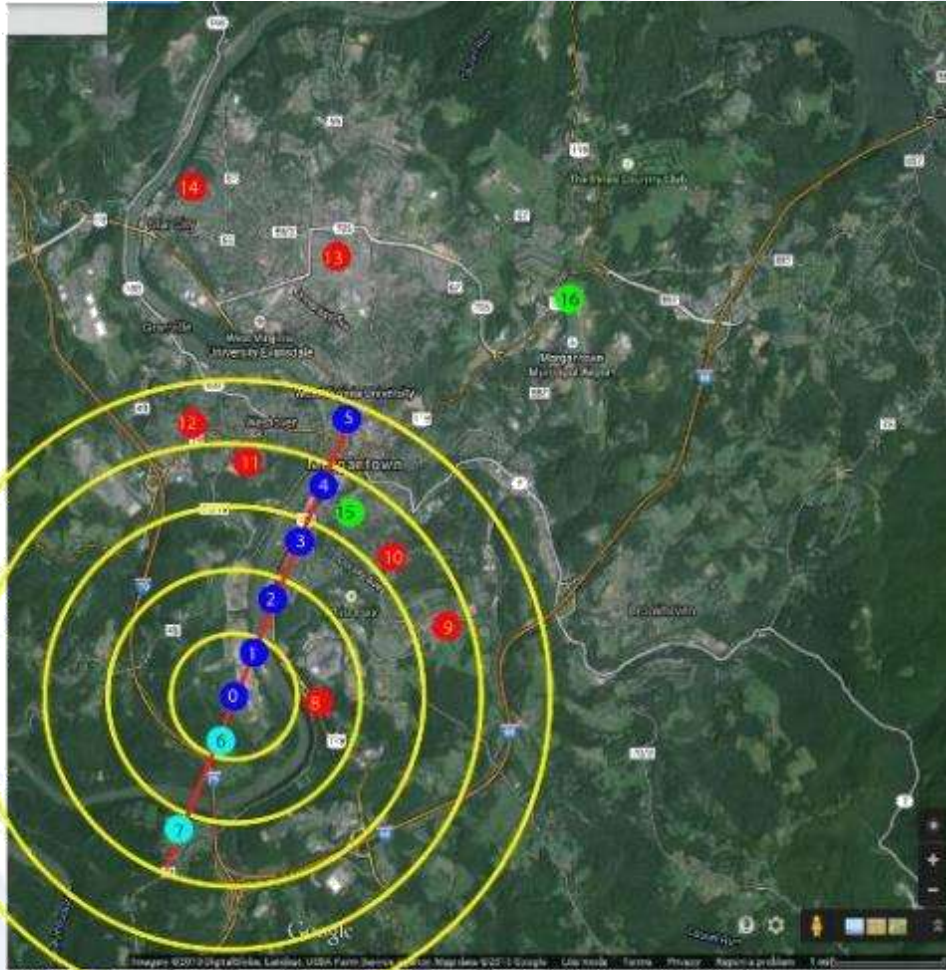
NO Parameters Exceeded TCLP

- In the Vertical and Horizontal (Marcellus) sections:
 - Drill Cuttings ~500-800 tons/well or 25 to 50 truckloads
 - Drilling Mud
- TCLP organics-no exceedances
- TCLP inorganics-no exceedances

TCLP - Toxicity Characteristic Leaching Procedure



MSEEL Environmental Monitoring Air Emissions



Radiochemistry: Drill Cuttings

Brazil nuts are about 12 pCi/g

Radionuclides (pCi/g)																
vertical	EPA 901.1									9310						
Marcellus	⁴⁰ K			²²⁶ Ra			²²⁸ Ra			alpha			beta			
	Act	Unc	MDC	Act	Unc	MDC	Act	Unc	MDC	Act	Unc	MDC	Act	Unc	MDC	
MIP 4400 3H	28	4.8	1.0	1.2	0.3	0.3	1.8	0.5	0.3	15.0	7.1	9.8	24.5	6.3	5.6	
MIP 5026 3H	24	4.4	1.4	1.4	0.3	0.2	1.9	0.5	0.3	10.5	5.8	9.2	19.4	4.8	4.1	
MIP 6798 5H	27	4.5	0.9	1.8	0.3	0.2	1.4	0.4	0.5	17.1	7.7	11.2	27.8	6.7	5.4	
MIP 8555 5H	26	4.2	1.1	4.7	0.7	0.2	1.3	0.4	0.4	27.0	9.6	10.2	36.9	8.6	6.6	
MIP 8555 5H DUP	25	4.6	1.5	4.6	0.7	0.3	1.1	0.6	0.6	38.1	11.1	9.1	29.8	6.8	4.9	
MIP 9998 5H	17	4.3	2.7	9.2	1.3	0.3	0.5	0.9	0.9	46.8	11.0	4.7	42.9	9.0	5.9	
MIP 11918 5H	22	3.7	1.1	4.0	0.7	0.2	0.7	0.5	0.5	24.4	9.2	10.3	23.0	6.2	6.2	
MIP 11918 5H	20	3.4	1.1	4.2	0.6	0.2	0.8	0.4	0.6	23.8	6.8	5.2	28.7	6.3	5.1	
MIP 13480 3H	18	3.2	1.2	9.2	1.3	0.2	0.8	0.6	0.5	55.7	14.7	11.5	35.4	8.2	5.8	
MIP 13480 3H DUP	18	3.5	1.4	9.7	1.4	0.3	1.1	0.4	0.3	59.2	14.9	9.3	35.0	7.8	4.6	
MIP 13480 3H Mud	13	3.0	1.1	5.6	0.9	0.2	0.5	0.3	0.8	60.0	15.9	10.5	42.5	9.6	6.1	
MIP 14454 5H	20	3.8	1.1	5.8	0.9	0.2	1.3	0.5	0.6	28.8	7.9	6.5	37.5	8.0	5.4	



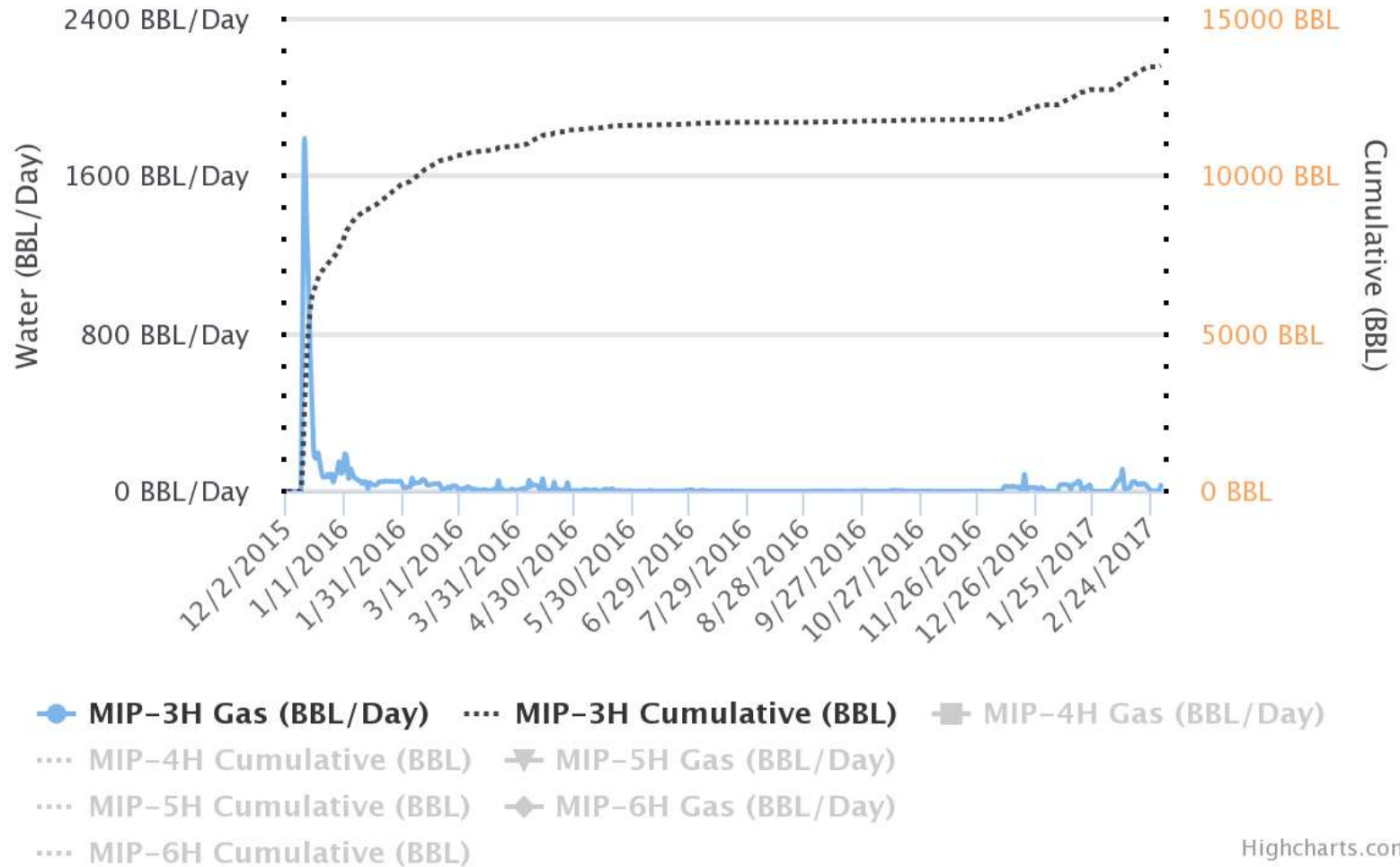
Flowback/Produced Water

- Extremely saline: 10,000 to 300,000 mg TDS/L
- Inorganics: Na, Mg, Ca, Sr, Ba, Cl, Br
- Organics: BTEX
- NORMs: $\alpha, \beta, ^{226}\text{Ra}, ^{228}\text{Ra}$,
- During flowback cycle
 - Discharge drops off rapidly
 - Initially 5,000 bpd to 175 bpd after 60 days
 - Ion concentrations increase
- Most of the contaminants come from the formation-**not frac fluid**



Flowback Volumes: MIP 3H

Water Production for MIP-3H, MIP-4H, MIP-5H, and MIP-6H



Highcharts.com



MSEEL data

Nearly all parameters were higher in flowback than frac fluid

Pink: exceeds drinking water MCL

MDL		units	SDWA MCL	MIP 3H		MIP 5H	
				HF	FB day 42	HF	FB day 42
0.0011	Al	mg/L	0.05	0.42	0.00055	0.02	0.00055
0.0007	As	mg/L	0.01	0.00	0.35	0.00	0.35
0.0002	Ba	mg/L	2	0.04	2500	0.048	1100
0.4	Ca	mg/L		35.5	6800	34	2900
0.0001	Cr	mg/L	0.1	0.003305	0.05	0.00005	0.05
0.01	Fe	mg/L	0.3	1.996	140	0.005	120
0.0001	Pb	mg/L	0.015	0.00	0.005	0.00	0.005
0.019	Mg	mg/L		9.70	710	8.00	330
0.0002	Mn	mg/L	0.05	0.11	11	0.00	1.8
0.0004	Ni	mg/L		0.01	0.2	0.00	0.2
0.03	K	mg/L		3.40	130	2.50	120
0.001	Se	mg/L	0.05	0.00	0.5	0.00	0.5
0.0001	Ag	mg/L	0.1	0.00	0.05	0.00	0.05
0.1	Na	mg/L		46.50	21000	30.00	13000
0.0003	Sr	mg/L		0.34	1400	0.27	630
0.02	Zn	mg/L	5	0.07	1.2	0.04	1.2
4.3	Alk	mg/L		70.00	140	64.00	240
0.09	Br	mg/L		0.17		0.95	
0.29	Cl	mg/L	250	31.50	61000	34.50	37000
3	SO4	mg/L	250	125.00	7	140.00	7
7.6	TDS	mg/L	500	340.00	88000	565.00	55000
0.25	Benzene	µg/L	5	0.13	10	0.13	27
0.2	Toluene	µg/L	1000	0.43	13	0.01	53
0.22	Ethylbenze	µg/L	700	0.11	1.1	0.11	4
0.62	Xylene tot	µg/L	10000	0.32	3.2	0.32	23
0.005	MBAS	mg/L	0.5	0.00	0.38	0.00	0.26



Subsurface Sampling



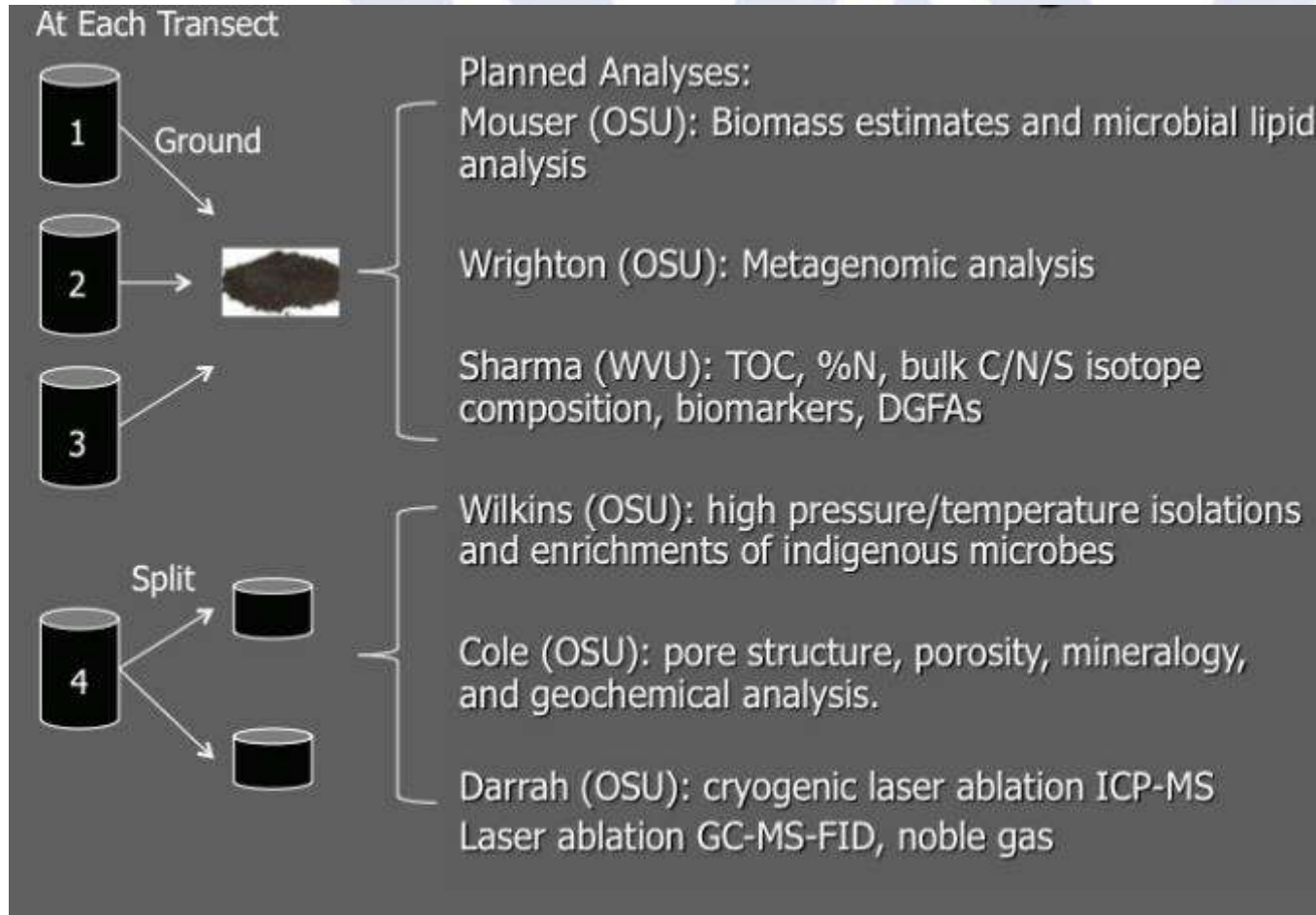
Retrieved 111' of a targeted 120' whole core



Sidewall Cores



Sidewall Cores Geochemistry

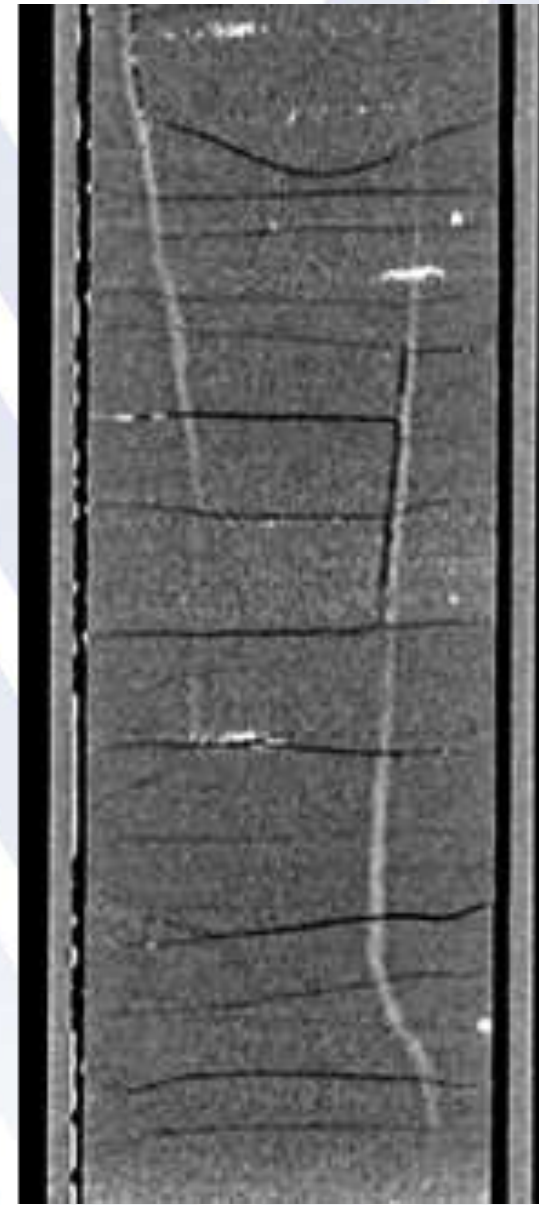
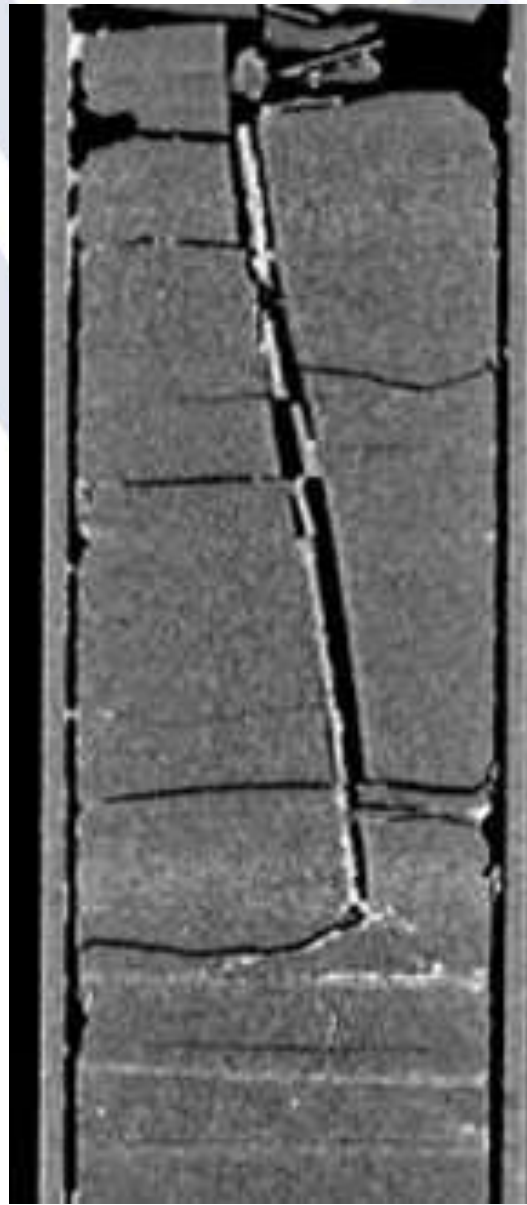


MSEEL

Completion MIPU 3H and 5H

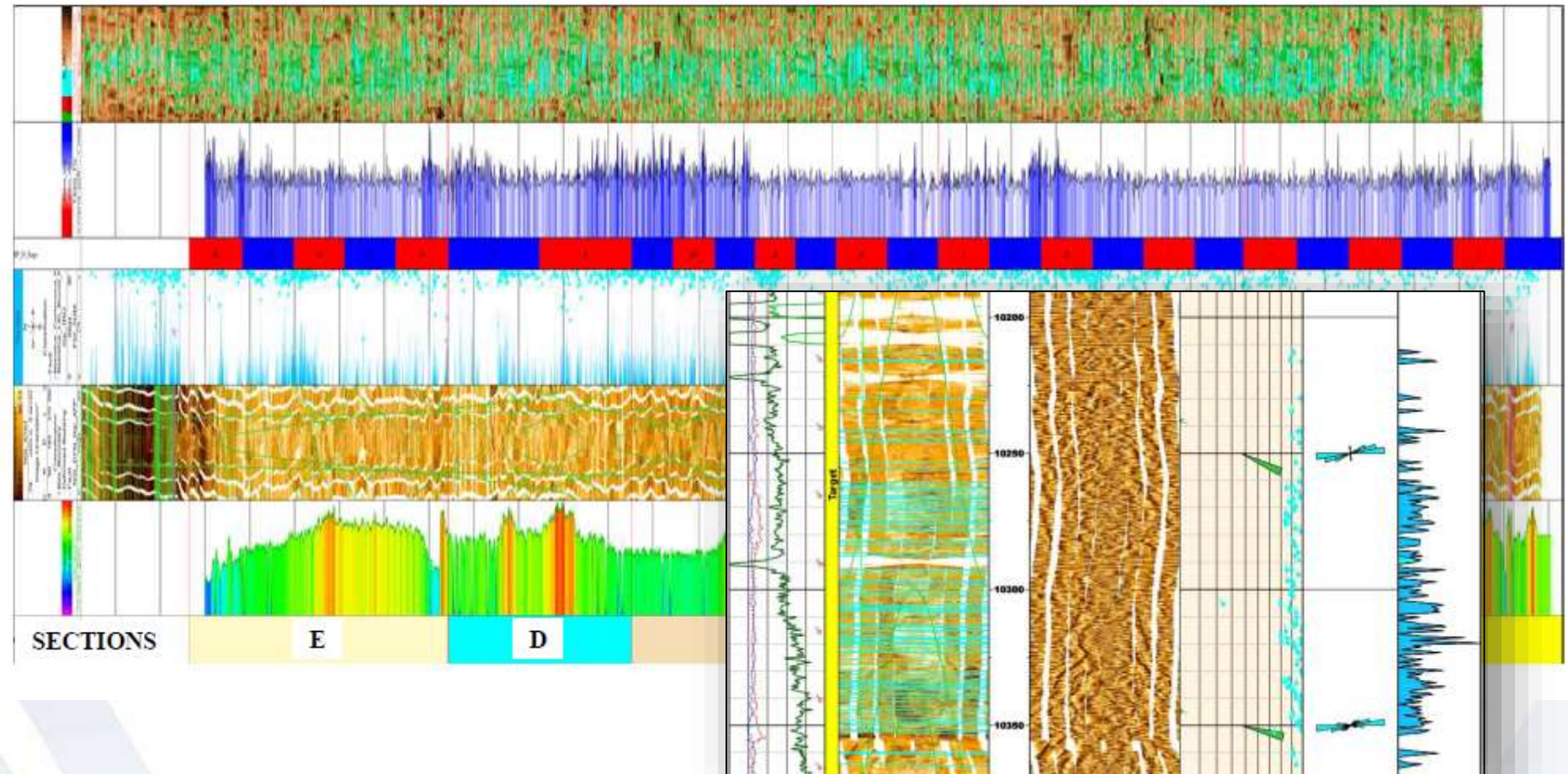


High Resolution CT Scanning – Fractures

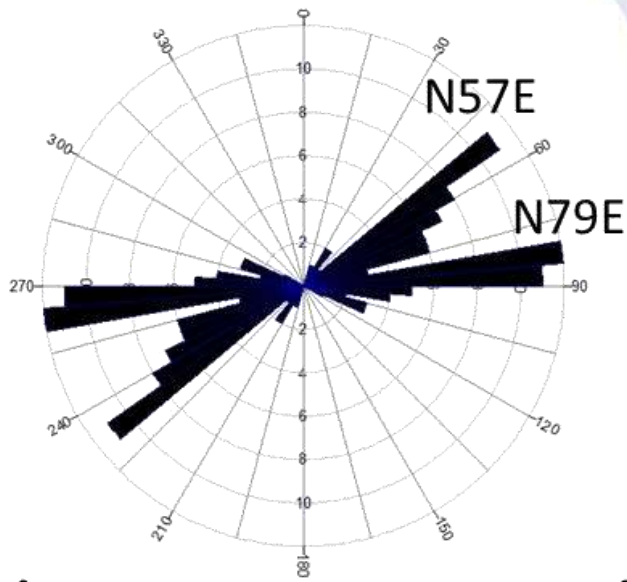


MSEEL - LOGGING LATERAL

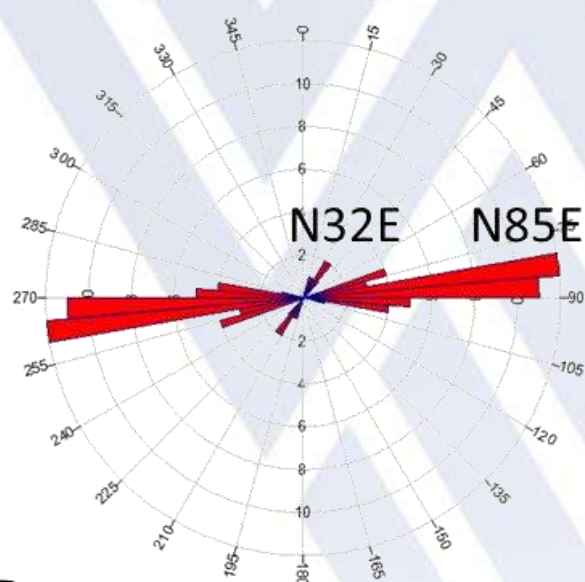
High Definition open hole logs in lateral with synthetic mud



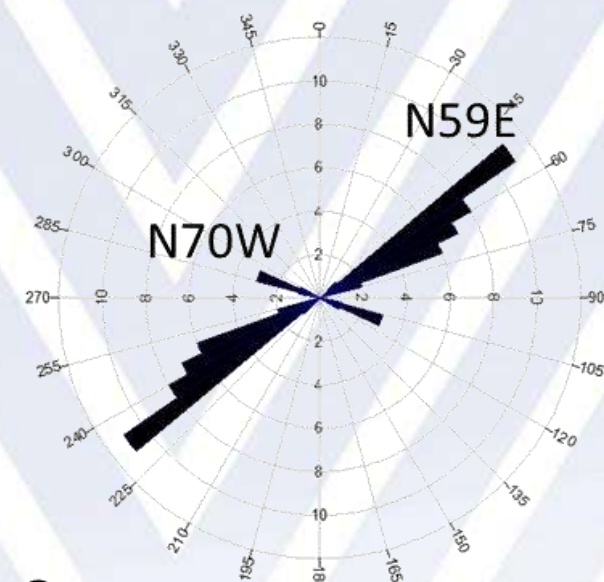
MSEEL - Microseismic



A.



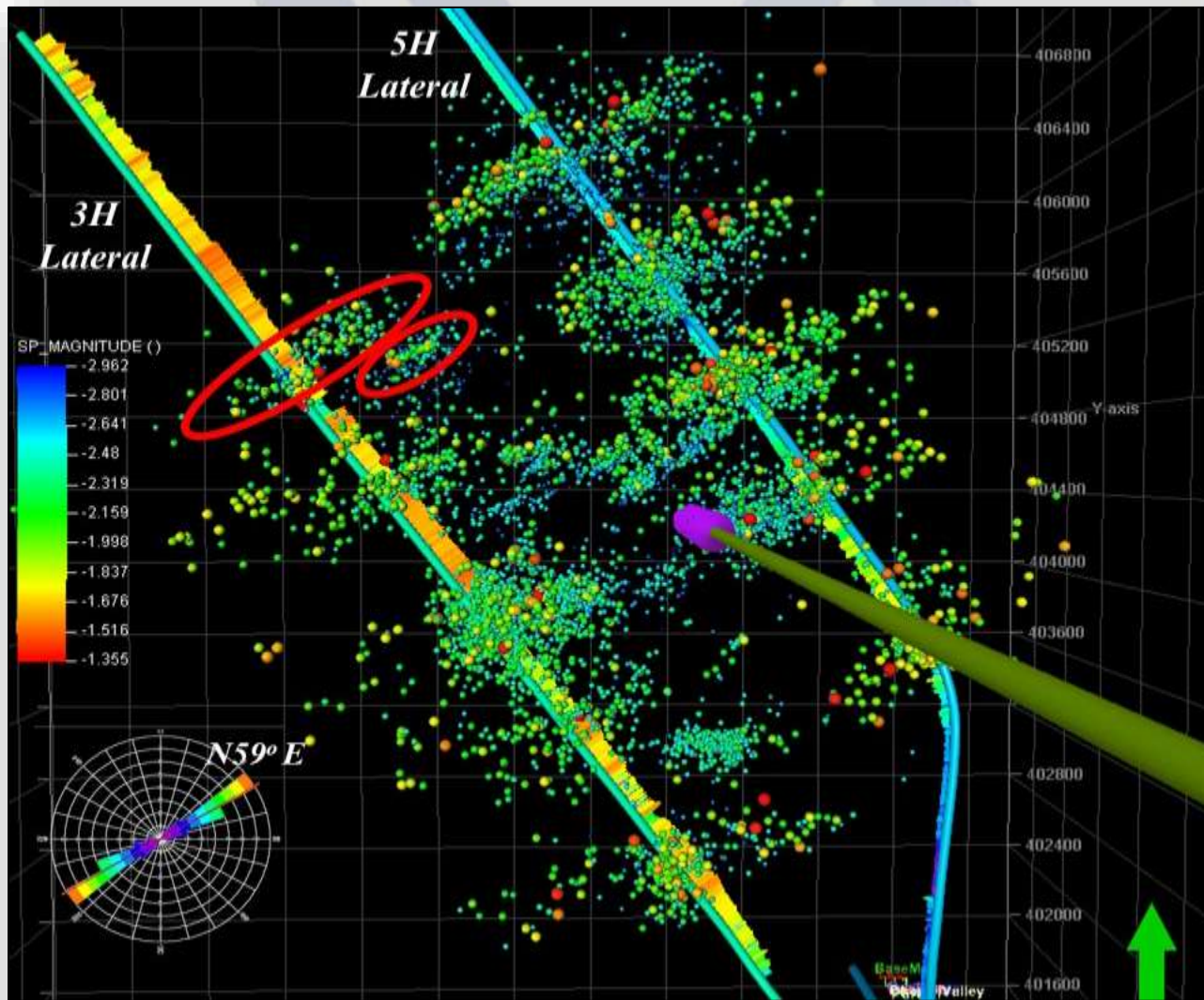
B.



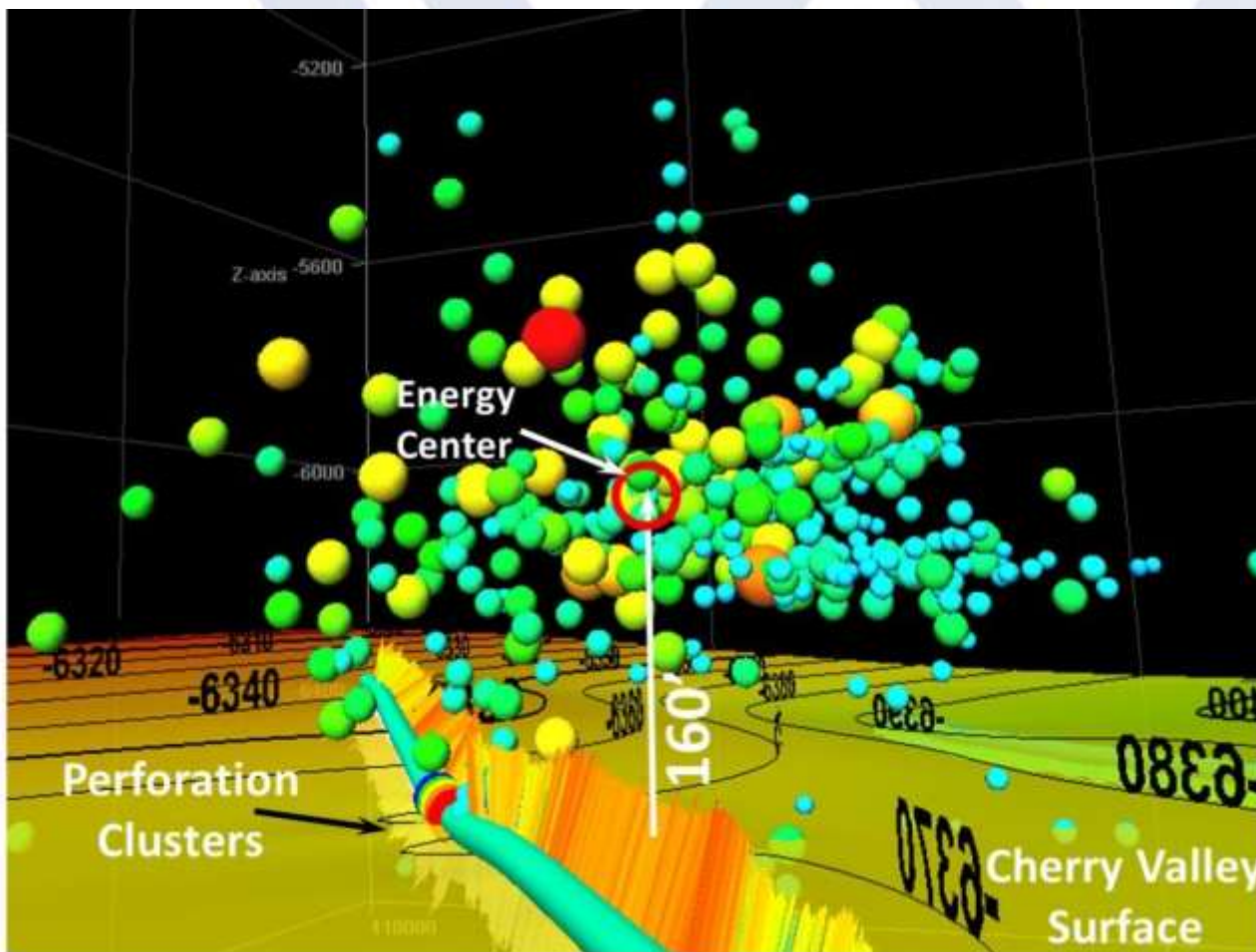
C.



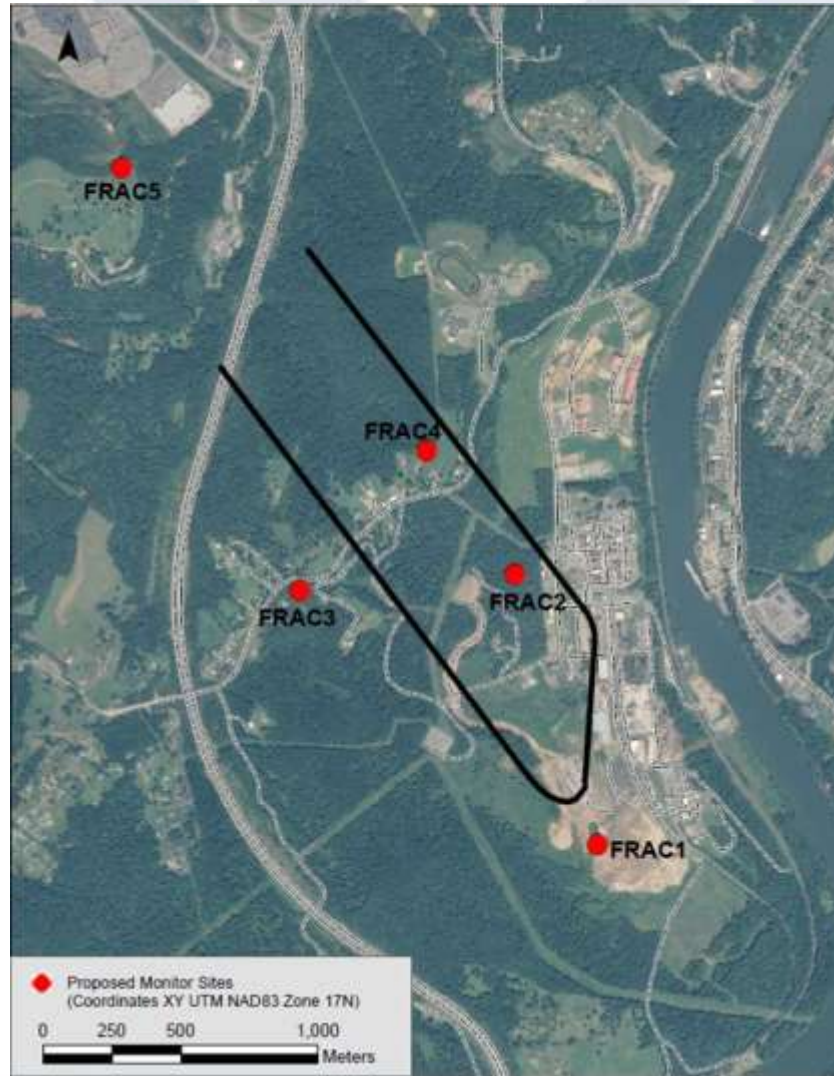
MSEEL - Microseismic



MSEEL - Microseismic



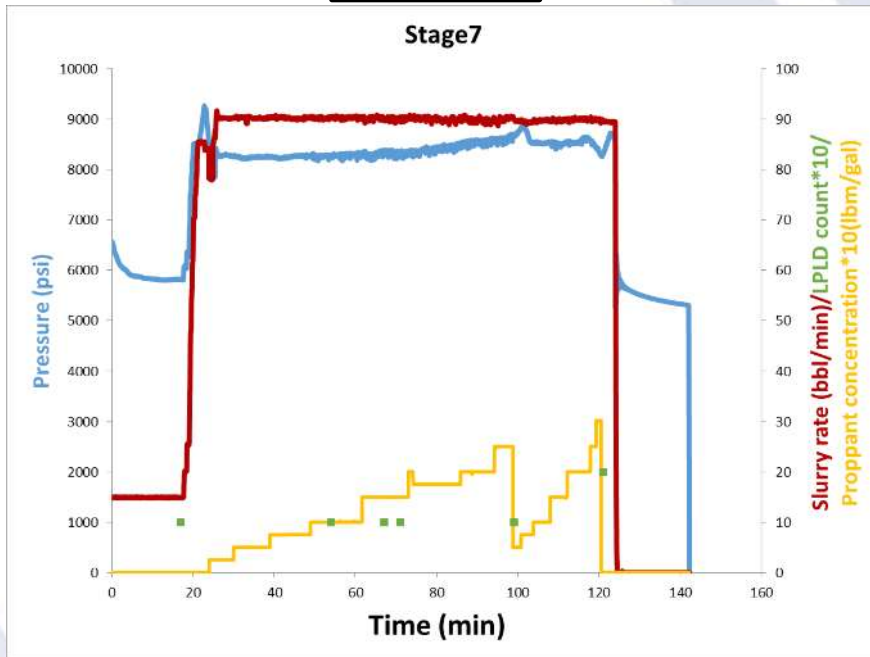
SURFACE MONITORING OF SLOW SLIP (LPLD)



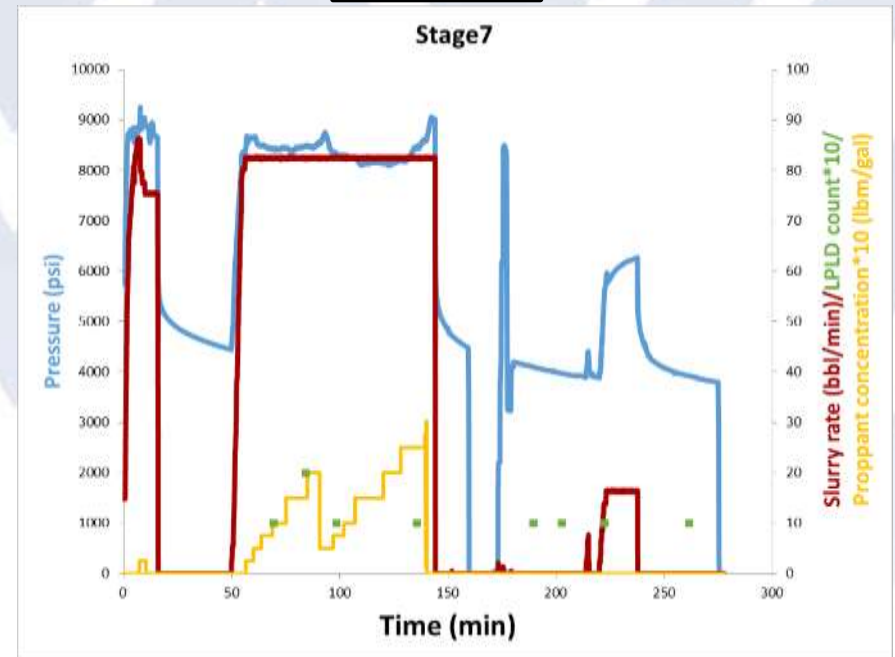
SURFACE MONITORING OF SLOW SLIP (LPLD)

LPLD and injection parameters

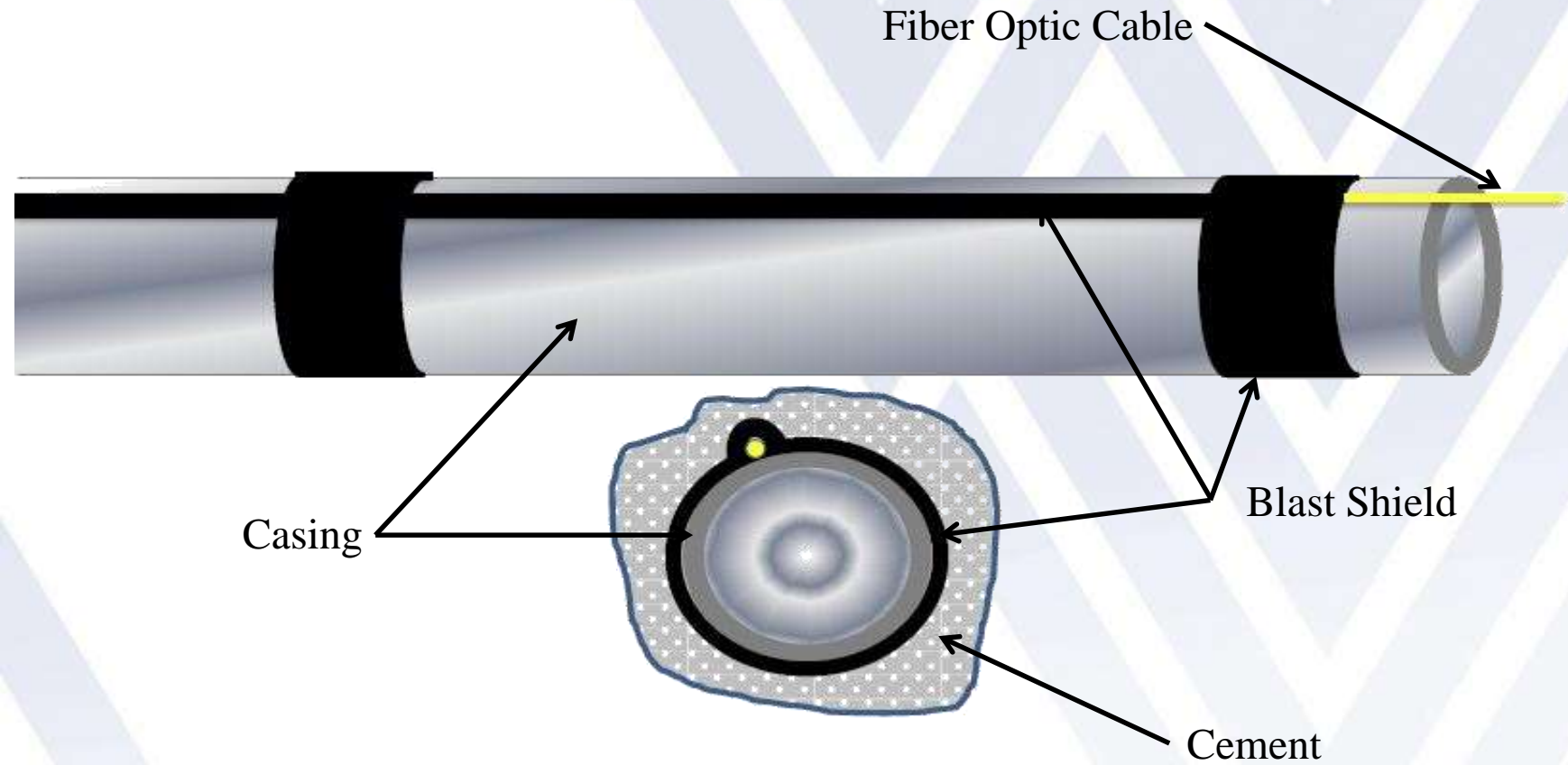
Well 3H



Well 5H



Fiber Optic Installation



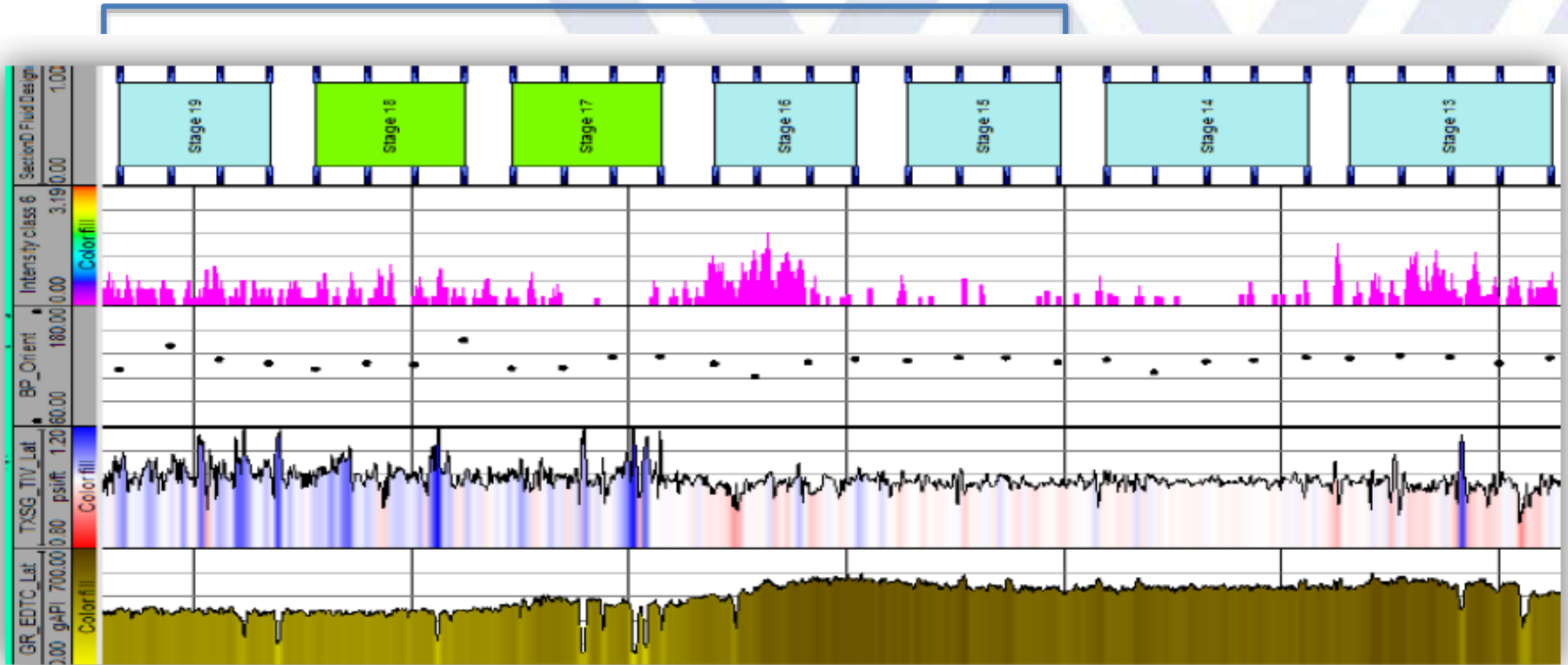
MIP 3H Completion Design

Section		Stage	Cluster Count	Total Shot Count	Shot Density (shot/ft)	Stage Length (ft)	Pump schedule
E	Best Practice Applied	28	4	40	6	191	A
		27	4	40	6	184	A
		26	5	40	6	225	A
		25	5	32	6	231	A
		24	5	30	6	222	A
		23	5	40	6	237	C
		22	5	40	6	220	C
D	Sapphire VEF	21	5	40	5	218	D
		20	5	40	5	240	D
C	SLB Engineered Completion	19	4	32	6	180	C
		18	4	32	8	180	C
		17	4	32	6	181	C
		16	4	26	6	178	C
		15	4	26	6	186	C
		14	5	30	6	228	A
		13	5	30	6	230	A
B	NNE 75% 100-Mesh	12	5	50	5	231	B
		11	5	50	5	232	B
		10	5	50	5	227	B
		9	5	50	5	237	B
		8	5	50	5	222	B
		7	5	50	5	224	B
A	NNE Standard 35% 100-Mesh	6	5	50	5	245	A
		5	5	50	5	234	A
		4	5	50	5	230	A
		3	5	50	5	238	A
		2	5	50	5	223	A
		1	5	50	5	233	A



MSEEL - LOGGING LATERAL

High Definition open hole logs in lateral with synthetic mud



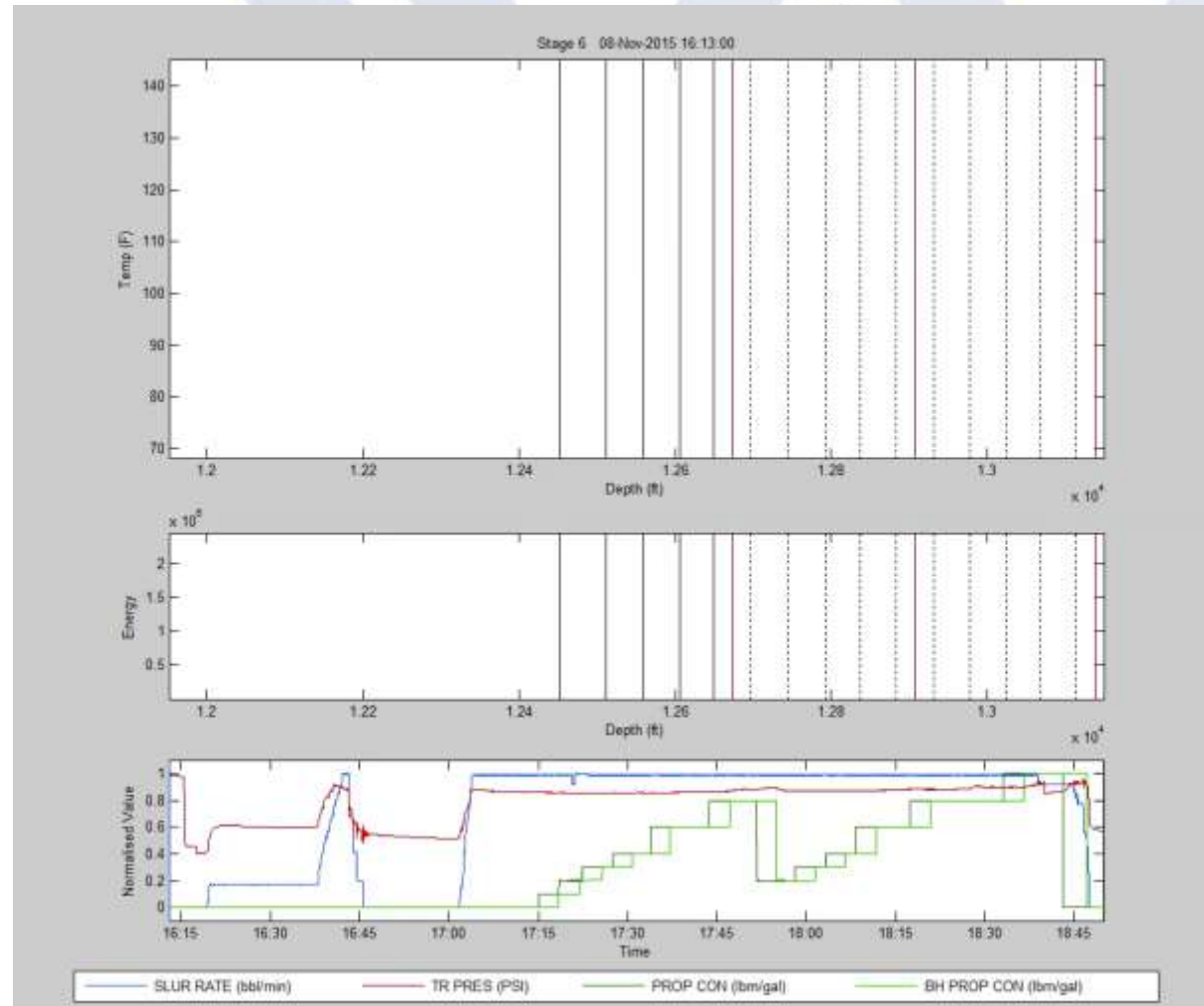
Mapped Faults & Fractures

For MIP-3H the number of faults and fractures encountered at each stage is reported as:

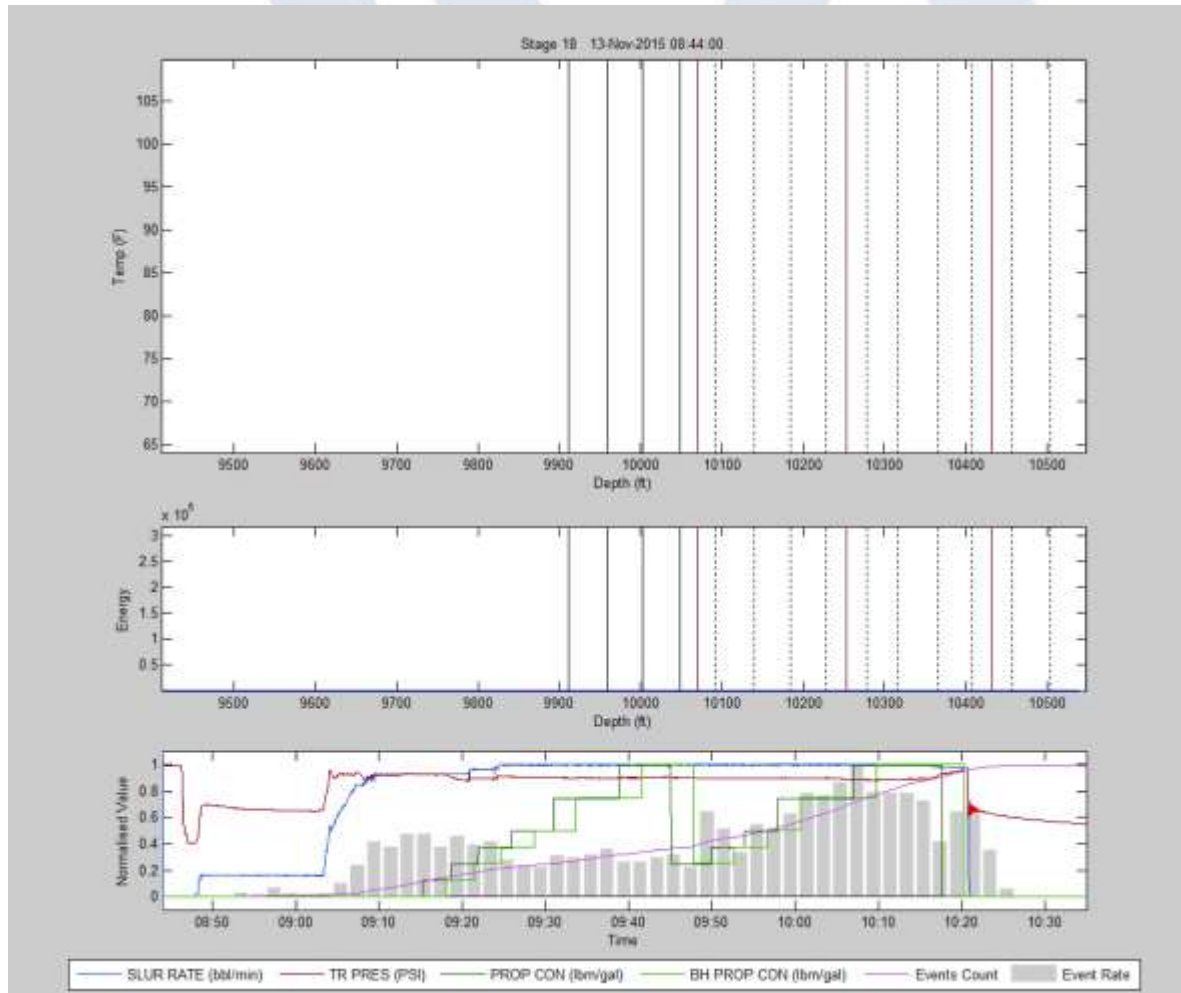
Fault/Fracture \ Stage	1	2	3	4	5	6	7	8	9	10	11	12	13	14	15	16	17	18	19	20	21	22	23	24	25	26	27	28
No of Faults	3				2	1				2	1																	
No of Fractures	41	25	48	29	15	69	47	51	97	160	86	65	72	17	14	90	25	56	68	71	37	46	21	41	42	89	66	28



MIP3H - Stage 6: Geometric Completion Uneven Distribution

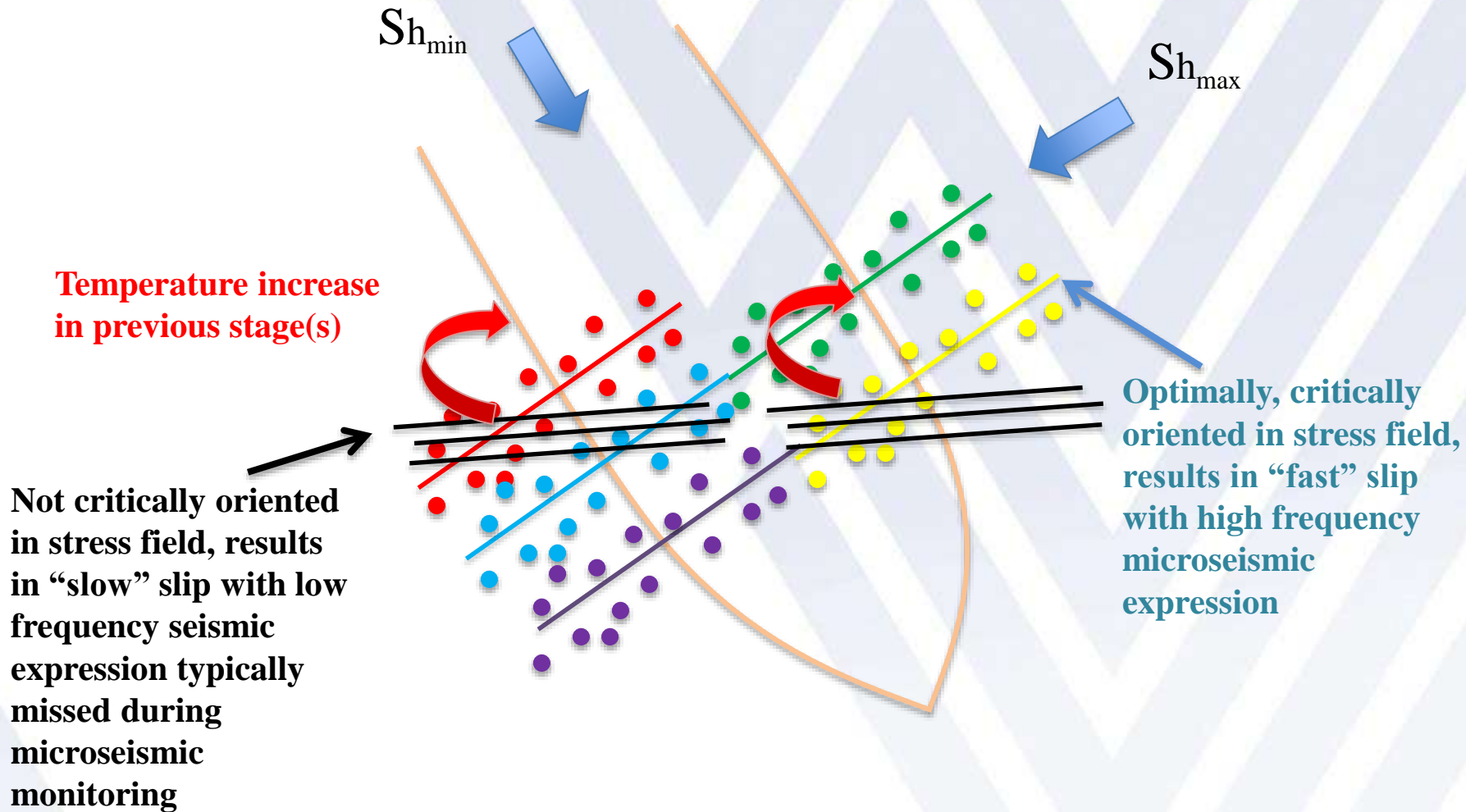


MIP 3H - Stage 18 Even Distribution



SURFACE MONITORING OF SLOW SLIP (LPLD)

Synopsis of slow-slip deformation



Temperature During Production

Jan 2016



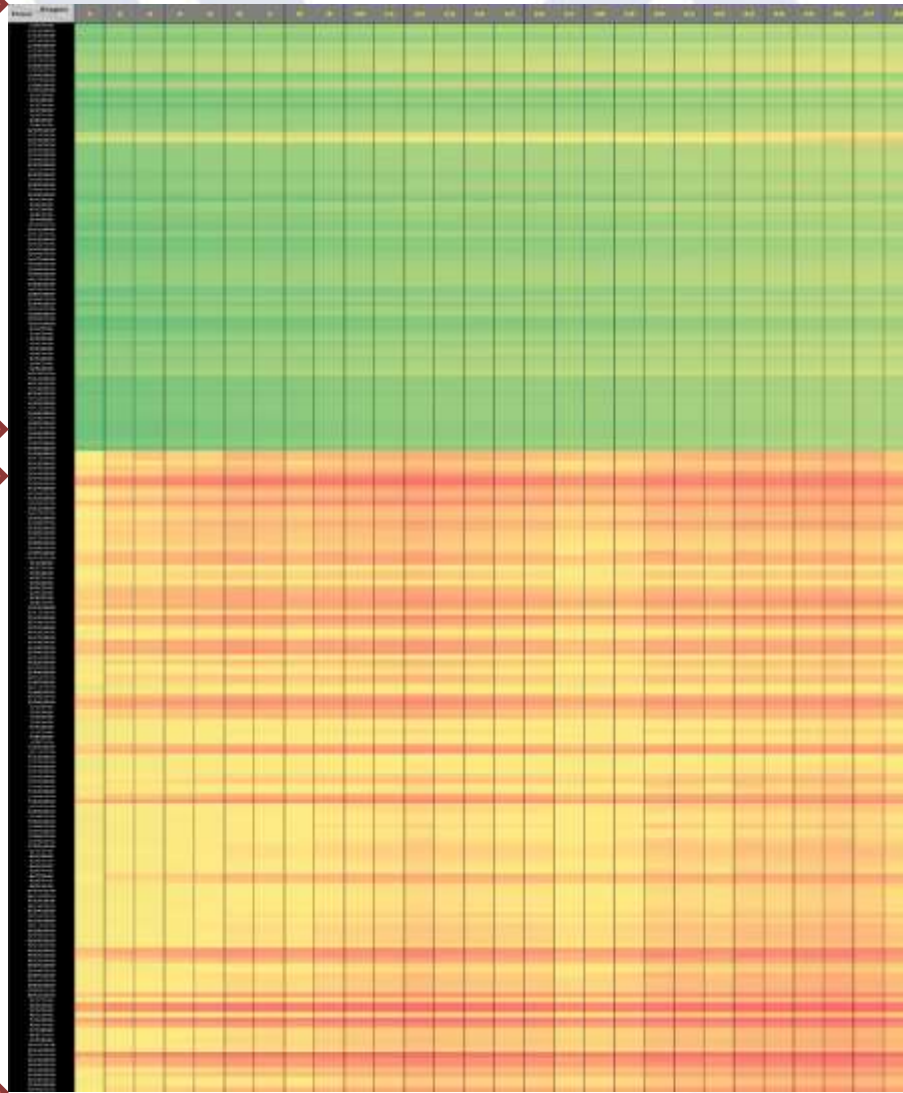
April 2016



May 2016

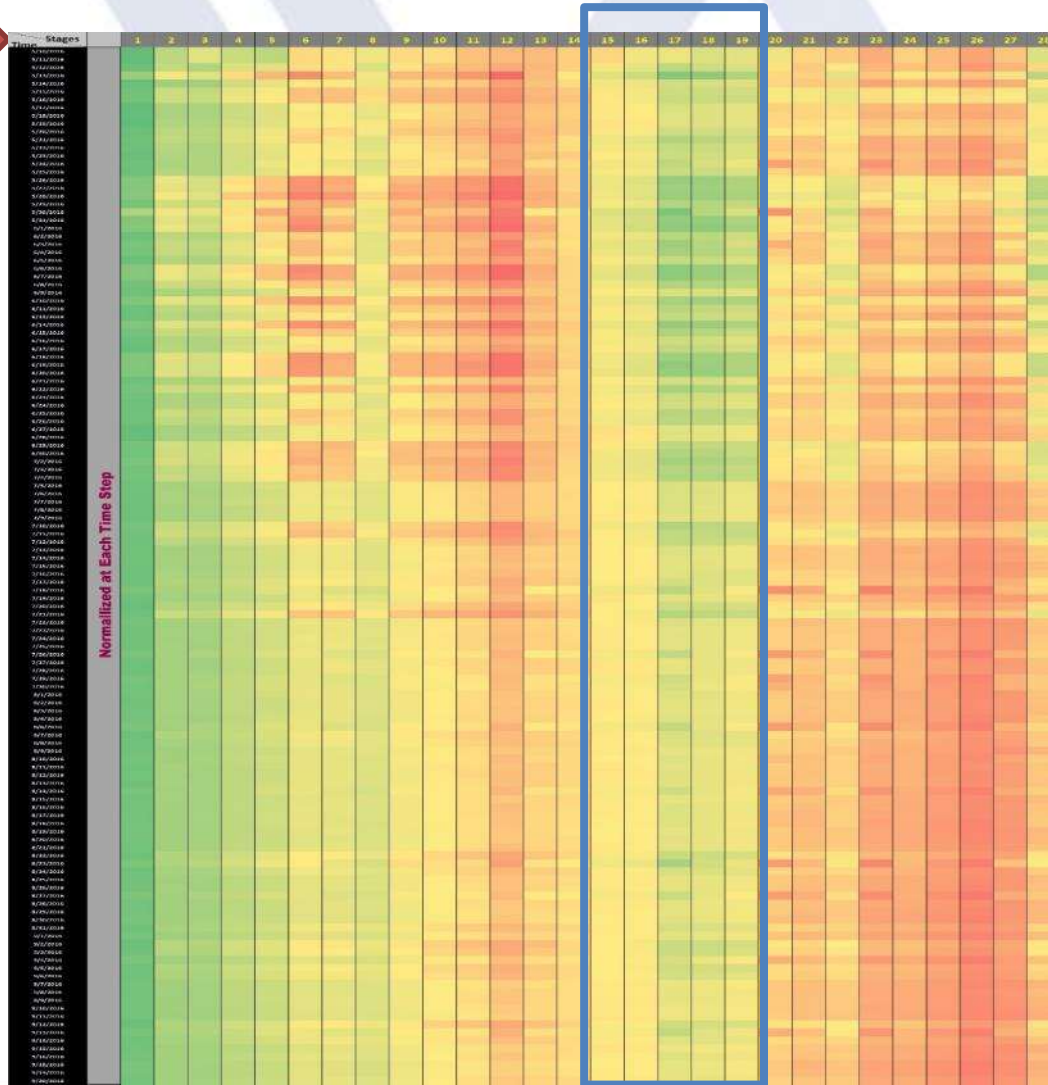


Sept 2016



Normalized Temperature During Production

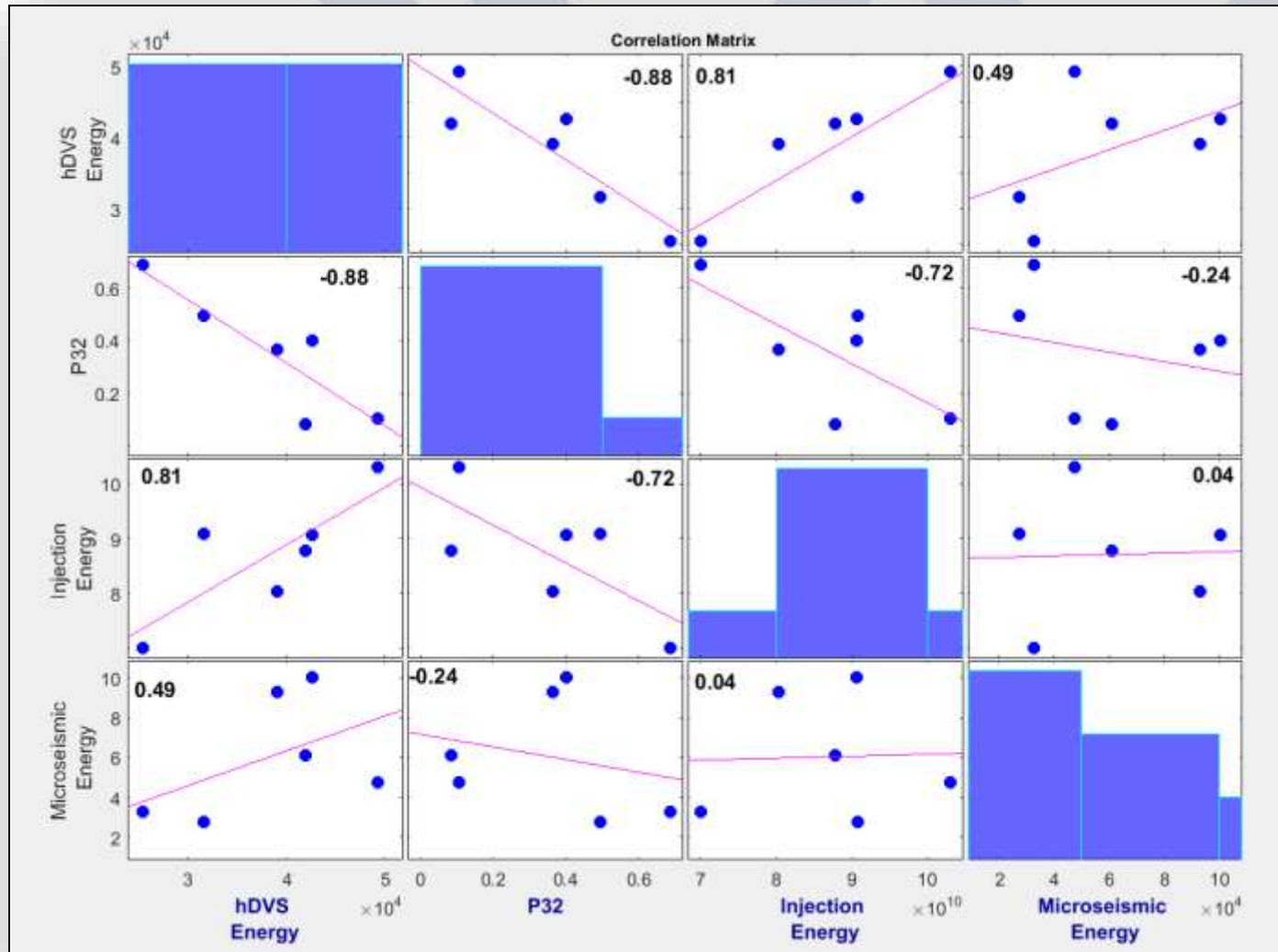
May 2016



Sept 2016

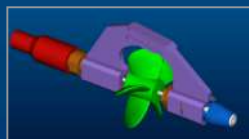


Microseismic, Injection Energy & Fractures



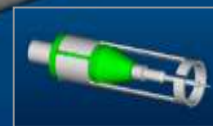
Horizontal Production Logging Schlumberger Flow Scanner (FSI)

Standard Tool: OD 1-11/16 in.



Fluid velocity

Five
Mini-Spinners



Six GHOST*
Optical probes

Gas holdup



Six DEFT*
Electrical probes

Water holdup

Real-Time Acquisition

Standard Assembly: 35.3 ft



Basic Measures: GR, CCL, CALI, DEVI, RB, Pressure, Temperature
Department of Geology and Geography

MSEEL Plans

● Production Logging During Winter

● Thin Data Analysis and Prediction

★ Drilling Parameters

★ Image Processing

● Continued Work on Core

★ Geochemistry

★ Geomechanics

★ Pore Networks

● Reservoir Modeling

★ Nano-Scale to Reservoir Scale

★ Geomechanical

★ Flow Simulation

● Integration Across Disciplines



Building Partnerships for Research, Education, and Outreach

Industry

MSEEL

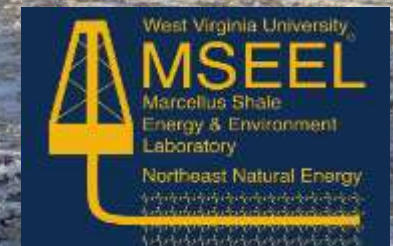


Community

Academia

Government

Tim Carr
Phone: 304.293.9660
Email: tim.carr@mail.wvu.edu



Appendix 2 – MSEEL Project Context: State of the Region

Regional Research Institute West Virginia University

Resource Document Series



MSEEL Project Context: State of the Region (2001-2014)

Caleb Stair, Regional Research Institute, West Virginia University;
Sriparna Ghosh, Regional Research Institute, West Virginia University;
Randall Jackson, Director, Regional Research Institute and Professor,
Department of Geography, West Virginia University.

RRI Resource Doc 2017-01

Date submitted: January 30, 2017

Key words/JEL Codes: Regional Economics, Regional Analysis,
Energy Economics, Environmental Economics; Q41, Q42, Q48, Q55

MSEEL Project Context: State of the Region (2001-2014)

Caleb Stair*
Sriparna Ghosh †
Randall Jackson‡

January 30, 2017

Contents

1	Introduction	3
2	General Data	4
2.1	Employment	4
2.2	Unemployment and Per Capita Personal Income	8
2.3	Gross Product and Per Capita GDP	12
3	Mining and Related Activities	13
3.1	Fracking Overview and Gas Production	13
3.2	Focus on mining and related activities	16
4	Summary	18
A	Data	20

*Regional Research Institute and Department of Agricultural and Resource Economics. West Virginia University. E-mail: Caleb.Stair@mail.wvu.edu

†Regional Research Institute and Department of Economics. West Virginia University. E-mail: Sriparna.Ghosh@mail.wvu.edu

‡Director, Regional Research Institute, and Professor, Department of Geology and Geography, West Virginia University. E-mail: Randall.Jackson@mail.wvu.edu

Abstract

The Marcellus Shale Energy and Environmental Laboratory, or MSEEL is the nation's first integrated research initiative on shale gas drilling. An experimental hydraulic fracturing gas well is the centerpiece of the MSEEL project, "which West Virginia University launched in fall 2014 in partnership with Northeast Natural Energy, the National Energy Technology Laboratory of the U.S. Department of Energy and Ohio State University. The five-year, \$11 million project is the first-ever long-term, comprehensive field study of shale gas resources in which scientists will study the process from beginning-to-end.¹" Because one dimension of the MSEEL analysis is the economic impacts and implications of well-drilling activity, this report has been prepared to provide a statistical overview and description of the local and regional economies leading up to the initiation of the MSEEL project, and to set the stage generally for subsequent socioeconomic analyses. The report includes various graphs and tables that describe the local economy during the 2001 to 2014 period, providing a context within which to view the role of gas extraction activities in the economy.

¹ "Drilling to begin at experimental science well to be monitored by WVU, OSU researchers," Posted: Jun 26, 2015 10:55 AM EDT, Updated: Jul 26, 2015 10:55 AM EDT State Journal. <http://www.statejournal.com/story/29416633/drilling-to-begin-at-experimental-science-well-to-be-monitored-by-wvu-osu-researchers>

1 Introduction

Several major events in U.S. history occurred during the 2001-2014 period. The period began with the catastrophic 9/11 terrorist attacks that arguably shaped other financial and political events of subsequent years. That September event was unprecedented in U.S. history. It marked only the third time in history that the New York Stock Exchange was shut down for a period of time. In this case, it was closed from September 10 - 17. Besides the tragic human loss of that day, the economic losses were high. Some estimate that there was over \$60 billion in insurance losses alone (Waugh, 2007). Approximately 18,000 small businesses were either displaced or destroyed in Lower Manhattan after the Twin Towers fell (Waugh, 2007). There was a buildup in homeland security on all levels. 9/11 was a catastrophic financial loss for the U.S. After the 9/11 terrorist attacks, the War on Terror was launched in Afghanistan and the Iraq War was launched shortly after in 2003. The cost of these wars is ongoing. In 2008, the Congressional Research Service had approved about \$944 billion for the operations overseas (Fitzgerald and Cordesman, 2008). This has placed an incredible financial strain on the economy and it is impossible to know what the final cost will be at this time.

Severe weather also played a role during this era. On August 25, 2005, Hurricane Katrina hit the Gulf Coast of the U.S. as a strong Category 3 or low Category 4 storm (Jonkman et al., 2009). It quickly became the biggest natural disaster in U.S. history, almost destroying New Orleans due to severe flooding (Jonkman et al., 2009). Hurricane Rita quickly followed Katrina only to make matters worse. Between the two, more than \$200 billion in damage was done (Plyer, 2016). 400,000 jobs were lost and 275,000 homes were destroyed (Plyer, 2016). Many of the jobs and homes were never to be recovered. Hundreds of thousands of people were displaced and over 1,000 were killed and more are missing (Plyer, 2016). The effect on oil and gasoline prices was long-lasting.

Financial issues also took a toll on the U.S. economy during this period. In September of 2008, a seemingly perfect storm of factors came together to engage the deepest economic downturn in not only the U.S., but across the globe, since the Great Depression (Stiglitz, 2010). The great investment banks that had stood on Wall Street began to collapse due to the sub-prime mortgage crisis and serious corporate fraud (Palley, 2011). During the last months of the Bush Administration, the federal government stepped in to bail out some of these institutions in order to keep the U.S. financial system afloat (Stiglitz, 2010). By the time the Obama Adminis-

tration reached the White House in January of 2009, the economy had contracted and the recession had taken hold. At the end of 2009, there are signs of recovery, but the process was slow (Palley, 2011). A few years later, the Affordable Care Act (Obamacare) began registering people for the expanded federal government health insurance program in 2013. This was in spite of a variety of waivers and problems in implementing the cumbersome rules and regulations of the program. Various states decided to allow the federal government to run the exchanges for them, while some states and the District of Columbia set up their own exchanges to sell the policies (Jones et al., 2014).

2 General Data

2.1 Employment

West Virginia’s top five largest private employers are Wal-Mart, West Virginia United Health System, Charleston Area Medical Center, Kroger, and Mylan Pharmaceuticals. The ranking of the top five employers was unchanged from 2014. The retail giant Wal-Mart has been the state’s largest private employer since 1998.

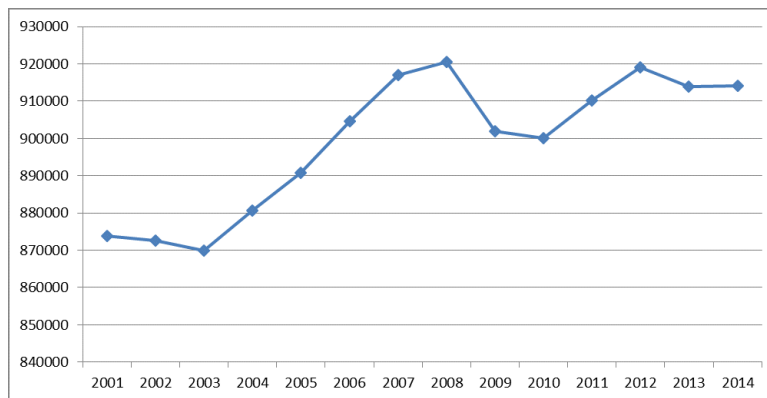


Figure 1: Total Employment (West Virginia)

A 2013 study indicated that 8.9 percent of employment in West Virginia was created by the oil and natural gas industry (PricewaterhouseCooper, 2013). The industry directly employed 35,925 people, or four percent of total state employment. Indirectly, the industry employed 22,374 people and induced 22,102 jobs (PricewaterhouseCooper, 2013). As Figure #1 shows West Virginia Experienced a sharp

increase in employment. This corresponded with the start of fracking’s new golden age as oil and gas producers began to explore the nation’s shale formations in earnest (Higginbotham et al., 2010).

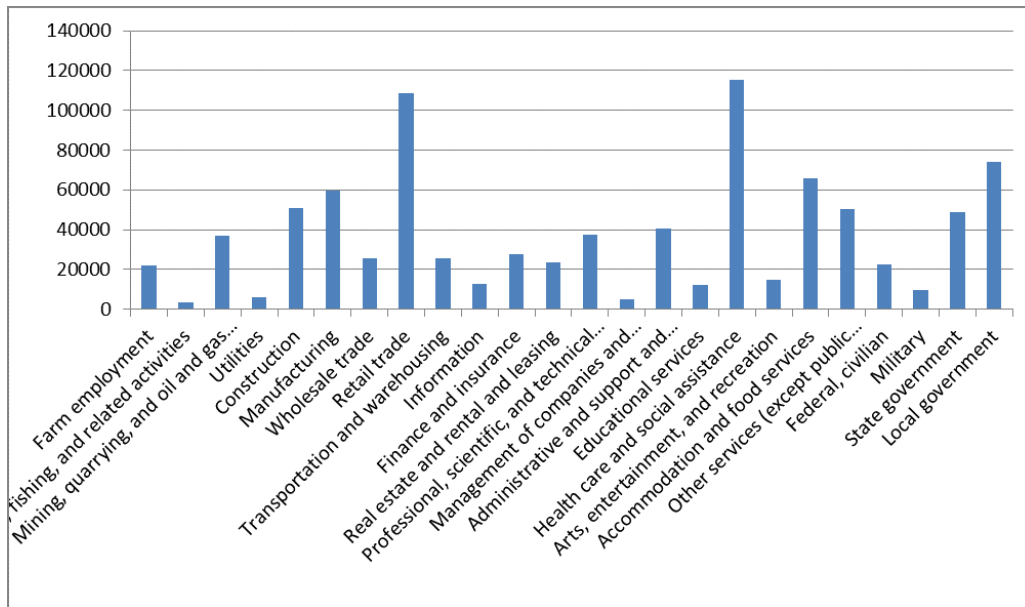


Figure 2: West Virginia: Average Sector Employment (2001-2014)

The most common industries in West Virginia by number of employees are Health Care and Social Assistance; Retail Trade; and Local Government. Compared to other states, West Virginia has an unusually high number of employees in the Mining sector (O’Leary and Boettner, 2012).

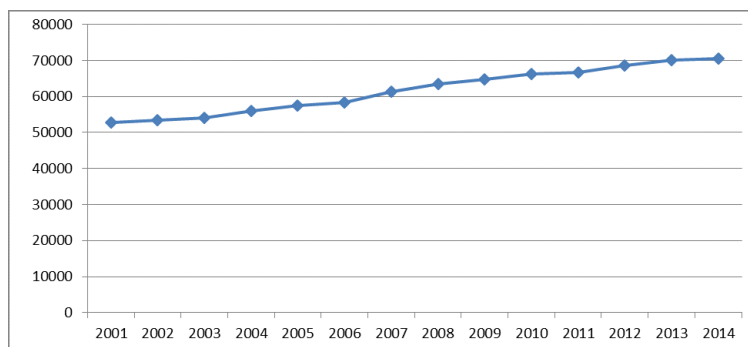


Figure 3: Monongalia: Total employment (number of jobs)

The top five employers in Monongalia County, the site of the experimental well, are West Virginia University, West Virginia University Hospitals, Mylan Pharmaceuticals, Inc., Monongalia County Board of Education and Monongalia General Hospital. Total employment in the county has steadily increased over the 2001-2014 time period reflecting its concentration in economically consistent sectors².

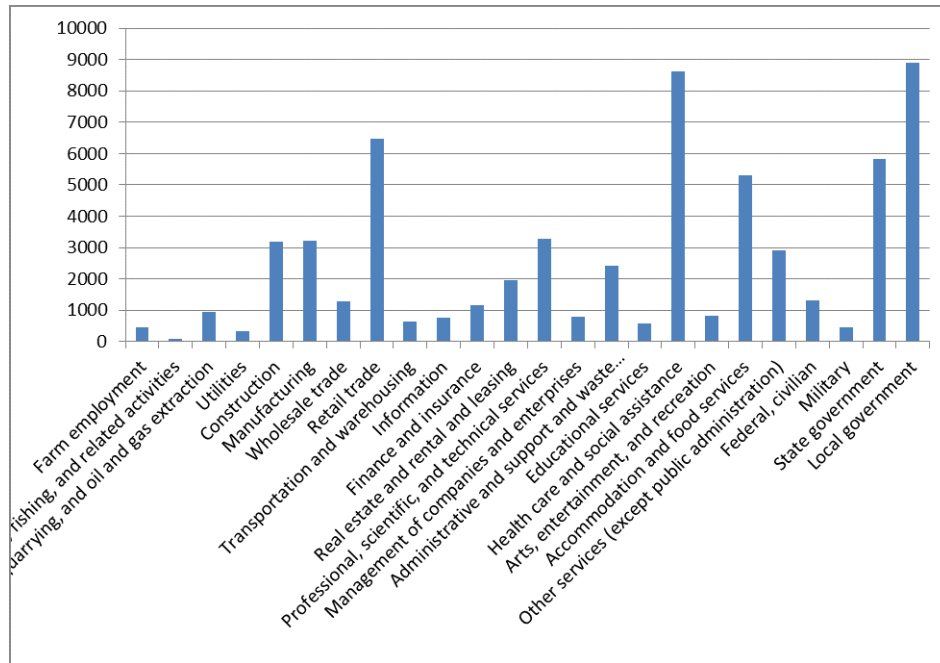


Figure 4: Monongalia: Average Sector Employment (2001-2014)

The most common industries in Monongalia County, WV by number of employees are Healthcare & Social Assistance; Retail trade; and Local Government. Its economy is driven by health and education resources, which are concentrated there in the city of Morgantown. West Virginia University (WVU), along with major hospitals and related health and social services, together generate almost 40% of the county’s jobs (Hammond, 2011).

²Health care and social assistance is listed as a recession resistant sector by the BEA and BLS.

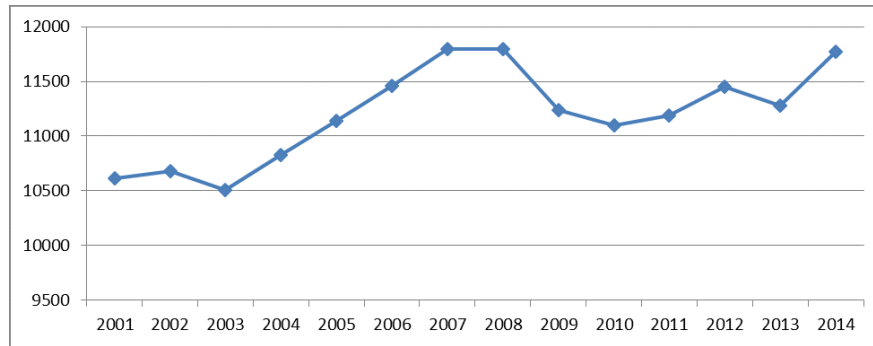


Figure 5: Preston: Total employment (number of jobs)

The top five employers in Preston County are the US Department of Justice, Preston County Board of Education, Preston Memorial Hospital, CW Wright Construction Company, Inc. and Wal-Mart Stores, Inc. The graph of total employment in Figure #5 closely mirrors that of state total employment in Figure #1. Preston started feeling the effects of the recession as early as 2008. The county experienced losses in total employment for the next two years. Fortunately in 2011 there was a rebound in job growth for Preston County.

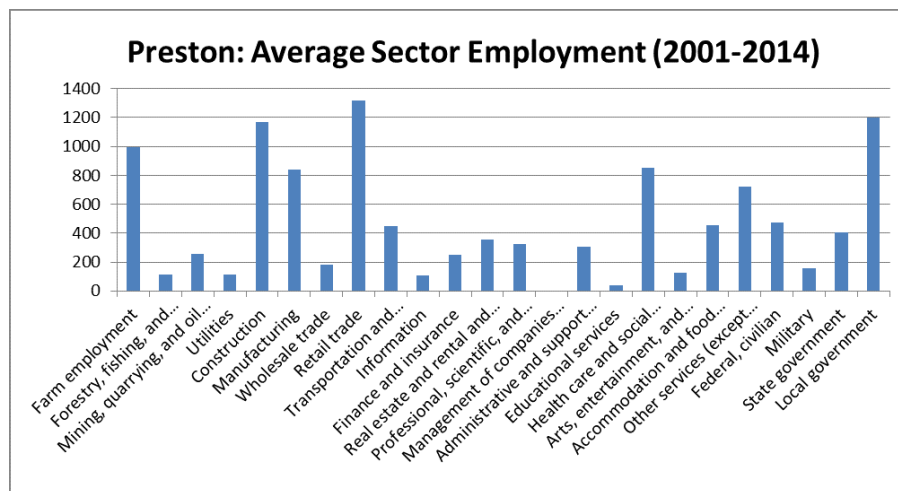


Figure 6: Preston: Average Sector Employment (2001-2014)

The most common industries in Preston County, WV by number of employees are Retail trade; Construction; and Local Government. The United States Penitentiary, Hazelton is a major employer in the state. It is a \$129 million high security facility

with a satellite minimum security prison camp. The rural West Virginia County also has a significant amount of farm employment.

2.2 Unemployment and Per Capita Personal Income

The recession began to affect West Virginia employment in October of 2008. Between October 2008 and January 2010, West Virginia lost 32,400 jobs. Since then, the state has slowly added 11,600 jobs. While the situation does seem to be improving there has been little effect on the unemployment rate. The unemployment rate in 2014 at 6.6 percent is about one-third higher than the 2007 level.

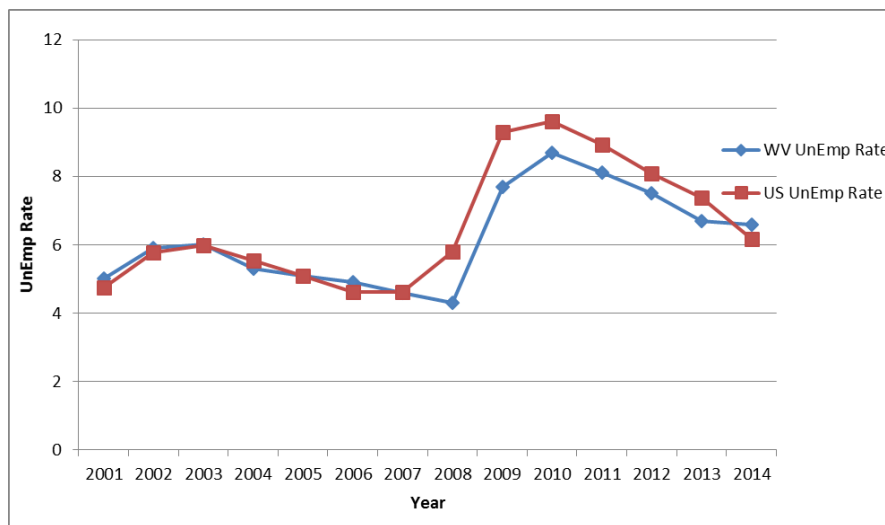


Figure 7: West Virginia v. US Unemployment Rate (2001-2014)

Further, the recovery has been unbalanced, with a net loss of jobs that paid high- or mid-level wages and a net increase of low-paying jobs. Of all the industries in the state, manufacturing and construction suffered the most. Construction saw a loss of 7,800 jobs, representing almost a quarter of all jobs lost. Manufacturing lost 7,200 jobs, over 22 percent of all jobs lost. Manufacturing jobs were already on the decline, the recession only accelerated the loss.

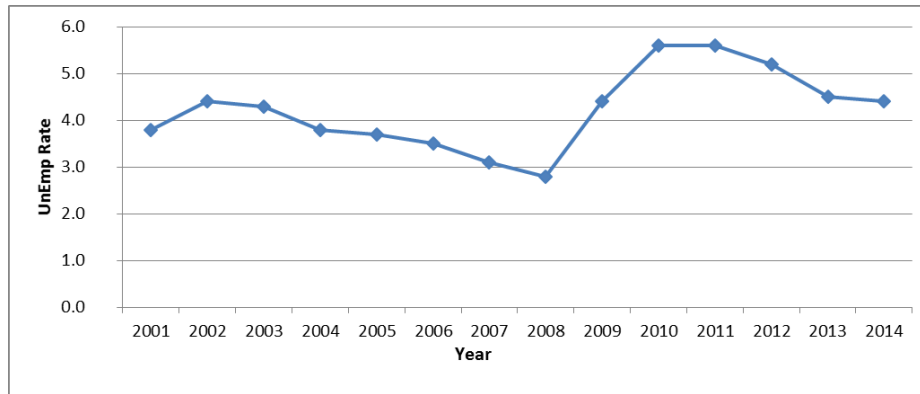


Figure 8: Monongalia Unemployment Rate (2001-2014)

Monongalia County has maintained a comparatively low unemployment rate over the 2001-2014 period. This is because Monongalia County, while having significant coal production, is primarily dependent on other sources of personal income. This income stems from education and health industries³. The economic conditions of the past few years have been extremely kind to employment needs in Monongalia County relative to the rest of the country. Unemployment rates were below five percent from 2001 to 2009 and below six percent for the entire 2001-2014 period. Monongalia County is well below the averages for West Virginia and the United States over the past ten years.

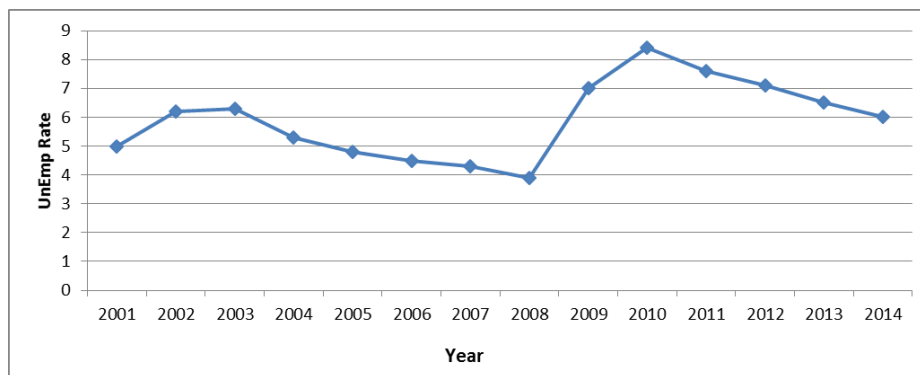


Figure 9: Preston Unemployment Rate (2001-2014)

Preston County suffered during the recession because it had a large number of construction jobs⁴. The county began to feel the effects of the recession as early

³Like West Virginia University and West Virginia University Hospitals.

⁴The CW Wright Construction Company is a major employer in the county.

as 2008 with an unemployment rate over 8% in 2010. However, like its neighbor Monongalia County, it has a large Healthcare & Social Assistance industry. The Hazelton Penitentiary also helped the county recover in the post-recession economy (Hammond, 2011).

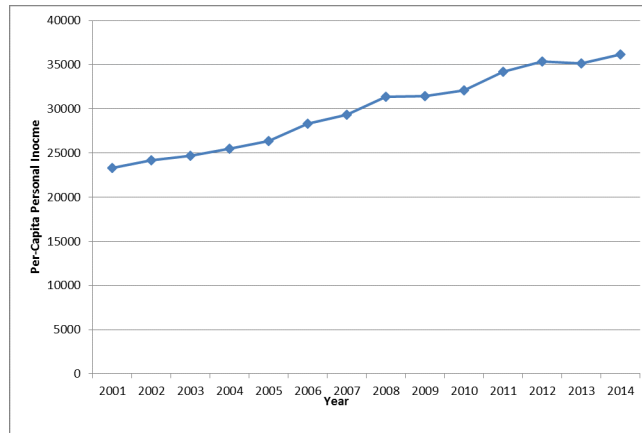


Figure 10: West Virginia Per-Capita Personal Income (2001-2014)

Historically, West Virginia has been one of the poorest states. It was the second poorest state in the United States of America in 2014. Its per capita personal income levels have lagged behind that of the nation for years. However, West Virginia’s Per capita personal income has steadily increased over the 2001-2014 period (Figure #10). In 2010, West Virginia’s personal income growth expanded while the national average fell 2.6 percent. There is a worry of a resource curse in the state. This happens where a reliance on extraction of natural resources ultimately lowers overall economic well-being (Higginbotham et al., 2010).

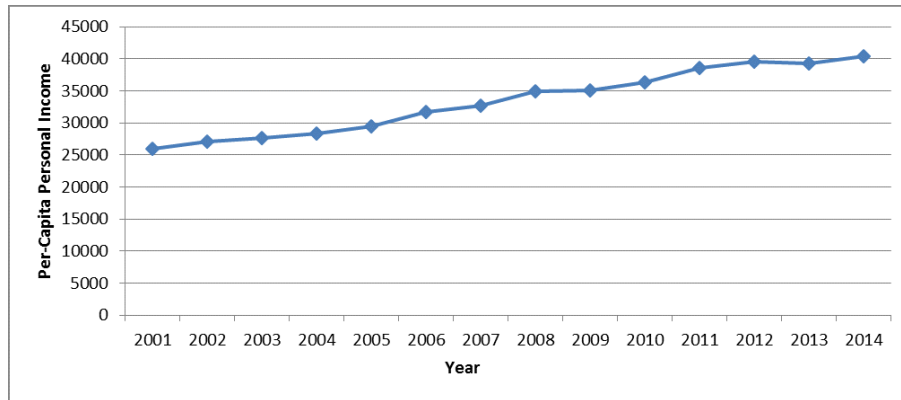


Figure 11: Monongalia, WV Per-Capita Personal Income (2001-2014)

Monongalia County has been above West Virginia in per capita income for the last few decades. By 2009, that difference had grown to 13.6%. Much of this disparity can be attributed to the multiplier effect of having West Virginia University and related services and facilities in Monongalia County. As shown by Figure #11, per capita income has increased steadily over the 2001-2014 period.

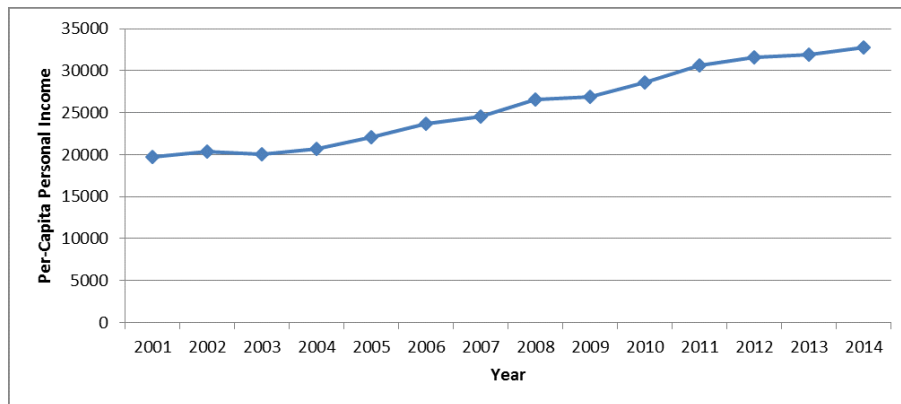


Figure 12: Preston, WV Per-Capita Personal Income (2001-2014)

Per-Capita income in Preston, WV has lagged behind the state and its neighbor Monongalia County. This is largely because its employment is in lower income industries. Figure #12 shows that the per capita income has steadily increased over the 2001-2014 period.

2.3 Gross Product and Per Capita GDP

West Virginia’s GDP is shown above in Figure #13. It has steadily increased over the 2001-2014 time period. Natural resources have played an important role in West Virginia’s economy for more than a century. With the discovery of coal and natural gas, extractive industries like mining and drilling developed to remove these resources, especially in the state’s more remote areas. West Virginia remains an energy state, with an estimated 11% of its gross state product coming from extractive industries.

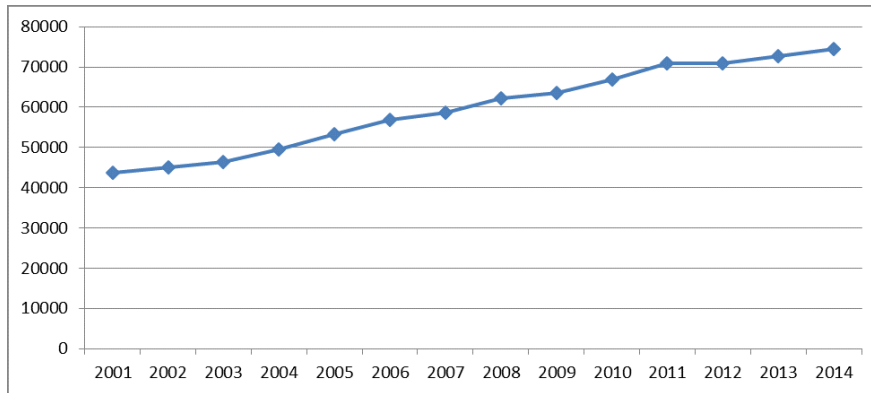


Figure 13: West Virginia: GDP (millions of current dollars)

The Morgantown Metropolitan Statistical Area (MSA), which includes both Monongalia and Preston Counties, continues to post solid growth in jobs and income. Figure #14 above shows that Per Capita Real GDP has consistently grown over the 2001-2014 period. These important indicators of an area’s economic strength have surged in the Morgantown MSA during the last two decades and its unemployment rate has remained low(Hammond, 2011). One of the reasons that the economy of the Morgantown MSA fared much better than the rest of the country in recent years is that it is heavily weighted toward higher education and health care employment which are growing and relatively recession resistant sectors (Hammond, 2011).

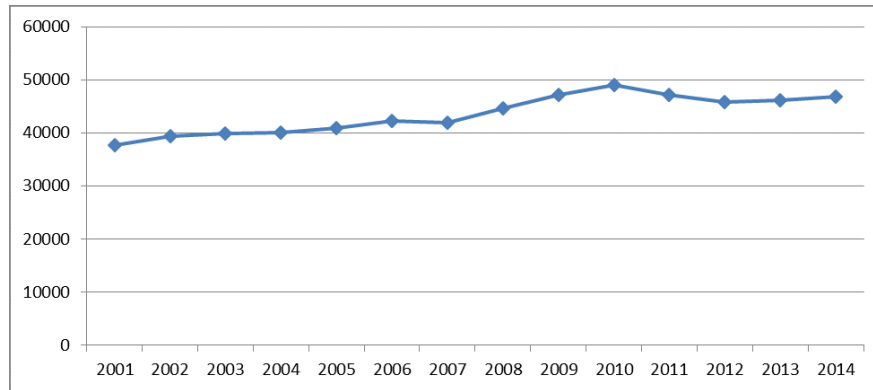


Figure 14: Morgantown, WV (MSA) Per Capita Real GDP

3 Mining and Related Activities

3.1 Fracking Overview and Gas Production

Fracking is the process of producing natural gas by injecting a mixture of water, sand and chemicals into the rock at high temperature and pressure. West Virginia also produces large amounts of natural gas. West Virginia is located in the heart of the Marcellus Shale Natural Gas Bed, which stretches from Tennessee north to New York in the middle of Appalachia (Moss, 2008). The Marcellus Shale is a major source of production of natural gas and oil and underlies an extensive area in West Virginia. In 2002, the United States Geological Survey (USGS) found that the Marcellus Shale contains about 1.9 trillion cubic feet of natural gas (USGS, 2002).

According to the U.S. Energy Information Administration (EIA), West Virginia has crude oil, natural gas, and coal bed methane and shale gas reserves. West Virginia is part of the Appalachian basin. Concerns about state losing coal jobs are being offset by the growth in the natural gas industry. Although West Virginia has benefited from natural gas drilling for many years, the recent discovery of the Marcellus Shale has set off a drilling boom. As a whole, the state’s natural resource extraction employment outlook is healthy.

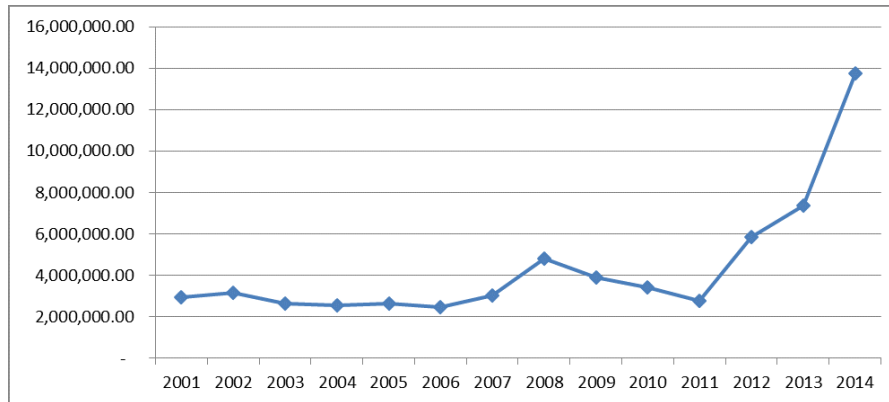


Figure 15: Monongalia, WV Gas Production (MCF)

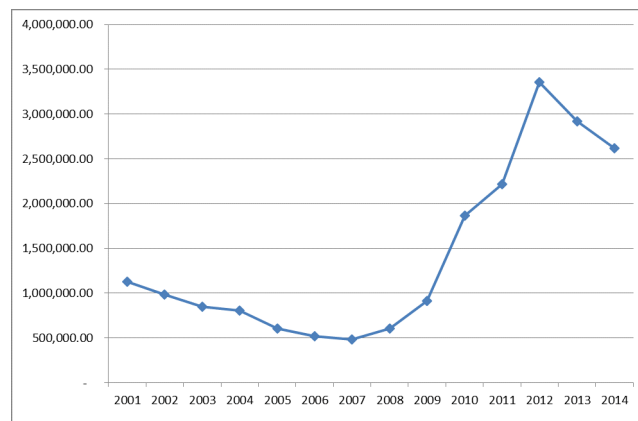


Figure 16: Preston, WV Gas Production (MCF)

As Figure #15 shows, gas production in Monongalia County has experienced rapid expansion over the last three years. Meanwhile, gas production in Preston County has fallen for the last three years. According to Drilling Edge there are currently 13 producing operators in Preston County and 21 producing operators in Monongalia County.

In 2002, the state issued one Marcellus Shale drilling permit. In 2008, over 800 permits were issued (Higginbotham et al., 2010). In 2009, however, only 426 permits were issued for wells⁵. Only 125 of those wells were actually drilled (Symonds and Jefferis, 2009). Currently, there are over 1,200 active Marcellus drilling sites in West

⁵ A combination of horizontal and vertical wells.

Table 1: Well Permits in Monongalia, WV

County	Permit status	Well Type	Year	Number of Wells
Monongalia	Application received	Horizontal	2011	8
Monongalia	Permit commenced	Horizontal	2011	6
Monongalia	Permit completed	Horizontal	2011	6
Monongalia	Permit issued	Horizontal	2011	7
Monongalia	Application received	Horizontal	2014	1
Monongalia	Application received	Vertical	2014	18
Monongalia	Permit commenced	Vertical	2014	2
Monongalia	Permit completed	Vertical	2014	2
Monongalia	Permit issued	Horizontal	2014	1
Monongalia	Permit issued	Vertical	2014	18

Table 2: Well Permits in Preston, WV

County	Permit status	Well Type	Year	Number of Wells
Preston	Application received	Horizontal	2011	14
Preston	Application received	Vertical	2011	2
Preston	Permit commenced	Vertical	2011	5
Preston	Permit commenced	Horizontal	2011	5
Preston	Permit completed	Horizontal	2011	5
Preston	Permit completed	Vertical	2011	5
Preston	Permit issued	Vertical	2011	1
Preston	Permit issued	Horizontal	2011	11
Preston	Application received	Horizontal 6A	2014	18
Preston	Permit issued	Horizontal 6A	2014	13

Table 3: Drilling in Preston, WV and Monongalia, WV

County	Year	Well Status	Well Type	Numbers
Monongalia	2011	Active well	Horizontal	7
Monongalia	2014	Active well	Horizontal 6A	2
Monongalia	2014	Permit issued	Horizontal 6A	17
Preston	2011	Active well	Horizontal	4
Preston	2014	Permit issued	Horizontal 6A	12

Virginia (Higginbotham et al., 2010). Table #1 shows that recent applications and permits in Monongalia County have been for conventional vertical and horizontal gas wells. Conversely, Table #2 shows that recent applications and permits in Preston County have been for horizontal 6A wells.⁶

3.2 Focus on mining and related activities

One of the major resources in West Virginia’s economy is coal. According to the Energy Information Administration (EIA), West Virginia is the second-leading coal producer in the United States (behind Wyoming), and the top coal-producing state in Appalachia. West Virginia’s historical ties with the coal industry have strongly influenced the economic, political, and social structures of the state. Nearly all of the electricity generated in West Virginia is from coal-fired power plants. West Virginia produces a surplus of electricity and leads the Nation in net interstate electricity exports. While some may attribute coal industry woes to a regulatory “war on coal,” other factors such as cheap natural gas and competition from other coal markets are driving forces.

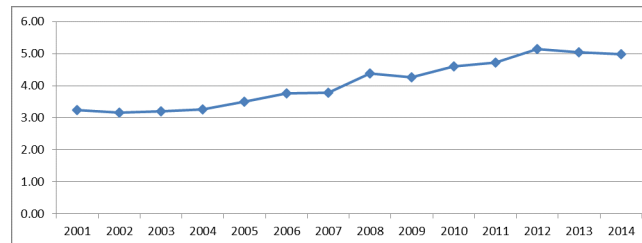


Figure 17: West Virginia Mining’s portion of total employment (2001-2014)

Mining’s portion of total state employment consistently increased from 2001-2012 with a slight drop in 2013 and 2014⁷. This is shown above in figure #17. The state is facing both an energy boom in north-central West Virginia and a coal bust in the south. Between 2008 and 2013, state coal production declined by 28% and almost 5,000 coal mining jobs has been lost (AFSC, 2014). Meanwhile, the north-central part of the state has seen an increase in coal and natural gas and oil jobs over the past five years.

⁶Article 6A of W.Va Code § 22-6A-12 applies to Natural gas well drilled using a horizontal drilling method that disturbs three acres or more, excluding pipelines, gathering lines and roads, or utilizes more than 210,000 gallons of water in any 30-day period.

⁷In this case Mining is comprised of mining, quarrying, and oil and gas extraction industries

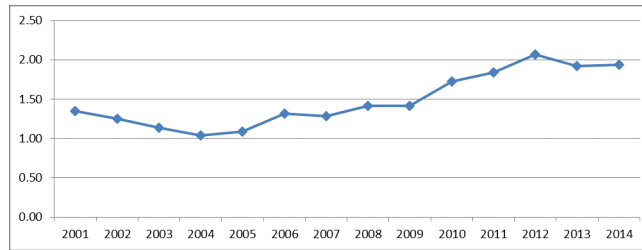


Figure 18: Monongalia, WV Mining’s portion of total employment (2001-2014)

Mining employment in Monongalia County followed a similar path as the state for the 2001-2014 period⁸. Mining’s portion of total state employment declined from 2001-2004, increased from 2005-2012, and dropped slightly in 2013 and 2014. In 2010, there were four companies operating underground mining operations at five mines. Notably, mining’s portion of total employment in the county is rather low. Only in 2012 was the portion higher than 2%.

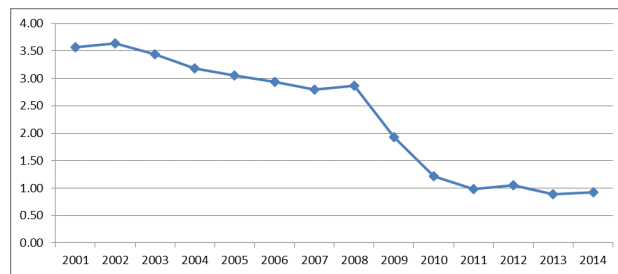


Figure 19: Preston, WV Mining’s portion of total employment (2001-2014)

Mining employment in Preston, WV steadily declined from 2001-2008⁹. In 2008 there beginning of a sharp decline in mining employment began. Alpha Natural Resources, Inc. announced that its subsidiary, Kingwood Mining Company, LLC, would cease coal mining operations at the Whitetail Kittanning mining complex in Preston County, WV at the end of December, 2008. Additionally, efforts by steel producers to match production capacity to declining demand for steel products prompted them to reduce their raw material requirements. These events lead to the sharp decrease in mining employment in Preston, WV.

⁸In this case Mining is comprised of mining, quarrying, and oil and gas extraction industries

⁹In this case Mining is comprised of mining, quarrying, and oil and gas extraction industries

4 Summary

West Virginia's economic recovery from the Great Recession has been assisted by growth in the state's natural gas and oil industries. Sadly, several of the jobs West Virginia lost in the recession may not come back. Manufacturing and non-durable goods production represented over a quarter of the jobs lost in the recession. Both of these sectors have been steadily losing jobs for over a decade. It may take a long time for those sectors to recover to pre-recession levels.

Meanwhile, the Morgantown Metropolitan Statistical Area (MSA), which includes both Monongalia and Preston Counties, continues to show growth in jobs and income. It has fared better than the rest of the country and state in recent years. The Morgantown MSA did not see large employment declines during the recession. Even at the height of the recession, employment growth in the Morgantown MSA was above 1.5 percent, and only fell off in 2011 when it grew by 0.7 percent. This is primarily because it is geared toward higher education and health care employment. These sectors are growing and relatively recession resistant.

References

- AFSC (2014). Economic Recovery and Transition in the Mountain State: State's Energy Economy Shifts north. Technical report.
- Fitzgerald, E. and Cordesman, A. (2008). Resources for Defeat: Critical Failures in Planning, Programming, Budgeting and Resourcing the Afghan and Iraq Wars. Technical report, Center for Strategic and International Studies.
- Hammond, G. W. (2011). Morgantown MSA Economic Monitor: Morgantown Leads State and Nation. Technical report, Bureau of Business and Economic Research.
- Higginbotham, A., Pellillo, A., Gurley-Calvez, T., and Witt, T. S. (2010). The Economic Impact of the Natural Gas Industry and the Marcellus Shale Development in West Virginia in 2009. Technical report, West Virginia University.
- Jones, D. K., Bradley, K. W., and Oberlander, J. (2014). Pascal's Wager: Health Insurance Exchanges, Obamacare, and the Republican Dilemma. *Journal of Health Politics, Policy and Law*, 39(1):97–137.

- Jonkman, S. N., Maaskant, B., Boyd, E., and Levitan, M. L. (2009). Loss of life caused by the flooding of New Orleans after Hurricane Katrina: analysis of the relationship between flood characteristics and mortality. *Risk Analysis*, 29(5):676–698.
- Moss, K. (2008). Potential development of the natural gas resources in the Marcellus Shale: New York, Pennsylvania, West Virginia and Ohio. *Denver, CO: National Park Service, US Department of the Interior, Geologic Resources Division.*
- O’Leary, S. and Boettner, T. (2012). In Depth: The Gas Boom and Coal Bust. Technical report, West Virginia Center on Budget and Policy.
- Palley, T. (2011). America’s flawed paradigm: macroeconomic causes of the financial crisis and great recession. *Empirica*, 38(1):3–17.
- Plyer, A. (2016). Facts for Features: Katrina Impact.
- PricewaterhouseCooper (2013). Economic Impacts of the Oil and Natural Gas Industry on the US Economy 2011. Technical report.
- Stiglitz, J. E. (2010). Interpreting the causes of the great recession of 2008. *Financial System and Macroeconomic Resilience: Revisited. Bank for International Settlements.*
- Symonds, J. E. and Jefferis, N. N. (2009). Thinking Horizontally in a Vertical World: Practical Considerations for Practitioners Advising Clients on Horizontal Development in the Marcellus and Big Sandy Fields. *Energy Miner Law Institute*, 30:417–445.
- USGS (2002). Assessment of Undiscovered Oil and Gas Resources of the Appalachian Province. Technical report.
- Waugh, W. L. (2007). Terrorism as disaster. In Rodríguez, H., Quarantelli, E. L., and Dynes, R. R., editors, *Handbook of Disaster Research*. 388-404. Springer.

A Data

Bureau of Economic Analysis. CA25N: Total Full-Time and Part-Time Employment by NAICS Industry.

Bureau of Economic Analysis. CA5N: Personal Income by Major Component and Earnings by NAICS Industry.

Bureau of Economic Analysis. GDP by Metro Statistical Area for all areas and components.

Bureau of Economic Analysis. Quarterly Gross Domestic Product by State

Drilling Edge. Oil & Gas Production in Monongalia County, WV. <http://www.drillingedge.com/west-virginia/monongalia-county>

Drilling Edge. Oil & Gas Production in Preston County, WV. <http://www.drillingedge.com/west-virginia/preston-county>

URTeC: 2670437

Insights from the Marcellus Shale Energy and Environment Laboratory (MSEEL)

Timothy R Carr*, Thomas H. Wilson, Payam Kavousi, Shohreh Amini, Shikha Sharma, West Virginia University: Jay Hewitt, Ian Costello, B. J. Carney, Emily Jordon, Northeast Natural Energy LLC: Malcolm Yates, Keith MacPhail, Natalie Uschner, Mandy Thomas, Si Akin, Oluwaseun Magbagbeola, Adrian Morales, Asbjorn Johansen, Leah Hogarth, Olatunbosun Anifowoshe, Kashif Naseem, Schlumberger: Richard Hammack, Abhash Kumar, Erich Zorn, Robert Vagnetti, and Dustin Crandall, National Energy Technology Laboratory, US Department of Energy.

Copyright 2017, Unconventional Resources Technology Conference (URTeC) DOI 10.15530-urtec-2017-2670437

This paper was prepared for presentation at the Unconventional Resources Technology Conference held in Austin, Texas, USA, 24-26 July 2017.

The URTeC Technical Program Committee accepted this presentation on the basis of information contained in an abstract submitted by the author(s). The contents of this paper have not been reviewed by URTeC and URTeC does not warrant the accuracy, reliability, or timeliness of any information herein. All information is the responsibility of, and, is subject to corrections by the author(s). Any person or entity that relies on any information obtained from this paper does so at their own risk. The information herein does not necessarily reflect any position of URTeC. Any reproduction, distribution, or storage of any part of this paper without the written consent of URTeC is prohibited.

Summary

The Marcellus Shale Energy and Environment Laboratory (MSEEL) involves a multidisciplinary and multi-institutional team undertaking integrated geoscience, engineering and environmental research in cooperation with the operator, Northeast Natural Energy LLC., numerous industrial partners and the National Energy Technology Laboratory of the US Department of Energy. The objective of MSEEL is to provide a long-term collaborative field site to develop and validate new knowledge and technology that can improve recovery efficiency while minimizing environmental implications of unconventional resource development

MSEEL consists of two legacy horizontal production wells completed in 2011, two new logged and instrumented horizontal production wells completed in 2015, a cored vertical pilot bore-hole, a microseismic observation well, and surface geophysical and environmental monitoring stations (Figure 1). Production from the new horizontal wells began in December 2015 and monitoring continues. Production logging to determine production efficiency was undertaken in early 2017 and is under evaluation. MSEEL has generated a large and diverse (multiple terabyte) dataset that provides significant insight into drilling operations, Marcellus Shale geology and fracture stimulation operations.

During drilling detailed geomechanical and image logs of the lateral and geochemical analysis of the whole core and sidewall cores were obtained. As part of the core analysis, kerogen was extracted from the different zones and analyzed to understand hydrocarbon generative potential, and interaction of the organic and inorganic matrix components with the fracture stimulation fluids (Agrawal et al., 2016; Agrawal et al., 2017; Agrawal and Sharma, 2017; Sharma et al., in press). Core and log data were coupled with microseismic and slow-slip seismic monitoring, and distributed temperature sensing (DTS) and distributed acoustic sensing (DAS) fiber-optic monitoring during completion. Subsequent production logging and continued DTS monitoring show the influence and interaction in the Marcellus Shale of both the present stress regime oriented northeast-southwest and the numerous preexisting healed and calcite cemented fractures oriented approximately east-west. The analysis of the comprehensive cluster-by-cluster completion data derived from surface and subsurface from the MSEEL project has contributed to an improved understanding of the effect of stage spacing and cluster density practices that could be used to significantly improve stimulation effectiveness and optimize recovery efficiency in the Marcellus and other unconventional reservoirs. The results provide an unprecedented picture of subsurface rock properties, stimulated reservoir volumes, faults and fracture systems. Understanding the distribution and strong influence of preexisting

fractures is demonstrated to lead to improved completions in an individual well, and strategies to improve completions across the southern portions of the Marcellus Shale play. Overall MSEEL is working to develop and validate new knowledge and technology and identify best practices for field implementation that can optimize hydraulic fracture stimulation and minimize environmental impacts of unconventional resource development.

Introduction

The Marcellus Shale Energy and Environment Laboratory (MSEEL) consists of a multidisciplinary and multi-institutional team undertaking integrated geoscience and engineering in cooperation with the operator Northeast Natural Energy, LLC., numerous industrial partners, and the Department of Energy. MSEEL consists of two legacy horizontal production wells (MIP 4H and MIP 6H) drilled in 2011, two new logged and instrumented horizontal wells (MIP-3H and MIP-5H) drilled and completed in 2015, a cored and logged vertical pilot bore-hole (MIP-3H), and a microseismic observation well (MIP-SW) (Figure 1). Production from the new horizontal wells began in December 2015 and is available online (<http://www.mseel.org>). Production is limited by pipeline distribution and consumption in the City of Morgantown, but the MIP wells are capable of producing multiple millions of cubic feet per day. MSEEL has integrated geophysical observations (microseismic and surface), fiber-optic monitoring for distributed acoustic sensing (DAS) and distributed temperature sensing (DTS) in the MIP-3H, advanced well logs, core data and production monitoring, to better characterize subsurface rock properties, and propagation pattern of induced fractures in the stimulated reservoir volume. We will concentrate on the evaluation of the completion efficiency of the MIP-3H undertaken in late 2015.

Data and Methods

Multistage hydraulic fracture stimulation is a required for viable production from unconventional shale-gas and tight-oil reservoirs. In the case of the MIP-3H stimulation over 28 stages involved injection, at high pressure, averaging 8500 psi (58.6 MPa), to break the formation and establish a complex network of permeable fracture pathways, of 1,900 pounds of proppant (20.2 cubic feet) and 1,760 gallons of fluid (235.3 cubic feet) along every foot of the 6,058 feet (1846m) of completed lateral (~255 cubic feet per foot of lateral, 23.7 cubic meters/meter). Generally, reservoir stimulation is thought to be associated with reactivation of pre-existing faults and fractures, with minor contribution from creation of new hydraulic fractures (Moos et al., 2011; Das & Zoback, 2013). Pre-existing natural fractures appear to affect the stimulation process. Gale et al., (2008) analyzed natural fractures of Barnett Shale core from Pecos County, Texas. The tensile testing on the cores showed failure along fractures even though fractures were sealed. They proposed that the Barnett Shale in the Fort Worth Basin has sealed natural fractures that affect hydraulic fracture propagation. This could be a result of reactivation of natural fractures and hence hydraulic fracture propagation at natural fracture tips. The distribution of microseismic events is most commonly used as a proxy for deformation along pre-existing faults and fracture, and opening of new fractures during hydraulic fracture treatment to outline the shape of stimulated reservoir volume (SRV). Evidence exists both in support of and opposed to microseismic as a method to image the SRV (e.g., Wilson et al., 2016a; Sicking et al., 2013).

The MIP 3H was drilled initially as a pilot, and cored and logged. A total of 111 feet (34m) of core was recovered from the top of the Marcellus Shale to the top of the underlying Onondaga Limestone. Core and related sidewall cores are undergoing analysis for geomechanical properties, geochemistry, porosity and permeability. Computerized tomography (CT) of the vertical core from the MIP-3H pilot hole displays the horizontal laminated nature of the shale and several vertical natural fractures in Marcellus Shale that are calcite cement filled (Figure 2).

The orientation of S_{Hmax} estimated from induced fractures in the Marcellus Shale observed in the vertical pilot hole is N57°E. A comprehensive suite of logs were collected in the vertical pilot hole and used to develop geomechanical properties and log derived parameters (Wilson et al., 2016b and Wilson et al., submitted). The logs being used to calculate geomechanical parameters (Poisson, Young's, Brittleness) are integrated with microseismic parameters (event count, b-value, and moment magnitude (Zorn et al., in press).

The MIP-3H lateral was targeted to and maintained within a 10 foot (3m) zone just above the Cherry Valley Limestone Member of the Marcellus Shale. A wealth of data concerning geomechanical properties, fracture orientation and intensity were acquired (Figure 3). The P32 fracture intensity was calculated using the wireline image logs. Medical computed tomography (CT) scanning of the vertical core from the MIP-3H pilot hole shows

several natural fractures in Marcellus Shale that are mineral filled (Figure 2). More than 1600 resistive (healed) fractures are documented from the wireline image logs in the MIP-3H. Based on image log data obtained in the vertical pilot well, natural fractures are dominated by two sets: a N57°E set consisting largely of open fractures and a N87°E set consisting entirely of healed fractures (Figure 4). Healed calcite-cemented fractures observed in the image log along the length of the lateral number more than 1,600 and have an average trend of N79°E (Figure 3). The first two groups of stages (1-13) were geometric with change in proppant size. The next three groups (14-28) used geomechanical data and fracture intensity acquired by well logging, along the lateral to modify the stage length, cluster spacing and treatment parameters. In addition to a limited entry approach, stages were strategically placed in segments with similar gamma ray, minimum horizontal stress, and natural fracture intensity (Anifowoshe et al., 2016).

MIP-3H completion

The MIP-3H well was completed in five sections from the toe to the heel: A, B, C, D, and E. Sections A and B are completed using a geometrical approach in which geomechanical parameters such as fracture closure stress, fracture intensity are not accounted for. Two types of proppants were used for hydraulic fracturing of MIP-3H: 100 mesh sand and 40/70 white sand. Section A has around 35% 100 Mesh proppants and 65% 40/70 white sand, while Section B has 75% 100 mesh and 25% 40/70 white sand. The completion extends to Section C, named as an engineered completion; Section C is designed by appraising geomechanical parameters from the well logs: each stages is set in a zone with similar fracture closure stress, fracture intensity, and gamma ray (Anifowoshe et al., 2016). The proportion of proppants varies between stages in Section C: Stages 13, 14, 15, 17, and 19 have 35% 100 mesh while Stage 16 has 67% mesh 100 and Stage 18 around 43% mesh 100. In addition, limited entry approach was undertaken by decreasing the number of shots per clusters to enhance stimulation efficiency (Anifowoshe et al., 2016). A new guar-free viscoelastic fracturing fluid known as Sapphire VF140, a trademark of Schlumberger, was used in Stages 20 and 21 (Section D). The Section E, involving stages 22 to 28, were completed using a combination of engineered approaches using variations in pumping schedule

Hydraulic fracture stimulation of both the MIP-3H and MIP-5H were monitored with a vertical microseismic array in the MIP-SW well located between the two laterals, and a set of five surface seismometers (figures 1 and 5). Clusters of microseismic events produced during stimulation of the MIP-3H well are oriented on average N59°E as expected from the regional patterns and from the induced fractures observed in the vertical pilot hole. Wilson et al, (2016b) calculated an average distance of 190 feet (58m) above the MIP-3H wellbore to the center of the radiated microseismic energy (Figure 6). The microseismic energy is distributed through the entire Hamilton Group and not localized in the vicinity of the lateral. Fiber optic cable, installed on the outside of the MIP-3H casing, provided distributed temperature (DTS) and acoustic (DAS) data. Acoustic energy and temperature were monitored with the fiber optic cable during fracture stimulation of individual stages, and production continues to be monitored via temperature.

There is a significant difference between the radiated microseismic energy produced during MIP-3H stimulation and injection energy obtained from pumping data available for each stage during well treatment. This analysis reveals that radiated microseismic represents less than 0.01% of the total injected energy (Kavousi et al., submitted). Similar observations of the disparity between energy of microseismic events and moment release expected from hydraulic fracture treatment have been made in other wells (Warpinski et al., 2012; and Das and Zoback, 2013). Much of this energy could be expressed as long period, long duration LPLD events (Das and Zoback, 2011). Numerous similar LPLD events were observed during hydraulic fracture stimulation of the Marcellus Shale at six wells in Pennsylvania and at the MSEEL pad (Kumar et al. 2016, Kumar et al. in press). Two probable mechanisms have been suggested for the occurrence of LPLD events including; higher clay content (>30%) at a local scale, and slip along pre-existing fractures that are unfavorably oriented in the ambient stress field (by Das and Zoback, 2011 and Zoback et al., 2012).

The extracted phase of DAS data (hDVS) measures the local vibrations around the fiber, and fracture stimulation in the Lower Marcellus Shale. Completion energy as expressed by hDVS is linearly correlated with the injection energy and has a strong negative correlation with natural fracture intensity (P32), but microseismic energy is not correlated with either injection energy or hDVS energy (Kavousi et al. submitted). DTS measures temperature changes and was monitored in all stages in the MIP-3H including the stimulated (S+0) stage and the adjoining two previous stages (S-1, S-2) and subsequent stages (S+1, S+2) (Figure 7) (Amini et al. in press). Cooling of the

treatment stage and the two following stages toward the heel of the well is expected due to injection of surface water used for fracture stimulation. However, as in Stage 6 (Figure 7), the previously treated stages toward the toe of the well often show an increase in temperature that approaches the temperature of the formation (~165°F). This increase in temperature in previous fracture stimulated stages is especially prevalent in areas with multiple fractures and faults as determined by log data (e.g., Stage 6, Figure 3c).

Discussion

A conceptual model is proposed as an attempt to explain the effect of the numerous preexisting N87°E healed fractures and faults observed in logs, open fractures and borehole breakouts observed in the vertical pilot hole oriented N57°E with observations during fracture stimulation in the MIP-3H (Figure 8). These observations during fracture stimulation include; the extreme disparity between energy of microseismic events and moment release expected from hydraulic fracture treatment, clusters of microseismic events centered well above the lateral and orientated N59°E, observed LPLD events during stimulation, correlation of hDVS with P32 and not with microseismic, and significant warming observed as measured by DTS in previous stages associated with fractures in the lateral. The rapid injection during fracture stimulation of an average of 255 cubic feet of proppant and fluid for every foot of the 6,058 feet (1846m) completed lateral would rapidly change both pore pressure, and vertical and lateral stresses. With the N36°W orientation of the MIP-3H lateral (Figure 1), fracturing and injection could occur along non-critically oriented N79°E preexisting fractures in the lower Marcellus Shale and predominately expressed in the aseismic “slow slip” with low frequency seismic events that are not picked up by standard microseismic monitoring. The oblique orientation of the lateral to preexisting fractures could explain the warming as detected by DTS of previous stages to near formation temperatures by movement of fluids previously injected and warmed by the formation through stimulated fractures communicating from one stage to the previous stage(s). This change in temperature in the previous stage(s) appears to be more prevalent between stages with numerous observed faults and fractures (e.g., Stage 6, figures 3c and 7). Microseismic events are centered significantly above the stimulated interval and follow optimal oriented fractures to the present day stress regime. The observed microseismic events may not be a direct expression of stimulated fractures and proppant placement in the targeted lower Marcellus shale, but indirect expression in the overlying stratigraphic units imposed by the injection of more than 250 cubic feet of sand and fluid per foot of lateral.

Conclusions

The following observations in the MIP-3H well indicate that the Marcellus Shale is a complex unconventional reservoir that does not respond in a straightforward manner during large scale hydraulic fracture stimulation. Completion efficiency along the lateral appears to be affected by preexisting fractures oriented at an angle to existing principal stresses and strongly influence hydraulic fracture propagation. The following conclusions support this interpretation:

- Open fractures and induced fractures in the vertical pilot well are oriented N57°E on average.
- Core from the vertical pilot hole displayed the horizontal laminations and several calcite cemented fractures in the Marcellus Shale.
- Logging of the MIP-3H lateral revealed more than 1600 healed (calcite cemented vertical fractures) with average orientation of predominately N79°E±18°.
- Microseismic clusters have average orientation of N59°E with radiated energy centered, on average, 190 feet (49m) above the MIP-3H lateral.
- The disparity between radiated microseismic energy and energy associated with fluid and proppant volumes and injection pressures during hydraulic fracture treatment is very significant.
- Completion energy (hDVS) generated from DAS is correlated with the injection energy and natural fracture intensity (P32), but microseismic energy is not correlated with either injection energy or hDVS energy
- Numerous LPLD events measured were observed during active fracture stimulation of individual stages.
- Warming of previous stages to near formation temperature was detected by DTS.

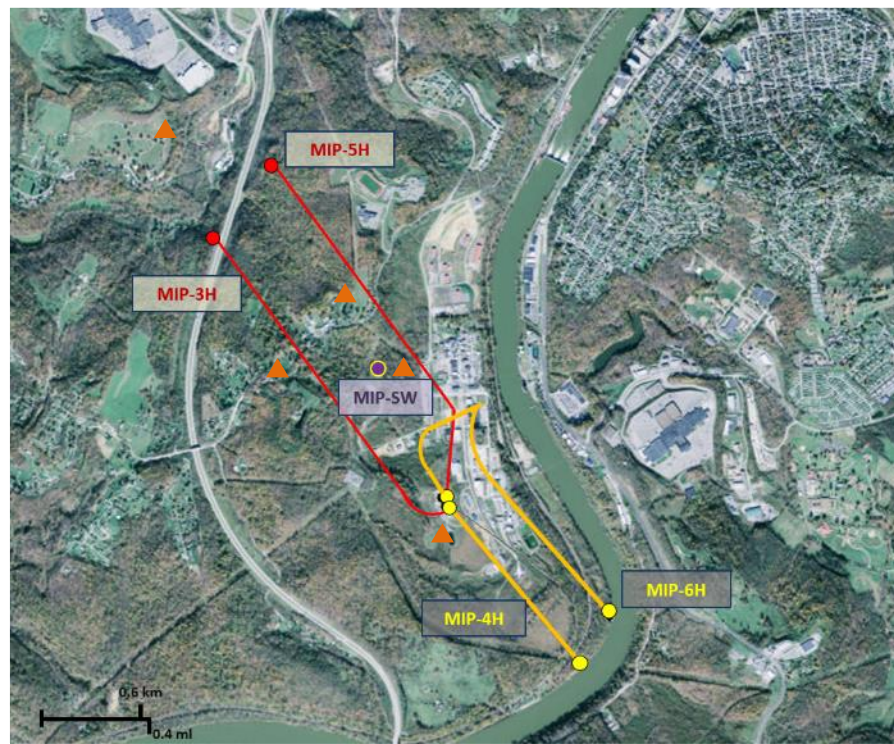
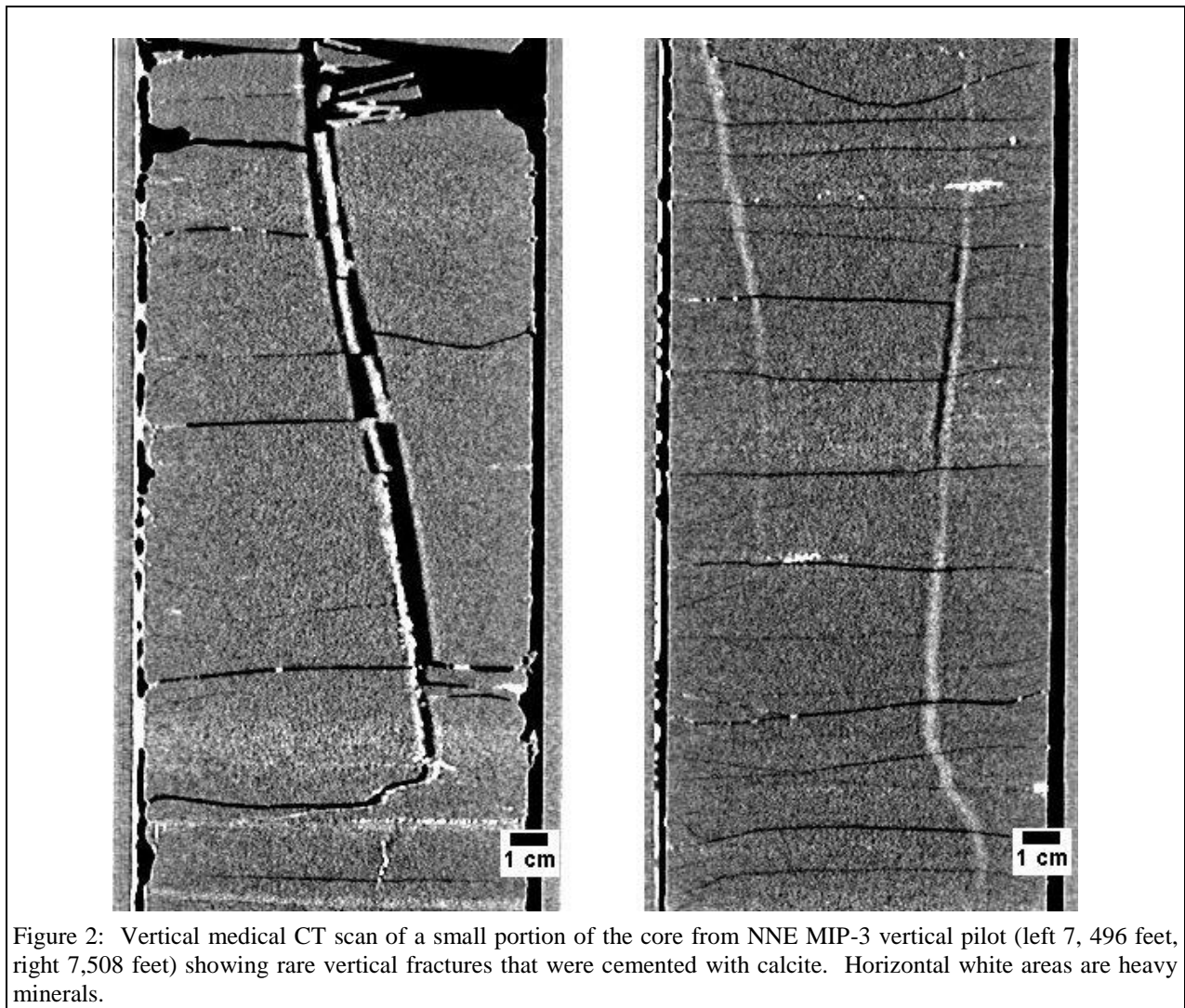
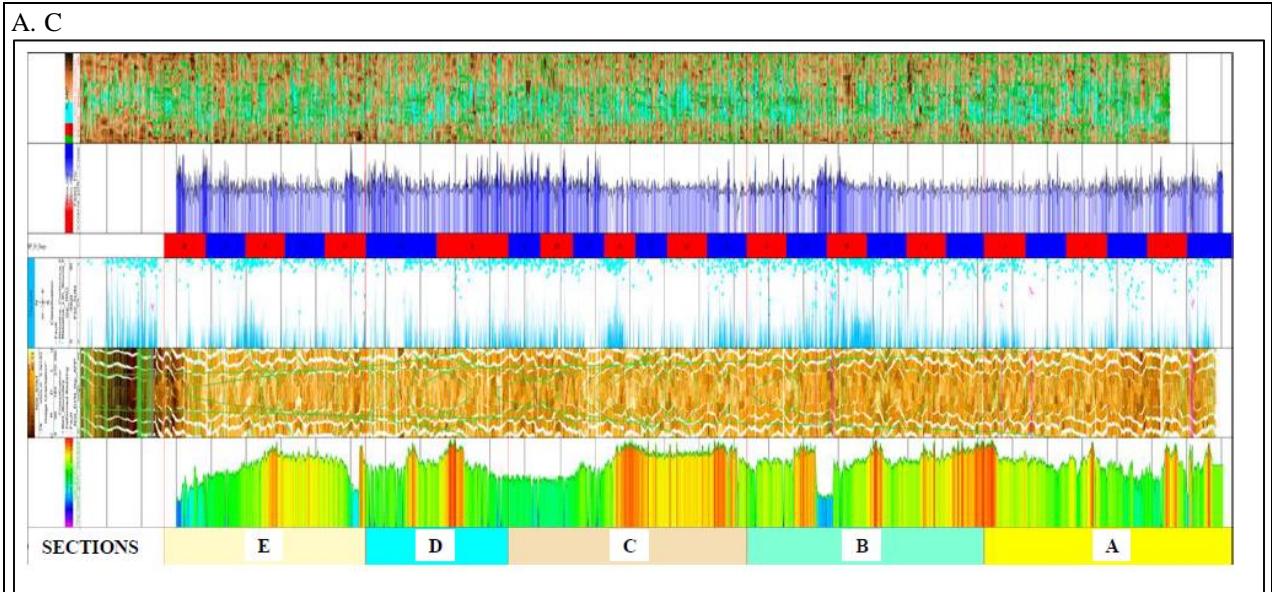
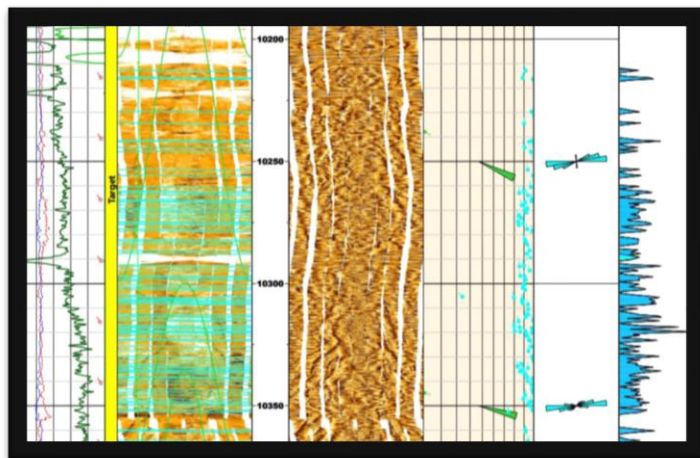


Figure 1: Marcellus Shale Energy and Environment Laboratory (MSEEL) just outside Morgantown, West Virginia, USA. The MSEEL site consists of four horizontal production wells operated by Northeast Natural Energy LLC. (MIP-3H, MIP-4H, MIP-5H, MIP-6H), two pilot holes (MIP-3 and MIP-4), a micro-seismic and sampled observation well (MIP-SW) and a grid of five surface seismometer (triangles). The Northeast Natural Energy MIP-3H (47-061-01707) surface location is longitude W79.976624° and latitude N39.602203°.





B.



C.

Stage	1	2	3	4	5	6	7	8	9	10	11	12	13	14	15	16	17	18	19	20	21	22	23	24	25	26	27	28
Fault/Fracture																												
No of Faults	3				2	1				2	1																	
No of Fractures	41	25	48	29	15	69	47	51	97	160	86	65	72	17	14	90	25	56	68	71	37	46	21	41	42	89	66	28

Figure 3: **A.** Logs acquired along the lateral of the MIP-3H. Curves from bottom to top are gamma-ray, QuantaGeo borehole image, natural fracture density (P32) with fracture/fault tadpoles, TIV closure stress and cement bond image. Over 1600 fractures were identified along the lateral. Leterred sections show five diffeernt completion strategies that were applied to the 28 stages of the MIP-3H lateral. **B.** Detail of portion of MIP 3H lateral showing QuantaGeo boreimage with sinusoids and fracture intensity and orientation. Fracture orientation is N87°E. **C.** Number of identified fractures and faults for each of the 28 stages of the MIP 3H.

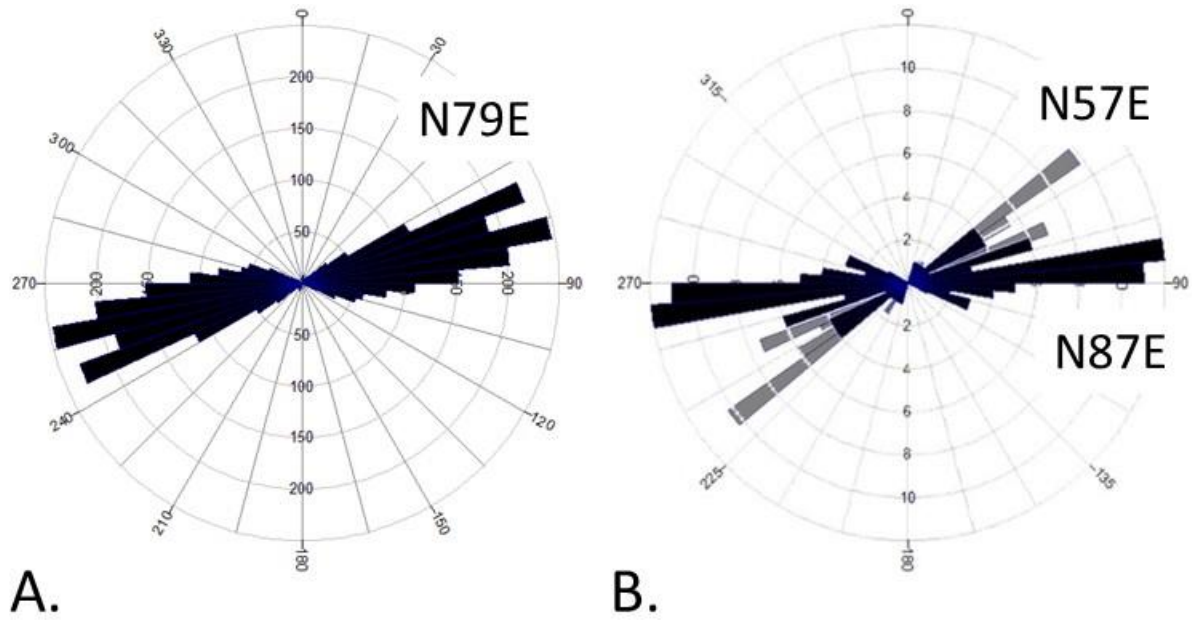


Figure 4: Rose diagrams of natural fractures a) observed along the length of the MIP-3H lateral (N=1640) and B) in the vertical pilot well (N=91). Fractures observed in the vertical well consist of 21 open fractures (light grey color) in the N57°E cluster and 70 healed fractures mainly concentrated in the N87°E cluster with a smaller fraction falling in the N57°E cluster.

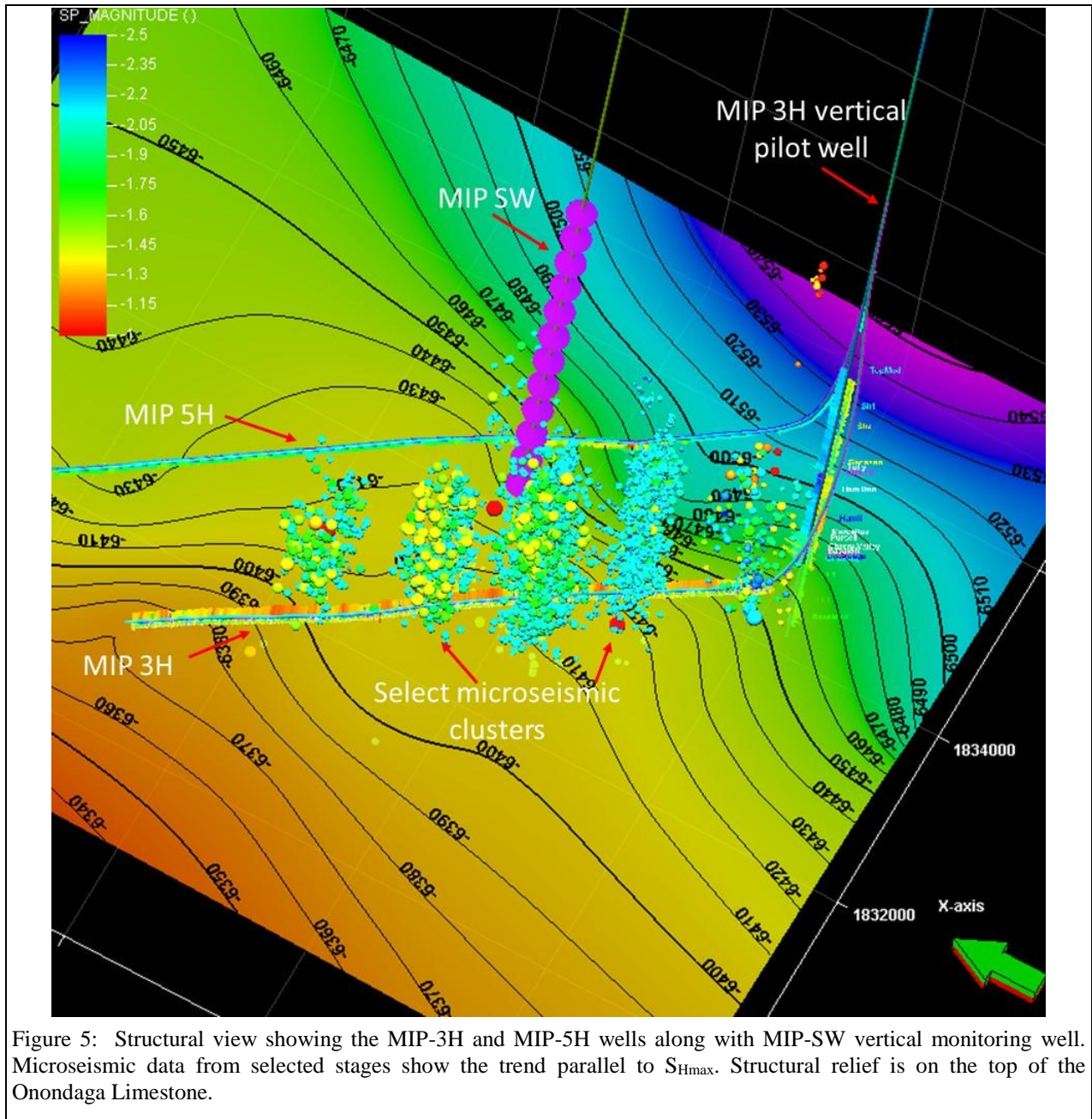


Figure 5: Structural view showing the MIP-3H and MIP-5H wells along with MIP-SW vertical monitoring well. Microseismic data from selected stages show the trend parallel to S_{Hmax} . Structural relief is on the top of the Onondaga Limestone.

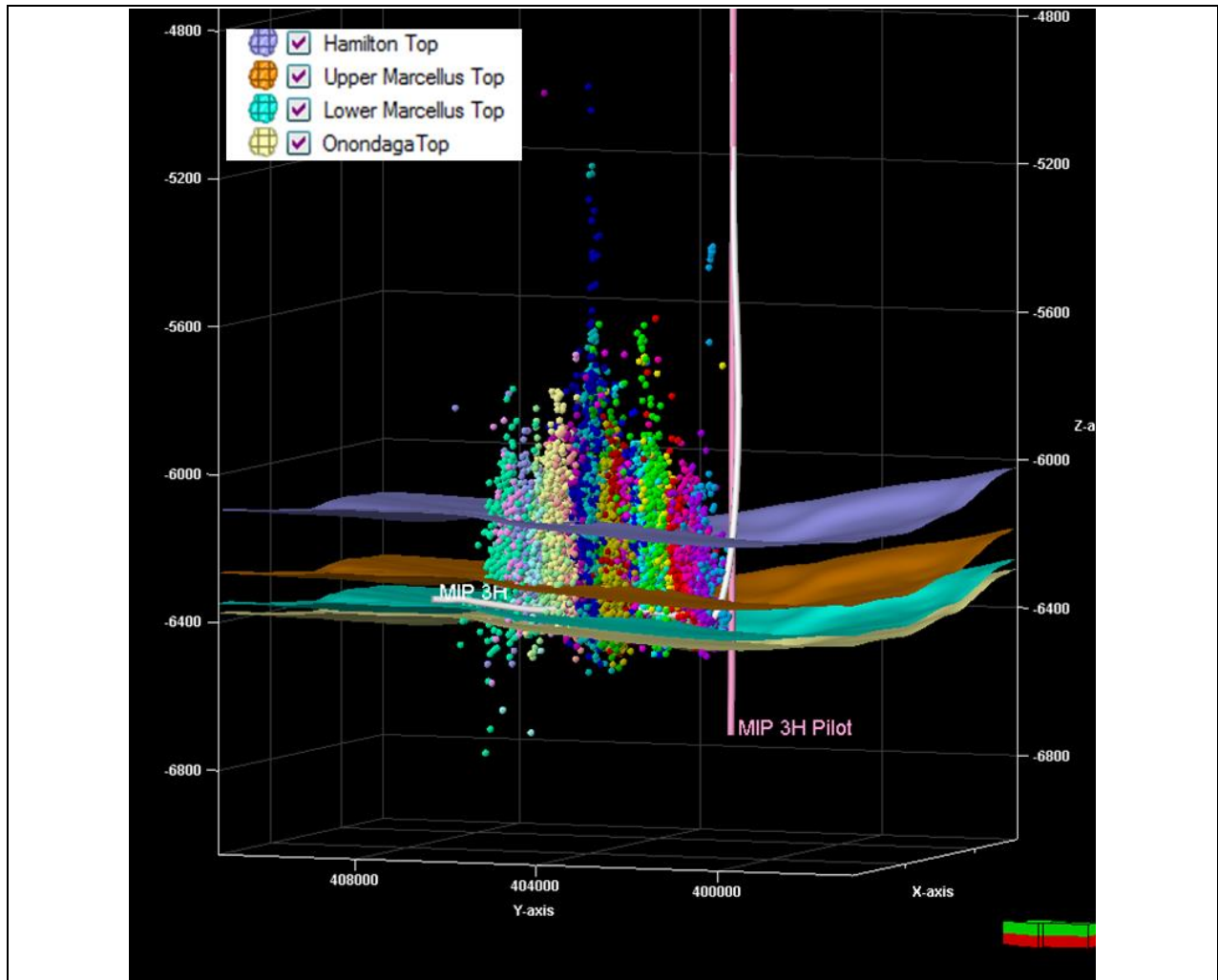


Figure 6: Microseismic data for Stages 7 to 28 recorded for well MIP-3H. The center of radiated microseismic energy is located 160 feet (49m) above the location of the lateral in the Lower Marcellus Shale as defined by the Cherry Valley Limestone and extends to well above the top of the Hamilton Group. (Kavousi and others, submitted; Wilson and others, submitted).

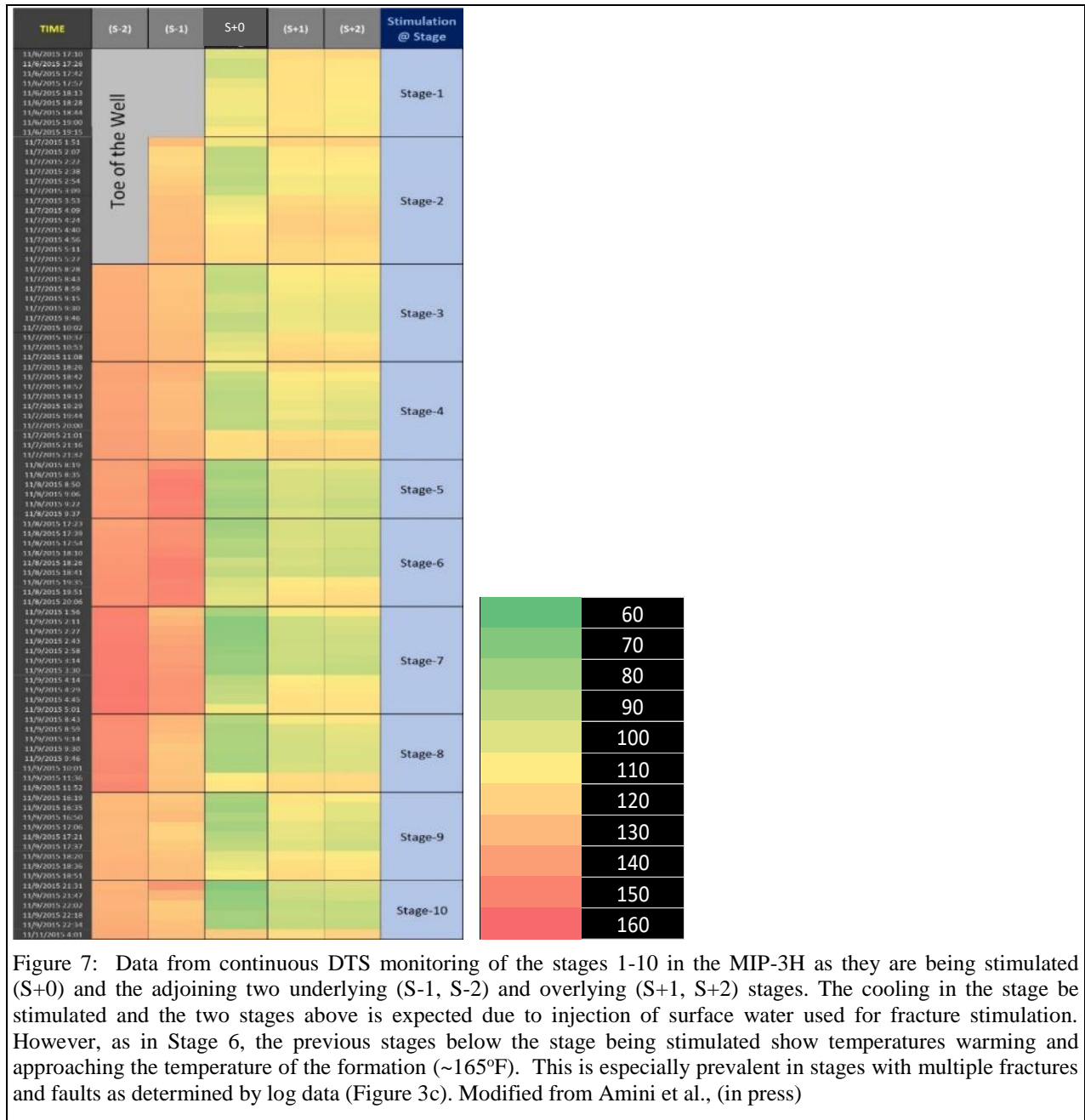


Figure 7: Data from continuous DTS monitoring of the stages 1-10 in the MIP-3H as they are being stimulated (S+0) and the adjoining two underlying (S-1, S-2) and overlying (S+1, S+2) stages. The cooling in the stage be stimulated and the two stages above is expected due to injection of surface water used for fracture stimulation. However, as in Stage 6, the previous stages below the stage being stimulated show temperatures warming and approaching the temperature of the formation (~165°F). This is especially prevalent in stages with multiple fractures and faults as determined by log data (Figure 3c). Modified from Amini et al., (in press)

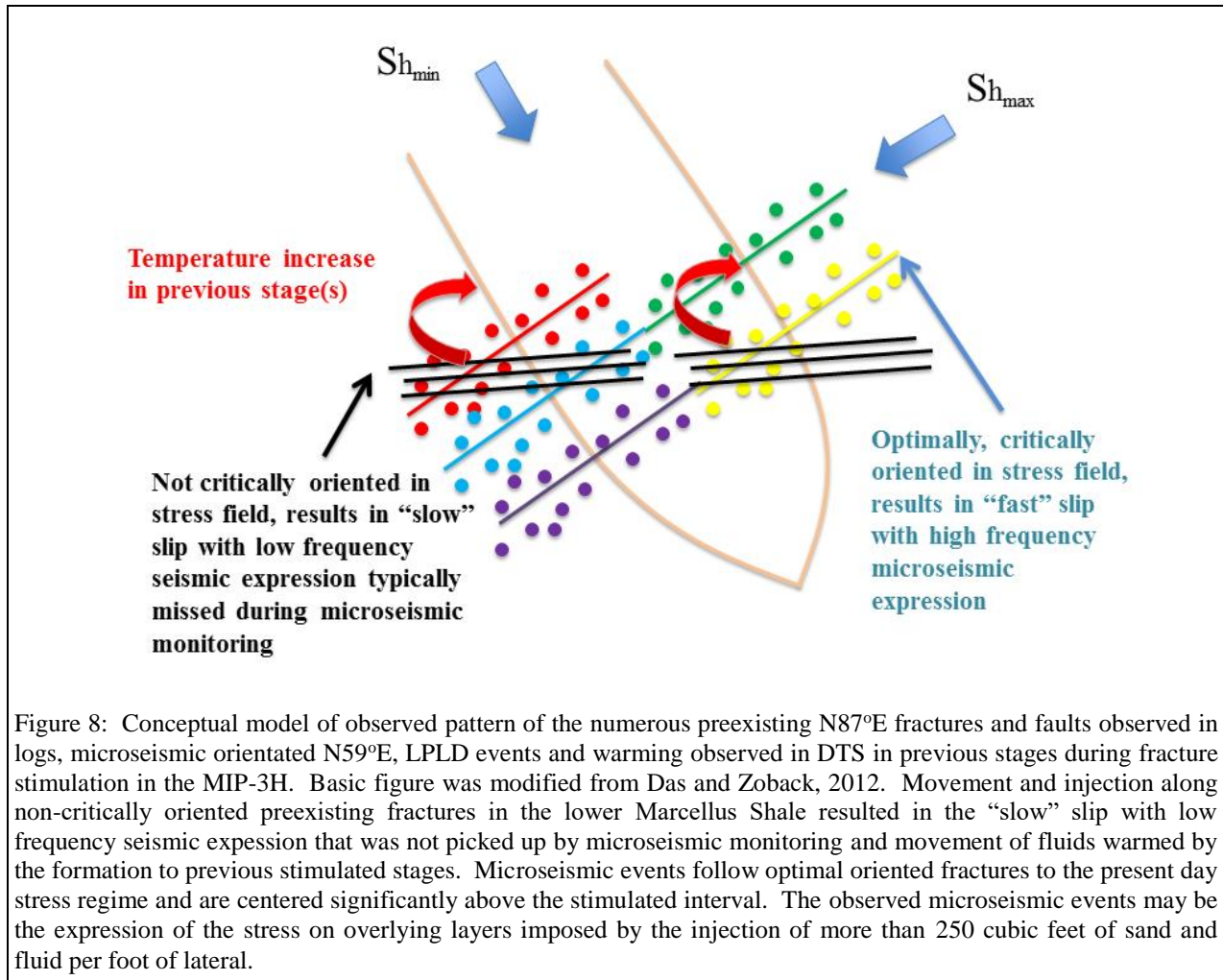


Figure 8: Conceptual model of observed pattern of the numerous preexisting N87°E fractures and faults observed in logs, microseismic orientated N59°E, LPLD events and warming observed in DTS in previous stages during fracture stimulation in the MIP-3H. Basic figure was modified from Das and Zoback, 2012. Movement and injection along non-critically oriented preexisting fractures in the lower Marcellus Shale resulted in the “slow” slip with low frequency seismic expression that was not picked up by microseismic monitoring and movement of fluids warmed by the formation to previous stimulated stages. Microseismic events follow optimal oriented fractures to the present day stress regime and are centered significantly above the stimulated interval. The observed microseismic events may be the expression of the stress on overlying layers imposed by the injection of more than 250 cubic feet of sand and fluid per foot of lateral.

References

- Agrawal, V., Sharma, S., 2017, Use of organic-geochemical proxies to assess organic matter sources, thermal maturity, and paleoredox conditions during deposition of Marcellus shale: *Journal of Petroleum Science and Engineering* (in review)
- Agrawal, V., Warriar, A., Sharma, S., 2017, Decoding molecular geochemistry of kerogen from Marcellus shale: American Association of Petroleum Geologists, Annual Convention and Exhibition, Houston, Texas.
- Agrawal, V., Sharma, S., Warriar, A., 2016, Understanding kerogen composition and structure in pristine shale cores collected from Marcellus Shale Energy and Environment Laboratory: Eastern Section AAPG 45th Annual Meeting in Lexington, KY.
- Amini, Shohreh, Payam Kavousi, and Tim Carr, in press, Application of Fiber-optic Temperature Data Analysis in Hydraulic Fracturing Evaluation: A Case Study in Marcellus Shale, Unconventional Resources Technology Conference, Unconventional Resources Technology Conference, Austin, Texas, July 24-26, DOI 10.15530-urtec-2017-2686732.
- Anifowoshe, O., Yates, M., Xu, L., Dickenson, P., Akin, J., Carney, B.J., Hewitt, J., Costello, I. and Arnold, Z., 2016, Improving Wellbore Stimulation Coverage in the Marcellus: Integrating Lateral Measurements with Enhanced Engineered Completion Design and Fiber Optic Evaluation: In SPE Eastern Regional Meeting. Society of Petroleum Engineers, SPE, paper no. 184051-MS, <https://doi.org/10.2118/184051>.
- Das, Indrajit, and M. D. Zoback, 2011, Long period long duration seismic events during hydraulic fracture stimulation of a shale gas reservoir: *The Leading Edge*, 30, 778–786, <http://dx.doi.org/10.1190/1.3609093>.

- Das, Indrajit and Mark D. Zoback, 2012, Microearthquakes Associated with Long Period, Long Duration Seismic Events During Stimulation of a Shale Gas Reservoir. SEG Technical Program Expanded Abstracts 2012: pp. 1-5, <http://dx.doi.org/10.1190/segam2012-1484.1>.
- Das, Indrajit, and M. D. Zoback, 2013, Long-period, long-duration seismic events during hydraulic stimulation of shale and tight-gas reservoirs—Part 1: Waveform characteristics: *Geophysics*, **78**, no. 6, KS107–KS118, <http://dx.doi.org/10.1190/GEO2013-0164.1>.
- Gale, J.F., Reed, R.M., Becker, S.P. and Ali, W., 2008, Natural Fractures in the Barnett Shale in the Delaware Basin, Pecos Co. West Texas: Comparison with the Barnett Shale in the Fort Worth Basin, AAPG Search and Discovery, http://www.searchanddiscovery.com/pdfz/documents/2010/10226gale/ndx_gale.pdf.html
- Kavousi, Payam. Timothy Carr, Thomas Wilson, and Shohreh Amini, Collin Wilson, Mandy Thomas, Keith MacPhail, Dustin Crandall, BJ Carney, Ian Costello, and Jay Hewitt, submitted, Correlating distributed acoustic sensing (DAS) to natural fracture intensity for the Marcellus Shale, SEG Technical Program Expanded Abstracts 2017.
- Kumar, Abhash, Richard Hammack, Erich Zorn, and William Harbert, 2016, Long period, long duration (LPLD) seismicity observed during hydraulic fracturing of the Marcellus Shale in Greene County, Pennsylvania. SEG Technical Program Expanded Abstracts 2016: pp. 2684-2688, <http://dx.doi.org/10.1190/segam2016-13876878.1>.
- Kumar Abhash, Erich, Zorn, Richard, Hammack, William Harbert, in press, Surface Seismic Monitoring of Hydraulic Fracturing Activity in Pennsylvania and West Virginia, Unconventional Resources Technology Conference, Expanded Abstracts 2017.
- Moos, D., G. Vassilellis, R. Cade, J. Franquet, A. Lacazette, E. Bourtembourg, and R. Cade, 2011, Predicting shale reservoir response to stimulation in the upper Devonian of West Virginia: Annual Technical Conference, SPE, paper no. 145849, <https://doi.org/10.2118/145849-MS>.
- Sharma, Sharma, Timothy Carr, Paula J. Mouser, Kelly Wrighton, David Cole, Michael Wilkins, Thomas Darrah, and Alexander Hakala, in press, Biogeochemical Characterization of Core, Fluids and Gas at MSEEL Site, Unconventional Resources Technology Conference, Unconventional Resources Technology Conference, Austin, Texas, July 24-26, DOI 10.15530-urtec-2017-2669965.
- Sicking, C., J. Vermiliye, P. Geiser, A. Lacazette, and L. Thompson, 2013, Permeability field imaging from microseismic: *Geophysical Society of Houston Journal*, **3**, 11–14, <http://dx.doi.org/10.1190/segam2012-1383.1>.
- Warpinski, N. R., J. Du, and U. Zimmer, 2012, Measurements of hydraulicfracture-induced seismicity in gas shales: Hydraulic Fracturing Technology Conference, SPE, paper no. 151597, <http://dx.doi.org/10.2118/151597-PA>.
- Wilson, Thomas, A. Hart, and P. Sullivan, 2016a, Interrelationships of Marcellus Shale gas production to frac-induced microseismicity, interpreted minor faults and fractures zones, and stimulated reservoir volume, Greene County, Pennsylvania: Interpretation, **4**, T15–T30, <http://dx.doi.org/10.1190/INT-2015-0045.1>.
- Wilson, Thomas, Timothy Carr, B. J. Carney, Jay Hewitt, Ian Costello, Emily Jordon, Keith MacPhail, Natalie Uschner, Miranda Thomas, Si Akin, Oluwaseun Magbagbeola, Adrian Morales, Asbjorn Johansen, Leah Hogarth, and Kashif Naseem, 2016b, Microseismic and model stimulation of natural fracture networks in the Marcellus Shale, West Virginia. SEG Technical Program Expanded Abstracts 2016: pp. 3088-3092. <http://dx.doi.org/10.1190/segam2016-13866107.1>.
- Wilson, Thomas, Malcolm Yates, Keith MacPhail, Ian Costello, Tim Carr, B. J. Carney, Jay Hewitt, , Emily Jordon, Natalie Uschner, Mandy Thomas, Si Akin, Oluwaseun, Magbagbeola, Adrian Morales, Asbjorn Johansen, Leah Hogarth, Olatunbosun Anifowoshe, Kashif Naseem, submitted, Marcellus Shale model stimulation tests and microseismic response yield insights into mechanical properties and the reservoir DFN, SEG/AAPG Journal Interpretation.
- Wilson Thomas, Payam Kavousi, Tim Carr, B. J. Carney, Natalie Uschner, Oluwaseun Magbagbeola and Lili Xu, submitted, Relationships of γ_p , μ_p , brittleness index, Young's modulus, Poisson's ratio and high TOC for the Marcellus Shale, Morgantown, West Virginia SEG Technical Program Expanded Abstracts 2017.
- Zorn Erich, William Harbert, Richard Hammack, and Abhash Kumar, in press, Geomechanics of the Microseismic Response in Devonian Organic Shales at the Marcellus Shale Energy and Environment Laboratory (MSEEL) Site, West Virginia, Unconventional Resources Technology Conference, Expanded Abstracts 2017.

URTeC: 2667397

Depositional Environment and Impact on Pore Structure and Gas Storage Potential of Middle Devonian Organic Rich Shale, Northeastern West Virginia, Appalachian Basin

Liaosha Song*, Tom Paronish, Vikas Agrawal, Brittany Hupp, Shikha Sharma, Timothy Carr; Department of Geology and Geography, West Virginia University, Morgantown, WV, USA

Copyright 2017, Unconventional Resources Technology Conference (URTeC) DOI 10.15530/urtec-2017-2667397

This paper was prepared for presentation at the Unconventional Resources Technology Conference held in Austin, Texas, USA, 24-26 July 2017.

The URTeC Technical Program Committee accepted this presentation on the basis of information contained in an abstract submitted by the author(s). The contents of this paper have not been reviewed by URTeC and URTeC does not warrant the accuracy, reliability, or timeliness of any information herein. All information is the responsibility of, and is subject to corrections by the author(s). Any person or entity that relies on any information obtained from this paper does so at their own risk. The information herein does not necessarily reflect any position of URTeC. Any reproduction, distribution, or storage of any part of this paper without the written consent of URTeC is prohibited.

Abstract

Characterizing the pore structure of a shale-gas reservoir is significant for calculating the original gas in place and fluid-flow characteristics. To better understand the impact of organic matter accumulation, redox condition, and depositional environment on pore structure and storage capacity, integrated geological and petrophysical characterization of the Devonian organic-rich shale was conducted. Core samples from a newly drilled science well from the Marcellus Shale Energy and Environment Laboratory (MSEEL) project and other wells in the Appalachian basin were selected to undertake this research. X-ray fluorescence (XRF), X-ray diffraction (XRD), and pyrolysis were performed to understand variations in composition, mineralogy and total organic carbon (TOC). Samples were examined from an interval including the overlying Tully Limestone, organic-lean Mahantango Shale, organic-rich Marcellus Shale and top of the underlying Onondaga Limestone.

We introduce the application of subcritical N₂ adsorption to measure pore volume, pore-size distribution, and pore-surface area, which are critical properties in characterization of the nano-scale pore regime of mudstone reservoirs. Results of the test are used to build models of the mudstone pore systems. With variations of TOC and mineralogy, changes in the characteristics of pore structure are observed. Middle Devonian shales have complex, heterogeneous pore size distributions as identified by subcritical N₂ adsorption. XRD results suggest a high content of clay minerals (mainly illite) through both Mahantango and Marcellus shales. Hysteresis of N₂ adsorption isotherm indicates slit-shape pores between 2nm and 50nm, possibly formed by clay particles. Organic matter shows strong influence on pore volume and pore surface area (BET specific surface area), which strongly influences storage mechanisms of shale-gas reservoirs. Carbonate-rich intervals show very low pore volume especially micropore (pore width smaller than 2nm) volume, and surface area. The results of N₂ adsorption are compared with NMR log to upgrade the evaluation.

Introduction

Micro- to mesoporous structures of unconventional reservoirs are challenging to characterize because of the extremely small pore sizes. Investigation of the micro- or mesoporous structures and their impact on flow properties requires experimental approaches, and sample preparation that will not affect the physical structure of samples while removing water, hydrocarbon, and other contaminants. To study shale pores more accurately, techniques such as gas adsorption and nuclear magnetic resonance (NMR), have been applied. The low-temperature nitrogen N₂ adsorption method can offer micro-pore volume, meso-pore size distribution, and pore surface area. Understanding the limitations of the analyses is also important, since at the scale of micro- to meso-pores, the measurement techniques influence the result. In this paper, we review some of the sample preparation procedures to find an appropriate and repeatable measurement. The NMR T2 spectra of core samples can be used to calculate porosity and permeability,

and characterize pore-throat structures of rock. Significant variations in pore structures can be expected within a formation due to lithologic variations resulting from depositional environment, sediment influx, and preservation.

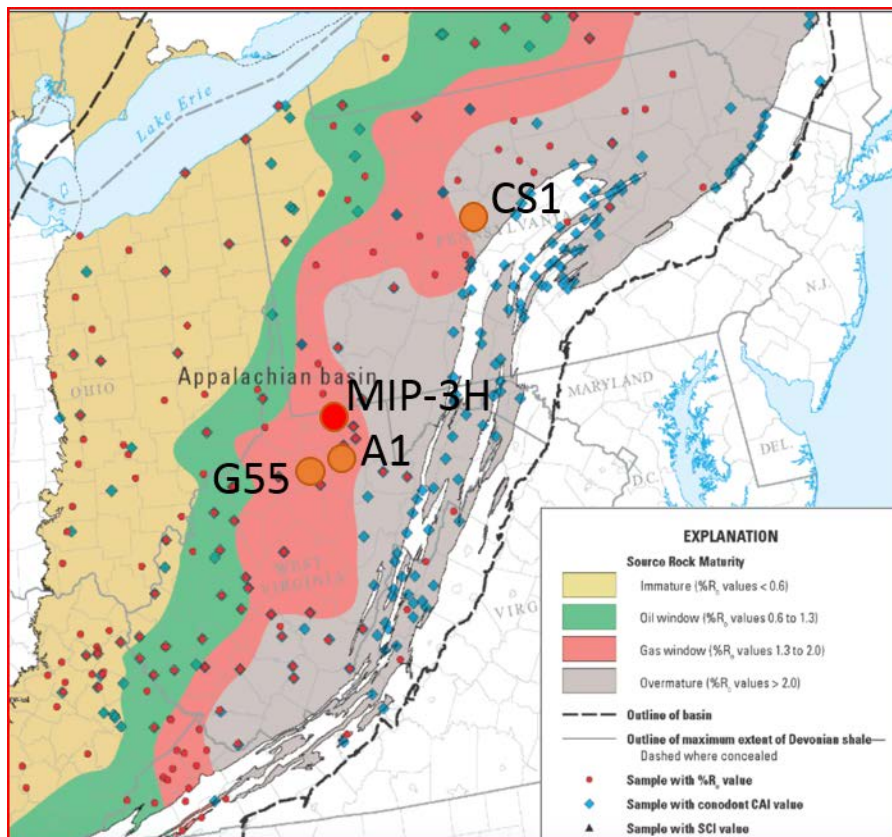


Figure 1: The Map shows the location of wells in West Virginia and Pennsylvania used in this paper, and the thermal maturity trend of the Marcellus Shale (modified after East et al., 2012).

In this research, shale samples were obtained from four wells penetrating Mahantango and Marcellus shale formations in West Virginia and Pennsylvania, covering a wide spectrum of thermal maturity (Figure 1). Total organic carbon content and mineralogy also vary significantly. Core samples from Marcellus Shale Energy and Environment Laboratory (MSEEL) project (MIP-3H well) were selected to run XRD, XRF, TOC and BET analyses and to compare to other wells. These techniques were used to characterize the pore-system characteristics of the Middle Devonian organic-rich shale in Appalachian basin, including the pore type, pore size, surface area, and pore volume. This research will help improve our understanding of the characteristics of the Marcellus and other organic-rich shale reservoirs and could further benefit evaluation of the storage capacity of shale-reservoirs.

Method

Source Rock Analysis (SRA)

Approximately 60 - 100 mg of pulverized rock was accurately weighed into an SRA crucible and placed in the SRA-Agilent autosampler, and held isothermally at 300°C for 3 minutes. During this isothermal heating, the free hydrocarbons are volatilized and detected by the FID detector where they are quantitatively detected and reported as milligrams (mg) of S1 per gram of rock. The free CO₂ is simultaneously liberated and detected by the IR cell and reported as milligrams (mg) of S3 per gram of rock up to 400°C. After the isothermal period, the temperature is ramped at 25°C/minute to 600°C. Between 300°C and 600°C organic hydrocarbons are generated from the pyrolytic degradation of the kerogen in the rock. The hydrocarbons are detected by the FID, labeled as S2, and reported as milligrams (mg) of S2 per gram of rock. Residual carbon is also measured and is recorded as S4 peak. TOC is calculated by using the equation: %TOC = 0.1 × [0.082 × (S1 + S2) + S4] (Espitalie et al., 1985). WFT Source Rock

Standard 533 (P/N 810-141) was run after every five samples. The standard deviation of the analysis was 0.07%. SRA analysis was performed at the National Energy Technology Laboratory in Morgantown.

X-ray Diffraction Geochemical Analysis

Sixty-two samples collected as side-wall plugs from the MSEEL project were analyzed for x-ray diffraction (XRD) geochemical analysis to determine bulk mineralogy. These samples were ground in a steel grinding container for 5-10 minutes until powdered. Powder samples were pressed into chemplex pellets for loading of samples into the diffractometer. XRD analysis was performed using the PANalytical X'Pert Pro X-ray Diffractometer at West Virginia University Shared Research Facilities. Samples for this project were analyzed at 2θ angles between 5° and 75° , with a step time of ~ 75 seconds, leading to each sample being ran for approximately 13.5 minutes. X-rays were concentrated through a 20mm brass opening. The raw spectra were interpreted using the X'pert HighScore Plus Program to establish percentage of various mineral phases present. Bulk mineralogical interpretations were semi-quantitatively determined using reference intensity ratios (RIR).

Portable X-ray Fluorescence Geochemical Analysis

X-ray fluorescence (XRF) was performed on the same 62 samples that were prepared for x-ray diffraction analysis. The chemplex pellets were analyzed using a Bruker portable x-ray fluorescence spectrometer Tracer III-SD provided by the Division of Plant and Soil Sciences at West Virginia University. Each sample was analyzed for 120 seconds. Runs were completed to acquire major and trace elemental concentrations reported as weight percent. All runs were calibrated using the Bruker Mudrock calibration.

Low-pressure N_2 adsorption (BET test)

Low-pressure N_2 adsorption were conducted on a Micromeritics ASAP-2020 instrument at -196°C (77K). About 1 gram of shale sample was crushed with mortar and pestle until the whole mass passes through a 60-mesh sieve to prevent potential sample biasing due to sieving. One sample from well CS1 is chosen to run the temperature test. About 5 gram of core sample was crushed and separated to 5 portions. Then samples were outgassed under high-vacuum apparatus at 120°C for 24 hours to remove adsorbed water and volatile matter before analyses with N_2 . The relative pressure (P/P₀) ranged from 0.009 to 0.990. Both adsorption and desorption data points were acquired. Adsorption branch of the isotherms were used to obtain information about micropores (<2 nm in diameter) and mesopores (2~50 nm in diameter). The classification of pore sizes used in this article follows the classification system of the International Union of Pure and Applied Chemistry. This classification of pore sizes has proven to be very convenient in coal and shale studies (Bustin et al., 2008; Clarkson et al., 2012; Mastalerz et al., 2013).

Specific surface area (SSA) was calculated based on Brunauer-Emmet-Teller (BET) theory Pore volumes, and pore distributions based on Barrett-Joyner-Halenda (BJH) model, t-Plot, H-K model (Brunauer et al., 1938; Barrett et al., 1951; Sing, 2001).

Results and Discussion

1. Selection of degassing conditions

Prior to the BET test, samples need to be degassed. The impact of degassing procedure on the results must be considered before the test, because the interpretation models are based on clean surfaces for the adsorbent. The ultimate goal of degassing is to remove all the water and volatiles (such as remaining hydrocarbons), and other impurities, so that N_2 can reach out to most of pore space of the sample, while avoiding irreversible damage to organic matter, minerals, and sample texture. For this purpose, the nano Darcy range permeability of shale makes it impractical to run this test on intact or large pieces of core sample. Most reservoir properties measurements of mudrocks are performed on crushed core samples, because with crushed powder, the total path length for the gas to access the entire pore structure is significantly shorter than intact core samples, thereby, the test can be finished within reasonable time (Luffel and Guidry, 1992; Kuila and Prasad, 2013).

Adesida et al., 2011 studied the effect of crushing on pore-structure parameters measured by N_2 gas adsorption. The results show that the specific surface area and total specific pore volume measured increases with decreasing sample particle size, which make sense since by crushing the sample to a finer size, extra surface area is created (Adesida et al., 2011). The increased pore volume is related to better pore accessibility at smaller grain sizes. When crushing the core sample, the different mechanical properties of the constituents (organic matter and minerals) of mudrocks are

noticed. This difference results in variance tendency to grind. By sieving the crushed sample into different sizes, it may result in a bias in the composition and mineralogy of each separated fraction (Kuila and Prasad, 2013). Therefore, the crushed samples are used for BET test. The crushing procedure will follow Kuila and Prasad (2013) with a different grain size. Samples are crushed until the entire mass passes through a 60-mesh sieve (40 mesh in their research) to prevent potential sample biasing due to sieving. The samples preparation procedure should also be repeatable. After literature review, most research on N₂ adsorption on mudrocks has been conducted on 60 mesh samples (Table 1). Thus the result can be compared with former research, and benefit future study.

Table 1 Sample preparation procedures of former researches

Authors	Year	Gas	T (°C)	Mesh Size	Time (hour)	Sample Location	BET SSA (m ² /g)
Lu et al.	1995	He, CH ₄	50~60	18~25	24	Antrim Shale from WV and KY	
Chalmers and Bustin	2006, 2007	N ₂ , CO ₂	105	60	>12	North America coal and shale	0.01~7.9
Chalmers and Bustin	2008	N ₂ , CO ₂	150	60	12	Lower Cretaceous NE British Columbia	N ₂ : 2.5~19.5; CO ₂ : 16.1~62.9
Ross and Bustin	2009	N ₂ , CO ₂	110	60	24	Jurassic, D-M, North British Columbia	3.4~44.5
Adesida	2011	N ₂	100	20~40	3	Barnett	0.06~11.16
Strapoc et al.	2010	N ₂ , CO ₂		60		New Albany Shale (D-M)	4~20
Mastalerz et al.	2012	N ₂ , CO ₂	110	60	14	New Albany Shale (D-M)	N ₂ : 0.2~2.4; CO ₂ : 10.9~12.8
Zhang et al.	2012	CH ₄	200	100	over night	Green River, Barnett	
Clarkson et al.	2012	N ₂ , CO ₂		4	over night	Triassic Montney, Western Canada	0.62~3.05
Clarkson et al.	2013	N ₂ , CO ₂	60	60	> 4 days	North America	2.3~17.1
Kuila	2013	N ₂	200	40	24	Haynesville	22.85~23.11
Heller and Zoback	2014	CO ₂	40	100~270		Eagle Ford, Barnett, Marcellus, Montney	
Maria-Fernanda Romero-Sarmiento	2014	N ₂	80		6	Mississippian Barnett Shale	14~39

Another import factor for degassing is the temperature. Olson, 2012 summarized degassing temperature for 6 categories of materials (Table 2). Unfortunately, there isn't a category for mudrock. While it still shed some light on the selection of temperature. Amorphous oxides (e.g. silica, alumina) are similar to numerous minerals in mudrock, and a temperature from 100°C to 200°C did not change the pore structure (Olson, 2012). To find the best temperature for this research, one sample was split into 5 portions and degassed under 5 different temperatures. Figure 2 shows the pore size distributions of this sample at these temperatures. The overall trends are the same over all the five tests. However, as temperature increases, we noticed an increase in pore volume. Samples degassing under 80°C and 120°C show almost the same pore size distribution (PSD), which agrees with another research on Barnett Shale (Adesida et al., 2011) and other research studies (Table 1). In the rest of this study, 120°C is used as the degas temperature.

2. Pore size distributions

Isotherms are the direct result from low pressure N₂ adsorption tests. Figure 3 shows the isotherms of the six samples from MIP-3H, all of which are type IV isotherm with H3 or H4 hysteresis loop. This shape of isotherm indicates that the shale samples are micro- to meso-porous materials, and this type of hysteresis loop often is observed with aggregates of plate-like particles forming slit-shaped pores. At high P/P₀ section (P/P₀ > 0.9), the

isotherm shows a steep increase and no limit when P/P0 close to 1. This is attribute to the sample also has macro pores, and the steep increase is representative of macro pore filling (Sing et al., 1982).

Table 2 Summary of outgassing conditions by material type (Olson, 2012)

Material Type	Flow or Vacuum	Temp. (°C)	Duration (hr)
Active pharmaceutical ingredients	Either	40 or ½ melting point	≥ 2
Activated carbon, zeolites, catalysts	Vacuum	90 then 300	1 then ≥ 3
Magnesium Stearate	Vacuum	40	2
Excipients, e.g. starches, celluloses, sugars, polymers	Either	20o < Tg or ½ melting point	≥ 2
Amorphous oxides, e.g. silica, alumina	Either	100 to 200	≥ ½
Metal oxide, e.g. titanium dioxide, zinc oxide, iron oxide, nickel oxide	Flow	300	≥ 2
Ionic salts & crystalline nonmetals	Either	300 or ½ melting point	≥ 2

The pore size distribution of the six samples from MIP-3H are calculated with BJH model (Figure 4). The variation in pore structure are mainly controlled by TOC and mineralogy (Figure 7). Tully Limestone and Onondaga Limestone show significantly less pores compared with the Marcellus Shale within the meso-pore zone (2~50nm), and very few pores below 20 nm. In the Marcellus Shale, the pore structure also varies. The Marcellus top sample has a spike at 7 nm and a bigger pore volume than upper Marcellus sample. The Marcellus top sample also has the highest clay content (Figure 7). Upper and middle Marcellus samples have similar PSD in 20nm to 50nm interval. The lower Marcellus sample, which has the highest TOC content, has the highest pore volume.

3. TOC, pore surface area, and pore volume

The specific surface area (SSA) of the six samples ranges from 1.09 m²/g to 52.9 m²/g (Table 3). The BJH pore volume of samples range from 0.003052 cm³/g to 0.051914 cm³/g (Table 3). The micro pore volume and surface area are calculated by T-plot. The BET specific surface area and BJH pore volume indicate an overall positive correlation with TOC (Figure 5, 6). MIP-3H, G55 and A1 (listed as 1.36<Ro<1.41) shows a better correlation compare to CS1 (listed as 2.67<Ro<2.89). There is a significant decrease in micro- to meso-pores with increasing carbonate content.

4. Mineralogy, lithology, and depositional environment

The MIP-3H well utilizes both common and advanced logging tools to provide insight into TOC and mineralogy at the log-scale (Figure 8). The Marcellus Shale at the MSEEL location is defined by three high gamma ray peaks (greater than 300 API) separated by thin carbonate intervals (lower than 110 API). Linear relations between SRA derived TOC measurements and uranium and gamma ray help to predict the organic content throughout the Marcellus Shale interval. Generally, there is an increase in organic content with depth from about 5 wt.% in the upper Marcellus to 15 wt.% in the most organic portion of the lower Marcellus. This trend is reiterated by an increase in resistivity (figure 8, tract 2 orange), which denotes organic matter and carbonate through this interval.

Mineralogy is determined using the XRD (Figure 7). The abundance of organic matter in volume percentage is calculated from TOC wt.% following Crain's workflow(Crain and Holgate, 2014). Then the XRD results are converted into volume fraction of minerals and organic matter with average mineral density. The average density of organic matter is set to be 1.26 g/cc (Crain and Holgate, 2014). Overall, there is a decrease in the clay content with depth in the Marcellus Shale with an increase in the organic matter. In lower Marcellus, the volume fraction of organic matter is 33% (Figure 7).

The NMR log shows relatively consistent porosity ranging from about 2 to 4% through the Marcellus Shale interval (Figure 8, tract 7). There is, however overall decrease in the T2 distributions, with slower T2 arrivals in the upper Marcellus (3ms and greater) and faster in most organic portion of the Lower Marcellus (<3ms). This trend could be related to a change in pore fluid type or an overall decrease in the pore size distribution.

The XRF data (Figure 8) provide general trends that relate the Marcellus unit to redox environment and the amount of detrital influence using relative quantities of major and trace elements, as well as, how they relate to one another. Descending through the stratigraphy, there is a decrease in detrital delivery which is represented by a decrease in Aluminum. In middle and lower Marcellus, the reduction of Al corresponds with GR log and TOC peaks. The interpreted redox conditions range from dysoxic in the upper Marcellus to anoxic to slightly euxinic in the middle and lower Marcellus. The covariance of Uranium (represent by TOC_URAN) and GR log readings indicate a reducing environment. The decrease of Th/U hinges with the TOC peaks, and the Th/U values remain less than 1 indicating a suboxic to anoxic environment. These are expressed by an overall increase in the concentration of trace elements, specifically in V+Cr trends, which show denitrification (Sageman et al., 2003; Lash and Blood, 2014; Chen et al., 2015; Chen and Sharma, 2017).

Table 3. Low-pressure N₂ adsorption test and TOC results

Depth(ft.)	Formation	BET SSA (m ² /g)	Micropore Area (m ² /g)	Micropore Volume (cm ³ /g)	BJH Pore Volume (cm ³ /g)	TOC wt. %
7201	Tully	1.09	0.1823	0.000078	0.004566	0.36
7452	Marcellus Top	19.43	4.3996	0.001861	0.027743	3.14
7466	Upper Marcellus	20.8849	5.6005	0.002382	0.024733	4.14
7508	Mid Marcellus	42.93	14.7628	0.006300	0.039927	6.48
7544	Lower Marcellus	52.90	10.5677	0.004379	0.051914	8.9
7555	Onondaga	1.74	0.5313	0.00022	0.003052	0.85

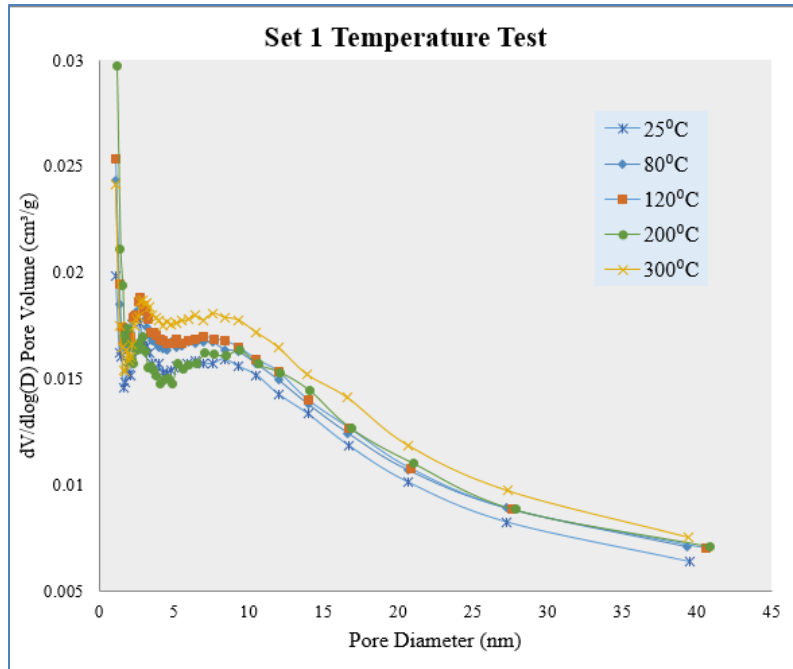


Figure 2. BJH pore-size-distributions of 5 samples degassed using 5 different temperatures.

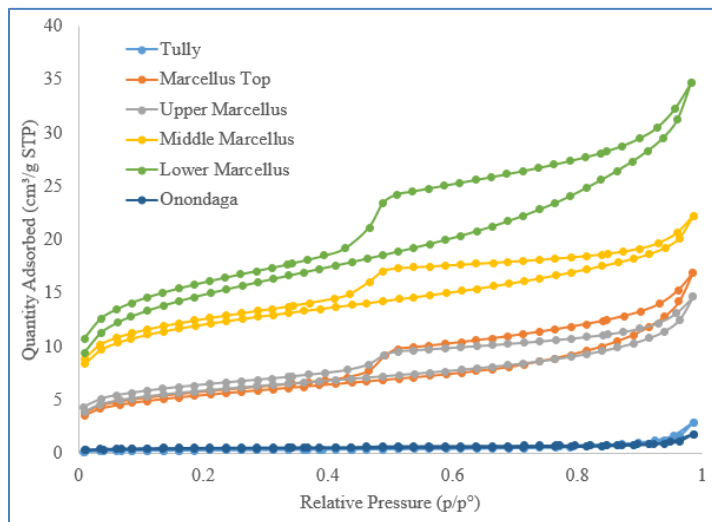


Figure 3. Isotherms of samples from MIP-3H.

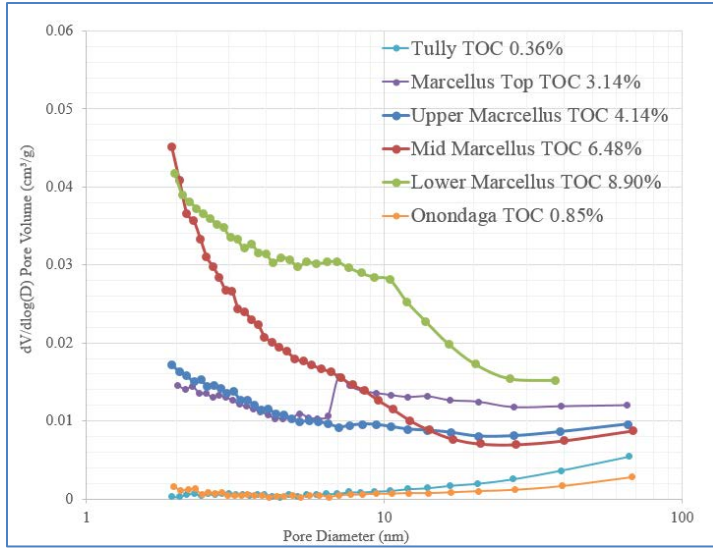


Figure 4: Pore size distribution of the samples across Tully Limestone, Marcellus Shale, and Onondaga Limestone with regard to the TOC weight percentage.

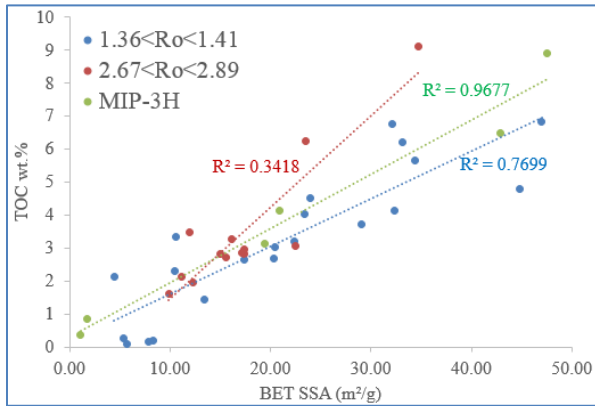


Figure 5: The relationship between BET specific surface area and TOC.

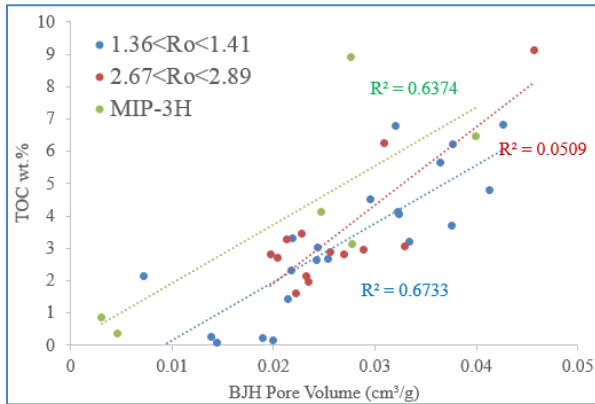


Figure 6: The relationship between BJH pore volume and TOC.

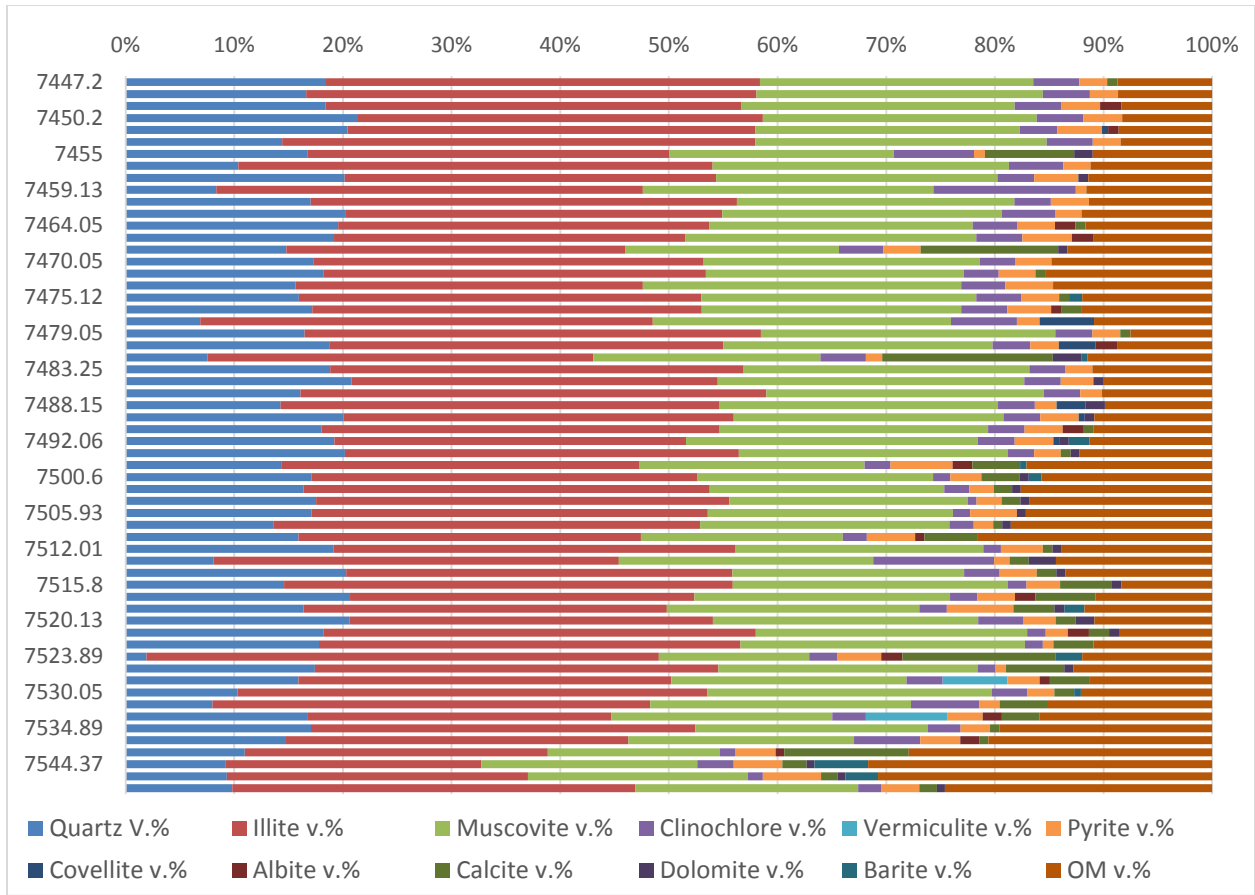


Figure 7: XRD data from well MIP-3H (in volume %) illustrating the mineralogical variations of the Marcellus Shale.

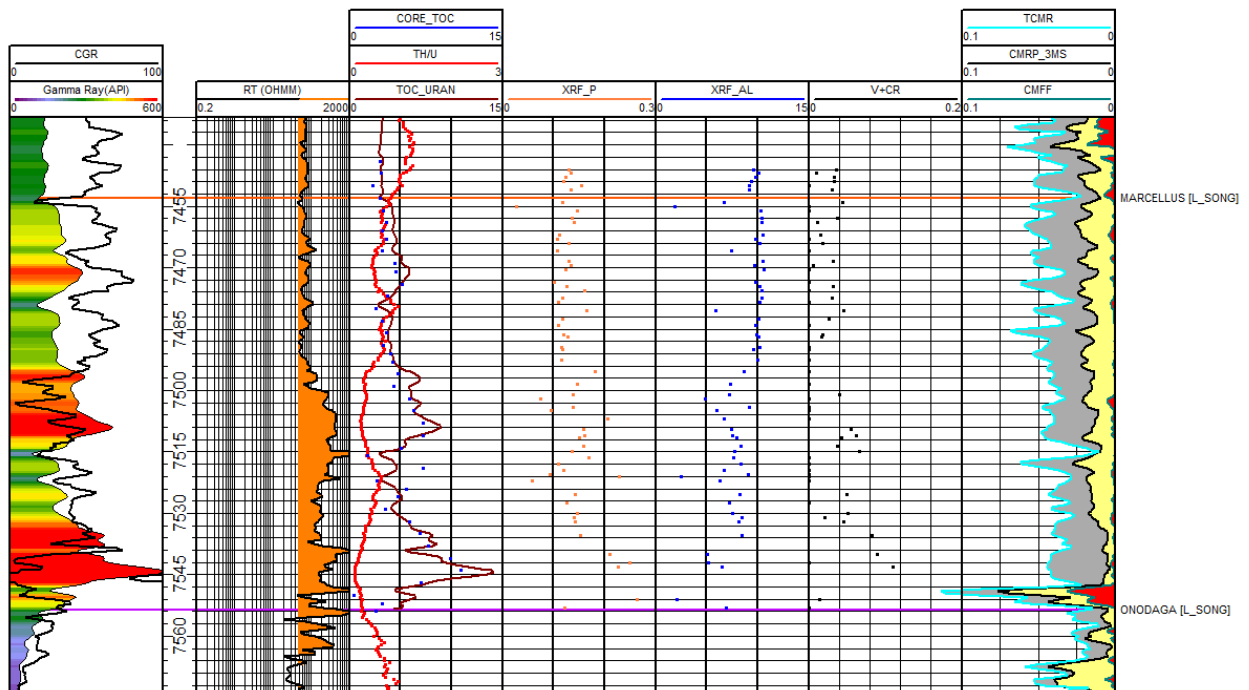


Figure 8. Geochemical and well-log profiles of the MIP-3H core showing abundances of P and Al from XRF test, Th/U from spectral GR, and NMR log.

Conclusions

Characterizing the pore structure of unconventional reservoirs is important for understanding the storage capacity and flow regime. Low pressure N₂ adsorption is a good method to study nano-scale pore structures especially micro- and meso-pores. It can provide pore surface area and pore volume information, which represents adsorbed gas and free gas storage capacity respectively. For accurate analysis, sample preparation is very important. We recommend crushing the sample until the entire mass passes through a 60-mesh sieve to prevent potential sample biasing due to sieving, then degas the sample at 120°C for 24 hours. The results indicate that micro- to meso-pores are concentrated in the organic content. Pore volume and pore surface area both show good positive correlations with TOC. Calibrated XRD results indicate that in lower Marcellus, the volume fraction of organic matter is approximately 30%, which offers great storage capacity especially for adsorbed gas.

Acknowledgement

The research undertaken in this study was funded through the U. S. DoE National Energy Technology Lab as part of their Marcellus Shale Energy and Environmental Laboratory (MSEEL) (DOE Award No.: DE-FE0024297). We also thank the Flexible Electronics for Sustainable Technologies (FEST) lab in the Mechanical and Aerospace Engineering Department of West Virginia University for offering the N₂ adsorption instrument.

References

- Adesida, A. G., I. Y. Akkutlu, D. E. Resasco, and C. S. Rai, 2011, SPE 147397 Kerogen Pore Size Distribution of Barnett Shale using DFT Analysis and Monte Carlo Simulations: SPE Annual Technical Conference and Exhibition, p. 1–14, doi:10.2118/147397-MS.
- Barrett, E. P., L. G. Joyner, and P. P. Halenda, 1951, The determination of pore volume and area distributions in porous substances. I. computations from nitrogen isotherms: *Journal of the American Chemical Society*, v. 73, no. 1, p. 373–380, doi:10.1021/ja01145a126.
- Brunauer, S., P. H. Emmett, and E. Teller, 1938, Adsorption of Gases in Multimolecular Layers: *Journal of the American Chemical Society*, v. 60, no. 1, p. 309–319, doi:citeulike-article-id:4074706\rdoi:10.1021/ja01269a023.
- Bustin, R. M., A. M. M. Bustin, B. Columbia, X. Cui, and D. J. K. Ross, 2008, SPE 119892 Impact of Shale Properties on Pore Structure and Storage Characteristics.
- Chen, R., and S. Sharma, 2017, Linking the Acadian Orogeny with organic-rich black shale deposition: Evidence from the Marcellus Shale: *Marine and Petroleum Geology*, v. 79, no. November, p. 149–158, doi:10.1016/j.marpetgeo.2016.11.005.
- Chen, R., S. Sharma, T. Bank, D. Soeder, and H. Eastman, 2015, Comparison of isotopic and geochemical characteristics of sediments from a gas- and liquids-prone wells in Marcellus Shale from Appalachian Basin, West Virginia: *Applied Geochemistry*, v. 60, no. June, p. 59–71, doi:10.1016/j.apgeochem.2015.01.001.
- Clarkson, C. R., J. M. Wood, S. E. Burgis, S. D. Aquino, and M. Freeman, 2012, Nanopore-structure analysis and permeability predictions for a tight gas siltstone reservoir by use of low-pressure adsorption and mercury-intrusion techniques: *SPE Reservoir Evaluation & Engineering*, v. 15, no. 6, p. 648–661, doi:10.2118/155537-PA.
- Crain, E. R., and D. Holgate, 2014, A 12-Step program to reduce uncertainty in kerogen-rich reservoirs: *Canadian Well Logging Society*, v. i, no. Spring, p. 10–16.
- Espitalie, J., G. Deroo, and F. Marquis, 1985, La pyrolyse Rock-Eval et ses applications. Deuxième partie.: *Revue de l'Institut Français du Pétrole*, v. 40, no. 6, p. 755–784, doi:10.2516/ogst:1985045.
- Kuila, U., and M. Prasad, 2013, Specific surface area and pore-size distribution in clays and shales: *Geophysical Prospecting*, v. 61, no. 2, p. 341–362, doi:10.1111/1365-2478.12028.
- Lash, G. G., and D. R. Blood, 2014, Organic matter accumulation, redox, and diagenetic history of the Marcellus Formation, southwestern Pennsylvania, Appalachian basin: *Marine and Petroleum Geology*, v. 57, no. November, p. 244–263, doi:10.1016/j.marpetgeo.2014.06.001.
- Luffel, D. L., and F. K. Guidry, 1992, New Core Analysis Methods for Measuring Reservoir Rock Properties of Devonian Shale, *in* SPE Annual Technical Conference and Exhibition: p. 1184–1190, doi:10.2118/20571-PA.
- Mastalerz, M., A. Schimmelmann, A. Drobnik, and Y. Chen, 2013, Porosity of Devonian and Mississippian New Albany Shale across a maturation gradient: Insights from organic petrology, gas adsorption, and mercury

- intrusion: AAPG Bulletin, v. 97, no. 10, p. 1621–1643, doi:10.130/04011312194.
- Olson, E., 2012, The Importance of Sample Preparation when Measuring Specific Surface Area: Journal of GXP Compliance, v. 16, no. 3, p. 52–62.
- Sageman, B. B., A. E. Murphy, J. P. Werne, C. A. Ver Straeten, D. J. Hollander, and T. W. Lyons, 2003, A tale of shales: The relative roles of production, decomposition, and dilution in the accumulation of organic-rich strata, Middle-Upper Devonian, Appalachian basin: Chemical Geology, v. 195, no. 1–4, p. 229–273, doi:10.1016/S0009-2541(02)00397-2.
- Sing, K., 2001, The use of nitrogen adsorption for the characterisation of porous materials: Colloids and Surfaces A: Physicochemical and Engineering Aspects, v. 187–188, p. 3–9, doi:10.1016/S0927-7757(01)00612-4.
- Sing, K. S. W., D. H. Everett, R. a. W. Haul, L. Moscou, R. a. Pierotti, J. Rouquérol, and T. Siemienińska, 1982, Reporting Physisorption Data for Gas / Solid Systems with Special Reference to the Determination of Surface Area and Porosity: Pure and Applied Chemistry, v. 57, no. 4, p. 603–619, doi:10.1351/pac198557040603.

URTeC: 2686732

Application of Fiber-optic Temperature Data Analysis in Hydraulic Fracturing Evaluation: A Case Study in Marcellus Shale

Shohreh Amini*, Payam Kavousi, Timothy R Carr, West Virginia University

Copyright 2017, Unconventional Resources Technology Conference (URTeC) DOI 10.15530/urtec-2017-2686732

This paper was prepared for presentation at the Unconventional Resources Technology Conference held in Austin, Texas, USA, 24-26 July 2017.

The URTeC Technical Program Committee accepted this presentation on the basis of information contained in an abstract submitted by the author(s). The contents of this paper have not been reviewed by URTeC and URTeC does not warrant the accuracy, reliability, or timeliness of any information herein. All information is the responsibility of, and, is subject to corrections by the author(s). Any person or entity that relies on any information obtained from this paper does so at their own risk. The information herein does not necessarily reflect any position of URTeC. Any reproduction, distribution, or storage of any part of this paper without the written consent of URTeC is prohibited.

Abstract

Technology advancement is a key parameter to gain more information, and valuable insight in the area where we lack proper knowledge to make the right decision at the right time. Development of unconventional resources is an area where application of advanced technology can play a significant role in shedding light on many unknowns pertaining to production from these resources.

Fiber-optic is among the new technologies that has recently received more attention in unconventional reservoir development. The data collected through optical fiber running along the horizontal or multi-lateral well, carry vast amount of information, which provides the operator with a near real-time monitoring opportunity.

This work is a part of Marcellus Shale Energy and Environment Laboratory (MSEEL) research, which is a unique multi-disciplinary research program, and aims at achieving a better understanding of the shale reservoirs and the best practices for producing from these resources. Despite the common practice of applying the same hydraulic fracturing design for all the stages of horizontal or multi-lateral wells in shale resources development, at MSEEL different stages of the well have been completed and stimulated with varying parameters. Perforation and hydraulic fracturing design along the lateral was performed based on reservoir characteristics, such as petrophysical parameters, geomechanical parameters, natural fracture density, amount of organic carbon, etc. Microseismic and fiber optic technology were used to monitor different stimulation operations performed on the well. Application of these technologies provided a large amount of information related to the performance of each operation.

This work is focused on the analysis of fiber-optic temperature data, collected from a multi-lateral well in Marcellus Shale. In this study, the performance of different hydraulically fractured stages of the well is investigated through evaluating the temperature changes along the wellbore during various operations. The analysis shows completion designs that lead to a better production from the corresponding stages. Using these results, best practice completion and stimulation plan can be suggested for infill drilling, re-fracturing or further development of the Marcellus Shale.

Introduction

During the last couple of decades, gas production from unconventional resources has grown rapidly. Shale gas is one of the unconventional resources, which is playing a major role in the world energy supply (EIA, 2016).

Due to the characteristics of the unconventional reservoirs (extremely low porosity and permeability) compared to the conventional reservoirs, utilization of hydraulic fracturing is required to make economic production. High volume hydraulic fracturing over multiple stages in horizontal well bores has employed relatively short history in our industry, and therefore there are many unknowns regarding different aspects of this operation.

Application of new technology is significantly beneficial to obtain more information and get more insights into the shale characteristics, fluid flow behavior within the shale formation, and production from multi-stage hydraulically fractured wells. However, the economic burden of utilizing advanced measurement tools on top of the already

expensive operation of horizontal drilling, and hydraulic fracturing makes it unappealing to the majority of the operators in shale. Therefore, most of the shale development operations are performed using a simple geometry design for the perforation and hydraulic fracturing, without considering any other parameters, such as the reservoir characteristics at the stage location.

This approach can result in a sub-optimal production from a shale reservoir, and lead to an adverse economic outcome. However, in shale development, the information that is gained through advanced measurements leads to a more insightful completion and stimulation design, which can eventually contribute to improved production rates and higher ultimate recovery from the wells. One of the advanced technologies that can be advantageous in shale development is fiber-optic, which can be applied in high-temperature/high-pressure condition to provide flow profiling and accurate wellbore monitoring (Denney, 2007).

Fiber-optic Technology Overview and Application

Real-time downhole data collected through optical fiber provides a means to greatly improve production management and ultimate reservoir recovery (Kragas, Williams, & Myers, 2001).

The distributed acoustic sensing (DAS) is a fiber-optic downhole measurement sensitive to local vibration around the fiber (Dickenson, et al., 2016). DAS technology is based on the Optical Time Domain Reflectometry (OTDR). A laser pulse travels inside the fiber and will be scattered back encountering natural imperfection in the fiber. The recorded backscatter contains information of local axial strain along the fiber (Parker, Shatalin, & Farhadiroushan, 2014). Distributed temperature sensing is another common fiber-optic measurement sensitive to temperature variations around the fiber. DAS and DTS measurements are often recorded in parallel to provide a more comprehensive understanding of stimulation (Molenaar & Cox, 2013).

Downhole fiber-optics was used to provide continuous measurement of pressure and temperature for West Coalinga Field in California (Karaman & Kutlik, 1996). Other applications such as water injection surveillance, leak detection analysis, acid injection profiling, and hydraulic fracturing have been documented (Rahman, Zannitto, & Reed, 2011), (Glasbergen, Yeager, Reyes, & Everett, 2010), (Sierra, Kaura, Gualtieri, Glasbergen, Sarker, & Johnson, 2008), (Holley & Kalia, 2015).

Employing fiber optic distributed measurements can be significantly beneficial in multiple stages of completion, post completion and production of a well.

Study Area

The well is located in Morgantown Industrial Park (MIP) site in the state of West Virginia (USA), and it is a part of the Marcellus Shale Energy and Environment Laboratory (MSEEL). MSEEL is a multi-disciplinary research program that aims at achieving a better understanding of the shale resources to ensure that energy is extracted in an economically efficient and environmentally responsible manner. Application of advanced technology such as comprehensive well logs, microseismic, Distributed Acoustic Sensing (DAS) and Distributed Temperature Sensing (DTS) at MSEEL, provides an opportunity to collect a large amount of data during various operations.

At the MIP site, two horizontal wells (MIP-4H and MIP-6H) were drilled in Marcellus Shale, and have produced natural gas since December 2011. Two new horizontal wells (MIP-3H and MIP-5H) were drilled from the existing pad, and placed on production in December 2015. MIP site also includes a vertical scientific observation well (MIP-SW) drilled approximately one half mile to the northwest between the two new horizontal wells for the purpose of additional subsurface data collection, and microseismic monitoring. The locations of the existing and newly drilled wells are depicted in Figure 1.

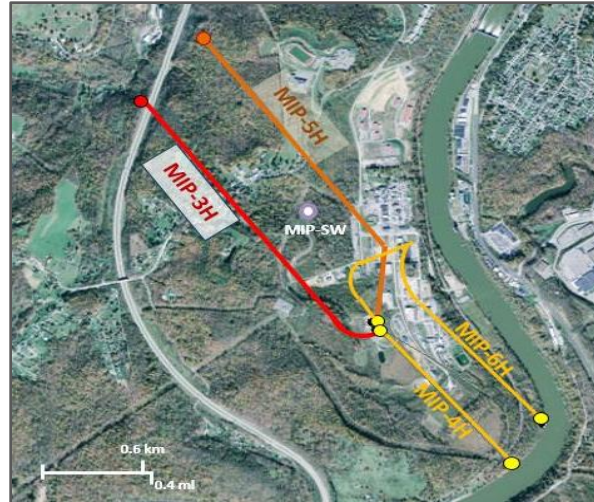


Figure 1. Marcellus Shale Energy and Environment Laboratory (MSEEL) just outside Morgantown, West Virginia, USA. The MSEEL site consists of four horizontal production wells operated by Northeast Natural Energy LLC. (MIP-3H, MIP-4H, MIP-5H, MIP-6H), two pilot holes (MIP-3 and MIP-4), a micro-sesimic and sampled observation well (MIP-SW). Fiber-optic cable was installed in the MIP-3H

MIP-3H Completion Specification

The MIP-3H well was completed over 28 stages in 5 sections from the toe to the heel Table 1. Section A and B are completed using a geometrical approach in which geomechanical parameters that does not account for geomechanical properties, fracture closure stress, fracture intensity. Two types of proppants are used for hydraulic fracturing of MIP-3H: 100 mesh sand and 40/70 mesh white sand. Section A has around 35% 100 Mesh proppants and 65% 40/70 white sand, while Section B has 75% 100 Mesh Sand and 25% 40/70 white sand.

The completion extends to Section C, labeled as Engineered Completion (Table 1). This section is designed by appraising geomechanical parameters from the well logs: each stage is set in a zone with similar fracture closure stress, fracture intensity, and gamma ray (Anifowoshe, et al., 2016). The proportion of proppants varies between stages in Section C: Stages 13, 14, 15, 17, and 19 have 35% 100 mesh while Stage 16 has 67% mesh 100 and Stage 18 around 43% mesh 100. In addition, limited entry approach was undertaken by decreasing the number of shots per clusters to enhance stimulation efficiency (Anifowoshe, et al., 2016).

A new guar-free viscoelastic fracturing fluid known as Sapphire VF® is used in stages 20 and 21(Section D) to maximize the well performance (Schlumberger, 2014). Sapphire fluids are designed to enhance proppants transport, deliver higher retained proppant pack permeability, improve fracture clean up, and lower the treatment pressure. Section E includes stages 22 to 28, which were completed using a combination of engineered approach along with using Sapphire fluid, and an accelerated pumping schedule.

Distributed Acoustic Sensing (DAS) and Distributed Temperature Sensing (DTS) fiber-optic devices are deployed in order to measure, and record high resolution energy band amplitude and temperature data along this well. Fiber-optic data is used for the purpose of well surveillance and long-term performance monitoring of the well bore as well as the reservoir.

Hydraulic fracturing design parameters for different stages of this well are summarized in Table 1.

Table 1. Hydraulic fracture designed parameters for MIP-3H by stage and zone

Section	Stage	Cluster Count	Total Shot Count	Shot Density (shot/ft)	Stage Length (ft)	Pump schedule	
E	Best Practice Applied	28	4	40	6	191	A
		27	4	40	6	184	A
		26	5	40	6	225	A
		25	5	32	6	231	A
		24	5	30	6	222	A
		23	5	40	6	237	C
		22	5	40	6	220	C
D	Sapphire VF	21	5	40	5	218	D
		20	5	40	5	240	D
C	SLB Engineered Completion	19	4	32	6	180	C
		18	4	32	8	180	C
		17	4	32	6	181	C
		16	4	26	6	178	C
		15	4	26	6	186	C
		14	5	30	6	228	A
		13	5	30	6	230	A
B	NNE 75% 100-Mesh	12	5	50	5	231	B
		11	5	50	5	232	B
		10	5	50	5	227	B
		9	5	50	5	237	B
		8	5	50	5	222	B
		7	5	50	5	224	B
A	NNE Standard 35% 100-Mesh	6	5	50	5	245	A
		5	5	50	5	234	A
		4	5	50	5	230	A
		3	5	50	5	238	A
		2	5	50	5	223	A
		1	5	50	5	233	A

DTS Data Acquisition

In order to collect temperature data, a strand of optical fiber, running inside the wellbore (outside the casing) sends a pulse of light, and the reflection signal is further processed to obtain the temperature at different locations along the well. Fiber-optic temperature data for MIP-3H are available during three intervals; stimulation, flow back, and production of this well. In the subsequent sections, the temperature distribution is visualized along the entire lateral, during several well operations.

1. Stimulation

Temperature data recorded during stimulation has the highest temporal and spatial resolution. Temperature data is recorded every 30 seconds, with a spatial sampling of 1.5 feet. To generate the temperature distribution an averaging filter, with a window length of 1 hour, was applied to all the stages along the lateral.

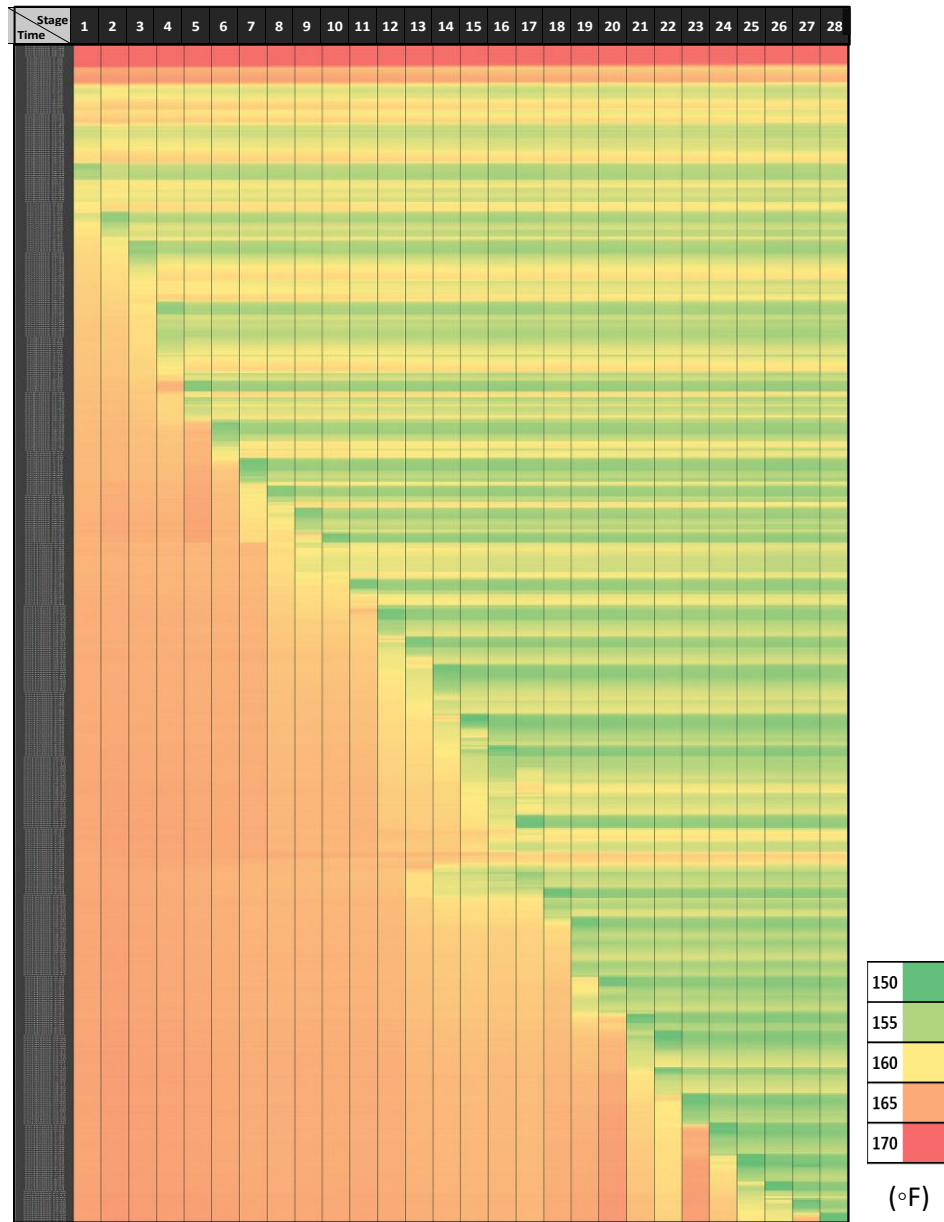


Figure 2. Temperature distribution in degrees Fahrenheit, at different stages of MIP-3H during stimulation. Stages 1 through 28 are shown on the horizontal axis and one-hour increments on the vertical axis.

In Figure 2, the 28 stages of the lateral are demonstrated in horizontal axis while simulation time is shown on the vertical axis. The very early time, with a uniform red color, represents the original reservoir temperature ($^{\circ}\text{F}$) that is followed by a green color, demonstrating the cooling effect of the fluid which is pumped through the wellbore. The area with darker green, shows the location of the stage which is being hydraulically fractured.

Observing the temperature distribution throughout the well during the entire stimulation operation provides us with valuable information. In some stages, at the time of fracturing, an increase in temperature is observed in the earlier stages (observed in stages 5, 6, 10, 12, 21 and 24). This is an indication of the existence of either a fault or conductive fractures in the vicinity of those stages which are activated by the stimulation operation and ultimately results in communication between the stages (Carr, et al., in press). In some cases, the temperature peaks and then falls back and, in some other cases the high temperature lasts for a longer while. This depends on the time during which generated communication between stages remains accessible.

2. Flow-back

Temperature measurement in flow-back period has time resolution of 5 minutes, and length resolution of 1.5 feet. Temperature values are normalized along the lateral to better demonstrate the temperature distribution along the lateral during the flow-back period (Figure 3).

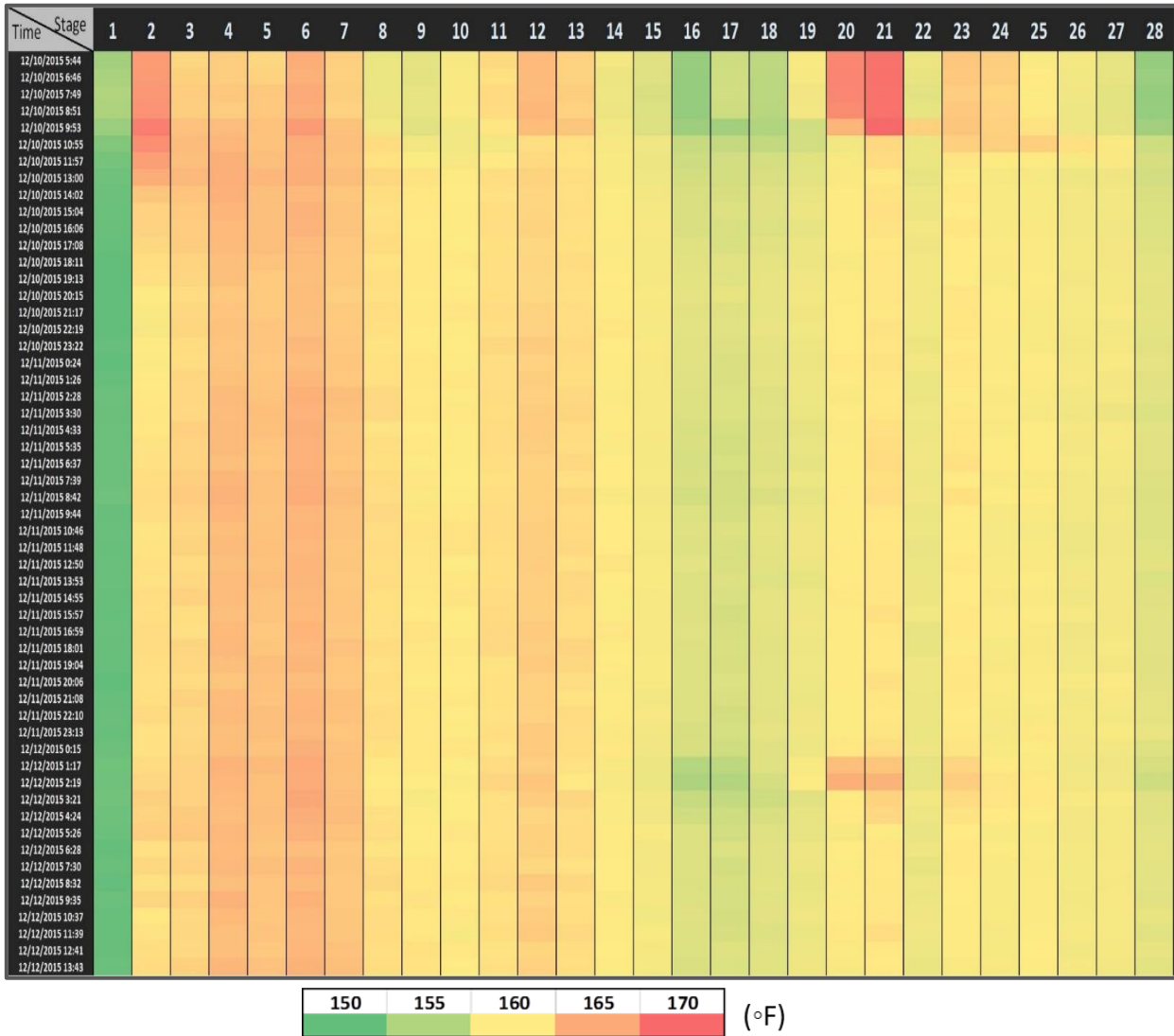


Figure 3. Normalized temperature distribution at different stages of MIP-3H during flow-back. Stages 1 through 28 are shown on the horizontal axis and three-hour increments on the vertical axis.

3. Production

During production a daily, 3-hour average temperature, is recorded at each 13 feet for the vertical section and each 5 feet for the lateral. Temperature distribution during production is presented in Figure 4.



Figure 4. Temperature distribution at different stages of MIP-3H during production. Stages 1 through 28 are shown on the horizontal axis and one-day increments on the vertical axis.

During this time interval, the average daily gas production of MIP-3H is 3.3 MMCF. Minimum temperature at this interval is 150 °F. From May 2016, gas production rate, due decreased demand from the City of Morgantown, was decreased to about half of the production in the first quarter (average daily gas production 1.7 MMCF). This causes a temperature increase along the lateral and therefore, the minimum temperature reaches to 164 °F.

Figure 5 illustrates the temperature distribution, which is normalized along the lateral, during the two time intervals of high and low production, separately.

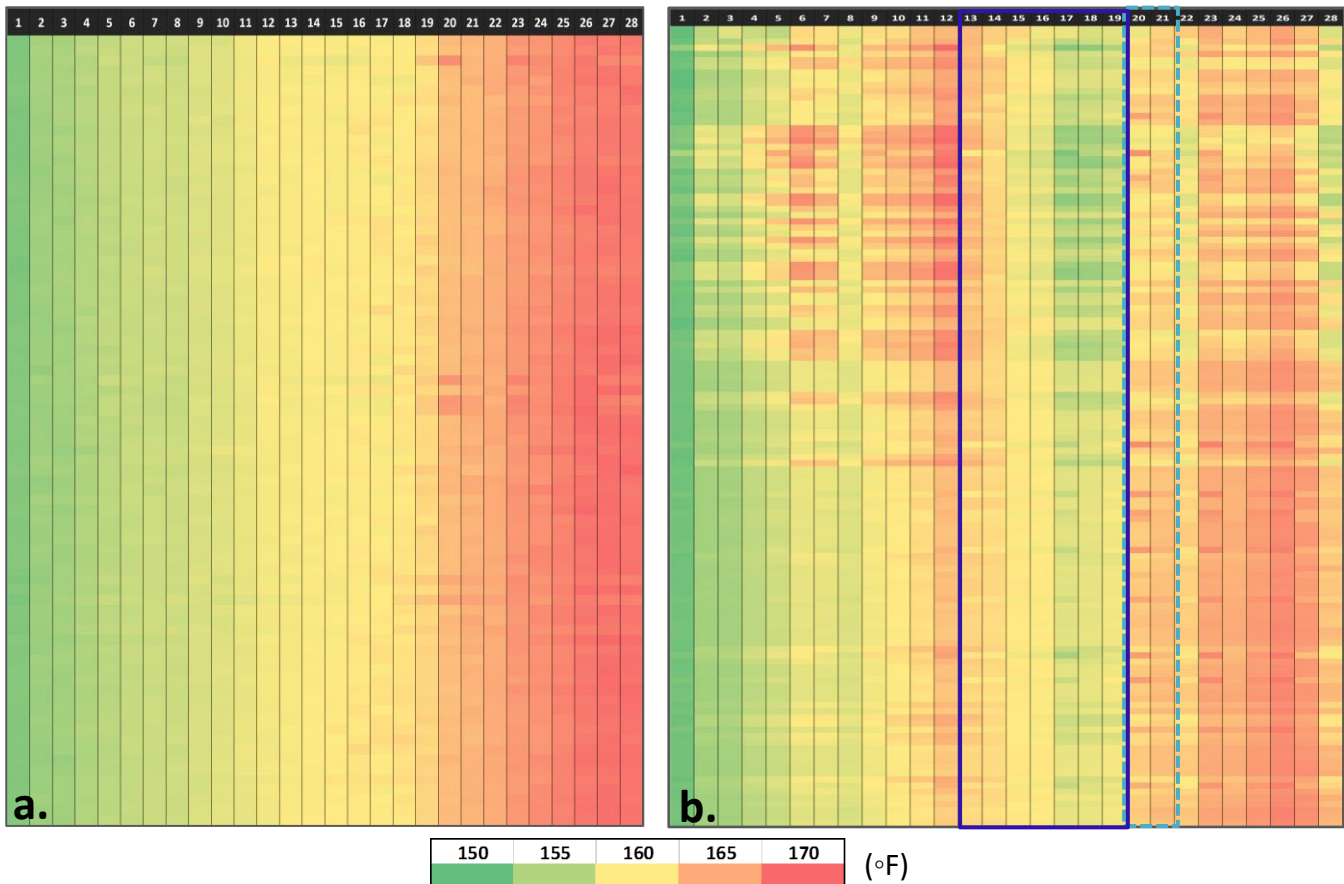


Figure 5. Normalized temperature distribution at different stages of MIP-3H during:
(a) High production period, (b) Low production period

During the high production interval, generally temperature increases from the toe towards the heel and the cooling effect is masked in the stages closer to the heel.

During the low production interval, the general trend of increased temperature from the toe to the heel is not seen due to the low amount of gas, and therefore the higher producing stages show lower temperature.

Summary and Conclusion

This study demonstrates how a different approach to analyzing the collected fiber-optics temperature data, provides us with valuable information. By summarizing and visualizing the data on stage-based format during each specific operation, completion efficiency of hydraulic fracturing are put into perspective.

Hydraulic fracturing of some stages of MIP-3H resulted in an increase in the temperature of the earlier stages. This is an indication of the existence of either MIP faults or conductive fractures in the vicinity of those stages. The faults or fractures are activated by the stimulation operation, and therefore a communication path is generated between the stages.

In the flow-back period a distinct pattern can be observed from the temperature of the differently completed stages (lower temperature between stages 13 to 19, and higher temperature in stages 20 and 21).

Evaluating the temperature data during the low rate production period shows lower temperature in stages 13 to 19 which is an indication of higher production in these stages. It should be noted that although these stages are all included in the section C of completion, with engineered design, they don't have similar performance. Looking more closely to the completion parameters it is observed that they have been completed with different stage length and different number of clusters. In fact shorter stage length, and fewer number of clusters resulted in higher production.

Stages 20 and 21 which are both generated using Sapphire VF® fluid, show a poor production performance. This can be related to the fact that the viscos hydraulic fracturing fluid is not effectively performing in this type of the reservoir.

Acknowledgements

This research was funded by a grant from Department of Energy's National Energy Technology Laboratory (DE-FE0024297).

References

- Anifowoshe, O., Yates, M., Xu, L., Dickenson, P., Akin, J., Carney, B. J., et al. (2016). Improving Wellbore Stimulation Coverage in the Marcellus: Integrating Lateral Measurements with Enhanced Engineered Completion Design and Fiber Optic Evaluation. *SPE Eastern Regional Meeting*. Canton, Ohio: Society of Petroleum Engineers.
- Carr, T. R., Wilson, T. H., Kavousi, P., Amini, S., Sharma, S., Hewitt, J., et al. (in press). Insights from the Marcellus Shale Energy and Environment Laboratory (MSEEL). *Unconventional Resources Technology Conference*. Austin, Texas: SPE.
- Denney, D. (2007). Real-Time Fiber-Optic Distributed Temperature Sensing: Oilfield Applications. *Journal of Petroleum Technology (JPT)*.
- Dickenson, P., Brants-Menard, S., Telsey, M., Stanbridge, A., Wilson, C., Akin, J., et al. (2016). Real-Time Interactive Remote Display of DTS and DAS Data for Well Treatment Optimization. *SPE Intelligent Energy International Conference*. Aberdeen, Scotland: Society of Petroleum Engineers.
- EAI. (2016). *International Energy Outlook*. Retrieved 2016, from US Energy Information Administration: [https://www.eia.gov/outlooks/ieo/pdf/0484\(2016\).pdf](https://www.eia.gov/outlooks/ieo/pdf/0484(2016).pdf)
- Glasbergen, G., Yeager, V. J., Reyes, R. P., & Everett, D. M. (2010). Fluid-Diversion Monitoring: The Key to Treatment Optimization. *SPE Production & Operations*.
- Holley, E. H., & Kalia, N. (2015). Fiber-optic Monitoring: Stimulation Results from Unconventional Reservoirs. *Unconventional Resources Technology Conference*. San Antonio, Texas: Unconventional Resources Technology Conference.
- Karaman, O. S., & Kutlik, R. L. (1996). A Field Trial to Test Fiber Optic Sensors for Downhole Temperature and Pressure Measurements, West Coalinga Field, California. *SPE Western Regional Meeting*. Anchorage, Alaska: Society of Petroleum Engineers.
- Kragas, T. K., Williams, B. A., & Myers, G. A. (2001). The Optic Oil Field: Deployment and Application of Permanent In-well Fiber Optic Sensing Systems for Production and Reservoir Monitoring. *SPE Annual Technical Conference and Exhibition*. Louisiana, New Orleans: SPE.
- Molenaar, M. M., & Cox, B. E. (2013). Field Cases of Hydraulic Fracture Stimulation Diagnostics Using Fiber Optic Distributed Acoustic Sensing (DAS) Measurements and Analyses. *SPE Unconventional Gas Conference and Exhibition*. Muscat: Society of Petroleum Engineers.
- Parker, T., Shatalin, S., & Farhadiroushan, M. (2014, February). Distributed Acoustic Sensing – a new tool for seismic applications. *First Break*.
- Rahman, M., Zannitto, P. J., & Reed, D. A. (2011). Application of Fiber-Optic Distributed Temperature Sensing Technology for Monitoring Injection Profile in Belridge Field, Diatomite Reservoir. *SPE Digital Energy Conference and Exhibition*. The Woodlands, Texas: Society of Petroleum Engineers.
- Shelumberger. (2014). *sapphire VF Guar-free viscoelastic fracturing fluid*. Retrieved October 2016, from http://www.slb.com/~media/Files/stimulation/product_sheets/sapphire_vf_ps.pdf.

Sierra , J. R., Kaura, J. D., Gualtieri, D., Glasbergen, G., Sarker, D., & Johnson, D. (2008). DTS Monitoring of Hydraulic Fracturing: Experiences and Lessons Learned. *SPE Annual Technical Conference and Exhibition*. Denver, Colorado: Society of Petroleum Engineers.

URTeC: 2669914

The Marcellus Shale Energy and Environmental Laboratory (MSEEL): Water and Solid Waste Findings—Year One

Paul F. Ziemkiewicz*, PhD

Director, Water Research Institute, West Virginia University

Copyright 2017, Unconventional Resources Technology Conference (URTeC) DOI 10.15530/urtec-2017-2669914

This paper was prepared for presentation at the Unconventional Resources Technology Conference held in Austin, Texas, USA, 24-26 July 2017.

The URTeC Technical Program Committee accepted this presentation on the basis of information contained in an abstract submitted by the author(s). The contents of this paper have not been reviewed by URTeC and URTeC does not warrant the accuracy, reliability, or timeliness of any information herein. All information is the responsibility of, and, is subject to corrections by the author(s). Any person or entity that relies on any information obtained from this paper does so at their own risk. The information herein does not necessarily reflect any position of URTeC. Any reproduction, distribution, or storage of any part of this paper without the written consent of URTeC is prohibited.

Summary

The Marcellus Shale Energy and Environment Laboratory (MSEEL) is centered on four producing, horizontal wells located across the Monongahela River from Morgantown WV. The wells are within 600m of the River and 950m from the Morgantown Utility Board (MUB) water intake. Two horizontal wells were completed in the Marcellus Formation in 2011. In 2015 WVU was awarded a contract by the USDOE/National Energy Technology Laboratory to implement a long-term field study around two new wells on the site to develop and validate new knowledge and technology to improve recovery efficiency and minimize environmental implications of shale gas development.

Prior to MSEEL, there had been no comprehensive field study coupling same site environmental baseline, completion and production monitoring with environmental outcomes. The water and solid waste component of the MSEEL project include monitoring the Monongahela River upstream of the MSEEL site, at the MUB water intake and downstream of MUB. Solid waste characterization includes drilling mud and drill cuttings through the vertical and horizontal well legs. Liquids analysis includes completion fluid, and time-series flowback and produced water sampling and analysis. Analytical parameters include organic, inorganic and radionuclides. MSEEL is generating an unprecedented body of data which will be available to researchers at NETL and researchers from other agencies and institutions for advancement of the science around shale gas development and evaluation of procedures needed to protect the public and the environment.

This presentation summarizes results of the first year: drilling, completion, flowback and produced water sampling as well as River monitoring. Important findings include the role of drilling fluids in determining the toxicity of drill cuttings, radioactivity levels in drill cuttings and time series trends in aqueous phase organic compounds (BTEX), radium, alpha and beta emitters and twenty inorganic ions. River monitoring indicated no effects attributable to well development and production. Risk reduction practices at the MSEEL well site will also be discussed.

Approach

The Marcellus Shale Energy and Environment Laboratory (MSEEL) is the first comprehensive field study coupling same site environmental baseline, completion and production monitoring with environmental outcomes. One year into the post completion part of the program, the water and solid waste component of MSEEL has systematically sampled flowback and produced water volumes, hydraulic fracturing fluid, flowback, produced water, drilling muds, drill cuttings and characterized their inorganic, organic and radio chemistries. In addition, surface water in the nearby Monongahela River was monitored upstream and downstream of the MSEEL drill pad. Toxicity testing per EPA method 1311 (TCLP) was conducted on drill cuttings in both the vertical and horizontal (Marcellus) sections to evaluate their toxicity potential.

The MSEEL production wells 3H and 5H were developed by Northeast Natural Energy, LLC (NNE) on the MIP well pad and completed in December 2015. The MIP pad contained two previous production wells: 4H and 6H.

The older wells were completed in 2011. The MIP pad is at an elevation 75 m above and a linear distance of 580 m from the Monongahela River, at a point 700 m upstream of the Morgantown Utility Board's primary drinking water intake. Prior to construction of the MIP pad NNE adopted a secondary containment strategy to minimize the risk of offsite contamination. This included a double HDPE liner and berms sufficient to contain any accidental leakage within the pad. Makeup water was taken from the Monongahela River and stored in a lined pond adjacent to the MIP pad. To ensure integrity of the water supply, the river was sampled at three stations: upstream, downstream and at the Morgantown Utility Board's water intake. Sampling began prior to installation of the 3H and 5H wells and continued for one year post completion.

Background

Hydraulic fracturing stimulates wells by injecting high volumes of water, sand and chemical additives into an otherwise non-producing, hydrocarbon rich formation at high pressures to induce porosity by developing and supporting fractures (US EPA 2010). Combined with horizontal drilling and development of extended, lateral well bores, hydraulic fracturing technology is critical to the viability of unconventional hydrocarbon plays.

Hydraulic fracturing requires significant quantities of water: Requirements commonly range from 11,000 to 19,000 m³ for a horizontal well, but volumes as high as 34,000 m³ have been reported (Xu et al., 2011; Lewis, 2012; Bai et al., 2013). Fracturing fluid typically consists of between 80 to 90 percent water; 8 to 15 percent proppant while the remaining 0.5- 1 percent consists of chemical additives. Commonly used additives include about 11 chemicals with different functions such as friction reducers, biocides, scale inhibitors, clay stabilizers, and surfactants (URS, 2011; McCurdy, 2011). Exposure pathways (Ziemkiewicz et al., 2014a) and protective measures (Ziemkiewicz et al., 2014b) have stressed the potential toxicity of produced water.

Methods

Produced water sampling. During well completion, hydraulic fracturing fluids are injected into the target formation and the injected fluids return to surface via the well bore as flowback. Figure 1 shows the general processes of fluid flow during hydraulic fracturing and gas production. Produced water is returned via the well bore along with gas during production phase. The distinction between flowback and produced water is not well defined and these two terms are sometimes used interchangeably in the vernacular.

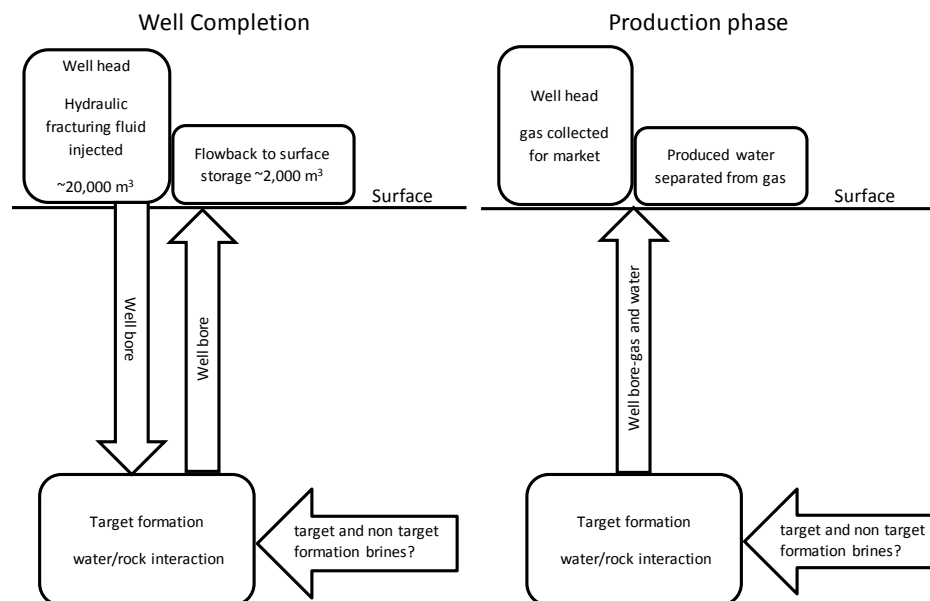


Figure 1. Flow of fluids during the well completion (hydraulic fracturing) and production phases of well operations (from Ziemkiewicz, 2014c)

Samples of frac makeup water, the hydrofrac fluid, flowback and produced water were sampled monthly over an interval of 392 days at the 3H and 5H wells. In addition, the 4H and 6H wells which were shut in when the newer wells came on line were re-activated and sampled starting in late 2016. Makeup water was pumped from the Monongahela River and mixed with the hydraulic fracturing fluids. Produced water samples were taken at the upstream end of each well's separator. Table 1 summarizes the analytical parameters: inorganic, organic and radiochemical.

Solid waste sampling and testing. Solid waste consisted of drill cuttings collected during the vertical and horizontal legs of the 3H and 5H wells. They were characterized according to the parameters listed in table 2. In addition both vertical and horizontal (Marcellus) samples were subjected to USEPA method 1311, the Toxic Characteristic Leaching Procedure (TCLP) to determine whether the drill cuttings constituted hazardous waste under the USEPA's Resource Conservation and Recovery Act (RCRA).

Table 1. Aqueous analytical parameters.

Aqueous chemistry parameters - HF fluids and PW					
Inorganics			Organics	Radionuclides	
pH	Anions	Cations*		Benzene	α
	TDS	Br	Ag		
TSS	Cl	Al	Mn	Ethylbenzene	^{40}K
Conductance	SO_4	As	Na	Total xylene	^{226}Ra
Alkalinity	sulfides	Ba	Ni	m,p-xylene	^{228}Ra
Bicarbonate	nitrate	Ca	Pb	o-xylene	
Carbonate	nitrite	Cr	Se	MBAS	
TP		Fe	Sr	O&G	
		K	Zn		

* total and dissolved

Table 2 Analytical parameters drill cuttings and mud.

Solids chemistry parameters - Cuttings & Muds								
Inorganics			Organics	Radionuclides	TCLPs			
alkalinity**	Anions	Cations*		Propane	α	Arsenic	1,4-Dichlorobenzene	Methyl ethyl ketone
	conductance	Br	Ag	Mg				
pH	Cl	Al	Mn	ORO	^{40}K	Benzene	1,1-Dichloroethylene	Pentachlorophenol
bicarbonate**	SO_4	As	Na	GRO	^{226}Ra	Cadmium	2,4-Dinitrotoluene	Pyridine
carbonate**	sulfide	Ba	Ni	Ethylbenzene	^{228}Ra	Carbon tetrachloride	Endrin	Selenium
TP	nitrate	Ca	Pb	m,p-xylene		Chlordane	Heptachlor	Silver
	nitrite	Cr	Se	o-xylene		Chlorobenzene	Heptachlor epoxide	Tetrachloroethene
		Fe	Sr	Styrene		Chloroform	Hexachlorobenzene	Toxaphene
		K	Zn	Toluene		Chromium	Hexachlorobutadiene	Trichloroethylene
				Total xylenes		o-Cresol	Hexachloroethane	2,4,5-Trichlorophenol
				TOC		m-Cresol	Lead	2,4,6-Trichlorophenol
				COD		p-Cresol	Lindane	2,4,5-TP (Silvex)
				O&G		Cresol	Mercury	Vinyl chloride
						2,4-D	Methoxychlor	

Results and Discussion

The MSEEL wells used green completion strategy including a synthetic based drilling fluid (Bio-Base 365). All drill cutting samples fell below TCLP thresholds for organic and inorganic components indicating that they are non-hazardous per the Resource Conservation and Recovery Act. Maximum specific isotopic activity in drill cuttings was recorded for ^{40}K which was 28.32 pCi/g. Gross alpha accounted for the highest reading at 60 pCi/g. The

maximum combined radium isotope values ($^{226+228}\text{Ra}$) was 10.85 pCi/g. These radioactivity levels are within the West Virginia standard of 5 pCi/g above regional background levels.

The composition of the hydraulic fracturing (HF) fluids in both wells was similar to the makeup water which was drawn from the Monongahela River. Its chemistry was typical of Monongahela River water. This is true of inorganics, organics and radioisotopes. Organic surrogate recoveries were in the range of 90 to 104% indicating good quality control at the analytical laboratory. There was no evidence that Monongahela River quality was influenced by well development, completion or production at the MSEEL site.

Produced water is severely contaminated indicating care in handling. Concentrations of all parameters increased through the flowback/produced water cycle. $^{226+228}\text{Ra}$ reached 20,000 pCi/L at post completion day 251 indicating an important trend that will be carefully assessed in ongoing monitoring.

Produced water volume trends in wells MIP 3,5H and MIP 4,6H. NNE's water production logs were used to estimate produced water volumes. While water production rates were similar in the first two months post completion, cumulative rates soon diverged yielding very different curves for each well (figure 2). It is noted that the older wells (4H, 6H) were shut in between 12 Dec 15 and 17 Oct 16, an interval of 315 days.

The proportion of injected hydraulic fracturing fluid returned as produced water, even after 1844 days (5 years) was only 12% at MIP 4H and 7.5% at MIP 6H (table 3). The reason for the variation among wells both with respect to cumulative and proportional produced water returns remains unclear.

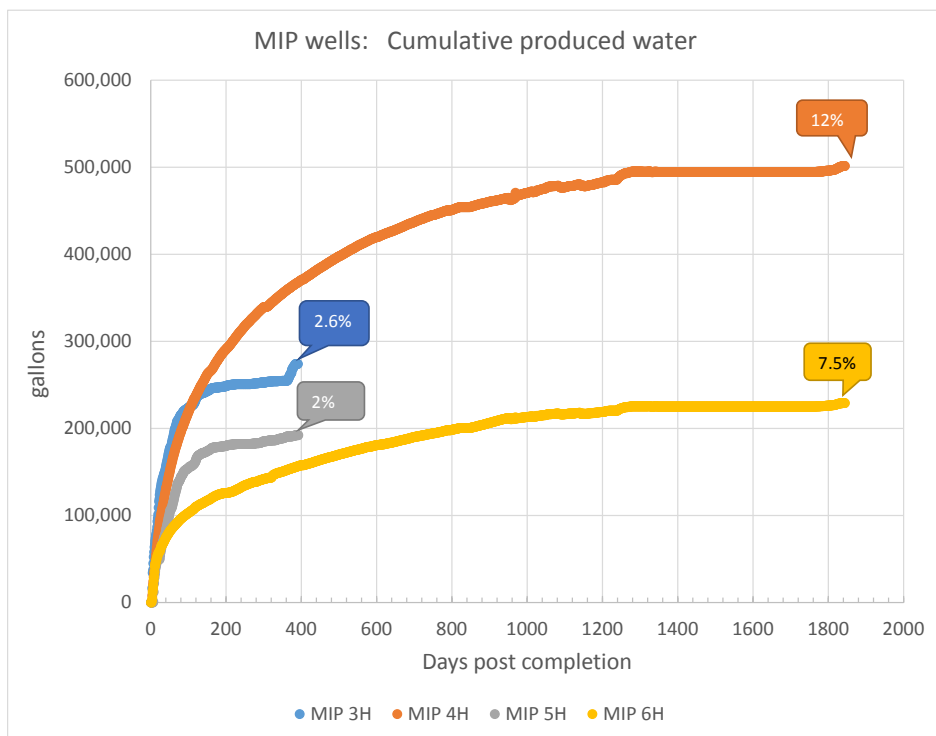


Figure 2. Cumulative water production at the four MSEEL wells. The estimated proportion of produced water to HF fluids are shown in the callouts.

Table 3. Produced water volumes relative to injected HF fluid for each MSEEL well.

	days post	cumulative produced water		HF injected
	completion	gal	% injected	gal
MIP 3H	392	274,102	2.6%	10,404,198
MIP 5H	392	192,134	2.0%	9,687,888
MIP 4H	1844	501,396	12.0%	4,160,982
MIP 6H	1844	229,183	7.5%	3,042,396

Trends in produced water chemistry

Major ions. While makeup water was characterized by low total dissolved solids (TDS) and a dominance of calcium and sulfate ions, produced water from initial flowback is essentially a sodium/calcium chloride water (figure 3). Other than slight increases in the proportion of barium and strontium, the ionic composition of produced changed very little through 314 days post completion.

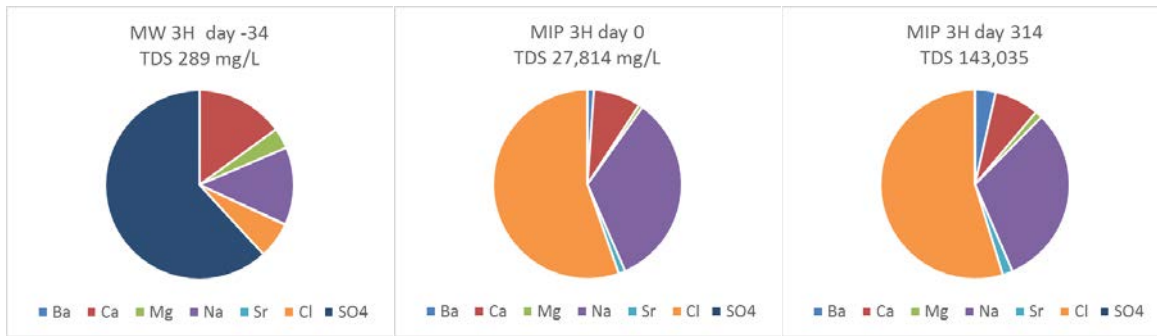


Figure 3 Changes in major ion concentrations in produced water from well MIP 3H. From left to right the charts represent makeup water from the Monongahela River, produced water on the first day of flowback and produced water on the 314th day post completion.

In fact, after 1858 days ionic composition in the older 4H and 6H wells remained nearly identical to the initial produced water from the 3H and 5H wells (figure 4).

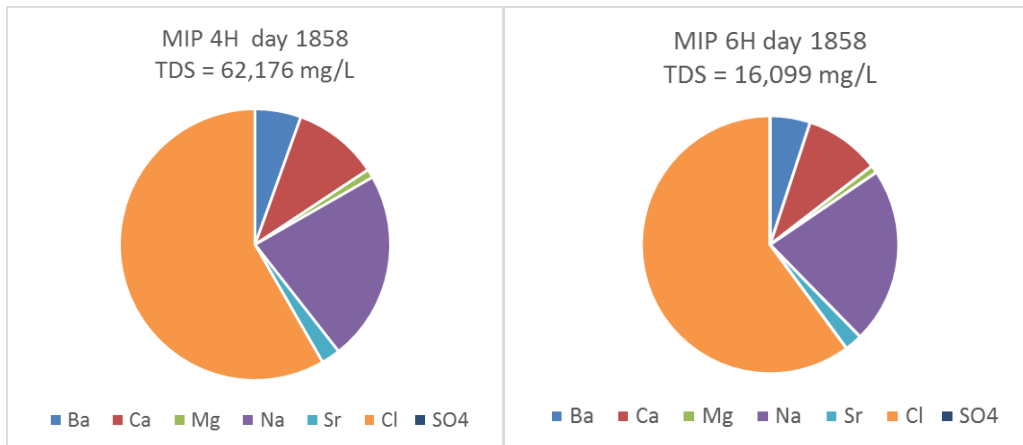


Figure 4 Major ion composition of wells MIP 4H and 6H 1858 days after completion.

While TDS increased rapidly over the initial 90 days post completion, it appears to have levelled off between 100,000 and 150,000 mg/L (figure 5). The older 4H and 6H wells offer insight into the longer term TDS trend.

Those wells only came back on line in October 2016 after a shut in period of 315 days and while those results vary they are much lower than the recent values for wells MIP 3H and 5H. Thus far, results are only available for two sampling dates: 16 Nov 16 and 14 Dec 16. TDS varied between 62,176 mg/L at well MIP 4H and 16,099 mg/L at MIP 6H. If these trends continue, it would suggest that available formation salt is being exhausted.

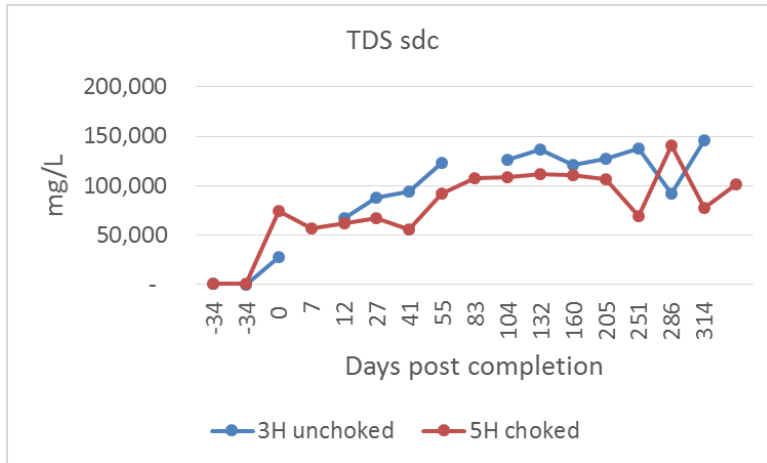


Figure 5 Changes in produced water TDS_{sdc} (sum of dissolved constituents) through the first 340 days post completion.

Water soluble organics. The water soluble aromatic compounds in produced water: benzene, toluene, ethylbenzene and xylene were never high. With one exception at post completion day 321, benzene has remained below 30 µg/L (figure 6). This may be a characteristic of dry gas geologic units and is consistent with Hayes (2009). After five years, benzene has declined below the drinking water standard of 5 µg/L.

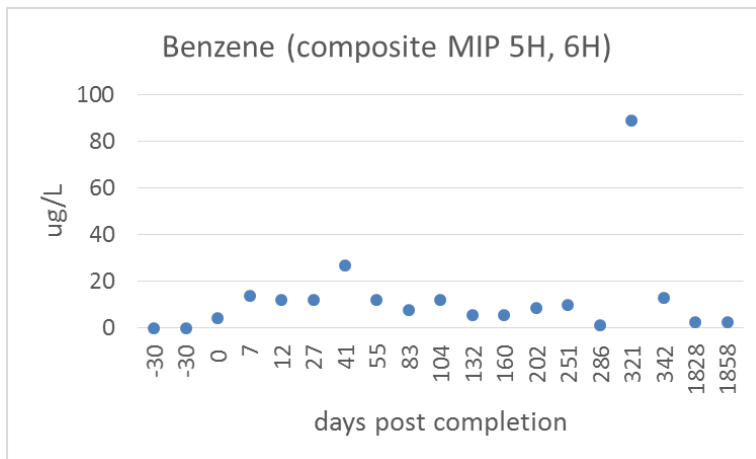


Figure 6 Changes in benzene concentration. The figure shows data from well 5H through the first 342 days post completion, followed by results from well 6H.

Radium isotopes. Radium concentrations generally increased over the 314 days post completion at wells MIP 3H and 5H. Maximum levels of the radium isotopes reached about 20,000 pCi/L at the unchoked 3H well and about half that amount at 5H (figure 7).

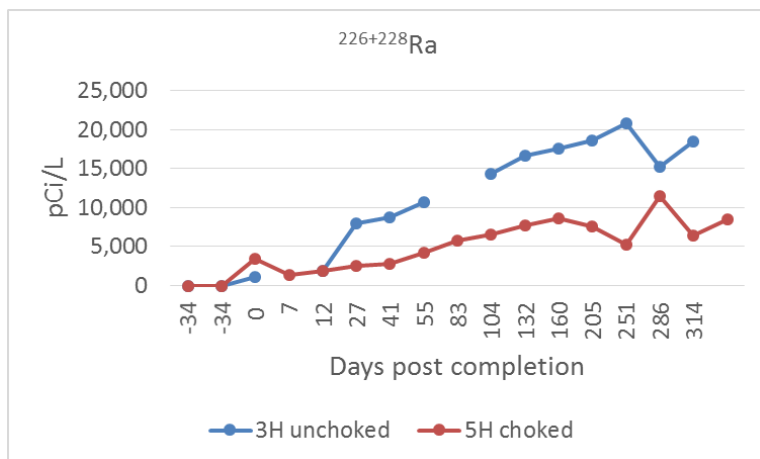


Figure 7 The radium isotopes are plotted against days post well completion. Well 5H was choked periodically. It produced less water and lower concentrations of radium.

At the older wells (MIP 4H and 6H), all isotope concentrations declined to low levels, often below the MDC (minimum detectable concentration) (table 4). This, like the apparent decline in TDS at the older wells is an interesting result and, if sustained by future sampling, would suggest exhaustion of contaminant reserves within the fracture field.

Table 4 Radiochemistry of the older wells 4H and 6H at 1828 (5 years) days post completion.

		16-Nov-16 MIP 4H			16-Nov-16 MIP 6H		
		days post completion: 1828			days post completion: 1828		
		act ¹	unc ²	mdc ³	act ¹	unc ²	mdc ³
α	pCi/L	228.0	53.6	27.2	57.7	10.9	1.6
β	pCi/L	48.7	20.1	29.2	7.4	1.6	0.8
²²⁶ Ra	pCi/L	353.3	260.6	309.2	199.3	333.5	390.3
²²⁸ Ra	pCi/L	31.1	31.9	48.6	0.0	20.9	54.6
⁴⁰ K	pCi/L	49.7	95.5	102.7	0.0	21.9	151.4

¹ activity

² +/- uncertainty

³ minimum detectable concentration

Solid waste. The TCLP (toxicity characteristics leaching procedure) or USEPA method 1311 is prescribed under the Resources Conservation and Recovery Act (RCRA) to identify hazardous solid waste. Both organic and inorganic TCLP was applied to thirteen drill cutting samples, twelve from MIP 3H and 5H and one from another well in western Monongalia County. All three wells had been developed using green, synthetic drilling fluid. All samples fell below the TCLP criteria for hazardous waste (RCRA subtitle C) and would be classified under RCRA subtitle D (industrial solid waste). Bio-Base 365 drilling fluid (Shrieve Chemical Products, Inc.) had been used at the MSEEEL wells and ABS 40 (AES Drilling Fluids Inc.) was used at the other well.

Conclusions

This paper summarizes the results of the first year of a planned four year study and should be regarded as preliminary. Nonetheless, important trends have developed. They are summarized below.

Risk Reduction

The study was centered on Northeast Natural Energy's MIP well pad near Morgantown WV. Several important risk reduction measures were taken in its construction, development and completion to protect offsite risk to water resources. These included secondary containment on the well pad consisting of HDPE lining within a berm that enclosed the entire 1.1 ha pad. The makeup water impoundment also included an HDPE liner with adequate freeboard. Condensate tanks were continuously monitored using a SCADA system with results accessible from multiple locations allowing real time access to remaining capacity and changes in stored volume. Finally, use of the green drilling fluid BioBase 360 rendered the cuttings and muds non-hazardous according to both organic and inorganic TCLP testing.

The nearest receiving stream, the Monongahela River serves as Morgantown's primary drinking water supply, river water quality was monitored at stations upstream of the MIP pad, at the city's water intake and also downstream of the MIP pad. No evidence of contamination with drilling fluids or produced water was detected.

Drill Cuttings

- Drill cutting radioactivity levels were within West Virginia DEP standards of 5 pCi/g above background. This was true of both vertical and horizontal (Marcellus) sections.
- Using the green drilling fluid Bio-Base 365, all drill cutting samples, vertical and horizontal, passed the USEPA's method 1311 (Toxicity Characteristics Leaching Procedure or TCLP) for inorganic and organic contaminants. This indicates that under Federal and West Virginia solid waste rules, these solid wastes would not be considered hazardous.
- The absence of hazardous TCLP findings suggest that drilling fluids, not the inherent properties of the Marcellus formation, play the dominant role in determining drill cutting toxicity.

Produced Water Quality

- Hydraulic fracturing fluid was nearly identical to makeup (Monongahela River) water. Initial produced water was radically changed in ionic composition and underwent a two order of magnitude increase in total dissolved solids (TDS).
- Produced water is highly saline and total dissolved solids (TDS) rapidly increased to a maximum between 100 and 150 g/L. However, there was negligible change in ionic composition between the initially produced water and that sampled five years post completion.
- Concentrations of both ^{226}Ra and ^{228}Ra increased rapidly through the produced water cycle to combined maximum concentrations of 20,000 pCi/L in the first year post completion. These radium isotopes are critical regulatory determinants.

Produced Water Quantity

- The volume of produced water decreased rapidly from nearly 500 bbl/day to less than 1 bbl/day after one year. Over this cycle produced water averaged about 6 bbl/day.
- After five years cumulative flowback and produced water represented only 7.5 and 12% of injected fluids at wells 6H and 4H respectively. After 392 days only 2% and 2.6% reported to the wellhead at the 5H and 3H wells respectively.

References

- Bai, B., Goodwin, S., and Carlson, K. 2013. Modeling of frac flowback and produced water volume from Wattenberg oil and gas field. *Journal of Petroleum Science and Engineering*. <http://dx.doi.org/10.1016/j.petrol.2013.05.003>.
- Hayes, T., 2009. Sampling and analysis of water streams associated with the development of Marcellus shale gas. Final report prepared for Marcellus Shale Coalition, Gas Technology Institute, Des Plaines, IL 60018.
- Lewis, A. 2012. Wastewater generation and disposal from natural gas wells in Pennsylvania. Master Thesis. Duke University.

- McCurdy, R. 2011. High rate hydraulic fracturing additives in non-Marcellus unconventional shales. Proceedings of the Technical Workshops for the Hydraulic Fracturing Study: Chemical and Analytical Methods. EPA 600/R-11/066.
- U.S. Environmental Protection Agency (USEPA), 2010. Office of Research and Development. Hydraulic Fracturing Research Study. Retrieved on May 2011, from <http://www.epa.gov/safewater/uic/pdfs/hfresearchstudyfs.pdf>
- URS, 2011. Water-related issues associated with gas production in the Marcellus shale. NYSERDA contract PO number 10666, Fort Washington, PA.
- Xu, P., Cath, T., and Drewes, J.E., 2011. Novel and emerging technologies for produced water treatment. US EPA Technical Workshops for the Hydraulic Fracturing, Arlington, VA.
- Ziemkiewicz, P.F., Quaranta, J.D., Darnell, A. and Wise, R. 2014a. Exposure pathways related to shale gas development and procedures for reducing environmental and public risk, *Journal of Natural Gas Science and Engineering*, Volume 16, January 2014, Pages 77-84, ISSN 1875-5100, <http://dx.doi.org/10.1016/j.jngse.2013.11.003>.
- Ziemkiewicz, P.F., Quaranta, J.D. and McCawley, M. 2014b. Practical measures for reducing the risk of environmental contamination in shale energy production. *Environ. Sci: Processes Impacts*. DOI:10.1039/C3EM00510K.
- Ziemkiewicz, P.F., He, Y.T. and Quaranta, J.D. 2014c. Characterization of waste waters from hydraulic fracturing. *In Proc: Am. Soc. of Civil Eng. Shale Energy Engineering Conference*. Pittsburgh PA. 21-23 July 2014.

URTeC: 2669965

Biogeochemical Characterization of Core, Fluids, and Gas at MSEEL Site

Shikha Sharma^{1*}, Timothy R. Carr¹, Paula J. Mouser², Kelly Wrighton³, David Cole⁴, Michael Wilkins⁴, Thomas Darrah⁴, Alexandra Hakala⁵

1. Geology & Geography, West Virginia University, Morgantown, WV, United States.
2. Civil, Envir & Geod Eng. , The Ohio State University, Columbus, OH, United States.
3. Microbiology, The Ohio State University, Columbus, WV, United States.
4. School of Earth Sciences, The Ohio State University, Columbus, OH, United States.
5. National Energy Technology Laboratory, Pittsburgh, PA, United States.

Copyright 2017, Unconventional Resources Technology Conference (URTeC) DOI 10.15530/urtec-2017-2669965

This paper was prepared for presentation at the Unconventional Resources Technology Conference held in Austin, Texas, USA, 24-26 July 2017.

The URTeC Technical Program Committee accepted this presentation on the basis of information contained in an abstract submitted by the author(s). The contents of this paper have not been reviewed by URTeC and URTeC does not warrant the accuracy, reliability, or timeliness of any information herein. All information is the responsibility of, and, is subject to corrections by the author(s). Any person or entity that relies on any information obtained from this paper does so at their own risk. The information herein does not necessarily reflect any position of URTeC. Any reproduction, distribution or storage of any part of this paper without the written consent of URTeC is prohibited.

Summary

The deposition and genesis of organic-rich shale create complex heterogeneities in the reservoir, which remain poorly understood despite their importance in the unconventional energy revolution. In addition, several questions need to be answered about the complex biogeochemical interactions that take place in the reservoir after injection of hydraulic fracturing fluids. Our interdisciplinary team is utilizing the core, fluids, and gas samples collected from the Marcellus Shale Energy and Environmental Laboratory (MSEEL) to develop a better understanding of these characteristics and processes to ensure that energy is extracted in an economically efficient and environmentally responsible manner.

The availability of well-preserved cores from MSEEL has given us the opportunity to significantly increase the resolution of subsurface stratigraphic characterization. We integrated geochemical, petrographic, molecular, and isotopic techniques to better understand the biogeochemical controls on temporal heterogeneities in quantity and quality of total organic carbon (TOC). The preliminary data from multiple proxies indicate that temporal variations in paleoredox condition, depositional environment, and microbial cycling effect both the type and amount of organic carbon preserved in the core. The composition, molecular structure, porosity and density of kerogen also appears to be affected by the same processes.

The unrestricted access to hydraulic fracturing fluid, drilling additives and produced fluid/gas samples with minimal exposure to the atmosphere has enabled our team to develop preliminary models of fluid-gas-shale and biogeochemical interactions in the reservoir. Our initial results on the produced water chemistry indicate that injection of hydraulic fracturing fluids results in dissolution of pristine biogenic carbonates in the reservoir. The increasing concentrations of redox-sensitive elements over time in produced water is strongly suggestive of the existence of an active anaerobic microbial community in the reservoir involved in fermentation of carbon compounds in hydraulic fracturing fluids, sulfur reduction, and methanogenic production. The molecular composition of produced gases in conjunction with the stable and noble gas isotopic signatures of produced gases and waters is being monitored over time to further constrain the biogeochemical interactions in the reservoir.

Introduction

The MSEEL site is located in the heart of the dry-gas area of the Marcellus Shale play in Monongalia County, West Virginia. Northeast Natural Energy LLC (NNE) drilled two previous wells the MIP 4H and MIP 6H in 2011. The two NNE wells are inside the gas “city gate”, where the gas is transferred to the local natural gas utility, and are constrained by the natural gas usage of Morgantown. Production from the old wells had declined and two wells (MIP 5H and 3H) drilled as part of the MSEEL project help meet the city demand. A dedicated scientific observation well was drilled in-between MIP 5H and 3H horizontal laterals to collect detailed subsurface data, and to monitor and test new hydraulic fracturing technologies in production wells drilled over the project lifetime. A diverse team of hydrologists, geochemists, health professionals and social scientists are conducting water/air quality and noise monitoring at this site over the five-year period. Researchers will also be given access to produced water and gas samples from the hydraulically fractured horizontal production well before they are disposed in holding tanks or pumped to production/distribution

Methods

Core collection and analysis

Complete 111 feet of vertical core and 50 sidewall cores were obtained from well 3H. In addition, 150 sidewall cores were collected from the scientific observation well. The cores were preserved on the site per the required protocols and available to all investigators for a wide variety of microbiological/geochemical/mineralogical/sedimentological analysis, macro and micro scanning and conducting high-pressure temperature experiments.

The core plugs samples collected from every foot of the vertical core and side wall cores were ground and homogenized and distributed among different investigators for geochemical and mineralogical analysis using ICP-MS, X-ray fluorescence (XRF), X-ray diffraction (XRD), and pyrolysis. Total organic carbon (TOC), stable carbon isotopic composition of bulk organic carbon ($\delta^{13}\text{C}_{\text{org}}$), and nitrogen ($\delta^{15}\text{N}_{\text{org}}$) were analyzed using a combustion elemental analyzer (EA), coupled to a Delta Advantage IRMS via a ConFlo IV interface while inorganic carbon ($\delta^{13}\text{C}_{\text{carb}}$) was measured using a GasBench coupled to a Delta Advantage IRMS. Samples and internal standards were analyzed in replicates to determine the precision of instrument which was better than $\pm 0.1\%$ for $\delta^{13}\text{C}$ and $\pm 0.2\%$ for $\delta^{15}\text{N}$. The internal laboratory standards and check standards (USGS 40 and USGS 41) were calibrated and reported in per mil (‰) relative to their respective IAEA standards (V-PDB and AIR) for $\delta^{13}\text{C}$ and $\delta^{15}\text{N}$ respectively.

Kerogen was also extracted from sidewall cores collected from Mahantango Formation and different zones of Marcellus Shale. The kerogen extraction procedure was standardized using both chemical and physical separation techniques, and was performed by extracting the maximum amount of unaltered kerogen with effective removal of soluble organic matter, carbonates, silicates and heavy minerals (Agrawal et al., 2016). Kerogen was analyzed using direct analytical techniques such as XPS (X-ray photoelectron spectroscopy), ATR-FTIR (Attenuated total reflection-Fourier transform infrared spectroscopy), ^{13}C solid state NMR (Nuclear magnetic resonance) and Raman spectroscopy to characterize its molecular structure.

Sidewall cores were collected using recommended practices in Wilkins et al., 2014 from a 360-foot span within the MIP 3H well targeting the Genesee, Tully, Mahantango, Marcellus and Onondaga formations. Briefly, fluorescent microspheres (0.5 μm , Polysciences Inc.) were added to the drilling mud at a concentration of ~ 105 beads per mL. After collection, cores were immediately transported to The Ohio State University anaerobically, on ice. Cores were surface sterilized using successive brine washes (sterile 1.5M NaCl solution). Microscopy was used to verify removal of microsphere tracers and cores were ground to a particle size less than 500 μm and homogenized. All ground core material was stored at -80°C until DNA extraction. Low biomass in the subsurface makes it important to develop methods of lipid extractions with the ability to yield higher and persistent recovery of microbial lipid biomarkers. We, therefore, conducted experiments and tested different established microbial lipid extraction procedures to avoid the underestimation of resulting profiles, biomass, and diversity. We tested three extraction methods: (i) modified Bligh and Dyer (mBD), (ii) Folch (FOL), and (iii) microwave assisted extraction (MAE) treatments. Within mBD method we utilized either a phosphate or citrate buffer. We also tested the effect of three different spikes on the extraction performance: (i) magnesium (Mg^{2+}), (ii) *Escherichia coli* biomass (*E.coli*), and (iii) intact phospholipid (POPC) to determine if the lipid yield and profile quality of the mBD extraction treatments could be enhanced.

Produced gas and fluid collection and analysis

Produced water samples were collected in 3-5 gallon (~11-18 litres) carboys just after the separator. The samples were transported, filtered and processed in Sharma Laboratory at WVU immediately after sampling. All water samples were collected in different containers using different methods and preservatives specified for different kinds of analysis. The geochemical analysis of water was analyzed via ICP-OES and ICP-MS. Ammonia and phosphate were measured on the Skalar nutrient analyzer. The samples were collected hourly during the initial phase of flowback followed by weekly to monthly sampling during later stages. Currently, samples are being collected every six weeks. The collected fluids are currently being processed for biomass, reactive chemistry, organic acids, and noble gas and stable isotope analysis at different institutes.

Produced gas samples were collected from well heads of the two production wells and transported to the Sharma Lab at WVU and analyzed for molecular composition and C/H isotope composition of methane, ethane, and CO₂ using GC Isolink connected to a Finnigan Delta Advantage mass spectrometer. A duplicate set of gas samples were sent to Darrah's lab at OSU for He, Ne, Ar, Kr, and Xe concentration analysis by quadruple mass spectrometry; and helium, neon, and isotopes by noble gas mass spectrometry. Both flow back fluids and produced gas samples have shown low levels of atmospheric gasses, indicating the acquisition of high-quality samples (a known challenge in sampling for noble gasses).

Results

The Total Organic Carbon (TOC) concentrations show a general decreasing trend from bottom (8-10%) to top (2-4%) of Marcellus. The $\delta^{13}\text{C}_{\text{org}}$ was relatively higher (-29‰ V-PDB) in the organic matter (OM) poor zone compared to the organic rich (OR) zone (-31‰ V-PDB) of the lower Marcellus, suggesting more influence of terrestrial OM in OM-poor zone compared to the OM-rich zone. Both $\delta^{13}\text{C}_{\text{org}}$ and $\delta^{15}\text{N}_{\text{org}}$ show larger fluctuations in the bottom OR zone indicating fluctuating redox and more nutrient recycling that might have fueled higher productivity and higher OM accumulation in that zone (Chen and Sharma 2016; Sharma et. al, 2016). The analysis of bulk geochemistry and pyrolysis data collected from all the plugs from the vertical core and sidewall cores is currently underway.

Bulk mineralogy of core samples, as determined with powder XRD, of core samples from well MIP 3H shows that Marcellus core is composed mainly of siliciclastic mudstones with interbedded carbonates. There is high content of illite in Mahantango and Marcellus Shale and overall the clay content decreases with depth and is accompanied by increase in TOC (Song et al., in press). Of the four sidewall cores targeted within the Marcellus, three (Marcellus top, depth 7451', middle (7509') and lower (7543') are mainly comprised of phyllosilicates (mostly illitic clay with minor chlorite), quartz, pyrite, alkali feldspar, calcite and dolomite. One (upper Marcellus, depth 7467') is a carbonate mudstone composed mostly of calcite, quartz, and dolomite, but with minor illite and chlorite detected. SEM images of unpolished fragments of this sample show sub-micron scale chlorite platelets and relatively small patches of organic matter (OM) disseminated throughout a dominant calcite matrix.

SEM analysis of unpolished, bedding-parallel cleavage fragments of Marcellus top (7451') show oriented, 100-200 micron diameter pods of organic material (OM), interpreted as preserved algal cysts containing large (several 10s of microns in dimension), euhedral dendritic chlorite crystals, as well as euhedral forms of calcite, quartz, and pyrite. Figure 1a shows an example of such an OM-rich feature that was targeted for dual beam FIB/SEM. Subsequent Gallium-ion beam slices of a large (40 x 40 μm) region of interest including one the pods, acquired at the Molecular Foundry (LBNL), also reveal small, porous patches of OM dispersed within the fine-grained illitic clay matrix, as well as pores formed at mineral phase boundaries and between OM and minerals (Figure 1b). In addition, large field BSE image analysis of bedding-perpendicular polished core sections of Mahantango, Marcellus top and lower Marcellus (Figure 2) show that these large algal OM features are common in several targeted depths. These data suggest that more than one type of OM exist within a single core sample, and that also they are distributed among different depths within the Mahantango and Marcellus. Detailed observations suggest, that OM/mineral/pore associations and rock fabric microstructure do vary with depth in the formation.

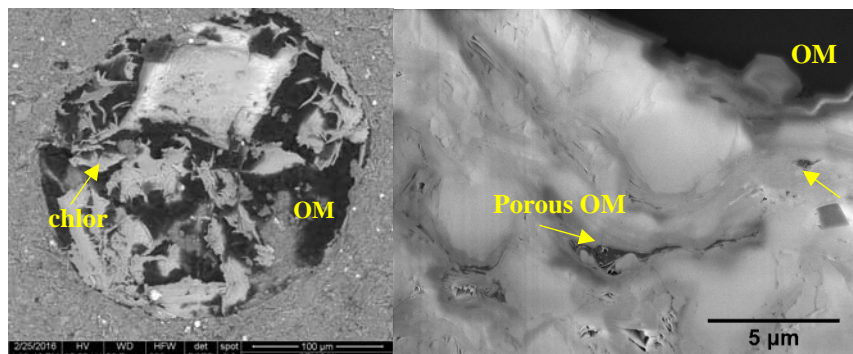


Figure 1a (left). Algal material replaced by OM (dark), euhedral dendritic chlorite, and other secondary minerals observed in Marcellus Top, depth 7451'. **Figure 1b** (right) is a dual beam FIB slice showing porous OM 1s of μm or less in length scale (yellow arrows), in addition to the large OM algal pod (upper right) without obvious pores.

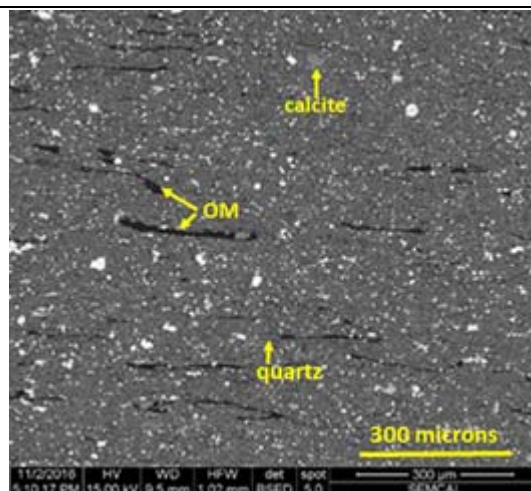
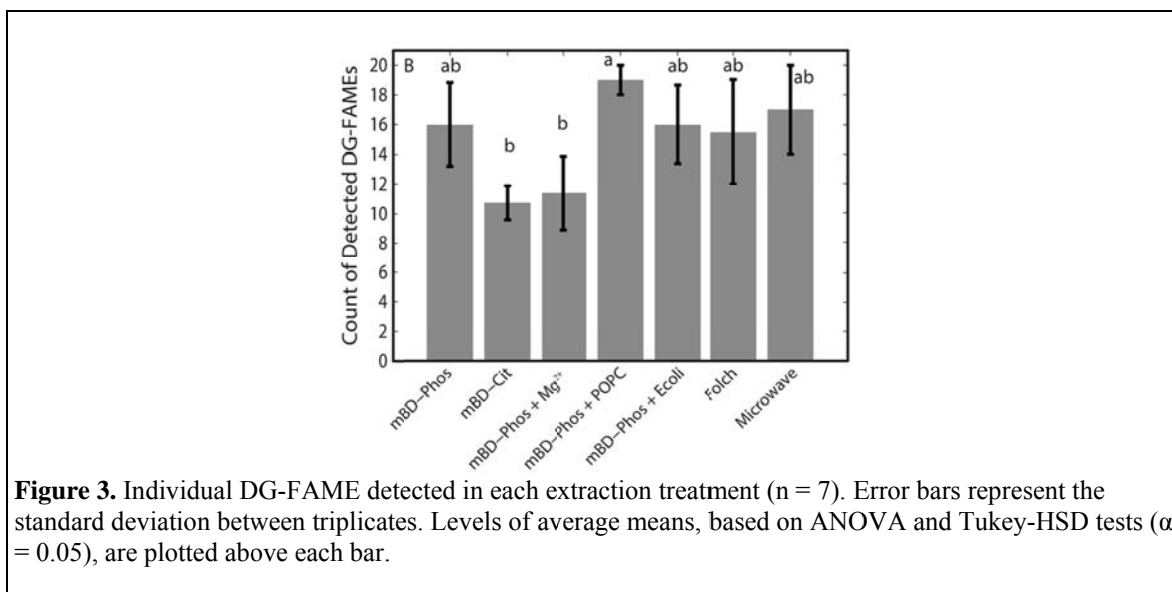
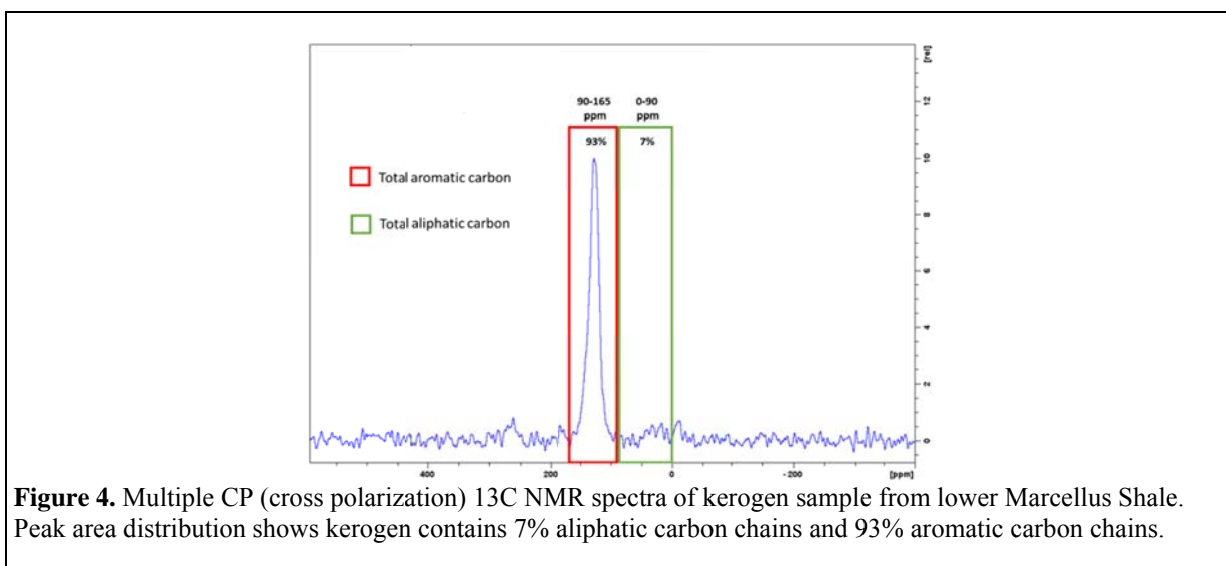


Figure 2. Example image of large field BSE scan for Lower Marcellus (depth 7543.0'). OM appears black, quartz and other siliciclastics appear medium gray; carbonates and phosphates appear light gray, and the strongest BSE scattering minerals (mainly pyrite) appear white.

The complex shale matrix, including high concentrations of organic constituents and salts as well as exceedingly low porosities, constitute serious challenges in extracting microbial lipids from shale. After testing different extraction methods and effect of the addition of spikes, we determined that the modified Bligh and Dyer method using a phosphate buffer and phospholipid spike (mBD+Phos+POPC) consistently provided reproducible results and higher recovery of phospholipid fatty acids (PLFAs) and diglyceride fatty acids (DGFA's) over other methods (Figure 3). This suggested that the addition of the POPC spike helped with the extraction of a pool of lipid material that was not accessible with the other methods. This method demonstrates that the extraction solvent mixtures are polar enough to release PLFA from microbial cell membranes and non-polar enough to release DGFA from neutral lipids (Akondi et al., 2016, 2017). This optimized method was used to extract lipid biomarkers from pristine sidewall cores collected from MSEEL site. Little evidence of intact lipid biomarkers was observed in Marcellus cores.



Preliminary direct kerogen analysis from samples collected at the MSEEL site suggests that majority of carbon chains present in kerogen are mainly aromatic in nature (Figure 4). This indicates that most of the aliphatic chains have been already thermally degraded at this maturity stage. Agrawal and Sharma, 2017 showed that aliphatic biomarkers and pyrolysis proxies at high maturity zones of Marcellus site can be used to determine thermal maturity and sources of organic matter. Aliphatic biomarkers of pristine sidewall cores collected from MSEEL show that contribution of organic matter from marine input increased from Marcellus top to lower Marcellus. However,



kerogen structural parameters determined by ¹³C solid-state NMR and Raman spectroscopy are very similar throughout Marcellus at MSEEL site. This indicates thermal maturity has the dominant control on kerogen structure (Agrawal et al., 2016, Agrawal et al., 2017). Using the structural parameters determined from direct kerogen analysis and S₂ values of SRA (source rock analysis), multiple regression models will be built to determine the HC generative potential of different carbon chains of kerogen.

The microbial community composition in pristine sidewall cores from the MIP3H well and input fluids (e.g. drilling muds) was compared to the microbial communities in produced fluids from MIP3H and MIP5H wells, using a combination of 16S rRNA sequencing and culturing. Fluids were filtered to collect microbial biomass. Comparison

of core material samples to the controls did not show any signature for indigenous microbial life in the MIP3H well. Comparison of the microbial communities in drilling muds and produced fluids show that many of the injected microorganisms thrive in the subsurface, eventually dominating the communities after 250 days. The dominant microorganisms in both wells are *Halanaerobium* spp. (up to 43% relative abundance) and *Orenia* spp. (up to 75% relative abundance), detected in the drilling muds between 4.0 and 8.5% relative abundance (Daly et al, 2016). DNA-based analyses from sidewall core material and produced fluids were complimented by anaerobic culturing enrichments. Although no cultures were obtained from pristine sidewall core material, the produced fluid enrichments resulted in the isolation of multiple *Halanaerobium* spp. and the dominant methanogen in produced fluids, a member of *Methanohalophilus*. Laboratory cultivation techniques confirmed that the *Methanohalophilus* is halotolerant (growing at or above 80 g/L NaCl) and piezotolerant (>3,000 psi). Several *Halanaerobium* spp. were isolated from the MIP3H and MIP5H wells, growing across broad pressure and salinity gradients, including salinities as high as 250 g/L NaCl (Borton et al, 2016). Together these results show that the microorganisms that dominate the produced fluid communities are introduced into the wells during the drilling and hydraulic fracturing process and that these microorganisms are well adapted to growing and persisting in fractured shales. Consistent, visual evidence of cells indicates viable microbial biomass exist in both wells through all stages of completion and production. Concentrations of carbon, nitrogen and phosphorus species confirm the shale system is not oligotrophic or limited for key macronutrients. The increasing concentrations of redox-active elements and reduced electron acceptors strongly suggests an active anaerobic microbial community exists in the well involved in the respiration of iron, manganese, and sulfur species (Booker et al, 2016, Evert et al., 2016).

The average molecular composition of produced gas samples collected from wells MIP3H and 5H indicates that gas is primarily composed of methane (97-98%) with little ethane (2.5%) and propane (.14%). The $\delta^{13}\text{C}_{\text{CH}_4}$ values of methane is around -36.4‰ V-PDB and is heavier than ethane which has value of around -39.2‰ V-PDB. The isotope values are higher than produced gas samples collected from Green County wells, PA (Sharma et al., 2015) but do show the characteristic isotope reversal observed in gas sources from Marcellus Shale. The bulk produced fluid geochemistry data from MIP 3H and 5H wells show that chloride concentrations range from approximately 55,000 to 84,000 mg/L. However, the Cl⁻ concentrations did not increase systematically over time, nor did these two wells exhibit similar changes. Dissolved sulfate was not detected in the flowback samples collected from April through September. Fluoride concentrations were approximately an order of magnitude lower during this time, as compared to the first month of flowback samples. Dissolved NH₃ followed a similar trend as Cl⁻, with concentrations ranging from approximately 80 to 100 mg/L N. Data reduction from trace metal analysis on the ICP-OES and ICP-MS continues. Core flood experiments with fracturing fluid and sidewall cores are being conducted to evaluate fluid-rock reactions in the fractured shale, and to date have shown chemical changes associated with pyrite oxidation and calcite dissolution (Hakala et al., 2017). The carbon isotopic composition of dissolved inorganic carbon ($\delta^{13}\text{C}_{\text{DIC}}$) in the produced fluids are highly enriched in ¹³C with values ranging from +10‰ to +31‰ V-PDB compared to the injected frac water which had values of -8.7‰ to -8.2‰ V-PDB. The highly enriched $\delta^{13}\text{C}_{\text{DIC}}$ are consistent with values reported from Marcellus produced waters collected from Greene County, PA (Sharma et al., 2014). The high carbon isotope values are indicative of microbial utilization of lighter carbon by methanogenic bacteria in the reservoir indicating biogenic methanogenesis in the reservoir (Sharma et al., 2014, Wilson and Sharma, 2016, 2017). Genomic analysis reveals that like other shale systems *Methanohalophilus* could be the dominant source of biogenic methane at MSEEL (Borton et al., 2016). The noble gas analysis is being conducted to identify the contribution of microbial methane to the total gas. The evidence of microbial methanogenesis raises the possibility of enhanced gas recovery from these shales using biological amendments.

Conclusions

The preliminary characterization of vertical and sidewall cores indicates there are many spatiotemporal biogeochemical heterogeneities in the shale from the molecular, pore to core scales. The highest TOC in the lower part of Marcellus is accompanied by isotopic and geochemical signatures of fluctuating redox and higher nutrient cycling that might have played a key role in higher organic matter production. The access to pristine sidewall cores at this site will enable us to accurately characterize viable and non-viable microbial life in different zones of Marcellus and its interfaces with overlying and underlying formation using lipid biomarkers. The modified Bligh and Dyer method that we developed using a phosphate buffer and phospholipid spike (mBD+Phos+POPC) appears to give the highest yield and reproducibility for PLFA's and DGFA's.

The complete access to water and gas samples from all stages of drilling and production at MSEEL has helped us to infer that variety of water-microbe-rock interactions are initiated in the reservoir after injection of nutrient enriched fracturing fluid. Isotopic and genomic data supports the existence of microbial methanogenesis in the Marcellus shale.

Acknowledgements

This research was funded by a grant from Department of Energy's National Energy Technology Laboratory (DE-FE0024297), two grants from National Science Foundation Division of Environmental Biology (NSF-DEB #1342732/1342701 to SS and PJM) and an Early career instrumentation grant (NSF EAR #1205596 to SS).

References

- Agrawal, V., Sharma, S., 2017, Use of organic-geochemical proxies to assess organic matter sources, thermal maturity, and paleoredox conditions during deposition of Marcellus shale: *Journal of Petroleum Science and Engineering* (in review)
- Agrawal, V., Warriar, A., Sharma, S., 2017, Decoding molecular geochemistry of kerogen from Marcellus shale. American Association of Petroleum Geologists Annual Convention, Houston, Texas, April 2-5
- Agrawal, V., Sharma, S., Warriar, A., 2016, Understanding kerogen composition and structure in pristine shale cores collected from Marcellus Shale Energy and Environment Laboratory. Eastern Section American Association of Petroleum Geologists' Meeting, Lexington, Kentucky, September 25-27
- Akondi R, Trexler RV, Pfiffner SM, Mouser PJ, Sharma S, 2016. Comparing Different Extraction Methods for Analyses of Ester-linked Diglyceride Fatty Acids in Marcellus Shale. Eastern Section American Association of Petroleum Geologists' Meeting, Lexington, Kentucky, September 25-27
- Akondi R, Trexler R, Pfiffner SM, Mouser PJ, Sharma S 2017. An Improved Lipid Extraction Method for Deep Subsurface Shale. *Frontiers in Microbiology* (in review)
- Booker, A.E., Borton, M.A., Daly, R.A., Welch, S.A., Nicora, C.D., Sharma, S., Mouser, P.J., Cole, D.R., Lipton, M.S., Wrighton, K.C. and Wilkins, M.J., Sulfide Generation by Dominant Colonizing Halanaerobium Microorganisms in Hydraulically Fractured Shales. Eastern Section American Association of Petroleum Geologists' Meeting, Lexington, Kentucky, September 25-27
- Borton, M.A., Daly, R.A., Morgan, D.M., Booker, A.E., Hoyt, D.W., Mouser, P.J., Sharma, S., Wilkins, M.J. and Wrighton, K.C., 2016 Methanohalophilus is the Dominant Source of Biogenic Methane in Hydraulically Fractured Shales. Eastern Section American Association of Petroleum Geologists' Meeting, Lexington, Kentucky, September 25-27
- Chen R, Sharma S. 2016. Role of oscillating redox conditions in formation of organic-rich intervals in the Middle Devonian Marcellus Shale, Appalachian Basin, USA. *Palaeogeography, Palaeoclimatology, Palaeoecology*, 446, 85-97.
- Rebecca A. Daly, Mikayla A. Borton, Travis A. Wilson, Susan A. Welch, David R. Cole, Shikha Sharma, Michael J. Wilkins, Paula J. Mouser, Kelly C. Wrighton. Microbes in the Marcellus Shale: Distinguishing Between Injected and Indigenous Microorganisms. Eastern Section American Association of Petroleum Geologists' Meeting, Lexington, Kentucky, September 25-27
- Evert M, Panescu J, Daly R, Welch S, Hespren J, Sharma S, Cole D, Darrah TH, Wilkins M, Wrighton K, Mouser P 2016. Temporal Changes in Fluid Biogeochemistry and Microbial Cell Abundance after Hydraulic Fracturing in Marcellus Shale. Eastern Section American Association of Petroleum Geologists' Meeting, Lexington, Kentucky, September 25-27

Hakala, J.A.; Crandall, D.; Moore, J.; Phan, T.; Sharma, S.; Lopano, C. Laboratory-scale studies on chemical reactions between fracturing fluid and shale core from the Marcellus Shale Energy and Environmental Laboratory (MSEEL) site. Unconventional Resources Technology Conference, Austin, TX, 24 – 26 July, DOI 10.15530-urtec-2017-2670856.

Sharma S, Mulder M, Sack A, Schroeder K, Hammack R. 2014. Isotope approach to assess hydrologic connections during Marcellus Shale drilling. *Groundwater* 52, 424-433.

Sharma, S., Bowman, L., Schroeder, K. and Hammack, R., 2015. Assessing changes in gas migration pathways at a hydraulic fracturing site: Example from Greene County, Pennsylvania, USA. *Applied Geochemistry*, 60, 51-58.

Sharma S, Agrawal V, Akondi R, and Warriar A, 2016 Understanding biogeochemical controls on spatiotemporal variations in total organic carbon in cores from Marcellus Shale Energy and Environment Laboratory. Eastern Section American Association of Petroleum Geologists' Meeting, Lexington, Kentucky, September, 25-27

Song L, Paronish T, Agrawal V, Hupp B, Sharma S, Carr T, 2017. Depositional Environment and impact on pore structure and gas storage potential of Middle Devonian organic rich shale, northeastern West Virginia, Appalachian Basin. Unconventional Resources Technology Conference, Austin, Texas, July 24-26, DOI 10.15530-urtec-2017-2667397.

Wilkins, M. J., R. A. Daly, P. J. Mouser, R. Trexler, S. Sharma, D. R. Cole, K. C. Wrighton, J. F. Biddle, E. H. Denis, J. K. Fredrickson, T. L. Kieft, T. C. Onstott, L. Peterson, S. M. Pfiffner, T. J. Phelps & M. O. Schrenk. 2014. Trends and Future Challenges in Sampling the Deep Terrestrial Biosphere. *Frontiers In Microbiology*, 1-8.

Wilson T, and Sharma S. 2017. Inferring biogeochemical interactions in deep shale reservoirs at the Marcellus Shale Energy and Environment Laboratory (MSEEL). Joint 52nd northeastern annual section/ 51st north-central annual section meeting March 19-21, Pittsburgh, PA.

Wilson T and Sharma S. 2016. Assessing biogeochemical interactions in the reservoir at Marcellus Shale Energy and Environment Laboratory. GSA Annual Meeting, Denver CO, September 25-28

URTeC: 2670856

Laboratory-Scale Studies on Chemical Reactions Between Fracturing Fluid and Shale Core from the Marcellus Shale Energy and Environmental Laboratory (MSEEL) Site

J. Alexandra Hakala*, National Energy Technology Laboratory
Dustin Crandall, National Energy Technology Laboratory
Johnathan Moore, AECOM National Energy Technology Laboratory
Thai Phan, ORISE National Energy Technology Laboratory
Shikha Sharma, West Virginia University
Christina Lopano, National Energy Technology Laboratory

Copyright 2017, Unconventional Resources Technology Conference (URTeC) DOI 10.15530/urtec-2017-2670856

This paper was prepared for presentation at the Unconventional Resources Technology Conference held in Austin, Texas, USA, 24-26 July 2017.

The URTeC Technical Program Committee accepted this presentation on the basis of information contained in an abstract submitted by the author(s). The contents of this paper have not been reviewed by URTeC and URTeC does not warrant the accuracy, reliability, or timeliness of any information herein. All information is the responsibility of, and, is subject to corrections by the author(s). Any person or entity that relies on any information obtained from this paper does so at their own risk. The information herein does not necessarily reflect any position of URTeC. Any reproduction, distribution, or storage of any part of this paper without the written consent of URTeC is prohibited.

Abstract

Injection of fracturing fluids into shales during hydraulic stimulation can result in various chemical reactions involving the injected fluid and host shale rock. Differences in chemical composition between the injected fluids and fractured rock can result in mineral precipitation along shale fractures and within the shale matrix, potentially affecting long-term gas recovery from the shale. Our prior research showed that mineral precipitation and dissolution occur along freshly-generated fractures, and within the shale matrix, during core flood experiments in which laboratory-fractured Marcellus Shale was exposed to simulated hydraulic fracturing fluids. Many of the mineral precipitation reactions were hypothesized to occur due to the inability for antiscaling compounds in the fracturing fluids to control mineral precipitation at elevated temperature and pressure. In some locations along the fracture, proppant was cemented to shale surfaces through secondary mineral precipitates. The present study focuses on core flood experiments using fresh core and site hydraulic fracturing fluid from the Marcellus Shale Energy and Environmental Laboratory site (MSEEL; Morgantown, WV) at reservoir pressure and temperature conditions. The objectives of this study are to evaluate the reproducibility of the earlier experiments using fresh core, and to identify causes for any observed differences with the prior outcrop-based experiments.

Introduction

Introduction of fracturing chemicals into shale formations can initiate chemical reactions that result in shale mineral dissolution and precipitation of secondary minerals within the shale matrix and along newly-generated fractures. These reactions can affect matrix and fracture permeability by generating new flow pathways in the case of mineral dissolution. Secondary mineral precipitation could be both beneficial and detrimental to gas flow within the reservoir, as depending on the mineral morphology and location, precipitation could result in additional propping of fractures, or could reduce matrix and fracture permeabilities. Recent attention to fracturing chemical-mineral reactions that could affect gas production have shown that both the formation mineralogy and injected fluid chemistry have a significant influence on the overall chemical changes during hydraulic fracturing. Barite has been of interest in the Marcellus Shale due to elevated concentrations of barium measured in produced waters and the shale. Barite scale in the wrong locations within the system can present a significant challenge for sustained long-term production as barite dissolution and removal are difficult and potentially costly.

Prior batch experimental studies focused on reactions between Marcellus Shale and fracturing fluids showed that, in the presence of elevated barium and fracturing chemicals, barite precipitation was either directly observed or predicted based on saturation indices calculations from experimental fluid chemistries (Dieterich et al., 2015; Marcon et al., 2017). In core flood experiments performed with laboratory-generated fracturing chemicals and core plugs derived from Marcellus Shale outcrop, barite precipitation was observed by computed tomography (CT) and scanning electron microscopy (SEM). Barite is also predicted based on saturation indices calculations with fluid chemistry, for fracturing fluids generated with both freshwater and recycled produced water compositions as the carrier fluid (Vankeuren et al., under review). In these experiments, barium was either leached from the shale (in the case of freshwater-based fracturing fluid) or present in the initial fracturing fluid (in the case of produced water-based fracturing fluids). Sulfate was generated through reaction of the ammonium persulfate breaker, and to a lesser extent, oxidation of pyrite in the shale. Replicate experiments designed to verify the Vankeuren (under review) study, and the integrity of the experimental system used for the present study, showed similar results (Moore et al., 2017)

The Marcellus Shale Energy and Environmental Laboratory (MSEEL) is a gas-producing research well located in Morgantown, West Virginia operated by North Northeast Energy (NNE) and managed by West Virginia University (WVU) as one of the National Energy Technology Laboratory/U.S. Department of Energy (NETL/DOE) hydraulically-fractured shale field sites. The site includes a production well that was vertically cored (MIP 3H) and hydraulically stimulated during November 2015. Samples from MSEEL include fresh core and fracturing chemical mixtures actually used on site, which can provide a new perspective on potential mineral reactions during hydraulic fracturing, as our prior studies were performed with a lab-generated fracturing fluid and Marcellus Shale core plugs extracted from outcrop samples. The focus for this study was to evaluate mineral dissolution and precipitation in MSEEL 3H core samples reacted with a sample of the hydraulic fracturing fluid developed for fracturing of the MIP 3H well (November 2015).

Methods

Experimental Design and Apparatus

Experiments were designed to represent diffusive flow and reaction of hydraulic fracturing fluids with the shale reservoir rock over a simulated four-day shut in period. The apparatus consisted of a dual core holder system, with an inlet reservoir leading to an injection pump (Figure 1). Fluids were introduced into a Hassler type core holder, which contained shale cored from MSEEL 3H samples for evaluating fluid-rock interactions, or remained empty for procedural blank tests. Injection was performed with a solvent pump at a constant rate, overburden pressure was maintained with a confining pump, and a back-pressure pump controlled system pressure and acted as the effluent reservoir. Fluids were sampled from the influent and effluent reservoirs for evaluating changes to fluid chemistry from the experimental apparatus (in the case of the system blank test) and fluid-rock interactions (in experiments containing MSEEL core). The confining reservoir chemistry was sampled and monitored to ensure a no flow boundary was maintained between the core sleeve and end plugs. Experiments and blank tests were performed at 150°F, 3000 psi confining pressure, 2800 psi pore pressure, and a fluid flow rate of 0.03 ml/min. Injected fluid was chilled to 5°C for the duration of the test to avoid microbial growth. Two core flood experiments were performed with MSEEL core, and one experiment was performed where 3H injection fluid was circulated through the experimental apparatus in the absence of core (referred to as the “blank experiment” in the results and discussion).

Core Selection, Preparation, and Hydraulic Fracturing Fluid

Two depths of the MSEEL 3H core were selected based on location associated with hydraulic fracturing of the 3H well, and based on the ability to sub-core from the existing slabs: 7498.4 ft, and 7504.6 ft. These samples were chosen because they were the most competent sections of core near the lateral kick off point, which was slightly lower at approximately 7500 ft. Samples were cut from 2/3 slab and core was drilled bedding concordant. Drilling performed perpendicularly to the bedding plane resulted in core diskings. The 1.5 inch diameter samples were cored with at least 4 inches total length and fractured by a modified Brazilian method (Atkinson et al., 1982); the cores were in two 2” long sections each as even the concordant cores tended to break. Fractures were filled with less than a single monolayer of 40/70 mesh >99% quartz Innoprop proppant, and loaded into core sleeves. Hydraulic fracturing fluid used for the experiments was sampled from the batch of fracturing fluid injected into the MIP 3H well during fracturing (date range 11/6/2015 through 11/15/2015). The composition of the fracturing fluid is presented in Table 1. A pump malfunction occurred at 24 h for the 7498.4 ft experiment resulting in a higher flow

rate through the experimental apparatus, which resulted in a higher volume accumulation in the effluent reservoir and may result in some differences of fluid chemistry measured at 24 and 48 h for this experiment.

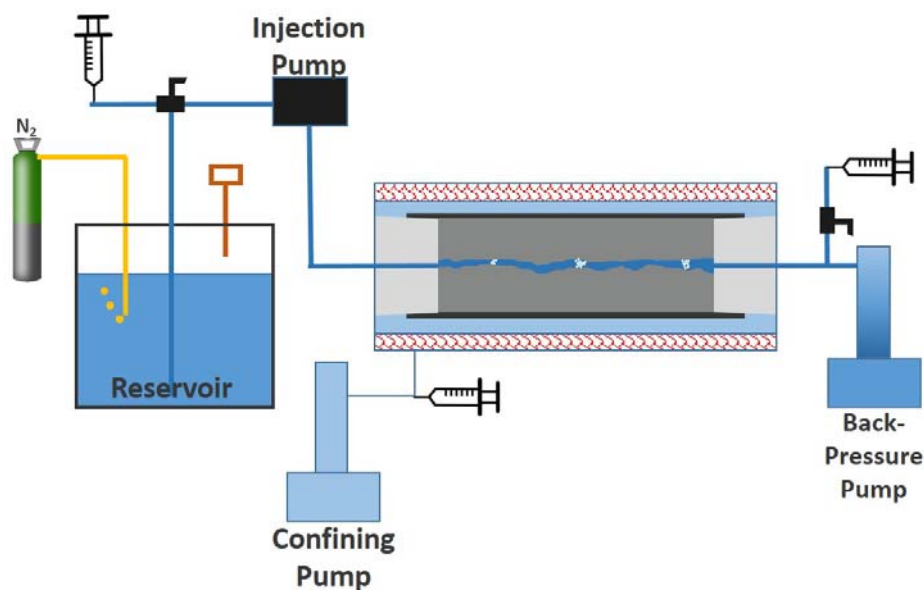


Figure 1: Schematic of experimental apparatus

Fluid Chemistry Analysis

Fluid sample analysis was performed by ion chromatography (IC), inductively coupled plasma mass spectrometry (ICP-MS), and inductively coupled plasma optical emission spectroscopy (ICP-OES). Influent and effluent reservoir fluids were sampled according to the following schedule after introduction of fluids into the experimental apparatus: 2, 24, 48, 72, and 96 h. Samples for IC analysis were filtered through 0.2 μm membrane and not-acidified, and samples for ICP-MS and ICP-OES were unfiltered and acidified with ultrapure nitric acid (Thermo Fisher, Optima grade) prior to analysis. The pH of the influent and effluent reservoir fluids were monitored during sampling. The temperature of fluids when sampled from the collection reservoir ranged from 21.25 ± 2.42 °C for the blank and both core-containing experimental runs.

Computed Tomography Scanning and Image Processing

The 3H cores were scanned before and after exposure with a North-Star Imaging M-5000 Industrial Computed Tomography (CT) scanner. Voxel resolution was 25.4 μm . Image processing was performed using ImageJ[®] and ilastik[®]. No discernable features of interest, which included reacted zones and precipitate, were detected using traditional or advanced techniques. Thus, post-processing of the images was not performed in a quantitative fashion.

Table 1: Hydraulic Fracturing Fluid Product Component Disclosure for MIP 3H Well from FracFocus.org

Trade name	Supplier	Purpose	Ingredients	Chemical Abstract Service Number (CAS #)	Maximum Ingredient Concentration in Additive (% by mass)	Maximum Ingredient Concentration in HF Fluid (% by mass)
Proppant Transport	Schlumberger	Corrosion Inhibitor, Scale Inhibitor, Biocide, AntiFoam Agent, Acid, Breaker, Gelling Agent, Friction Reducer, Iron Control Agent, Fluid Loss Additive				
			Water (Including Mix Water Supplied by Client)	N/A		87.63568
			Quartz, Crystalline silica	14808-60-7	99.06784	12.21724
			Hydrochloric acid	7647-01-0	0.66726	0.08228
			Ammonium sulfate	7783-20-2	0.06845	0.00844
			Guar gum	9000-30-0	0.05865	0.00724
			Acrylamide, 2-acrylamido-2-methylpropanesulfonic acid, sodium salt polymer	38193-60-1	0.05052	0.00623
			Glutaraldehyde	111-30-8	0.02831	0.00349
			Ethanol, 2,2',2''-nitrotris-1,1',1''-tris(dihydrogen phosphate), sodium salt	68171-29-9	0.00971	0.00120
			Diammonium peroxidisulphate	7727-54-0	0.00601	0.00074
			Polymer of 2-acrylamido-2-methylpropanesulfonic acid sodium salt and methyl acrylate	136793-29-8	0.00541	0.00067
			Alkyl(c12-16) dimethylbenzyl ammonium chloride	68424-85-1	0.00506	0.00062

Table 1, continued

Trade name	Supplier	Purpose	Ingredients	Chemical Abstract Service Number (CAS #)	Maximum Ingredient Concentration in Additive (% by mass)	Maximum Ingredient Concentration in HF Fluid (% by mass)
			Sodium erythorbate	6381-77-7	0.00436	0.00054
			Trisodium ortho phosphate	7601-54-9	0.00427	0.00053
			Urea	57-13-6	0.00332	0.00041
			Polypropylene glycol	25322-69-4	0.00294	0.00036
			Methanol	67-56-1	0.00252	0.00031
			Fatty acids, tall-oil	61790-12-3	0.00156	0.00019
			Thiourea, polymer with formaldehyde and 1-phenylethanone	68527-49-1	0.00129	0.00016
			Ethylene glycol	107-21-1	0.00121	0.00015
			Non-crystalline silica (impurity)	7631-86-9	0.00084	0.00010
			Vinylidene chloride/methylacrylate copolymer	25038-72-6	0.00080	0.00010
			Sodium sulfate	7757-82-6	0.00078	0.00010
			Alcohols, C14-15, ethoxylated (7EO)	68951-67-7	0.00061	0.00008
			Ethanol	64-17-5	0.00061	0.00007
			Propargyl alcohol	107-19-7	0.00041	0.00005
			2-Propenamid (impurity)	79-06-1	0.00017	0.00002
			Hexadec-1-ene	629-73-2	0.00014	0.00002
			1-Octadecene (C18)	112-88-9	0.00007	0.00001
			Dimethyl siloxanes and silicones	63148-62-9	0.00005	0.00001
			Tetrasodium ethylenediaminetetraacetate	64-02-8	0.00009	0.00001
			Dodecamethylcyclohexasiloxane	540-97-6		
			Poly(tetrafluoroethylene)	9002-84-0	0.00001	
			Formaldehyde	50-00-0	0.00001	
			Copper(II) sulfate	7758-98-7		
			Decamethyl cyclopentasiloxane	541-02-6		
			Magnesium silicate hydrate (talc)	14807-96-6	0.00002	
FR Pro 150	ECM	Friction Reduction				
			Water	7732-18-5	50.00000	0.01575

Table 1, continued:

			Polyacrylamide-co-acrylic acid	9003-06-9	32.00000	0.01008
			Sodium chloride	7647-14-5	15.00000	0.00472
			Alcohol ethoxylate surfactants	Trade	5.00000	0.00157
			Petroleum distillate	64742-47-8	25.00000	

Results

Calcium shows an increase in the MSEEL 7504.6 ft and 7498.4 ft core flood experiments relative to the influent and blank effluent Ca concentrations (Figure 2A,C). The effluent pH value for the MSEEL 7504.6 ft experiment was consistently lower compared to the pH of the influent and blank effluent, and the pH of the influent and effluents for the blank and MSEEL 7498.4 ft experiment remained within the same range (Figure 2B,D). The influent pH remained between 7.56 ± 0.37 . The blank effluent pH ranged from 7.30 ± 0.06 , the MSEEL 7504.6 ft effluent pH ranged between 6.89 ± 0.06 , and the MSEEL 7498.4 ft effluent pH ranged from pH: 7.09 ± 0.12 . Elevated Ca in effluent from the MSEEL core flood experiments, along with lower pH, suggests that Ca-bearing mineral dissolution (likely calcite) occurred during the experiments concurrently with chemical reactions that caused a pH decrease.

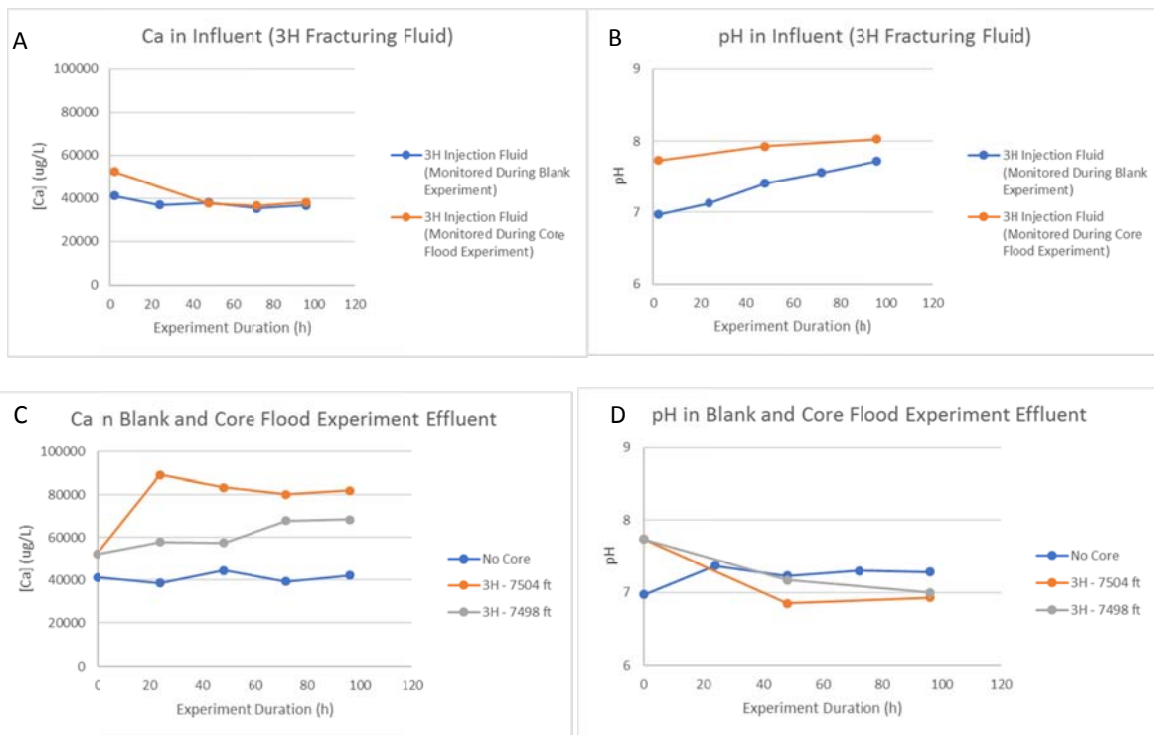


Figure 2: Calcium (A,C) and pH (B,D) for the influent, blank, and core flood experiments with MSEEL 7504.6 ft and 7498.4 ft cores. Lines are included to show the data trend and do not constitute a fit of the data. The influent data show changes to the 3H injection fluid over the time frame of the experiment, prior to introduction into the experimental system (A,B). The blank and core flood panels show changes in effluents for experiments with and without core (C,D). The 0 hour time point in plots C and D represents the value for the influent for more direct comparison of changes in fluid chemistry detected in the effluent.

Barium and strontium are both present in the fracturing fluid and do not vary significantly in the influent during the course of the experiment (Figure 3A,B). Barium concentrations during the MSEEL 7504.6 ft experiment were similar to the core-free blank experiment, suggesting that Ba behavior in the system was mainly influenced by existing Ba within the experimental apparatus. This likely is residual barite precipitate that was difficult to remove

during cleaning of the apparatus after prior experiments (Figure 3C). The elevated initial Ba concentrations in the MSEEL 7498.4 ft experiment reflect influences of the pump malfunction on the solution composition (Figure 3C). Strontium exhibits similar trends in the MSEEL core flood effluents as with the blank effluent, which may result from chemical memory effects in the experimental system (Figure 3B,D).

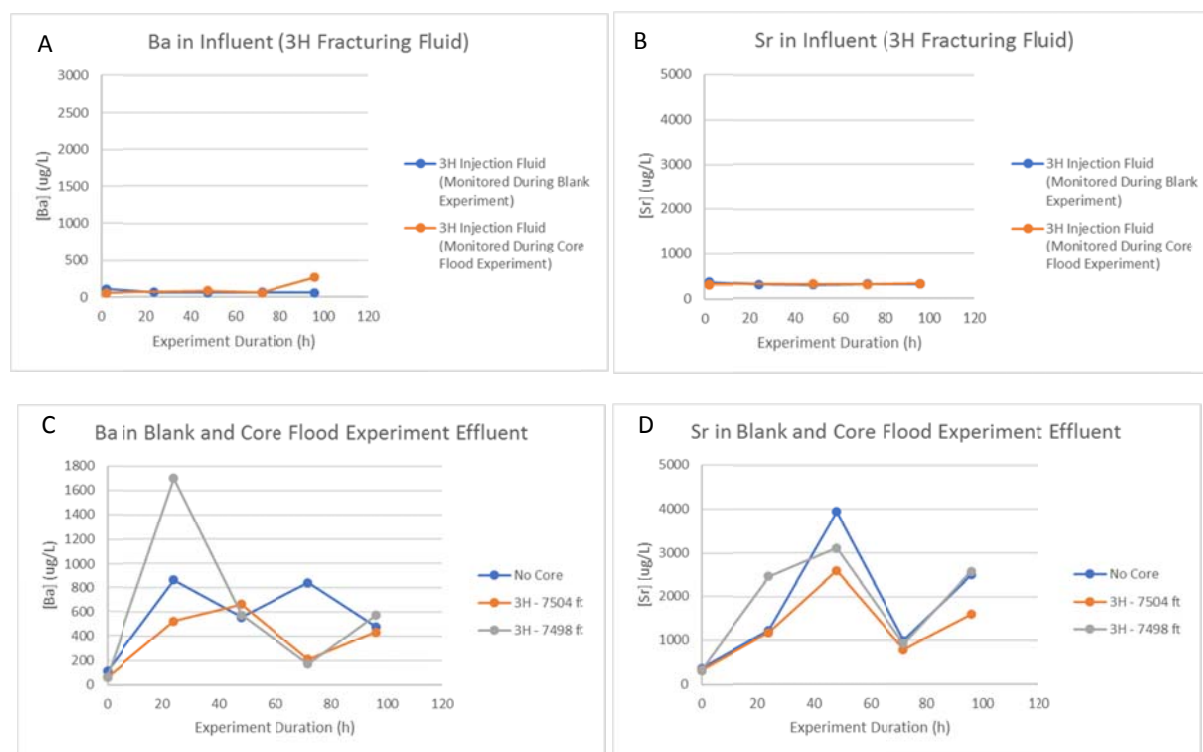


Figure 3: Barium and strontium chemistry for the influent (A,B) and the blank and core flood experiments with MSEEL 7504.6 ft and 7498.4 ft cores (C,D). Lines are included to show the data trend and do not constitute a fit of the data. The influent data show changes to the 3H injection fluid over the time frame of the experiment, prior to introduction into the experimental system (A,B). The blank and core flood panels show changes in effluents for experiments with and without core (C,D). The 0 hour time point in plots C and D represents the value for the influent for more direct comparison of changes in fluid chemistry detected in the effluent.

Sulfate concentrations for both MSEEL core flood effluents are elevated relative to the blank, and show similar trends over time (Figure 4A,B). The control experiment sulfate concentrations remain similar to the influent concentration, suggesting minimal contribution of sulfate from the experimental apparatus to the fluid chemistry (Figure 4A,B).

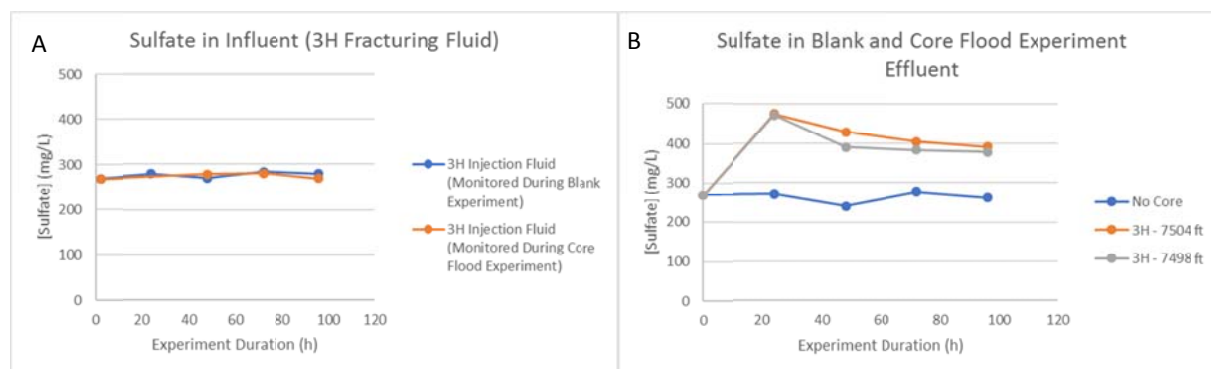


Figure 4: Sulfate concentrations for the influent (A) and blank and core flood effluents (B). Lines are included to show the data trend and do not constitute a fit of the data. The influent data show changes to the 3H injection fluid over the time frame of the experiment, prior to introduction into the experimental system (A). The blank and core flood panels show changes in effluents for experiments with and without core (B). The 0 hour time point in plot B represents the value for the influent for more direct comparison of changes in fluid chemistry detected in the effluent.

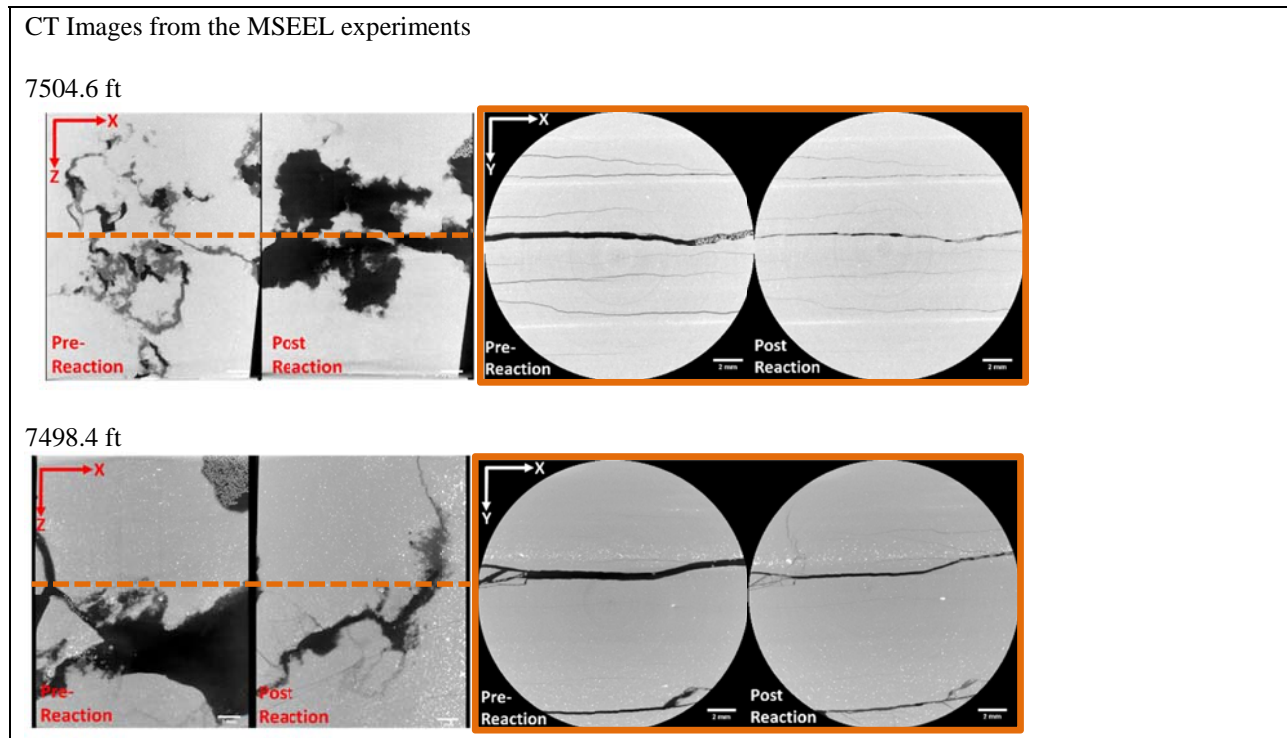


Figure 5: CT grayscale images of the rock cores before and after reaction. Images on the left are looking perpendicular to the fracture plane while images on the right are looking parallel to the fracture or along flow direction. Apertures variation is a result of the pre-reaction scans being done before confining pressure and post reaction scans after confining pressure was applied and then released. Brighter elements within the images are proxies for highly attenuating minerals while dark sections are filled with air or water.

Discussion

Evidence for barite precipitation was not observed, either in the fluid chemistry or the CT images of the experiments with the MSEEL MIP 3H core. CT images did not show any variation in matrix attenuation (grayscale) nor did it show any additional mass gained along the fracture margin as was observed in previous experiments.

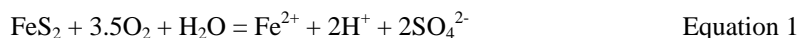
Influence from memory effects of Ba and Sr within the experimental apparatus prevents further interpretation of Ba and Sr mineral scale chemistry resulting from fracturing fluid-shale reactions in the MSEEL experiments presented here. This differs significantly from prior experiments with Marcellus Shale outcrop core reacted with lab-generated fracturing fluids, where barite and Sr-bearing carbonate secondary precipitation was observed within the core (Vankeuren et al., under review). However, precipitation at the core inlet also was observed (Vankeuren et al., under review), and a check of barite saturation indices with MINTeq for the 2h time point of the 3H injection fluid and blank effluent show that both fluids are saturated with barite.

The blank and MSEEL core flood experiments do show elevated solution-phase Ba and sulfate. Although mineral scale is expected to form in the presence of elevated solution-phase Ba and sulfate, other fluid-phase species may affect barite solubility. Examples include the concentration of total dissolved solids present in solution, and the presence of organic acids and antiscalant compounds, which can increase barite solubility. Similar interpretations were presented in prior studies performed with Marcellus Shale in batch experiments (Marcon et al., 2017) and in barite solubility studies (Edenborn et al., 2016; He and Vidic, 2016; Hakala et al., 2017).

Differences in the influent fluid chemistry between the MSEEL experiments in this study, and prior experiments performed with Marcellus Shale outcrop, also may explain differences in the experimental results. A Schlumberger chemical treatment was applied to the MIP 3H well, while the prior experiments applied a fracturing fluid design

based on results from a review of FracFocus data, and generated with fracturing chemicals supplied by a different service company (Vankeuren et al., in review; Moore et al., 2017). The fracturing fluid mixtures between the MSEEL and prior experiments therefore contained different fracturing chemicals, and different concentrations of fracturing chemicals where similarities existed. For example, ammonium persulfate, considered to significantly control sulfate generation and resulting barite precipitation in the prior experiments, is present in different concentrations in the lab-generated solution from prior experiments and the MIP 3H fracturing fluid. Ammonium persulfate was 0.02% of solution in the experiments performed by Vankeuren et al (under review) and Moore et al. (2017). In the experiments reported here, the maximum amount of ammonium persulfate in solution is 0.00074% by mass, and likely was lower during our MSEEL core flood experiments (performed during March 2017) due to oxidant degradation during storage after the November 2015 preparation of fracturing fluid at the well pad.

Sulfate is present in the influent due to existing concentrations in the make-up water, and due to addition of fracturing chemicals (such as ammonium persulfate, and copper sulfate; Table 1). Sulfate increases in both MSEEL core flood experiments, and does not change in the blank experiment relative to the influent concentration (Figure 4A,B), indicating that reaction between the influent and cores resulted in sulfate generation. Sulfate can be generated from the fracturing fluid and from reactions with minerals in the shale. Shale mineral reactions likely to generate sulfate concentrations observed in the MSEEL experiments include ion exchange, gypsum dissolution and pyrite oxidation. Sulfate release via ion exchange was observed in ultrapure water extracts of MIP 3H sidewall cores (Hakala et al., 2017). Because of the slight pH decrease observed in the MSEEL core flood effluents, pyrite oxidation is also a potential contributor to sulfate in the system as the reaction produces sulfate and lowers the solution pH. Pyrite may oxidize due to the presence of oxygen (Eq. 1) or Fe^{3+} (Eq. 2) in solution (Rimstidt and Vaughan, 2003).



Lowering of the pH concurrent with increases in Ca concentrations in the MSEEL core flood effluents provides evidence for calcite dissolution, which has been observed in prior batch and core flood experiments with Marcellus Shale (Dieterich et al., 2016; Marcon et al., 2017; Vankeuren et al., under review). Concurrent calcite dissolution during pyrite oxidation within shales has been observed in other studies focused on shale-fracturing fluid interactions (Wilke et al., 2015).

Conclusions

Composition of the hydraulic fracturing fluid will affect observed secondary mineral precipitates that form in newly-generated fractures and the shale matrix. The presence of oxidants, especially persulfate-based compounds, can have a significant effect on scale mineral precipitation; certain reactions may not be observed if the oxidant isn't as active, or in a low concentration. Concurrent pyrite oxidation and calcite dissolution occur in the MSEEL core flood experiments. The MSEEL core flood experiments showed no change between the pre- and post-reaction CT scans, indicating a difference in fracturing fluid-shale reactions that result in mineral scale formation, compared to prior studies. Further characterization of the shale post-reaction is planned. Additional studies exploring interactions between fracturing fluids and shale involving a range of concentrations of specific fracturing chemicals will provide information on how to best control mineral scale formation during hydraulic fracturing of shale gas reservoirs.

Acknowledgements

This research was supported through the Oil and Gas Program, Office of Fossil Energy, U.S. Department of Energy.

References

- Atkinson, D.; Smelser, R.E.; Sanchez, J. Combined mode fracture via the cracked Brazilian disk test. *International Journal of Fracture*, **1982**, *18*(4), 279-291.
- Dieterich, M.; Kutchko, B.; Goodman, A. Characterization of Marcellus Shale and Huntersville Chert before and after exposure to hydraulic fracturing fluid via feature relocation using field-emission scanning electron microscopy. *Fuel*, **2016**, *182*, 227-235.

Edenborn, H.M.; Hakala, J.A.; Paukert, A. Gel diffusion studies on factors affecting barite scaling in Marcellus shale gas wells. Geological Society of America Northeastern Section Meeting, Albany, NY, March 20 – 23, 2016.

FracFocus www.FracFocus.org. Accessed April 23, 2017.

Hakala, J.A.; Phan, T.; Stuckman, M.; Edenborn, H.M.; Lopano, C.L. Role of Organic Acids in Controlling Mineral Scale Formation During Hydraulic Fracturing at the Marcellus Shale Energy and Environmental Laboratory (MSEEL) Site. Unconventional Resources Technology Conference, Austin, TX, 24-26 July 2017, DOI 10.15530-urtec-2017-2670833

He, C.; Vidic, R.D. Impact of antiscalants on the fate of barite in the unconventional gas wells. *Environmental Engineering Science* **2016**, *33* (10), 745-752.

Marcon, V.; Joseph, C.; Carter, K.E.; Hedges, S.W.; Lopano, C.L.; Guthrie, G.D.; Hakala, J.A. Experimental insights into geochemical changes in hydraulically fractured Marcellus Shale. *Applied Geochemistry* **2017**, *76*, 36-50.

Moore, J.; Hakala, A.; Vankeuren, A.; Phan, T.; Crandall, D. Experiments evaluating geochemical alteration of matrix minerals adjacent to simulated hydraulic fractures. Geological Society of America Northeastern Section Meeting, Pittsburgh, PA, March 19, **2017**.

Rimstidt, J.D.; Vaughan, D.J. Pyrite oxidation: a state-of-the-art assessment of the reaction mechanism. *Geochimica et Cosmochimica Acta*, **2003**, *67*(5), 873 – 880.

Vankeuren, A.N.; Hakala, J.A.; Jarvis, K.; Moore, J. Under Review, *Environmental Science and Technology*

Wilke, F.D.H.; Vieth-Hillebrand, A.; Naumann, R.; Erzinger, J.; Horsfield, B. Induced mobility of inorganic and organic solutes from black shales using water extraction: implications for shale gas exploitation. *Applied Geochemistry*, **2015**, *63*, 158 – 168.

URTeC: 2670833

Role of Organic Acids in Controlling Mineral Scale Formation During Hydraulic Fracturing at the Marcellus Shale Energy and Environmental Laboratory (MSEEL) Site

J. Alexandra Hakala*, National Energy Technology Laboratory
Thai Phan, ORISE National Energy Technology Laboratory
Mengling Stuckman, AECOM National Energy Technology Laboratory
Harry M. Edenborn, National Energy Technology Laboratory
Christina L. Lopano, National Energy Technology Laboratory

Copyright 2017, Unconventional Resources Technology Conference (URTeC) DOI 10.15530/urtec-2017-2670833

This paper was prepared for presentation at the Unconventional Resources Technology Conference held in Austin, Texas, USA, 24-26 July 2017.

The URTeC Technical Program Committee accepted this presentation on the basis of information contained in an abstract submitted by the author(s). The contents of this paper have not been reviewed by URTeC and URTeC does not warrant the accuracy, reliability, or timeliness of any information herein. All information is the responsibility of, and, is subject to corrections by the author(s). Any person or entity that relies on any information obtained from this paper does so at their own risk. The information herein does not necessarily reflect any position of URTeC. Any reproduction, distribution, or storage of any part of this paper without the written consent of URTeC is prohibited.

Abstract

Gas production from hydraulically-fractured shales requires an ability to recover gas stored in tight shale matrices through newly-generated fractures. We previously found that geochemical reactions between hydraulic fracturing fluids and Marcellus Shale may result in the precipitation of scale-forming minerals along primary fractures. Organic acids present within fractured shale, either naturally-present in the shale or from reaction of injected frac chemicals, can affect scale-forming mineral solubility. To date limited information exists on water-soluble organic acids present in the Marcellus Shale that can affect the solubility of minerals such as barite. This study investigates which water-soluble organic substances are present in Marcellus Shale core collected from the Marcellus Shale Energy and Environmental Laboratory site (MSEEL; Morgantown, WV), and how these organic substances affect barite scale formation. Results to date suggest that the water-soluble component of shale minerals likely contributes organic acids to the produced water. On-going work is focused on using measured organic acid concentrations, along with measured dissolved solutes in MSEEL produced waters, to estimate the potential for barite and other mineral scales to form in hydraulically-fractured Marcellus Shale.

Introduction

Organic acid composition and concentrations measured in produced waters from hydraulically-fractured Marcellus Shale wells varies (Akob et al., 2015). This is a result of organic variability across the Marcellus Shale formation, chemicals and procedures applied during fracturing treatments for gas recovery, and sample handling and analytical approaches for produced waters (Orem et al., 2014; Akob et al., 2015).

Barite and other mineral scales are an issue in oil and gas wells due to their potential to affect hydrocarbon recovery flow pathways (He and Vidic, 2015). Ba^{2+} and sulfate co-exist in Marcellus Shale produced waters (Haluszczak et al., 2013), and have been observed to co-exist in experimental fluids associated with fracturing fluid-shale reactions involving Marcellus Shale (Dieterich et al., 2016; Marcon et al., 2017; Vankeuren et al., under review). Both field and experimental data suggest that organic acids affect barite solubility in hydraulically-fractured Marcellus Shale, and their presence was noted as a cause for increased concentrations of Ba and sulfate in produced waters (He et al., 2014).

In this study, we measured organic acid concentrations from ultrapure water extracts of Marcellus Shale side wall cores collected from the Marcellus Shale Energy and Environmental Laboratory MIP 3H well (Sharma et al., 2017). These values, along with produced water chemistry data collected during flowback of the MIP 3H well, were used to

model the effect of organic acids on mineral saturation indices. The primary focus was on barite as a potential mineral scale in hydraulically-fractured Marcellus Shale, however results for other sulfate-bearing scale minerals (gypsum, celestine) and halite are presented for comparison.

Methods

Produced waters were collected from the MSEEL MIP 3H well gas-water separator during flowback and transported to the Sharma Isotope Laboratory at West Virginia University for filtration (0.45 μm) and preservation. For ion chromatography (IC) measurements, no additional preservation was performed prior to analysis at NETL Pittsburgh. Samples were preserved with ultrapure nitric acid after filtration for the inductively coupled plasma mass spectrometry (ICP-MS) and optical emission spectroscopy (ICP-OES) measurements performed at NETL Pittsburgh. Data presented are from direct measurements, except for sulfate. Because sulfate in MIP 3H produced water was not measured by IC, total sulfur values from ICP-OES measurements were used to calculate moles of total sulfur, which then were converted to sulfate. This approach results in an over-estimation of sulfate relative to actual concentrations in the produced water, which are anticipated to be lower than the total sulfur concentration. However, the values calculated are within the range of sulfate extracted from 3H sidewall cores (described below), and represent an upper limit of the possible total sulfate in the MIP 3H produced waters.

MIP 3H sidewall cores were recovered from the Union Springs member of the Marcellus Shale, with depths from 7521.22 ft (2292 m) to 7552.95 ft (2302 m), at the MSEEL site in Morgantown, WV, USA. Rock chips were crushed using a ball mill mixer prior to extraction for water soluble components using ultrapure water (18.2 M Ω .cm) at 20:1 (water:rock) ratio. Slurry mixture of water and rock powder was centrifuged and syringe filtered through a 0.2 μm membrane filter. The water leachates were measured for cation and anion concentrations, including organic acids, by ion chromatography (Thermo Scientific Dionex ICS-5000+) and additional cation concentrations were measured by ICP-MS (NexION 300X).

Visual MINTEQ v. 3.1 (Gustafsson, 2013) was used to calculate saturation indices in MIP 3H produced waters with solution chemistries from the MIP 3H field data (days 1, 5, 10, and 56 after flowback). Modeling was performed with and without organic acids to evaluate the effect of organic acids on mineral saturation indices. Organic acid concentrations for acetate, formate, and butyrate were from measurements of the ultrapure water leachates from the MIP 3H sidewall cores.

Results and Discussion

Produced waters collected from the MIP 3H well show an increase in most dissolved solutes during the first 56 days after initiation of flowback (Table 1).

The ultrapure water extracts of MSEEL MIP 3H sidewall cores show that acetate, formate, and butyrate are extracted by ultrapure water, along with Ba and sulfate (Table 2). Ultrapure water leachates of Marcellus Shale contain relatively high sulfate in comparison to chloride. This easily water soluble component of Marcellus Shale could release sulfate into frac fluid that leads to enhancement of barite scaling, consistent with low sulfate concentrations in produced waters from the gas-water separator. Ba release from exchange sites of clays and organic matter (Phan et al., 2015; Renock et al., 2016) are a source for Ba in produced water, in addition to being present in existing formation water.

Saturation indices for Ba, Ca, and Sr sulfate scales, and halite for comparison, are shown in Figure 1, with values reported in Table 3. Saturation indices in the absence of organic acids are greater compared to calculations performed with organic acids present. This shows that organic acids present in concentrations that are water-leachable from the shale can affect the solubility of potential scaling minerals in the system. Barite is the only mineral with saturation indices that show precipitation can occur in the system, and the value increases during the course of flowback (Figure 1; Table 3). The fraction of free cations is reduced in the presence of organic acids (Figure 2). Saturation indices of barite, gypsum, and celestine in produced water are lower in the presence of organic acids because the organic acids form complexes with Ba²⁺, Ca²⁺, and Sr²⁺, resulting in a decrease in the fraction of free cations.

Table 1: Produced water chemistry data for MIP 3H.

		Day 1 ^a	Day 5 ^a	Day 10 ^a	Day 56 ^a
Ag ^b	µg/L	746	746	746	746
Al ^b	µg/L	41	41	41	41
B	µg/L	8870	10220	10980	9916
Ba	µg/L	226193	649893	1101993	2945993
Ca	µg/L	1615584	2772584	4027584	8291584
Fe	µg/L	39650	40910	60950	193500
K	µg/L	101370	93017	114421	137998
Li	µg/L	19524	34573	42993	68374
Mg	µg/L	197783	328583	452083	897683
Mn	µg/L	2751	5148	6478	12484
Na	µg/L	7307495	10979495	14469495	22939495
H ₄ SiO ₄	µg/L	32698	65444	69987	62212
Sr	µg/L	238392	475692	708592	1580992
Ti ^b	µg/L	83	83	83	83
Zr	µg/L	101	116	57	119
Fluoride	mg/l	10	6	9	3
Chloride	mg/l	15592	25496	33207	59619
Nitrite	mg/l	NM	NM	NM	NM
Bromide	mg/l	159	287	363	646
Nitrate	mg/l	3	3	1	3
Sulfate ^c	µg/L	8880	21192	32534	85351
Phosphate	µg/L	69395	117961	83626	53483

^aColumn headers indicate number of days after flowback when the water sample was collected.

^bValue reported is the detection limit; analyte was present however not quantifiable because it was below the detection limit.

^cCalculated from total sulfur measured by ICP-OES. Actual sulfate values were not measured due to being below the 2.5 mg/L detection limit in prior samples.

Table 2: Ultrapure water extracts of MSEEL MIP 3H Marcellus Shale sidewall cores (n=11)

Constituents	Unit	Min	Max	Average
Acetate	mg/kg	1.8	6.5	3.0
Formate*	mg/kg	0.5	1.0	0.8
Butyrate	mg/kg	1.9	14.3	6.3
Sulfate	mg/kg	116	1465	878
Ba ²⁺	mg/kg	2.7	5.1	3.5

*values are below the method detection limit of 5.7 mg/kg

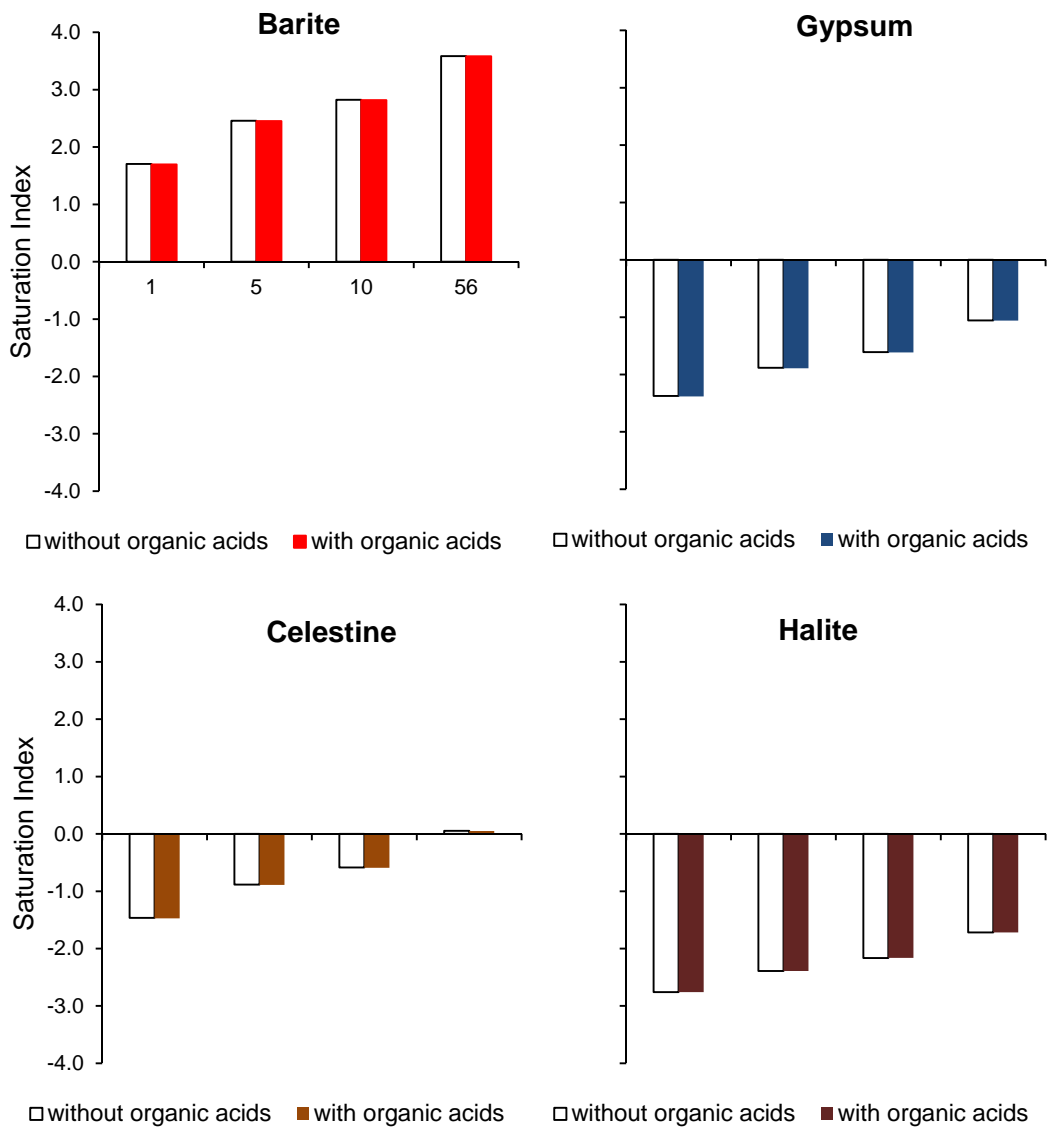


Figure 1: Effect of organic acids on the saturation indices of some minerals in MIP 3H produced water collected on day 1, day 5, day 10, and day 56 (numbers on the X axis) after flowback. Organic acids form complexes with divalent cations (Ba^{2+} , Ca^{2+} , and Sr^{2+}) resulting in a decrease in the fractions of free divalent cations, lowering the saturation indices of barite, gypsum, and celestine. However, organic acids show little effect on the saturation index of halite (Table 3).

Table 3: Effect of organic acids on the saturation indices, $\log(Q/K)$, of some minerals in MSEEL MIP 3H produced water calculated by Visual MINTEQ 3.1

Minerals	Time after flowback	Without organic acids	With organic acids*
Barite	1	1.704	1.696
	5	2.459	2.453
	10	2.824	2.819
	56	3.586	3.582
Gypsum	1	-2.373	-2.383
	5	-1.884	-1.891
	10	-1.609	-1.615
	56	-1.056	-1.060
Celestine	1	-1.465	-1.474
	5	-0.884	-0.89
	10	-0.587	-0.592
	56	0.054	0.051
Halite	1	-2.760	-2.760
	5	-2.390	-2.390
	10	-2.164	-2.163
	56	-1.719	-1.719

*Assuming water:rock ratio of 0.01 during hydraulic fracturing, predicted concentrations of acetate, formate, and butyrate in produced water attributed by water soluble components of Marcellus Shale are 300, 80, and 630 mg/L, respectively.

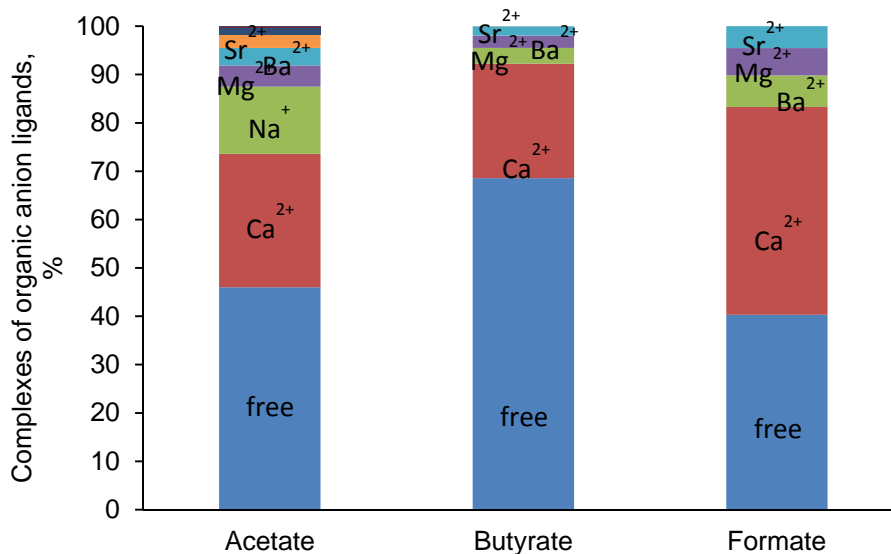


Figure 2: Complexes of acetate, butyrate, and formate in MIP 3H produced water collected on day 56 after flow back. Complexes of organic acids with Ba²⁺, Sr²⁺, Ca²⁺, and Mg²⁺ result in a decrease of free ions, thus, suppress the scaling potential of sulfate scales containing these divalent cations.

Conclusions

Organic acids measured in the water-soluble leachate of Marcellus Shale include acetate, butyrate, and formate. These organic acids, along with dissolved mineral-forming solutes such as Ba²⁺ and sulfate, may be present in fractured shale formations after interaction between hydraulic fracturing fluids and the shale. Mineral saturation indices calculated in the presence of acetate, butyrate, and formate show a decrease relative to those calculated in the absence of organic acids. This study showed that organic acids are present in water-extractable fractions of Marcellus Shale, and that their presence could affect the precipitation of mineral scale within the shale.

Acknowledgements

This research was supported through the Oil and Gas Program, Office of Fossil Energy, U.S. Department of Energy.

References

- Akob, D.M.; Cozzarelli, I.M.; Dunlap, D.S.; Rowan, E.L.; Lorah, M.M. Organic and inorganic composition and microbiology of produced waters from Pennsylvania shale gas wells. *Applied Geochemistry*, **2015**, *60*, 116-125.
- Dieterich, M.; Kutchko, B.; Goodman, A. Characterization of Marcellus Shale and Huntersville Chert before and after exposure to hydraulic fracturing fluid via feature relocation using field-emission scanning electron microscopy. *Fuel*, **2016**, *182*, 227-235.
- Edenborn, H.M.; Hakala, J.A.; Paukert, A. Gel diffusion studies on factors affecting barite scaling in Marcellus shale gas wells. Geological Society of America Northeastern Section Meeting, Albany, NY, March 20 – 23, 2016.
- Gustaffson, J.P. Visual MINTEQ Ver. 3.1, **2013**, <https://vminteq.lwr.kth.se/>
- He, C.; Li, M.; Liu, W.; Barbot, E.; Vidic, R.D. Kinetics and equilibrium of barium and strontium sulfate formation in Marcellus Shale flowback water. *Journal of Environmental Engineering*, **2014**, *140*, B4014001, 3-8.
- Marcon, V.; Joseph, C.; Carter, K.E.; Hedges, S.W.; Lopano, C.L.; Guthrie, G.D.; Hakala, J.A. Experimental insights into geochemical changes in hydraulically fractured Marcellus Shale. *Applied Geochemistry* **2017**, *76*, 36-50.
- Orem, W.; Tatu, C.; Varonka, M.; Lerch, H.; Bates, A.; Engle, M.; Crosby, L.; McIntosh, J. Organic substances in produced and formation water from unconventional natural gas extraction in coal and shale. *International Journal of Coal Geology*, **2014**, *126*, 20-31.
- Phan, T.T.; Capo, R.C.; Stewart, B.W.; Graney, J.R.; Johnson, J.D.; Sharma, S.; Toro, J. Trace metal distribution and mobility in drill cuttings and produced waters from Marcellus Shale gas extraction: Uranium, arsenic, barium. *Applied Geochemistry*, **2015**, *60*, 89-103.
- Renock, D.; Landis, J.D.; Sharma, M. Reductive weathering of black shale and release of barium during hydraulic fracturing. *Applied Geochemistry*, **2016**, *65*, 73-86.
- Sharma, S.; Carr, T.R.; Mouser, P.J.; Wrighton, K.; Cole, D.; Wilkins, M.; Darrah, T.; Hakala, A. Biogeochemical characterization of core, fluids, and gas at MSEEL site. Unconventional Resources Technology Conference, Austin, TX, 24 – 26 July, 2017, DOE 10.15530-urtec-2017-2669965.
- Vankeuren, A.N.; Hakala, J.A.; Jarvis, K.; Moore, J. Under Review, *Environmental Science and Technology*

URTeC: 2669946

Geomechanics of the Microseismic Response in Devonian Organic Shales at the Marcellus Shale Energy and Environment Laboratory (MSEEL) Site, West Virginia

Erich Zorn^{1*}, William Harbert^{1,2}, Richard Hammack¹, Abhash Kumar^{1,3}

¹ National Energy Technology Laboratory, US Department of Energy, Pittsburgh, PA

² Department of Geology and Environmental Science, University of Pittsburgh, PA

³ AECOM

Copyright 2017, Unconventional Resources Technology Conference (URTeC) DOI 10.15530/urtec-2017-2669946

This paper was prepared for presentation at the Unconventional Resources Technology Conference held in Austin, Texas, USA, 24-26 July 2017.

The URTeC Technical Program Committee accepted this presentation on the basis of information contained in an abstract submitted by the author(s). The contents of this paper have not been reviewed by URTeC and URTeC does not warrant the accuracy, reliability, or timeliness of any information herein. All information is the responsibility of, and, is subject to corrections by the author(s). Any person or entity that relies on any information obtained from this paper does so at their own risk. The information herein does not necessarily reflect any position of URTeC. Any reproduction, distribution, or storage of any part of this paper without the written consent of URTeC is prohibited.

Abstract

Using an innovative workflow incorporating microseismic attributes and geomechanical well logs, we have defined major geomechanical drivers of microseismic expression to understand reservoir stimulation response in engineering and geological contexts. We sampled microseismic data from two hydraulically fractured Marcellus wells in the Appalachian Basin, northern West Virginia, vertically through the event cloud, crossing shale, limestone, sandstone, and chert. We focused our analysis on the Devonian organic shale and created pseudo-logs of moment magnitude (M_w), b-value, and event count. The vertical moving-average sampling of microseismic data was completed such that the sample interval matched that of the geophysical well log. This technique creates robust, high-resolution microseismic logs that show subtle changes in microseismic properties and allows direct cross-plotting of microseismic versus geophysical logs. We chose five geomechanical properties to form the framework against which to interrogate the microseismic data: Young's modulus (YM), Poisson's ratio (PR), brittleness, lambda-rho ($\lambda\rho$), and mu-rho ($\mu\rho$). Additionally, we included natural gamma as a useful measure of organic content. Having defined this microseismic-geomechanical cross-plot space, we derived insights into the response of these units during hydraulic fracturing. Observations include: 1) larger magnitude microseismicity occurs in high PR, high YM rocks; high event counts are found in low PR rocks; 2) low b-value (high in-situ stress) is consistent with the occurrence of larger magnitude events and low event counts; and 3) YM and PR act as bounding conditions, creating "sweet spots" for high and low M_w , event count, and stress. In our cross-plot space, there is a meaningful link between microseismicity and the elastic properties of the host rock. In light of this dependence of stimulation potential on elastic properties, the calculation of microseismic pseudo-logs at stimulation sites and application of our cross-plot framework for microseismic-geomechanical analysis in unconventional shale will inform operators in planning and forecasting stimulation and production, respectively.

Introduction

In late 2015, two parallel, horizontal wells in Monongalia County, West Virginia were drilled and hydraulically fractured in the Marcellus Shale over 58 stages (Figure 1). The wells were stimulated separately from each other, with the more northerly well (Well 5) completed first, then the southerly well (Well 3) second, as opposed to a "zipper-frac" or simulfrac. Microseismic monitoring was completed by Schlumberger, deploying one 12-level (100 foot spacing) Versatile Seismic Imager (VSITM) array down one vertical deep well. Additionally, standard well logs including p-sonic, s-sonic, bulk density, total porosity, and natural gamma were acquired in the vertical well, and a full suite of geomechanical well logs were acquired along the length of one of the horizontal wells.

25,116 microseismic events were recorded at the geophones over the course of 52 out of the 58 stages of treatment (Figure 1), ranging between moment magnitude (M_w) -3.15 and -0.05, with a mean value of M_w -2.14. The seismicogenic b -value is simply the slope of the linear portion of the \log_{10} (frequency) versus magnitude distribution in a seismic catalog, and is an indicator of in-situ stress conditions. We employed the seismological toolset ZMAP (Wiemer 2001). The completeness magnitude (M_c) is the minimum magnitude above which the distribution still follows the Gutenberg-Richter power law relationship. M_c for this dataset varies between -1.8 and -2.2 depending upon the method of calculation. M_c can be calculated by modelling the catalog for the entire magnitude range and determining the point at which the distribution becomes non-linear or non-self-similar. This is known as the EMR method (Woessner 2005). A simpler method is to find the point of maximum curvature (MaxC) in the frequency-magnitude distribution. The overall b -value for the entire catalog from both wells ranges between 1.2 and 1.5, depending upon the M_c calculated.

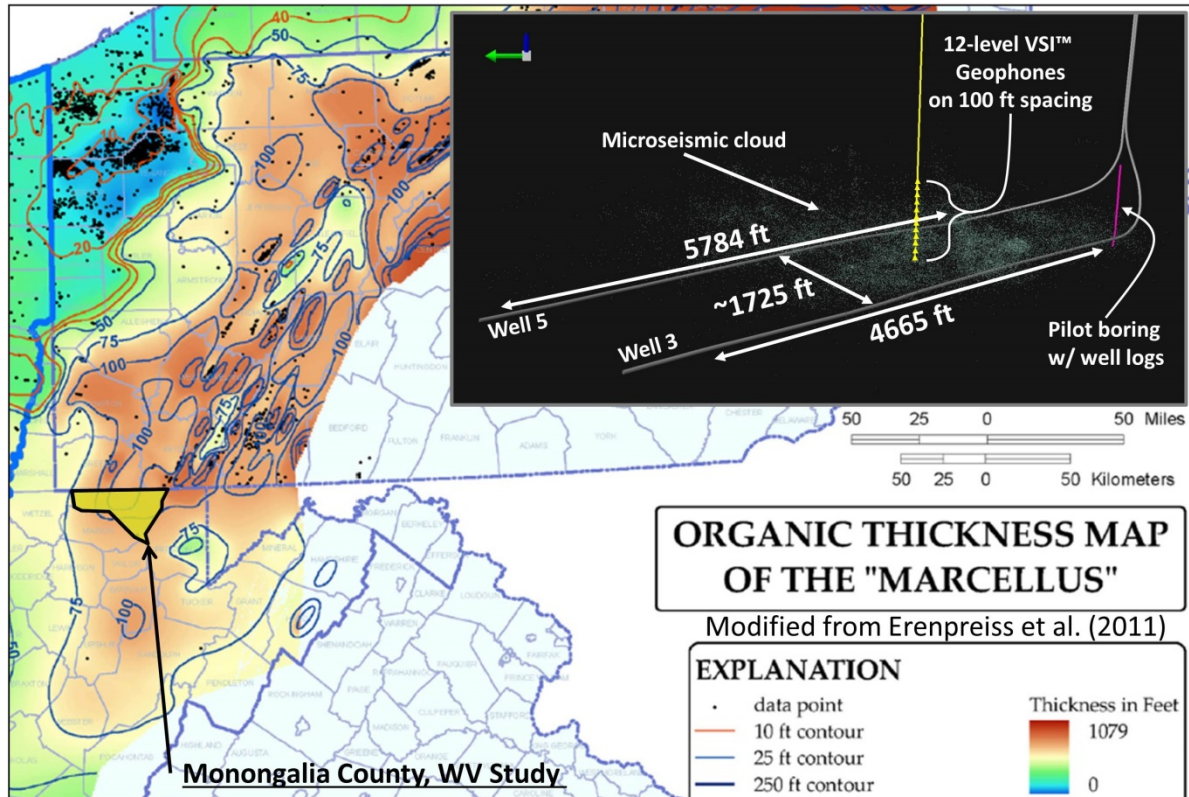


Figure 1. Location map, modified from Erenpreiss et al. (2011). Inset is a view of the lateral well geometry and spacing, monitoring well location and configuration, logged pilot hole location and depth, and the microseismic cloud.

In the development of unconventional resources like the Marcellus Shale, where natural gas is trapped within tight and/or poorly interconnected porosity, direct stimulation of the source/reservoir layer through hydraulic fracturing is critical to the recovery of hydrocarbons. Microseismic monitoring provides direct evidence of fracture formation by detecting the resulting seismic events, as documented in Maxwell et al. (2002) and other studies. However, not all of the hydraulic energy transferred downhole is applied to the task of creating fractures in the zone of interest. Much of this energy is lost to heat, fluid energy dissipation, and aseismic deformation (Lee et al. 1991, Boroumand and Eaton 2012). Furthermore, the majority of microseismicity occurs outside of the zone of interest. The inefficiency described above should be accounted for when using microseismic data as a measure of stimulation. A too simplistic approach in which abundant microseismicity should correspond to high hydrocarbon production can lead to over- or under-estimates of production. However, the distribution of microseismicity over a vertical span that includes four distinct shale units and multiple limestone units presents the opportunity to examine the relationship between rock mechanical properties and microseismic characteristics. Roche and van der Baan (2015) performed similar work in which they investigated the effect of in-situ stress, pore pressure, lithological layering and coupling, and geomechanical rock properties on the distribution and characteristics of microseismicity at two hydraulic fracturing sites.

Methods

In order to directly compare properties of the microseismic catalog such as event magnitude and event count to the geophysical well logs, the microseismic cloud was sampled using a five-foot vertical window that was advanced through the cloud at the same interval and elevation as the well logs (Figure 2a). First, using ZMAP (Wiemer 2001), the b-value was calculated for the entire microseismic catalog, and the corresponding completeness magnitude (M_c) was used as a cutoff (Figure 2a; Figure 3), eliminating events with magnitudes too small to be detectable uniformly across the entire site, as described in Maxwell (2012). M_c is represented on Figure 2a by the sharp cutoff in the microseismic cloud. The moment magnitude of events within the window at each sampling point was averaged to create a moment magnitude “log”. The number of events within the moving window at each sampling point was also used to create an event count log. Lastly, using the complete dataset, the slope of the frequency-magnitude distribution (b-value) of microseismicity within a dynamically sized, sliding sample window containing 300 events, was calculated to create a b-value log. This robust b-value log was then interpolated to match the well log sample interval. Figure 2b shows the core set of geomechanical and microseismic logs used in this study.

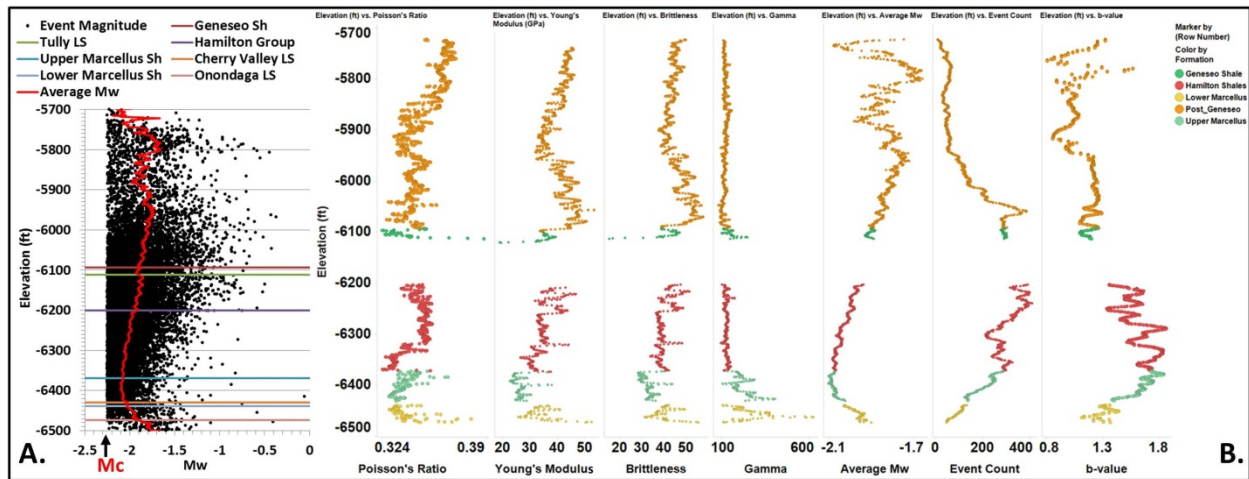


Figure 2. (A) The moment magnitude “log” superimposed on the microseismic cloud from which it was calculated. (B) The geomechanical / dynamic moduli logs and microseismic logs forming the foundation of the analyses in this study.

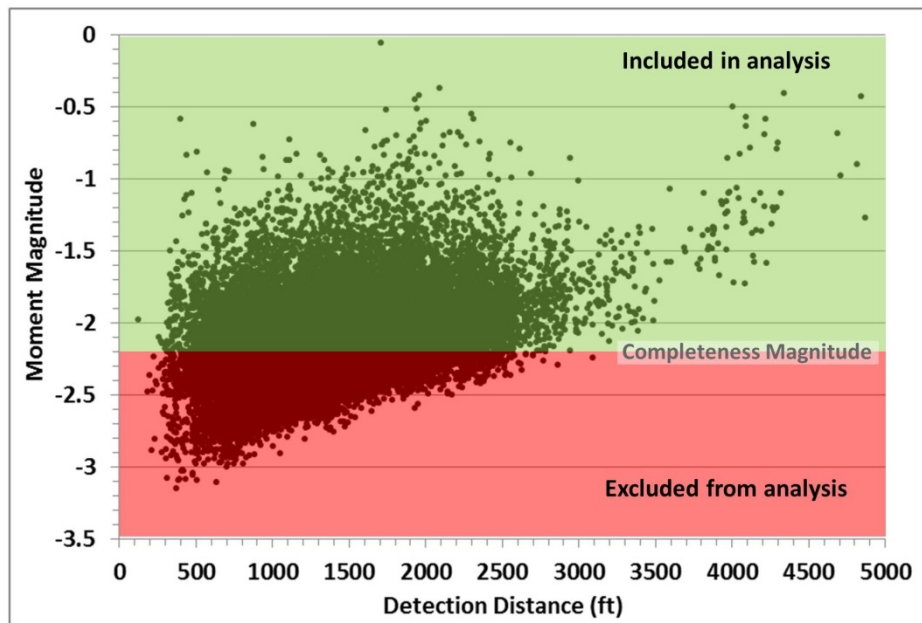


Figure 3. Moment magnitude versus detection distance (ft), showing the naturally inclined detection threshold, indicating a decrease in small magnitude detection ability with increased distance. The plot is divided into two panels, based upon a completeness magnitude of -2.2.

The mu-rho versus lambda-rho (MRLR) crossplot forms the foundation upon which these other properties are imposed because they are invariant and form the basic elements of the other moduli. Goodway et al. (2010) illustrated the usefulness of the MRLR space in describing changes in lithology, porosity, elasticity, and fluid content (among other properties) (Figure 4). Our approach in this study is to crossplot MRLR and color the data cloud by one of the microseismic parameters, while superimposing useful reference iso-lines of PR, YM, and brittleness, and shading the plot by gamma value. We consider this crossplot space the most useful in interpreting our attributes. This approach of displaying seven attributes in a single reference plot helps to identify the principal components that drive change in microseismic expression. Brittleness is calculated according to Rickman et al. (2008), in which PR and YM alone describe brittleness:

$$BRIT_YM = ((YM - 1)/(8 - 1)) * 100$$

$$BRIT_PR = ((PR - 0.4)/(0.15 - 0.4)) * 100$$

$$BRIT_TOTAL = ((BRIT_YM + BRIT_PR) / 2)$$

In these equations, it is important to note the YM and PR threshold values that affect the total brittleness calculation. When YM = 8 Mpsi and PR = 0.15, the resulting material will be “100%” brittle. YM = 1 Mpsi and PR = 0.4 will produce a “0%” brittle material. Reasonable combinations of values are likely constrained within these bounds, resulting in brittleness values of between 0 and 100%. As YM increases, brittleness increases; as PR increases, brittleness decreases.

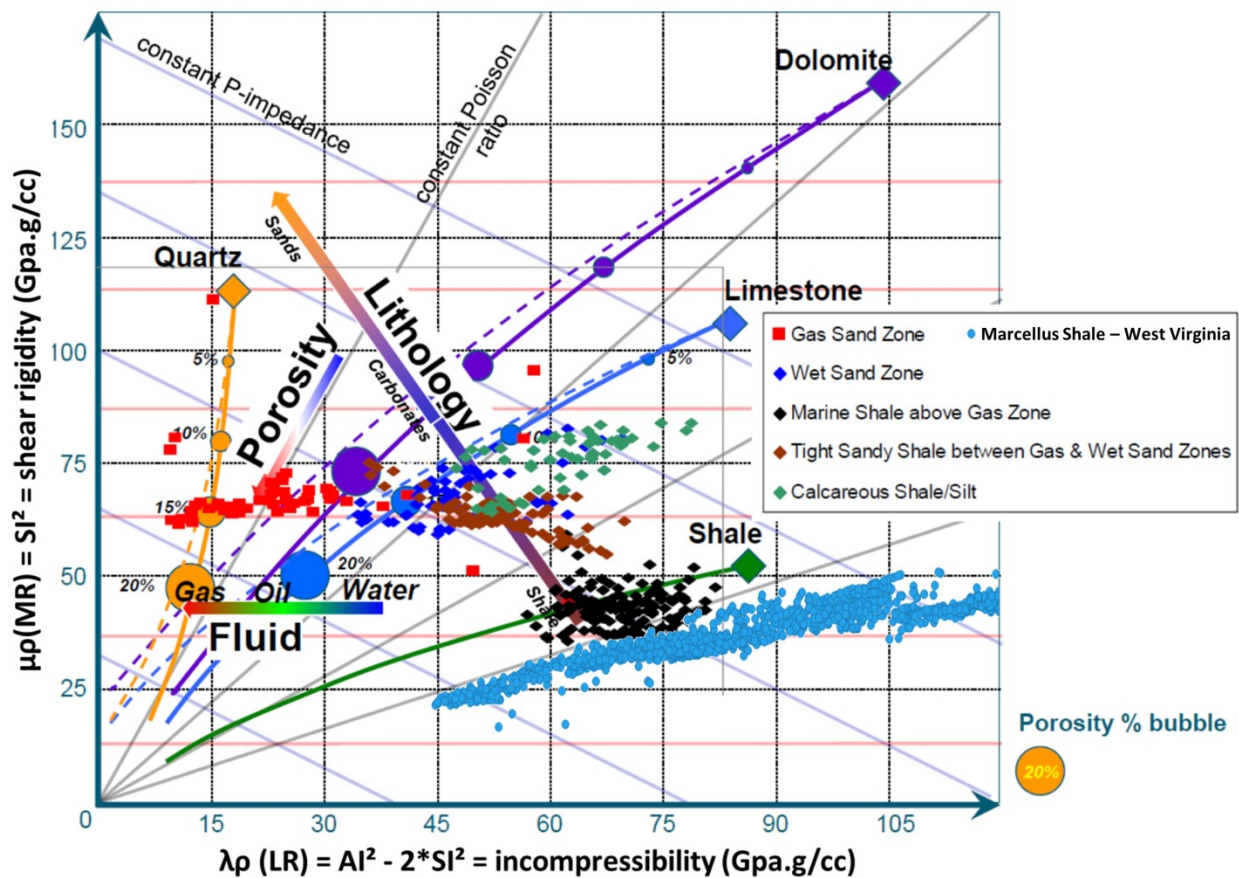


Figure 4. The utility of Mu-Rho versus Lambda-Rho space, with West Virginia Devonian Shale data superimposed in light blue. Modified from Goodway (2009).

To reduce detection bias in the microseismic data, we excluded all events with a moment magnitude smaller than the magnitude of completeness (-2.2) of the microseismic catalog, as defined by the b-value of the frequency-magnitude

distribution (Figure 2a, identified by Mc; Figure 3). Location uncertainty ranges from an average of 160 feet in the maximum eigenvector dimension to 42 feet in the minimum dimension. To minimize error we excluded all microseismic events with a signal to noise ratio < 2 . Stratigraphically, at the project scale, rock units are relatively flat lying and laterally continuous. This is important due to the nature of the sampling and analysis methods being employed here, in which well log properties are treated as laterally applicable and uniform. As this present study concentrates only on the geomechanical and microseismic properties of organic shale, we excluded any non-shale rocks from the analysis, such as limestone and chert. In an effort to be consistent with a previous study completed in Clearfield County, PA (Zorn et al. 2017), we decided to use the same basic log set of V_p , V_s , and Rho_B (bulk density) as the starting point for all calculations. It is understood that there is uncertainty in both the location and magnitude of microseismic events, and also in the assumption that rock layers are flat lying and laterally continuous. We feel that the sampling methods employed in this study (sliding/overlapping sampling windows, average magnitudes, etc.) are robust enough to soften the effects of this uncertainty.

Results

In order to approach the interpretation of this projection of seven different variables, we first examine the data for gradients present at orthogonal angles to iso-lines of each variable. In examining the data-cloud against YM, we see direct correlation between increasing or decreasing YM and the presence of relatively large or small moment magnitude events, respectively (Figure 5). Additionally, when we examine the data compared to iso-lines of PR, a relationship emerges in which the smallest magnitude microseismicity generally occurs in the zone of lowest PR and the largest magnitude microseismicity occurs in the zone of highest PR.

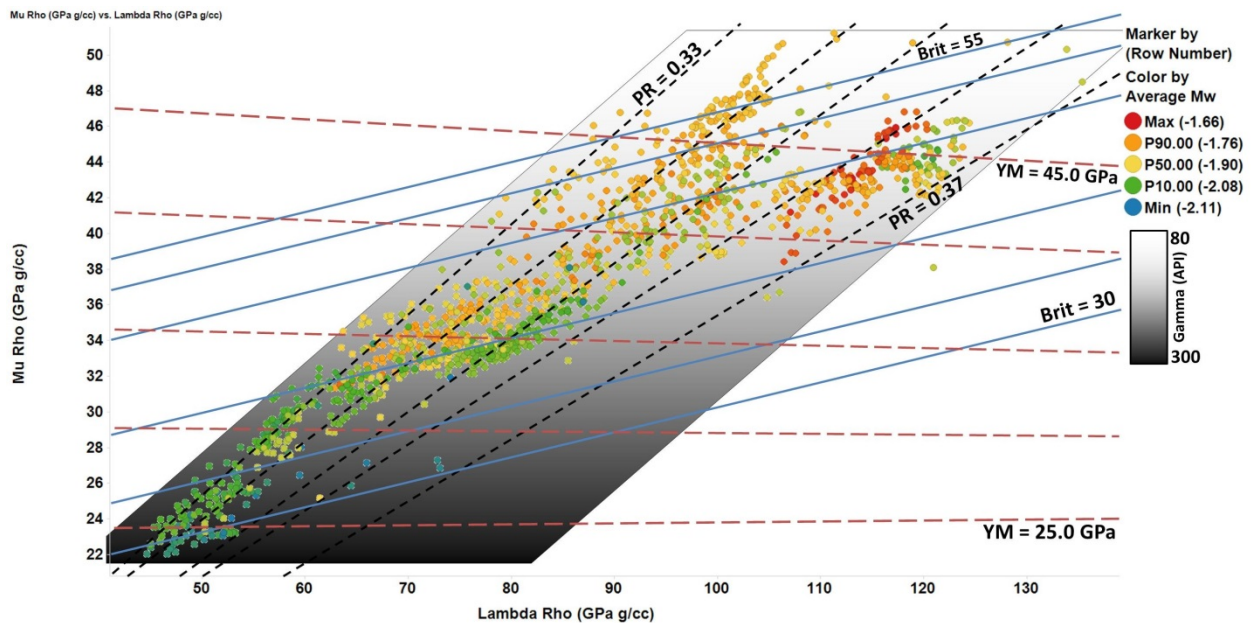


Figure 5. The MRLR analysis space colored by average moment magnitude of microseismicity.

It appears that PR exerts first order control over the relative abundance of microseismicity (Figure 6). There is a striking juxtaposition of the highest event count next to lowest event count, within the same zone of YM (> 40 GPa). However, the lowest number of events occurs at the highest PR, and microseismicity is most abundant where PR is lowest. Examination of the zone of low PR reveals there is a secondary gradient in which a combination of high YM and low PR conditions will result in more microseismicity than a low YM / low PR condition.

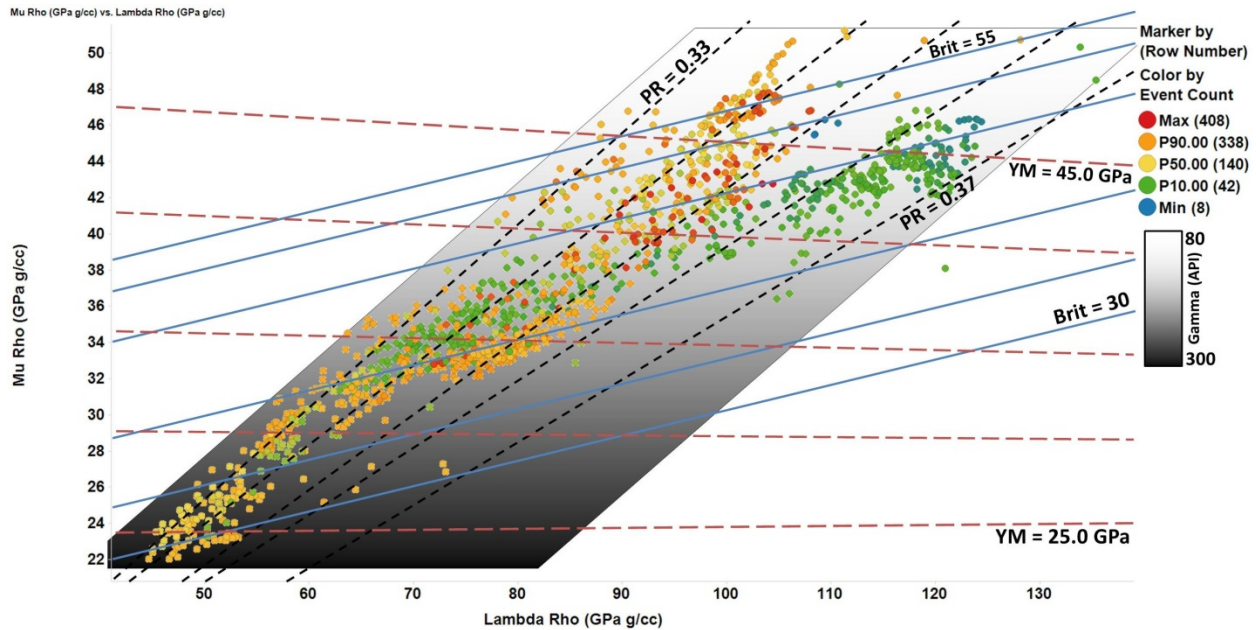


Figure 6. The MRLR analysis space colored by microseismic event count.

The seismogenic b -value can be interpreted as an indicator of stress condition (Schorlemmer et al. 2005, Goertz-Allmann and Wiemer 2013). A low b -value indicates that a larger proportion of the event catalog is comprised of larger magnitude seismicity, conceivably a result of higher stress conditions at failure. Conversely, a high b -value (>1) indicates a distribution of seismicity weighted more toward smaller magnitudes as a result of failure in a lower stress condition. In MRLR space, according to Goodway, the state of in-situ stress increases with increasing MR and LR. We observe the lowest b -values in the region of the crossplot that generally corresponds to the largest moment magnitudes and lowest event counts (Figure 7). Relating to rock physical properties, low b -values occur in mid to high YM and lower gamma (organic content) rocks. Conversely, the highest b -values occur in rocks with a low YM and the highest organic content. A low YM and high organic content would presumably allow internal stresses to be redistributed more readily, discouraging a high stress condition and resulting in a higher b -value.

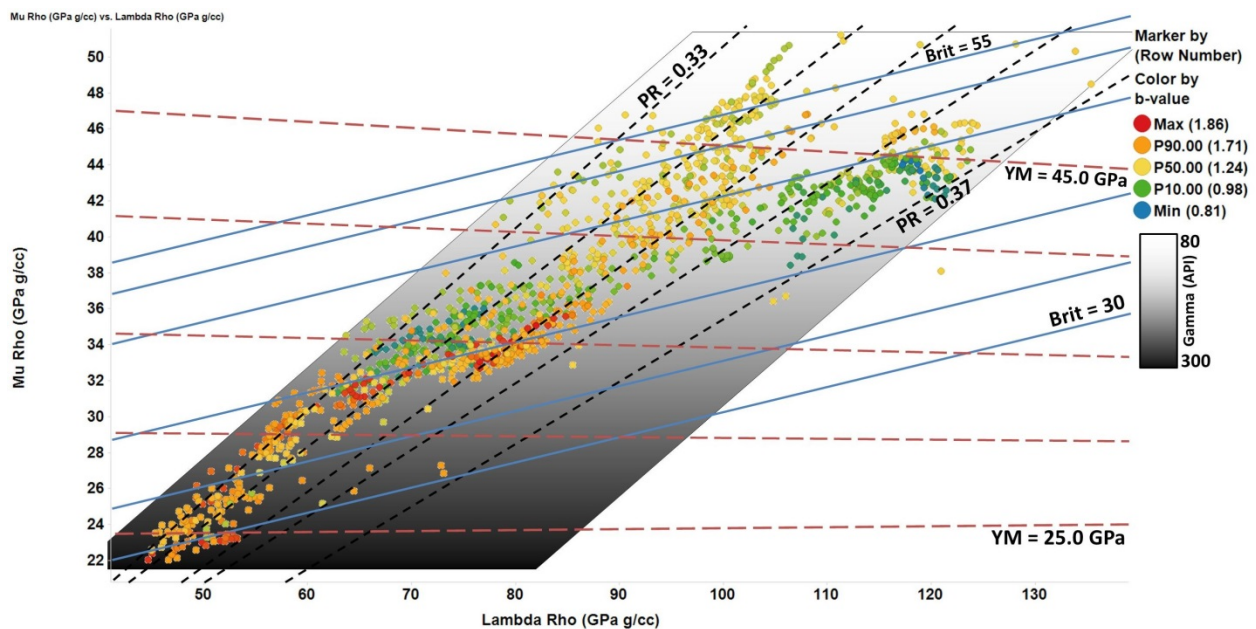


Figure 7. The MRLR analysis space colored by the seismogenic b -value of microseismicity.

Discussion

Young's modulus (axial stress / axial strain) is a measure of material stiffness and Poisson's ratio (axial strain / lateral strain) is a measure of material toughness (Figure 8). Stiffness is the resistance to deformation when stressed, while toughness is the resistance to fracturing when stressed. Stiff materials are generally more brittle and prone to fracturing, and resistant to deformation, while less stiff materials are tougher. A material that possesses a high PR will likely have a low YM, and vice versa, but there is a natural spread in the possible physical value combinations such that at a given stiffness, materials can be more or less tough, and at a given toughness, materials can be more or less stiff. We believe that the observed relationships between microseismic properties and elastic properties of organic shale rocks are a result of these subtle interactions between YM and PR. Of course, there are second-order variables which undoubtedly influence these relationships, such as existing structures (expulsion features, fractures, faults, or other stress risers), in-situ pore pressure, pore shape, permeability/diffusivity, clay and kerogen content, differential stress/closure stress, anisotropy, pumping pressure, rate, volume, and duration. We have tried to address the matter of stress state through the inclusion of b-value analysis. The effect of relative organic content and its relationship with geomechanical and microseismic properties can be seen in the gamma value overlay.

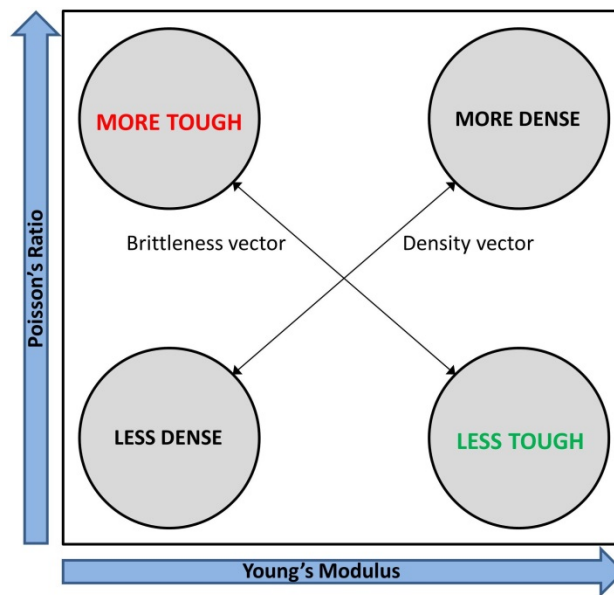


Figure 8. Poisson's Ratio versus Young's Modulus crossplot space and the distribution of elastic rock properties.

We observe in Figure 5 that the reservoir rocks with the highest PR and YM also host the largest average magnitude microseismicity. These are both the toughest and stiffest rocks, meaning they are both resistant to fracturing and resistant to deforming. The inverse is also apparent: the smallest magnitude microseismicity occurs in formation rocks with the lowest YM and the lowest PR.

In the examination of microseismic event count in the context of geomechanical properties (Figure 6), we see a first order gradient in which rocks with the lowest PR host the largest number of microseismic events. A second order gradient orthogonal to YM indicates that at any value of PR, an increasing YM will cause an increase in the occurrence of microseismicity. No data resides in the low YM, high PR zone of the crossplot, as this combination of rock mechanical properties does not exist in this stratigraphic sequence. However, one can extrapolate that in a rock that is highly resistant to fracturing and amenable to deformation, the formation of brittle fractures and associated microseismicity would be a rare occurrence. The zone of maximum event count on the MRLR plot spans the spectrum of YM values but is focused on the low PR area, where rocks are more prone to fracturing. It should be noted that in comparing the distribution of moment magnitude and event count in Figure 5 and Figure 6, we observe that the small to mid-size magnitudes coincide with a greater abundance of microseismicity and the largest magnitudes coincide with the lowest event counts. This is important as it demonstrates, in an induced microseismic catalog, adherence to frequency-magnitude laws set forth by Gutenberg and Richter (1944).

The analysis and discussion of b-value is relevant because it directly relates the magnitude to the abundance of microseismicity and we have shown that these three seismological attributes are in agreement, i.e. large $M_w \rightarrow$ low event count \rightarrow low b-value, and small $M_w \rightarrow$ high event count \rightarrow high b-value. More importantly, however, is the interpretation of b-value as an indicator of the in-situ stress state at the point of failure. Locally, the state of stress is influenced by the ability of the rock to distribute that stress, which is a function of the shale lithology and microstructure in the area of failure. Figure 7 illustrates that the highest b-values correspond to the lowest values of YM and PR, indicating that an increased ability to deform and/or sustain a fracture in response to stress discourages the development of a high local state of stress. The opposite relationship is also observed, in which the region of highest YM and PR corresponds to the presence of the lowest b-values. Additionally, it appears that there is a relationship between b-value and gamma value. If gamma is treated as a gross estimator of relative organic or kerogen content, then the most organic-rich shale will be least resistant to deformation in response to stress, and therefore have a tendency to host high b-value microseismicity.

Conclusions

We have approached a greater understanding of the fundamental geomechanical influences on the microseismic response to hydraulic fracturing. Utilizing standard sonic and density well logs, we calculated the dynamic elastic moduli, and employed a novel approach to create comparable microseismic “logs”. A multi-dimensional MRLR crossplot facilitated a dense and efficient display of meaningful data and uncovered subtle relationships between elastic properties of organic shale and the seismological attributes of recorded microseismicity. PR exerts a strong influence on the average moment magnitude of seismicity. PR and YM influence the abundance and frequency-magnitude distribution of seismicity. The elasticity of the rock, in the context of toughness and stiffness, directly affects the local in-situ state of stress, which in turn, affects the magnitude and abundance of microseismicity.

In terms of importance to energy industry applications, this knowledge can help to refine the concepts of “fracability” and “stimulated” reservoir. Traditionally, more microseismicity translates to “more fracable”. Targeting low PR rocks will result in increased event counts. Additionally, low PR is thought to correlate with higher exploitable organic content and a larger number of existing micro-fractures and/or expulsion features. However, these events will generally be the smallest magnitudes. Moment magnitude (M_w) is related to the area of the rupture plane and the stress drop at the failure, and the energy release of the failure increases logarithmically on the M_w scale. There may be some validity to targeting organic shale at the highest end of the PR scale and mid-high YM. Although event count will decrease, energy release and area of the failure plane will increase. High PR translates to larger average moment magnitude, and mid-high YM translates to a greater ability to sustain a propped fracture.

Finally, there are myriad other factors that can be less accessible but need to be kept in mind. These may act as additional controls on the microseismic response, including: existing macro and micro-structure (expulsion features, fractures, faults, or other stress-risers), in-situ pore pressure, pore shape, permeability/diffusivity, clay and kerogen content, differential stress/closure stress, anisotropy, pumping pressure/rate/volume/duration. We have established a foundation of understanding from fundamental material properties upon which to build in additional complexity.

Acknowledgements

We would like to thank the US Department of Energy’s National Energy Technology Laboratory and their industry partners for making this work possible.

References

- Boroumand, N., and D. W. Eaton, 2012, Comparing energy calculations: Hydraulic fracturing and microseismic monitoring: GeoConvention 2012: Vision, 1-4.
- Erenpreiss, M. S., L. H. Wickstrom, C. J. Perry, R. A. Riley, and D. R. Martin, 2011, Regional organic thickness map of the Marcellus Shale. Ohio Department of Natural Resources, Division of Geological Survey, 6 April 2011, https://geosurvey.ohiodnr.gov/portals/geosurvey/Energy/Marcellus/Regional_Marcellus%20thickness_cntrlpts_8x11.pdf (accessed 12 June 2017).
- Goertz-Allmann, B. P., and S. Wiemer, 2013, Geomechanical modeling of induced seismicity source parameters and implications for seismic hazard assessment: *Geophysics*, 78, no. 1, KS25-KS39.
- Goodway, W., M. Perez, J. Varsek, and C. Abaco, 2010, Seismic petrophysics and isotropic-anisotropic AVO methods for unconventional gas exploration: *The Leading Edge*, 29, no. 12, 1500-1508.
- Gutenberg, B., and C. F. Richter, 1944, Frequency of Earthquakes in California: *Bulletin of the Seismological Society of America*, 34, no. 4, 185-188.
- Lee, T. S., S. H. Advani, and J. M. Avasthi, 1991, Characteristic-time concept in hydraulic fracture configuration evolution and optimization: *SPE Production Engineering*, 6, no. 3, 323-333.
- Maxwell, S., 2012, Comparative microseismic interpretation of hydraulic fractures, Paper SPE-162782: SPE Canadian Unconventional Resources Conference, Proceedings, 1-8.
- Maxwell, S. C., T. I. Urbancic, N. Steinsberger, and R. Zinno, 2002, Microseismic imaging of hydraulic fracture complexity in the Barnett Shale, Paper SPE-77440: SPE Annual Technical Conference and Exhibition, Proceedings, 1-9.
- Rickman, R., M. Mullen, E. Petre, B. Grieser, and D. Kundert, 2008, A practical use of shale petrophysics for stimulation design optimization: all shale plays are not clones of the Barnett Shale, Paper SPE-115258: SPE Annual Technical Conference and Exhibition, Proceedings, 1-11.
- Roche, V., and M. van der Baan, 2015, The role of lithological layering and pore pressure on fluid-induced microseismicity: *J. Geophys. Res. Solid Earth*, 120, no. 2, 923-943.
- Schorlemmer, D., S. Wiemer, and M. Wyss, 2005, Variations in earthquake-size distribution across different stress regimes: *Nature*, 437, 539-542.
- Wiemer, S., 2001, A software package to analyze seismicity: ZMAP: *Seismological Research Letters*, 72, no. 2, 374-383.
- Woessner, J. (2005). "Assessing the Quality of Earthquake Catalogues: Estimating the Magnitude of Completeness and Its Uncertainty." *Bulletin of the Seismological Society of America*, 95, no. 2. 684-698.
- Zorn, E.V., W. Harbert, R. Hammack, A. Kumar, 2017, Geomechanical lithology-based analysis of microseismicity in organic shale sequences: a Pennsylvania Marcellus Shale example: *The Leading Edge*, In Press.

URTeC: 2670481

Seismic Monitoring of Hydraulic Fracturing Activity at the Marcellus Shale Energy and Environment Laboratory (MSEEL) Site, West Virginia

Abhash Kumar^{1,2, *}, Erich Zorn¹, Richard Hammack¹, William Harbert^{1,3}

¹National Energy Technology Laboratory, Department of Energy, Pittsburgh, PA;

²AECOM; ³Department of Geology and Environmental Science, University of Pittsburgh, Pittsburgh, PA

Copyright 2017, Unconventional Resources Technology Conference (URTeC) DOI 10.15530/urtec-2017-2670481

This paper was prepared for presentation at the Unconventional Resources Technology Conference held in Austin, Texas, USA, 24-26 July 2017.

The URTeC Technical Program Committee accepted this presentation on the basis of information contained in an abstract submitted by the author(s). The contents of this paper have not been reviewed by URTeC and URTeC does not warrant the accuracy, reliability, or timeliness of any information herein. All information is the responsibility of, and, is subject to corrections by the author(s). Any person or entity that relies on any information obtained from this paper does so at their own risk. The information herein does not necessarily reflect any position of URTeC. Any reproduction, distribution, or storage of any part of this paper without the written consent of URTeC is prohibited.

Summary

Hydraulic fracturing is a well-established completion technique to extract significant volumes of natural gas from organic-rich shale, which would otherwise behave as impermeable formations. Diffusion of water outward from the newly created hydraulic fractures into the reservoir helps reactivate the preexisting faults and initiates shear failure on complex network of preexisting planes of weaknesses. Microseismic events recorded on downhole arrays are a manifestation of associated shear failure along both preexisting and newly created fractures. Some of the recent studies focused on energy balance calculations suggest that the cumulative moment of microearthquakes is a small portion of the moment release expected for the amount of fluid injected into the formation. This suggests some other sources of deformation in the reservoir rock, contemporaneous with microseismic activity that need to be considered to get a balance in the energy budget during hydraulic fracturing process. Recent findings on long period, long duration tremors suggest that “slow slip emission” along weaknesses that are misaligned with respect to the present day stress field is likely the dominant mechanism of deformation and plays a crucial role in reservoir stimulation. In Monongalia County, Morgantown, we carried out surface seismic monitoring of the hydraulic fracturing operation at an active well pad with five seismometers. Upon investigating the waveforms from surface monitoring, we identified 89 high-amplitude, impulsive events and 436 long period, long duration (LPLD) events, with highly emergent waveform characteristics. The time of occurrence of these observed LPLD events have no temporal correlation with the events reported in the regional earthquake catalogs and data from CEUSN stations, suggesting that these LPLDs are not weakened records of regional earthquakes. We observed a significant concentration of energy in the 0.8-3 Hz frequency range for these observed LPLD events. During various stages of hydraulic fracturing, LPLD events were found to occur most frequently when the pumping pressure and rate were at maximum values. As the main purpose of hydraulic fracturing operation is to stimulate oil and gas production from the less permeable reservoir, we compared the relative production contribution per stage to the frequency of occurrence of LPLD events. We found good correlation between the frequency of LPLD events and production data, highlighting the potential contribution of slow deformation processes and its effectiveness in the reservoir stimulation.

Introduction

Hydraulic fracturing of organic-rich shale and tight gas reservoirs is routinely performed to enhance the secondary permeability of the reservoir and increase access to trapped hydrocarbon resources. Application of this engineering technology involves the injection of millions of gallons of water at high pressure to establish a complex network of permeable fracture pathways that enhances hydrocarbon production from an otherwise low-permeability reservoir.

Productivity enhancement and reservoir stimulation is generally thought to be associated with the reactivation of pre-existing fractures, with minor contribution from creation of new hydraulic fractures (Moos et al., 2011; Das & Zoback, 2013). The deformation along pre-existing fractures and the opening of new fractures is likely recorded as microseismic events during hydraulic fracturing treatment. The distribution of microseismic events is most commonly used as a proxy to calculate the stimulated reservoir volume (SRV). For the most part, this correlation is still unsettled in the literature, with evidence both in support of and against the practice (Wilson et al., 2016 and Sicking et al., 2013).

Although the history of hydraulic fracturing treatment dates back to as early as the 1940's (Montgomery & Smith, 2010), the nature of subsurface deformation during hydrofracturing is still unclear. The response of a shale reservoir to hydraulic stimulation has been reported to be extremely variable among different fracturing sites. A simple energy balance calculation suggests that the cumulative moment of micro-earthquakes is a small portion of the moment release expected for the amount of fluid injected into the formation (Warpinski et al., 2012). This energy deficit suggests that other sources of deformation may play a dominant role during hydraulic stimulation. In a recent study of hydraulic fracturing in the Barnett Shale, Das and Zoback (2011) found evidence of low-frequency events (seismic frequencies ranging between 10 and 80 Hz) that persist for a long time period (between 10 to 100 seconds in duration). The LPLD events are low in displacement amplitude, with a mostly emergent arrival that makes phase picking very difficult (Das & Zoback, 2011; Eaton et al., 2013). Two probable mechanisms have been suggested by Das and Zoback (2011) and Zoback et al. (2012) for the occurrence of LPLD events associated with hydrofracturing. These include: (1) high clay content (>30%) at a local scale, which increases shale ductility and promotes slow slip failure along fractures with a stable deformation rate; (2) slip along pre-existing fractures that are unfavorably oriented in the ambient stress field and deform in LPLD events. Waveform analyses by Das and Zoback (2013) indicate deformation along a relatively larger fracture in the case of LPLD events, relative to brittle microseismic event failures, with LPLD events releasing as much as 1000 times the energy of an average microseismic event.

With these considerations about slow slip deformation and their probable role in reservoir stimulation, we have analyzed surface seismic data collected from Monongalia County in West Virginia (Figure 1). We examined the spectral characteristics of the recorded waveforms to accurately record and analyze the characteristics of energy release at low seismic frequencies (0.8-3 Hz) and clearly identify the presence of LPLD slow slip events associated with hydrofracturing. Our spectrogram analyses show bursts of seismic energy in the 0.8-3 Hz frequency range for several discrete arrivals. Waveform characteristics of these low frequency arrivals are similar to tectonic tremors and LPLD events previously reported from the subduction zone environments and hydraulic fracturing operation in the Barnett Shale in Texas respectively (Shelly et al., 2006; Das & Zoback, 2011) and likely indicate the existence of slow deformation processes during hydraulic fracturing.

Data and Method

We used surface seismic network of five broadband seismometers (Nanometrics-Trillium Compact Posthole) to collect data during the hydraulic fracturing of two horizontal Marcellus wells in Monongalia County, West Virginia (Figure 1). We deployed the seismometers within 2 miles of the treatment well pad, with the nearest station (FRAC1) within 700 feet of the well pad. The approximate range of recording frequency for the broadband seismometer is 0.05-100 Hz, with a low noise floor, and it is highly sensitive to detect earthquakes from both local and regional seismicity. We optimized the geometry of the seismic network by placing seismometers around the northwest trending laterals (Figure 1). Of the two laterals (MIP 3H and MIP 5H), well 5H was hydraulically fractured during October 28 – November 5, 2015 and well 3H during November 6 – 15, 2015. We present our analysis of observed data from three months of recording between September to November 2015 in the current study.

We applied instrument response corrections to the raw amplitude counts recorded by our surface seismometers to obtain the actual measure of ground motion in nm/s at each site. For a preliminary search of low-frequency signals, we calculated the power spectral density for 10 consecutive windows of 1 hour each, before and after the start of hydraulic fracturing. We compared the power spectral density of the 10-hour windows before and during fluid injection for both stimulation phases (October and November 2015) as shown in Figures 2a and 2b. In an exhaustive search for long duration events, we filtered the seismic waveform in multiple different frequency range of 1-30Hz, 1-5 Hz and 0.8-3 Hz to remove the masking effect of high frequency signal and manually inspected the filtered data. We observed the best coherent signals between stations in the 0.8-3Hz-frequency range. We initially identified 535

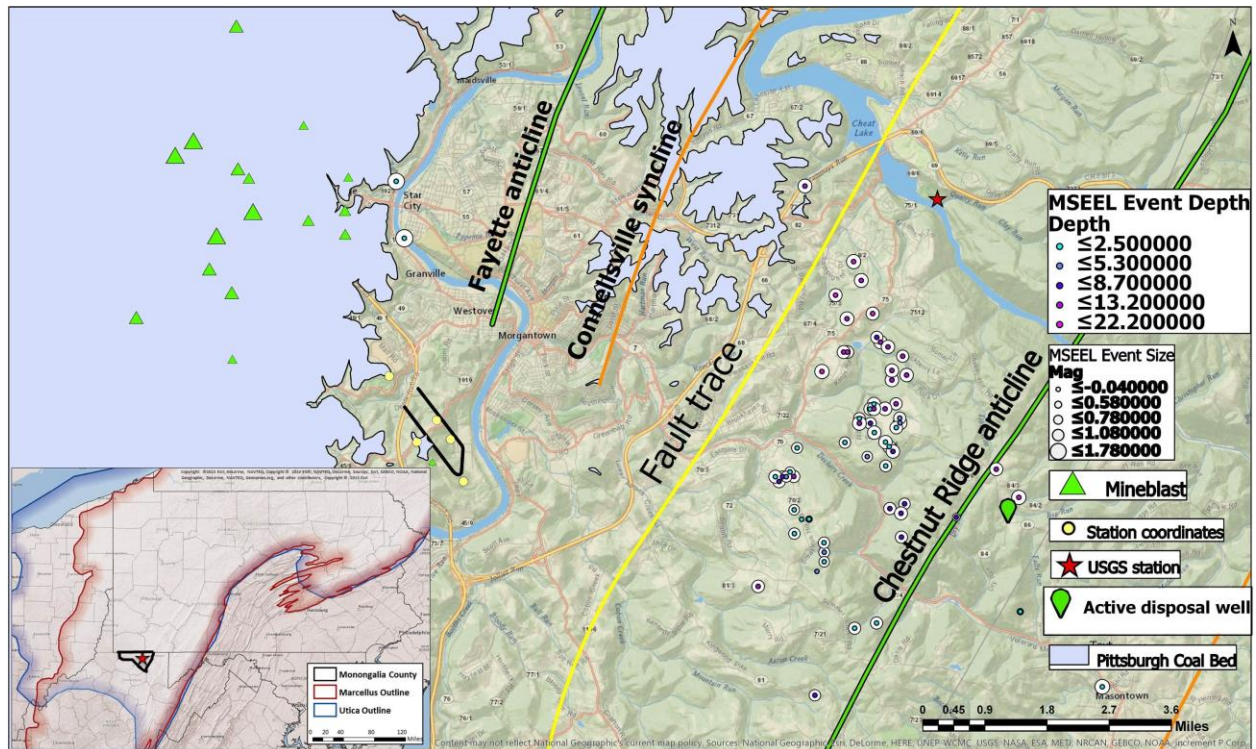


Figure 1. Map showing the location of two horizontal wells (solid black lines) in Monongalia County, with a small inset in the bottom left showing the study area and outline of Marcellus shale in West Virginia. Open circles represent the earthquake locations and the green triangles are mining or construction blasts located in the current study. Shaded grey area represents the outline of mined portion of the Pittsburgh Coalbed in Monongalia County, West Virginia.

discrete events, with waveform characteristics typical of an LPLD event, as discussed in Das and Zoback (2013). Each of these events is approximately 40-50 seconds in duration, with no impulsive phase arrival and waveforms dominantly composed of S-wave signal. This larger contribution of energy from the S wave arrival is similar to the waveform characteristics of previously reported long duration seismic tremor in the subduction zone environment and LPLD events from the Barnett Shale, respectively (Shelly et al., 2006; Das & Zoback, 2013).

In our analyses of long duration signal, it is imperative to rule out the possibility of mispicking regional or global earthquakes as potential LPLD events. Regional earthquakes could be a potential pitfall for the identification of LPLD events due to their overlapping frequency content and similar waveform characteristics, as pointed in recent studies (Caffagni et al., 2015; Zecevic et al., 2016). We carefully examined the USGS earthquake catalog for reported seismicity during the time period of observed LPLD events and found temporal overlap with some small magnitude regional events within 1000 km radius of our study area (Figure 3). We checked the arrival time of individual LPLD events and did not find any temporal overlap with the expected arrival time of these small magnitude regional events within 1000 km radius. We also compared the temporal records of our observed LPLD events with the events reported in a larger search radius of 2000 km in the Advanced National Seismic System [ANSS] composite catalog. From our list of 535 events, we found temporal overlap with 22 events reported in the ANSS catalogs. This suggests that either the 513 events are small magnitude regional events below the detection threshold of standard catalogs or they are local events in close proximity to our seismic network. To rule out the possibility of mis-picking small magnitude regional events as local earthquakes, we examined the waveform data from two stations of the nearby Central and Eastern US network (CEUSN), less than 70 miles from our study area (red pyramids, Figure 4). Of 513 non-catalog events, we found temporal correlation with 77 events in the CEUSN. We calculate the spectrogram of the north-south component signal for our final list of 436 unique LPLDs that are missing from both regional catalogs and nearby stations of the USArray.

We also compared the time of occurrence of LPLD events with the pumping pressure records to check for any first order correlation with pressure variation. As pointed by Zoback et al. (2012), long period events are likely

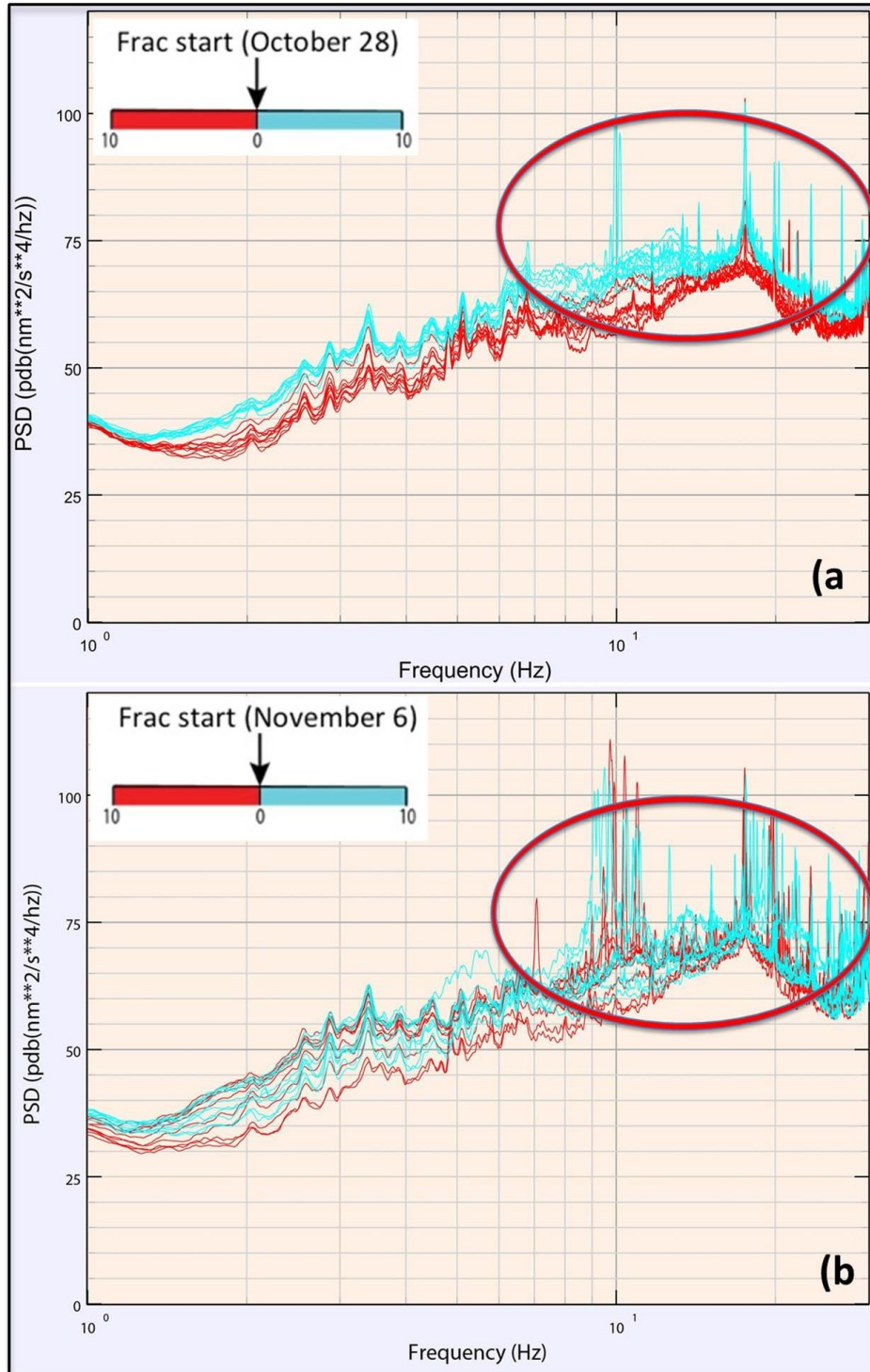


Figure 2. Spectral variation of power before (red) and after (cyan) fracturing started on (a) October 28, 2015 for well 5H and (b) November 6, 2015 for well 3H

associated with shear deformation along the preexisting fractures of relatively larger size and contribute more significantly to the stimulated reservoir volume (SRV) than its conventional estimate based on the microseismicity alone. The oil and gas production from unconventional reservoir is assumed to be inherently related to the SRV due to hydraulic fracturing (Warpinski et al., 2012). We compared the time of occurrence of long period events observed

during the hydraulic fracturing of well 3H with the stage-by-stage production data to highlight their contribution in reservoir productivity.

While searching for long duration events, we found some high amplitude discrete seismic arrivals with strongly impulsive waveform characteristics. Some of the impulsive events have waveform characteristics similar to a mine blast (these events displayed a pseudo-isotropic pressure pulse), with insignificant energy contribution from S-wave arrivals. We are able to pick P and S-arrivals for all other impulsive events on both the vertical and horizontal components. We used the single-station location procedure in SEISAN (Havskov & Ottemoller, 1999) to locate a final list of 89 impulsive events, including 21 probable mine blasts. We also estimated their moment magnitude by utilizing the spectral parameters of displacement spectra in SEISAN.

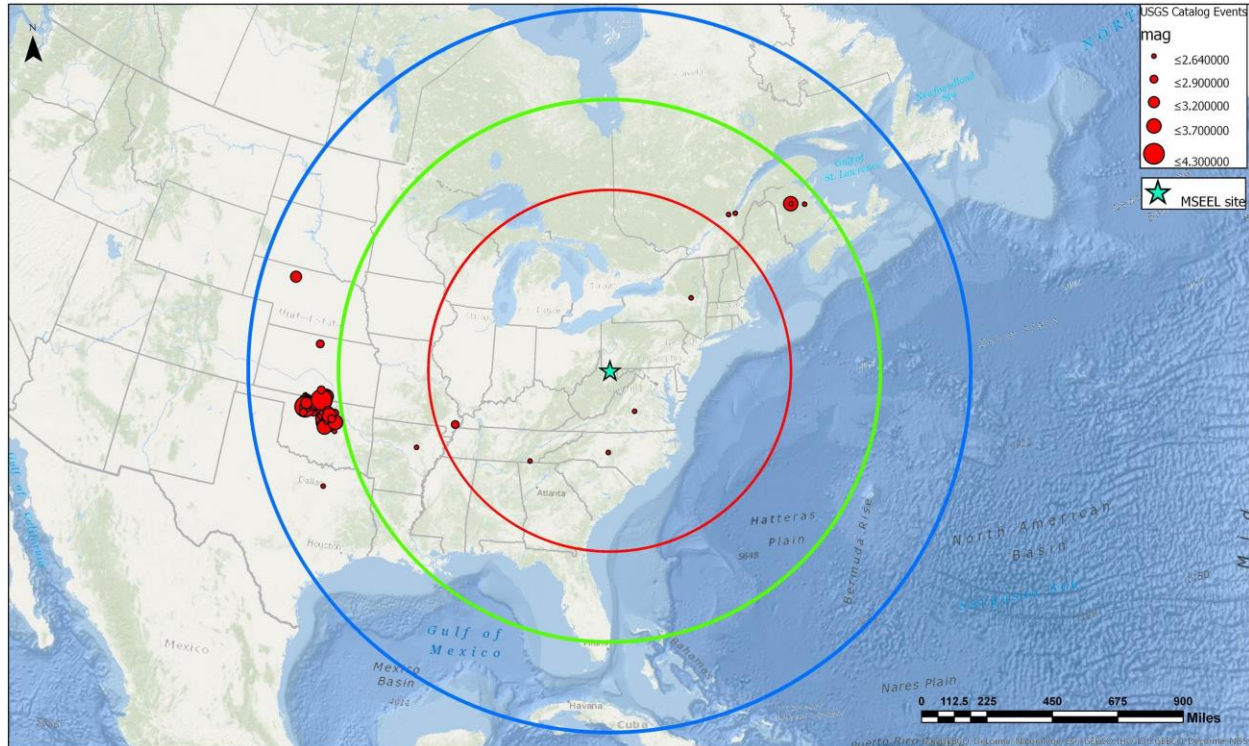


Figure3. Map showing the location of regional events (solid red dots) reported in the USGS catalog during the fracturing of well 5H and 3H. The red, green and blue circles drawn on the map have a radius of 1000 km, 1500 km, and 2000 km respectively

Results and Discussions

The locations of high amplitude impulsive events are shown in Figure 1. We observed two types of impulsive events with differing waveform characteristics. The two groups of events are geographically separated from each other and located on opposite ends of the two horizontal wells. The first group of events, located northwest of the horizontal wells, is composed of sparsely distributed hypocenters with waveform characteristics similar to a mine blast (green triangles in Figure 1). The range of hypocentral depth varies between 0 and 3 km for the first group of events. Review of the USGS record of mined areas for the Pittsburgh coal bed in West Virginia (Fedorko, 1990) shows an excellent spatial correlation between the location of these blast-type events and the southeastern edge of old underground mines in Monongalia County (grey shaded area in Figure 1). This suggests that the impulsive events, having waveform signature similar to pseudo-isotropic pressure pulse, are perhaps related to roof collapse in the old mine or blasts associated with civil construction and other mining activities. Southeast of the horizontal wells, we located a second group of events (open circles in Figure 1) with waveform characteristics similar to a natural earthquake. Events within the second group have hypocentral depth varying in the range of 0 to 22 km, with local magnitude in the range of $M_L 0$ to $M_L 1.78$. It forms a linear cluster of events, dominantly oriented north-south, with a minor extension in the northeast-southwest direction. We do not observe any spatial overlap between the location of these normal earthquakes and lateral Marcellus Shale wells. Majority of the events from this distant cluster have less

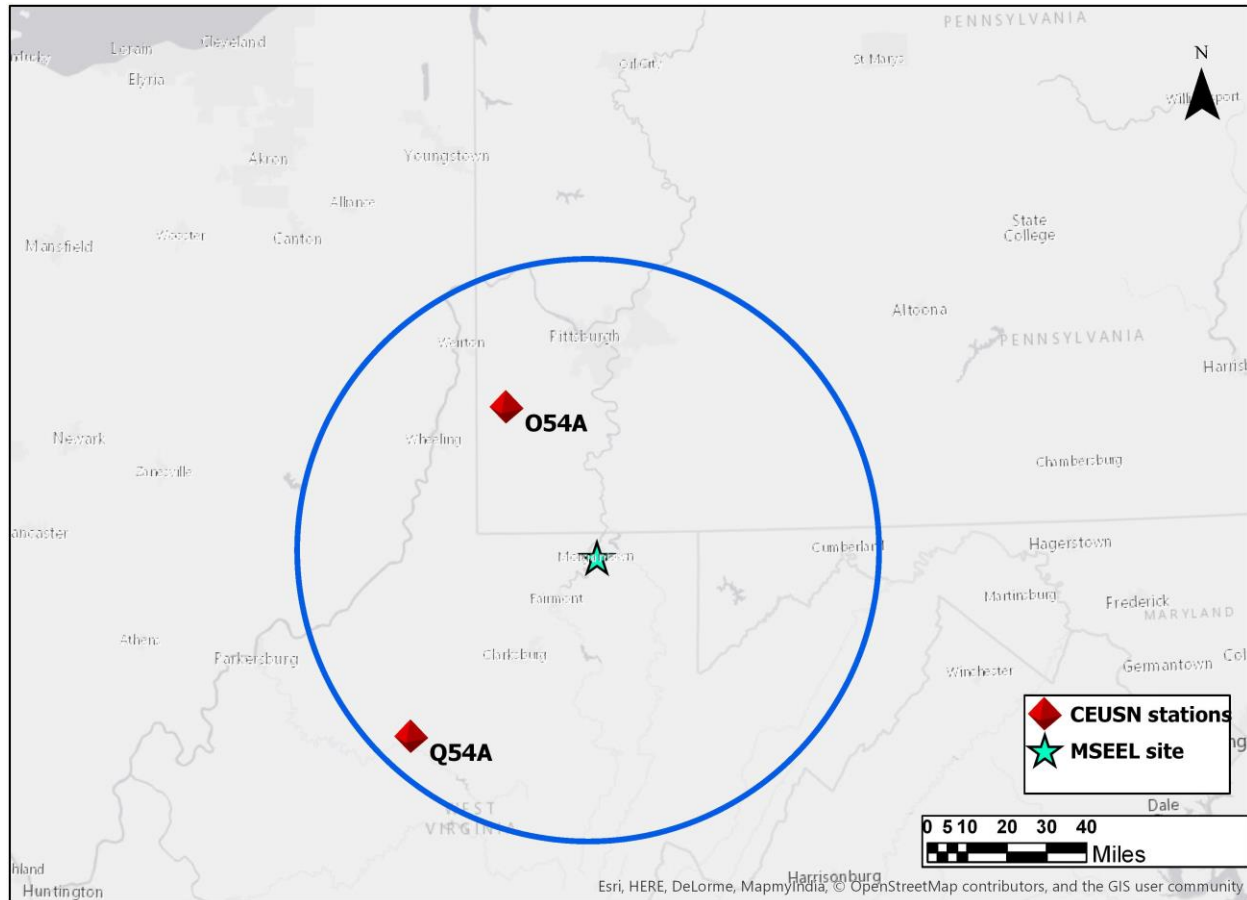


Figure4. Map showing the locations of nearby stations from Central and Eastern United States Network (red pyramids) used for waveform comparison with LPLD events recorded at Monongalia County site (cyan star). The circle (blue) drawn on the map has a radius of 70miles.

well-constrained hypocentral depth with large mean depth error (~25 km) that can be attributed to wide azimuthal gap (~360°, angle between two straight lines connecting an earthquake location with the two adjacent seismic stations in the network). This linear cluster apparently coincides with the western flank of Chestnut Ridge anticline, the westernmost ridge in the Appalachian Plateau Physiographic Province (Figure 1). We also found a class II injection well along the eastern edge of this earthquake cluster that is actively being used for commercial brine disposal at ~8000 ft (green place mark, Figure1). As widely evidenced in Central Oklahoma, the saltwater disposal could potentially increase the level of background seismicity (Walsh and Zoback, 2015). Considering the large error in hypocentral depth, it is difficult to quantify the exact nature of subsurface deformation related to this distant earthquake cluster. It is possible that the shallow events within this cluster are related to the subsurface variation in pore pressure resulting from brine disposal and deeper events are perhaps related to the tectonic deformation in the lower crust under this portion of the Central Appalachians.

During hydraulic fracturing, we observed a significant increase in the power spectral density between 7 and 30 Hz, with a larger number of peaks as compared to the pre-fracture time interval (Figure 2). The difference in spectral peaks before and during the hydraulic fracturing is significant at three seismometer locations (FRAC1, FRAC2 and FRAC4) for both laterals (wells 5H and 3H). We observed a subtle difference in power spectral peaks for FRAC5 that can be attributed to greater loss of energy due to its distal location from the two horizontal Marcellus Shale wells. At FRAC3, data recording was discontinuous due to solar charging shortcomings and we are unable to calculate power spectra at the time when fracturing started. The increase in power spectral peaks during stimulation indicates a significant contribution of energy from the low frequency (<30 Hz) signal.

Our detailed analyses of the LPLD events and their spectrograms show abrupt flares of energy in the seismic frequency range between ~0.8 to 3 Hz, with occasional spikes up to 4 Hz (Figure 5). Although our spectrograms for

the LPLD events are similar to those discussed by Das and Zoback (2011), spectral content is significantly different with lower dominant frequencies. This difference in spectral content is perhaps related to the different positioning of the recording system between ours and previous studies. We used data from surface seismometers for spectral analyses as opposed to borehole geophones used by Das and Zoback (2011). Seismic waves attenuate as they propagate through the earth, with larger attenuation for higher frequencies due to the inherent high-cut/low-pass filtering property of the earth. As the borehole geophones are likely to be closer to the origin point of LPLD seismicity in the subsurface, attenuation of higher frequencies will be less significant due to a shorter travel path. For the surface seismometers, higher frequencies will be comparatively more attenuated due to a longer travel path and the seismic signal will be left with dominantly lower frequencies. Of the 436 LPLD events, 55% (242 events) of the LPLD events were identified during the stimulation of well 5H and 45% (194 events) during the hydraulic fracturing of well 3H. Although there are no obvious differences in the hydraulic treatment strategies between well 5H and 3H to account for the difference in observed LPLD counts, one possibility is the difference in the number of stimulation stages between well 5H and 3H. Well 5H was stimulated over more stages than well 3H (30 versus 28 stages), which would create an elevated fluid pressure condition in the reservoir for a longer period of time and perhaps be responsible for the increased LPLD count during the treatment of well 5H. Another possibility is the closer proximity of seismometers (FRAC2 and FRAC4) to well 5H, leading to improved detection for small magnitude LPLD events.

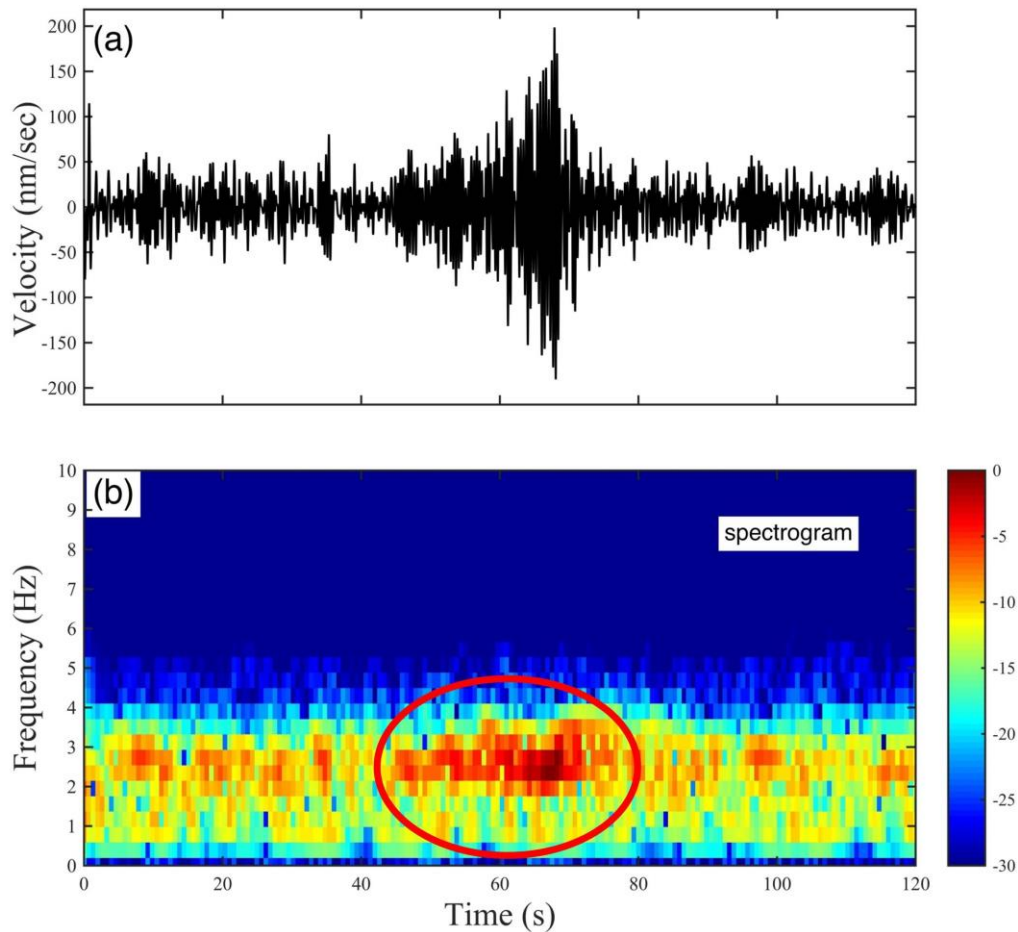


Figure 5. Stacked waveform (panel-a) and spectrogram (panel-b) of a long duration event identified during November stimulation period of well 3H. Color scale shows amplitude in decibel, with warmer colors corresponds to higher amplitude and vice-versa.

As mentioned in the previous section, we made diligent efforts of checking standard earthquake catalogs and data from nearby stations of CEUSN to avoid misinterpreting any small to large magnitude regional events as potential LPLD events. From our final list of 436 LPLD events, we carefully selected some high quality LPLD events with high signal to noise ratio and analyzed 2-minute long records of CEUSN data spanning the arrival times of these

selected LPLD events. We found no indication of small magnitude events during the relevant time intervals at both stations (O54A and Q54A) from CEUSN (Figure 6). The seismic waveforms recorded at both CEUSN stations appear to contain a uniform record of background noise, without any noticeable change in the amplitude level or frequency content with time. The direct comparison of seismic waveforms of individual LPLD events to the CEUSN data also highlights the static amplitude level at both CEUSN stations with no signs of regional phase arrival before and after the origin time of LPLD events (Figure 7). The absence of LPLD record from the CEUSN data is an important observation that likely suggests a local source of deformation for the causality of LPLD signal rather than small magnitude regional earthquakes not listed in the standard catalogs.

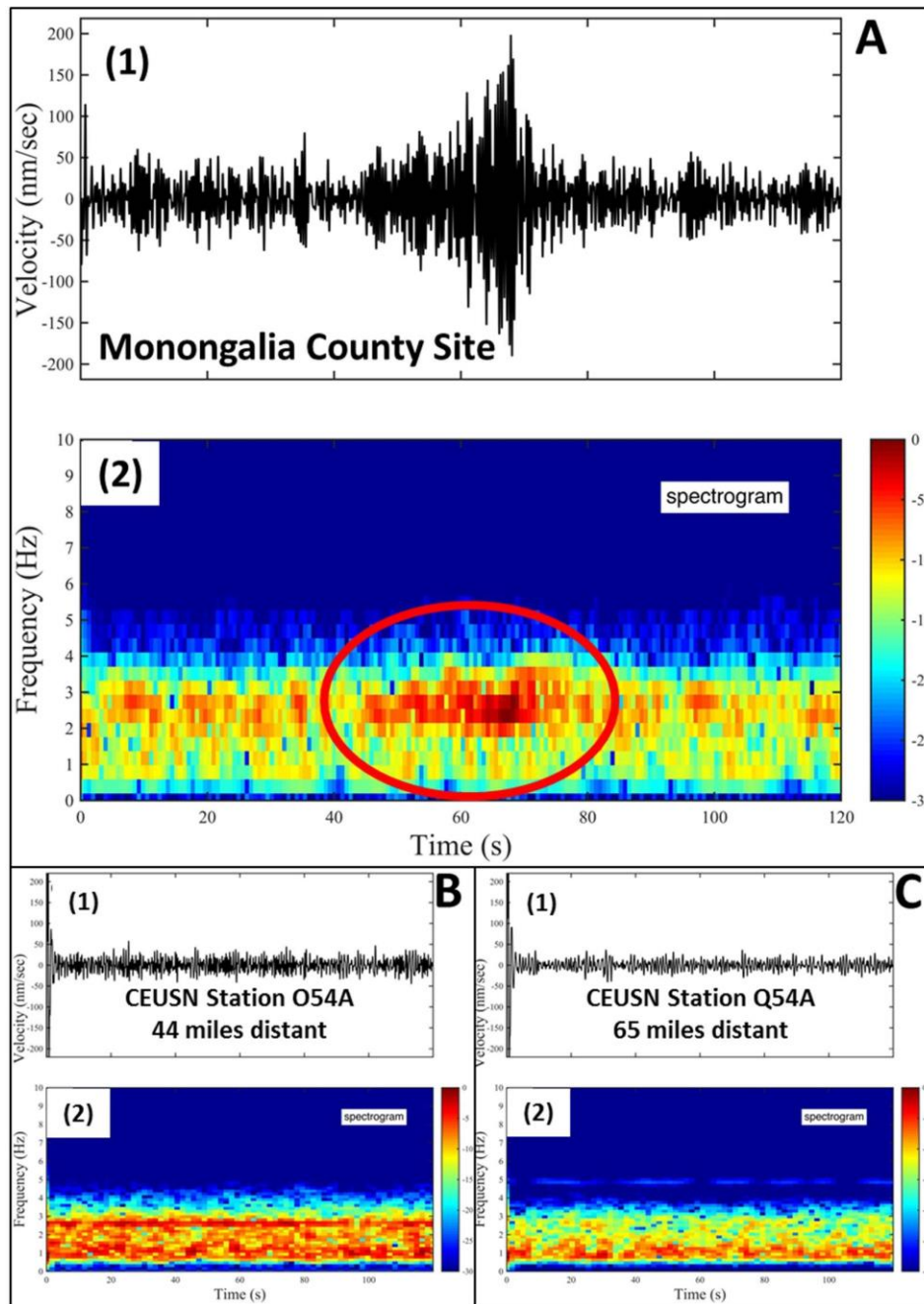


Figure 6. Stacked seismic traces (panel 1) and spectrogram plots (panel 2) of (A) a long duration event recorded at MSEEL site from treatment well 3H (B-C) Central and Eastern United States Network (CEUSN) data recorded at O54A and Q54A respectively for similar timeframe as used for panel A

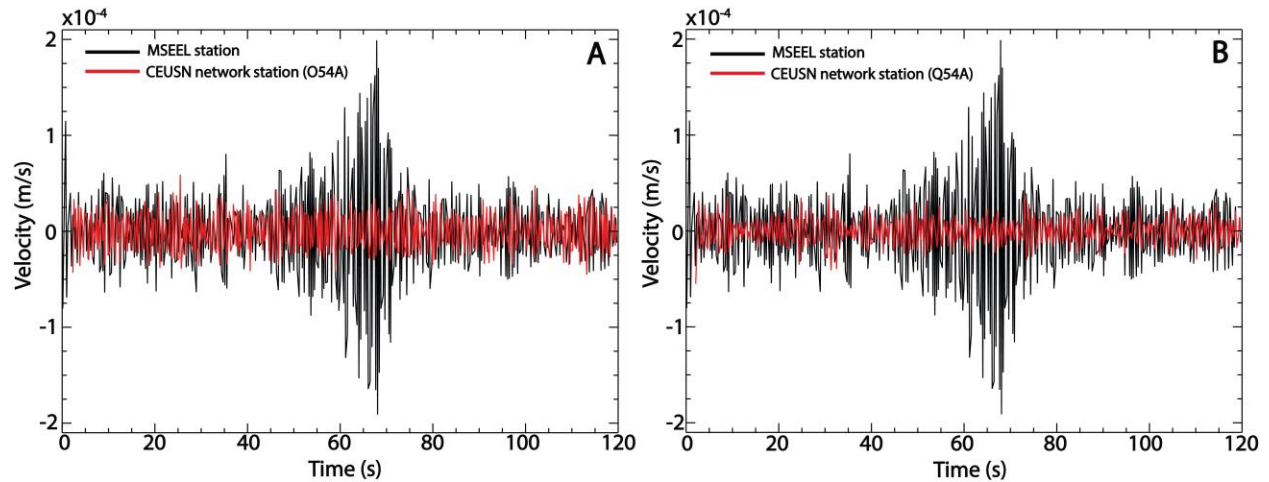


Figure 7. Stacked seismic traces showing the waveform comparison of a LPLD event recorded at MSEEL site (black trace) and CEUSN data (red trace) (A) at O54A station (B) at Q54A station. This is the same LPLD event as shown in Figure 6 (A). The timeframe for both MSEEL stations and CEUSN stations is same

Our attempt of finding a temporal correlation, if any, between the time of occurrence of LPLD events and variation in the pumping parameters reveals that LPLD events mainly occur during the pad and proppant phases of pumping, when pumping pressure and pumping rate are plateaued at their maximum (Figure 8). This is similar to the previous observation of Das and Zoback (2011) for the hydraulic fracturing of Barnett Shale and associated LPLD events. As suggested by Das and Zoback (2011) and Zoback et al. (2012), LPLD events during hydraulic fracturing are triggered by shear deformation along sub-optimally oriented natural fractures by an exceptional increase in pore pressure. Our observed correlation between the time of occurrence of majority of LPLD events and increased pumping pressure and rate is therefore logical given that the maximum pore-pressure perturbation is likely to correlate with the maximum pressure and rate.

How to maximize the effects of reservoir stimulation for better access to hydrocarbons is still a looming question even after 80 years of operational history of hydraulic fracturing technology. This is in most part related to the complexity of the geomechanical response of the reservoir during hydraulic fracturing, to which a clear understanding is still lacking. This incomplete realization of reservoir response adversely affects the recovery efficiency of oil and gas from the unconventional shale reservoirs. A recent study by Boroumand and Eaton (2012) that focuses on the energy budget estimate during hydraulic fracturing, clearly highlights the energy deficiency based on the microseismicity alone. This also suggests that the expected production of oil and gas and SRV estimate, based on the microseismicity alone, is perhaps an underestimate. To reduce the gap in the energy budget or estimated production, other deformation mechanisms (non-brittle deformation) need to be taken into account. We attempt to highlight the contribution of non-brittle deformation and associated LPLD events to reservoir productivity by comparing the production contribution per stage from well 3H to the observed frequency of LPLD events during hydraulic fracturing, as discussed in the method section. There are several cycles of high and low production that indicate a significant variation in the overall production of 28 different stages for well 3H (Figure 9). We observe correlation between the stage-by-stage gas production and the frequency of LPLD events recorded during stimulation. We do notice some mismatch between peaks in production and peaks in the LPLD count, likely due to uncertainty in the location of LPLD events. Though the LPLD may have occurred during a particular stage, the actual stimulated volume of rock may be closer to an adjacent stage. This correlation between the occurrence of LPLD activity and production data strongly suggest a significant contribution from non-brittle deformation in the SRV, which ultimately correlates with early-life gas production. We can use this correlation between production data and surface seismic observation to make better completion strategies and stimulation designs for other prospective projects in future.

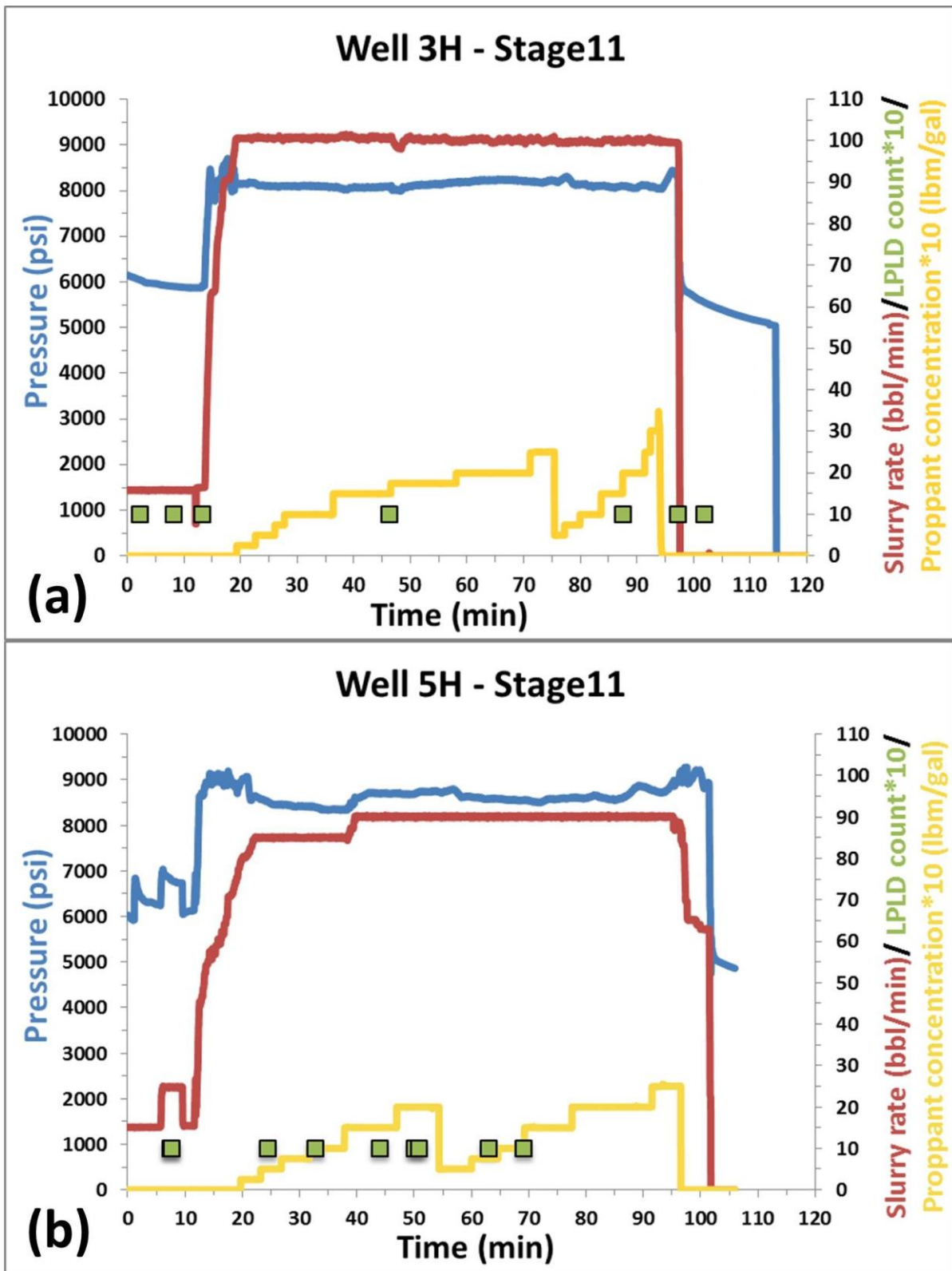


Figure8. Comparison between frequency of occurrence of LPLD events and injection parameters. Long duration events are shown as green rectangles for stage 11 of wells 5H and 3H, with solid lines representing surface pressure recording (blue), slurry rate (red), and proppant concentration (yellow)

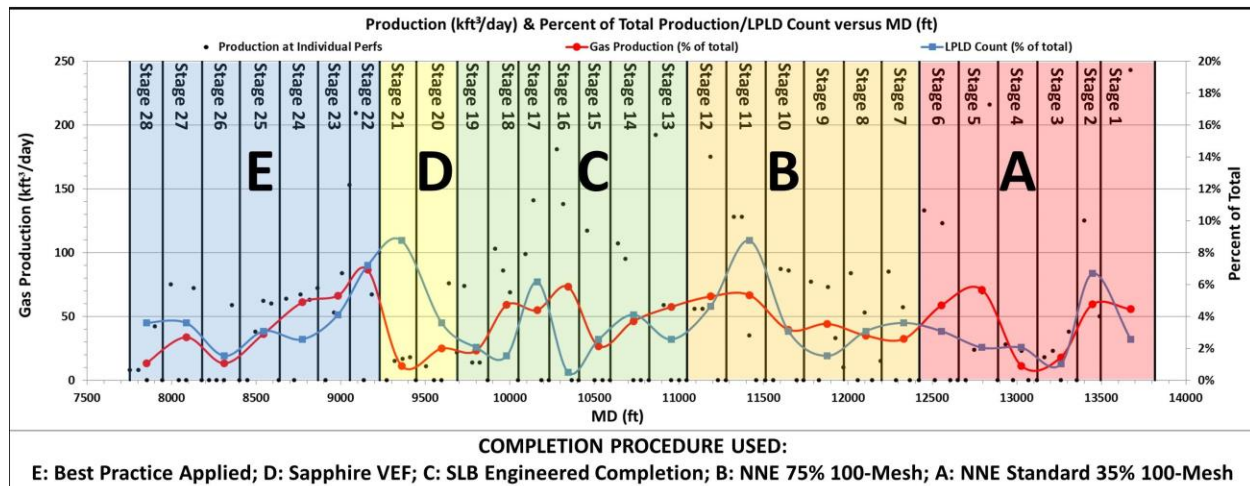


Figure9. Comparison between relative production contributions per stage (red curve) from well 3H to the frequency of occurrence of observed LPLD events (blue curve)

Conclusions

We present new 3-component surface seismic data collected during the hydraulic fracturing of horizontal Marcellus Shale wells in Monongalia County, West Virginia. We observed seismic events with waveform characteristics varying from impulsive to emergent, with high and low frequency content, respectively. We found an excellent spatial correlation between coal mining areas and impulsive events with waveform characteristics similar to a mine blast. These events are likely related to mine roof collapse and other mining related activities in the nearby region. We also noticed a linear cluster of impulsive events in Monongalia County that aligns with the western flank of Chestnut Ridge Anticline and close to an active wastewater disposal well in this proximity. This distant cluster of seismic events is perhaps related to the reactivation of basement faults triggered by disposed fluids and/or small-scale crustal deformation in this tectonically complex portion of the Central Appalachians. Most seismic events exhibit waveform characteristics similar to long period, long duration (LPLD) events previously observed in the Barnett Shale, Texas. These events are characterized by emergent waveforms with no clear arrival of the body wave (P and S) phases. We observed a significant difference in the power spectral peaks before and during hydraulic fracturing. This suggests a significant contribution of energy from the low frequency signal during stimulation. Spectral characteristics of these LPLD events are similar to those observed in Barnett Shale, but differ in terms of frequency content, having lower dominant frequencies. This difference in spectral content is likely due to attenuation of higher frequency component from the seismic signal as it covers a longer travel path to the surface seismometer. During various stages of hydraulic fracturing, LPLD events were found to occur most frequently when the pumping pressure and rate were at maximum values. These observations suggest that long period, long duration events are generated in response to highly elevated fluid pressure. We also noticed a positive correlation between the variations in LPLD counts and the stage-to-stage production for one of the two laterals suggesting a significant contribution from the non-brittle deformation in the reservoir stimulation and early-life gas production.

Disclaimer

This project was funded by the United States Department of Energy, National Energy Technology Laboratory, through a support contract with AECOM. Neither the United States Government nor any agency thereof, nor any of their employees, nor AECOM, nor any of their employees, makes any warranty, expressed or implied, or assumes any legal liability or responsibility for the accuracy, completeness, or usefulness of any information, apparatus, product, or process disclosed, or represents that its use would not infringe privately owned rights. Reference herein to any specific commercial product, process, or service by trade name, trademark, manufacturer, or otherwise, does not necessarily constitute or imply its endorsement, recommendation, or favoring by the United States Government or any agency thereof. The views and opinions of authors expressed herein do not necessarily state or reflect those of the United States Government or any agency thereof.

Acknowledgement

We are grateful to National Energy Technology Laboratory, Department of Energy for permission to publish this work. This research was supported in part by an appointment to the U.S. Department of Energy (DOE) Postgraduate Research Program at the National Energy Technology Laboratory administered by the Oak Ridge Institute for Science and Education and partly in support of the National Energy Technology Laboratory's ongoing research under the RES contract DE-FE0004000. We would also like to acknowledge the National Science Foundation (NSF), United States Geological Survey (USGS), United States Nuclear Regulatory Commission (USNRC) and Incorporated Research Institutions for Seismology (IRIS) for the seismic waveform data from Central Eastern US Seismic Network (CEUSN) and regional mine blasts.

References

Boroumand, N. and D. W. Eaton, 2012, Comparing energy calculations - Hydraulic fracturing and microseismic monitoring: 74th Conference and Exhibition, EAGE, Extended Abstracts, C042.

Caffagni, E., D. Eaton, M. van der Baan, and J. P. Jones, 2015, Regional seismicity: A potential pitfall for identification of long-period long-duration events: *Geophysics*, **80**, no. 1, A1-A5, doi:10.1190/geo2014-0382.1.

Das, I., and M. D. Zoback, 2011, Long period long duration seismic events during hydraulic fracture stimulation of a shale gas reservoir: *The Leading Edge*, **30**, 778–786, doi: 10.1190/1.3609093.

Das, I., and M. D. Zoback, 2013, Long-period, long-duration seismic events during hydraulic stimulation of shale and tight-gas reservoirs—Part 1: Waveform characteristics, *Geophysics*, **78**, KS107–KS118, doi: 10.1190/GEO2013-0164.1.

Eaton, D., M. Van der Baan, J. B. Tary, B. Birkelo, N. Spriggs, S. Cutten, and K. Pike, 2013, Broadband microseismic observations from a Montney hydraulic fracture treatment, northeastern British Columbia: *CSEG Recorder*, **38**, 45–53.

Fedorco, Nick, 1990, Pittsburgh coal structure contours- working map, Paden City quadrangle, WV-OH: West Virginia Geological and Economic Survey Open File Report-014.

Havskov, J., and L. Ottemoller, 1999, SeisAn Earthquake Analysis Software: *Seismological Research Letters*, **70**, 532-534, doi:10.1785/gssrl.70.5.532.

Montgomery, C. T., and M. B. Smith, 2010, Hydraulic fracturing: History of an enduring technology: *Journal of Petroleum Technology*, **62**, 26, doi: 10.2118/1210-0026-JPT.

Moos, D., G. Vassilellis, R. Cade, J. Franquet, A. Lacazette, E. Bourtembourg, and R. Cade, 2011, Predicting shale reservoir response to stimulation in the upper Devonian of West Virginia: Annual Technical Conference, SPE, Paper 145849.

Shelly, D. R., G. C. Beroza, S. Ide, and S. Nakamuta, 2006, Low-frequency earthquakes in Shikoku, Japan, and their relationship to episodic tremor and slip: *Nature*, **442**, 188–191, doi: 10.1038/nature04931.

Sicking, C., J. Vermiliye, P. Geiser, A. Lacazette, and L. Thompson, 2013, Permeability field imaging from microseismic: *Geophysical Society of Houston Journal*, **3**, 11–14, doi: 10.1190/segam2012-1383.1.

Walsh, F., and M. D. Zoback (2015). Oklahoma's recent earthquakes and saltwater disposal, *Sci. Adv.* **1**, e1500195, doi: 10.1126/sciadv.1500195.

Warpinski, N. R., J. Du, and U. Zimmer, 2012, Measurements of hydraulicfracture- induced seismicity in gas shales: Hydraulic Fracturing Technology Conference, SPE, Paper 151597, doi: 10.2118/151597-PA.

Wilson, T., A. Hart, and P. Sullivan, 2016, Interrelationships of Marcellus Shale gas production to frac-induced

microseismicity, interpreted minor faults and fractures zones, and stimulated reservoir volume, Greene County, Pennsylvania: *Interpretation*, **4**, T15-T30, doi: 10.1190/INT-2015-0045.1.

Zecevic, M., G. Daniel, and D. Jurick, 2016b, On the nature of long-period long-duration seismic events detected during hydraulic fracturing: *Geophysics*, **81**, no. 3, KS113-KS121, doi: 10.1190/geo2015-0524.1.

Zoback, M. D., A. Kohli, I. Das, and M. McClure, 2012, The importance of slow slip on faults during hydraulic fracturing stimulation of shale gas reservoirs: Americas Unconventional Resources Conference, SPE, Paper 155476, doi: 10.2118/155476-MS.

National Energy Technology Laboratory

626 Cochrans Mill Road
P.O. Box 10940
Pittsburgh, PA 15236-0940

3610 Collins Ferry Road
P.O. Box 880
Morgantown, WV 26507-0880

13131 Dairy Ashford, Suite 225
Sugarland, TX 77478

1450 Queen Avenue SW
Albany, OR 97321-2198

2175 University Ave. South
Suite 201
Fairbanks, AK 99709

Visit the NETL website at:
www.netl.doe.gov

Customer Service:
1-800-553-7681

